Fission-barriers and energy spectra of odd-mass actinide nuclei in self-consistent mean-field calculations

Meng Hock Koh

Numéro d'ordre:

UNIVERSITY OF BORDEAUX

and

UNIVERSITI TEKNOLOGI MALAYSIA

PhD CO-DIRECTED THESIS

by

KOH Meng Hock

(辜 明 福)

Fission-barriers and energy spectra of odd-mass actinide nuclei in self-consistent mean-field calculations

Thesis defended on 29 October 2015

Rapporteurs :

Héloïse Goutte	Research director	CEA Saclay, France
Paul Stevenson	Senior Lecturer	University of Surrey, UK

Members of the jury :

Michael Bender	Research director	CENBG Bordeaux-Gradignan, France	**President of the jury**
Héloïse Goutte	Research director	CEA-Saclay, France	**Rapporteur**
Paul Stevenson	Senior lecturer	University of Surrey, UK,	**Rapporteur**
Olivier Bouland	Researcher	CEA Cadarache, France	**Examiner**
Norsarahaida bt. Saidina Amin	Professor	Universiti Teknologi Malaysia	**Examiner**
Ludovic Bonneau	Doctor Hb.	CENBG Bordeaux-Gradignan, France	**Thesis co-supervisor**

Invited members:

Philippe Quentin	Professor	CENBG Bordeaux-Gradignan, France	**Thesis co-supervisor**
Husin Wagiran	Professor	Universiti Teknologi Malaysia	**Thesis co-supervisor**

To my parents, my wife and our soon-to-be born child.

ACKNOWLEDGEMENT

First and foremost, I would like to thank to Prof. Philippe Quentin and Dr. Ludovic Bonneau for whom I have the opportunity to work closely with, since I started my masters degree study six years ago. I am most grateful for their advices both with regards to research and practical daily experiences, as well as their immense patience in the course of writing this thesis. I would also like to express my appreciation to Prof. Husin Wagiran for his encouragement in pursuing this research work, and for making the necessary arrangements for the success of this co-directed thesis between Universiti Teknologi Malaysia and University of Bordeaux.

My appreciation also goes to manuscript reviewers and panel of examiners; Dr. Héloise Goutte, Dr. Paul Stevenson, Dr. Olivier Bouland, Dr. Micheal Bender, Prof. Norsarahaida, Prof. Ahmad Termizi bin Ramli, Prof. Noorddin bin Ibrahim and Assoc. Prof. Wan Saridan for their suggestions to the thesis manuscript, and for participating in the oral thesis defense.

I would also like to thank the Centre Etudes Nucléaires de Bordeaux Gradignan (CENBG) for the excellent working conditions, as well as the many wonderful people there, in particular Sylvie Perrève and Abdelaziz Habbouse of whom I have benefited tremendously from their assistance. My gratitude also goes to Prof. Bernard Hass and Prof. Philippe Moretto, the former and current director of CENBG for their administrative support for my research work.

My appreciation also to Universiti Teknologi Malaysia for the financial support rendered to me throughout these three years of study.

Many thanks to my friends; Lam Yi Hua (whom I met on my first trip to CENBG for a research attachment in 2010), Hou Xian and Lu Xing Heng (who have made my stay in Bordeaux more memorable), Yap Yung Szen (for assistance with the UTM thesis template) and Ng Theng Pin (for encouragement to persevere in my research).

A big thank you to my parents for their unwavering love and belief they have in me, my adorable twin sisters for their moral support, and my loving wife for being there for me in these long years of academic struggle. Finally, I would also like to record my appreciation to my late maternal grandmother for her love and care - the memories of the time we had together will always remain close to my heart.

ABSTRACT

While there have been numerous microscopic calculations on fission barriers of even-mass compound nuclei, there are however, relatively few such work dedicated to odd-mass nuclei. This is due to the complications posed by the breaking of the time-reversal symmetry at the mean-field level due to the presence of an unpaired nucleon. In order to circumvent this difficulty, previous fission-barrier calculations of odd-mass nuclei have been performed by neglecting the effect of time-reversal symmetry breaking. This work aims to improve on the description of fission barriers as well as the spectroscopic properties of ground and fission-isomeric state, of some odd-mass actinide nuclei by taking the effect of time-reversal symmetry breaking into account. This has been perfomed within a Skyrme-Hartree-Fock-plus-BCS framework with blocking, where the BCS formalism has been adapted to accomodate this symmetry breaking. The Skyrme nucleon-nucleon effective force has been used with various sets of parameters (SIII, SkM*, SLy5*). The residual pairing interaction has been approximated by seniority forces whose neutron and proton parameters have been fitted to reproduce the odd-even mass differences of some actinide nuclei. The low-lying rotational band-head energies evaluated within the Bohr-Mottelson unified model have been determined for four well-deformed odd-nuclei (^{235}U, ^{239}Pu, ^{237}Np, ^{241}Am) yielding a good qualitative agreement to the data for odd-neutron nuclei. The agreement was significantly less good for the odd-proton nuclei, possibly due to the use of the Slater approximation for the exchange Coulomb interaction. The deformation energies of two odd-neutron nuclei (^{235}U and ^{239}Pu) have been calculated for some single-particle configurations up to a point beyond the outer fission-barrier. Axial symmetry nuclear shape has been assumed while a breaking of the left-right (or intrinsic parity) symmetry has been allowed around the outer fission-barrier. The fission-barrier heights of such odd-neutron nuclei depend significantly on the particle configurations. A special attention has been paid to the very important rotational correction to deformation energies. In particular, the correction of the moment of inertia calculated from the usual Belyaev expression was considered. Overall, a qualitative agreement with available data on fission-barrier heights for the considered odd-neutron nuclei and their even neighbours has been obtained.

RÉSUMÉ

Alors qu il existe de nombreux calculs microscopique de barrières de fission pour des noyaux composé de masse paire, il n'y a cependant que relativement peu de tels calculs pour des noyaux de masse impaire. Ceci est dû aux complications induites par la brisure de la symétric de reversement du sens du temps au niveau du champ moyen qui est engendrée par la présence d'un nucleon non-apparié. Pour eviter cette difficulté, des calculs existants pour des noyaux de masse impaire ont tout simplement negligé ces effets de brisure de la symétrie de reversement du sens du temps. Dans ce travail, on se donne pour but d'améliorer la description des barrières de fission, aussi bien que des propriétés spectroscopiques du niveau fondamental et de l'etat isomerique de fission, pour quelques isotopes de masse impaire dans la région des actinides en prenant en compte de tels effets. Ceci a été realisé dans le cadre du formalisme de Skyrme–Hartree–Fock plus BCS avec blocking en adaptant ce formalisme à la brisure de la symétrie considérée. L'interaction résiduelle d'appariement a été approchée par une force de séniorité dont les paramètres ont été ajustés pour reproduire les différences de masse pair-impair de quelques noyaux de la région des actinides. Les énergies des têtes de bande rotationnelle de basse énergie ont été calculées dans le cadre du modèle unifié de Bohr-Mottelson pour quatre noyaux bien déformés (^{235}U, ^{239}Pu, ^{237}Np, ^{241}Am) produisant un bon accord qualitatif avec les données pour les noyaux impairs en neutrons. L'accord significativement moins bon obtenu pour les noyaux impairs en protons pourrait résulter de l'usage de l'approximation de Slater pour l'interaction d'échange de Coulomb. Les énergies de déformation de deux noyaux impairs en neutrons (^{235}U, ^{239}Pu) ont été calculées pour quelques configurations de particule individuelle, jusqu'après la barrières de fission externe. La symétrie axiale a été imposée tandis que la brisure de la symétrie droite-gauche (ou de parité intrinsèque) a été permise dans la région de la seconde barrière. Les hauteurs des barrières de fission pour ces noyaux impairs dépendent significativement des configurations de particule individuelle. Un accord qualitatif avec les données disponibles pour les hauteurs de barrières des noyaux impairs considérés et leurs voisins pairs a été généralement obtenu.

TABLE OF CONTENTS

Cover **i**

ACKNOWLEDGEMENT . . . iii
ABSTRACT . . . iv
RÉSUMÉ . . . v
TABLE OF CONTENTS . . . vii
LIST OF TABLES . . . ix
LIST OF FIGURES . . . xii

1 INTRODUCTION **1**

2 FISSION CROSS-SECTIONS CALCULATIONS **5**
2.1 Experimental study of the fission phenomenon . . . 5
2.1.1 Fission as a nuclear reaction . . . 5
2.1.2 Structures in the (n,f) cross-sections . . . 5
2.2 Fission cross-section modeling . . . 8
2.2.1 Fission reaction mechanism . . . 8
2.2.2 Optical model for fission . . . 11
2.3 Nuclear structure input . . . 14
2.3.1 Potential-energy surface . . . 14
2.3.2 Nuclear spectra . . . 15
2.3.3 Inertia parameters . . . 16

3 THEORETICAL FRAMEWORK **17**
3.1 The mean-field approach . . . 17
3.1.1 The Skyrme approximation to the effective nucleon-nucleon interaction . . . 17
3.1.2 The Hamiltonian density in the case of time-reversal symmetry breaking . . . 18
3.1.3 The Hartree-Fock equations . . . 21
3.1.4 Self-consistent blocking calculation (SCB) . . . 22
3.1.5 Self-consistent symmetries . . . 24
3.1.6 Constrained Hartree-Fock . . . 24
3.2 Treatment of pairing correlation . . . 28
3.2.1 The BCS approximation . . . 28
3.2.2 The BCS approximation with a seniority force . . . 30
3.3 The center-of-mass correction . . . 34
3.4 From HF+BCS energies to nuclear energies . . . 35
3.4.1 The case of even-mass nuclei . . . 35
3.4.2 The case of odd-mass nuclei . . . 38

4 TECHNICAL ASPECTS OF THE CALCULATIONS 43
4.1 Choice of the Skyrme parametrization . . . 43
4.2 Pairing strengths in the BCS framework . . . 46
4.2.1 Determining the neutron and proton pairing strengths . . . 46
4.2.2 Effect of pairing on fission-barrier heights . . . 50
4.3 Some numerical aspects . . . 52
4.3.1 Expansion of the single-particle wavefunctions on an axially symmetrical harmonic oscillator basis . . . 52
4.3.2 Optimization of basis parameters . . . 53
4.3.3 Numerical integration . . . 57
4.4 Locating the top of the barrier using the modified Broyden's method . . . 58
4.5 Implementation of the blocking procedure . . . 61

5 SPECTROSCOPIC PROPERTIES OF ODD-MASS ACTINIDES 62
5.1 Static moments in the ground state well . . . 62
5.2 Band-head spectra at the ground state deformation . . . 66
5.3 Spectroscopic properties in the isomeric well . . . 71
5.4 Effect of the neglected time-odd densities in the fit of the Skyrme forces . . . 76
5.5 Effect of time-reversal symmetry breaking on the ground-state band heads energy . . . 78

6 FISSION BARRIERS OF ACTINIDE NUCLEI 79
6.1 Even-even nuclei . . . 80
6.1.1 Results with a conserved parity symmetry . . . 80
6.1.2 Sensitivity of the fission-barrier heights of even-even nuclei to the moment of inertia . . . 84
6.2 Odd-mass nuclei . . . 87
6.2.1 HF+BCS results with a conserved parity symmetry . . . 87
6.2.2 Effect of neglected time-odd terms on the fission barriers . . . 92
6.2.3 HF+BCS results with parity symmetry breaking . . . 96
6.2.4 Fission-barrier heights within the Bohr-Mottelson unified model . . . 105
6.3 The specialization energy of odd-mass nucleus . . . 108
6.4 Connection with fission cross sections . . . 110
6.4.1 Comparison of barrier heights with empirical values and other calculations . . . 110
6.4.2 Transition states at the top of the inner-barrier . . . 113
6.4.3 Additional nuclear structure ingredients for fission transmission coefficients . . . 113

7 CONCLUSION & PERSPECTIVES 115

REFERENCES 119

A SKYRME PARAMETERS AND THE VARIOUS COUPLING CONSTANTS 128

B HF CALCULATIONS WITH ADJUSTMENT OF LINEAR CONSTRAINTS 130
B.1 Principle of the method . . . 130
B.2 Application to the constrained Hartree-Fock calculation . . . 131

C THE MOMENT OF INERTIA AND $\langle \hat{J}^2 \rangle$ TERM USING BELYAEV FORMULA 133

D ROTATIONAL ENERGY AS A FUNCTION OF ANGULAR VELOCITY 135

LIST OF TABLES

3.1 Rotational energy (given in MeV) calculated from Belyaev formula (IB) and the Intrinsic Vorticity Model (IVM) at the ground-state deformation as a function of the total angular momentum I_{av} with $I_{av}(I_{av}+1) = \langle \hat{J}^2 \rangle$. 37

3.2 Rotational energy (given in MeV) calculated from Belyaev formula (IB) and those using the moment of inertia deduced from R_{av} spin value at the ground-state deformation for ^{235}U and ^{239}Pu nuclei. The $1/2^+$ configuration in ^{235}U is not included for comparison due to the possible influence of the Coriolis coupling. 41

4.1 Calculated values of the odd-even mass difference $\Delta_q^{(3)}$ (in keV) with the SkM* parametrization for two pairs of pairing strengths (G_n, G_p) in comparison with experimental data (exp). The quoted values for the blocked state corresponds to the experimental I^π quantum numbers. 49

4.2 Root-mean-square energy deviation of the calculated $\Delta_q^{(3)}$ quantities (in keV) with corresponding data given in Table 4.1. These results are presented for three groups: considering the sets of nuclei for (I) neutron pairing only, (II) proton pairing only and (III) both proton and neutron pairing strengths. 49

4.3 Odd-even mass difference $\Delta_n^{(3)}$ obtained with the SLy5* interaction 50

4.4 The retained pairing strengths for the three considered Skryme parametrizations. 50

4.5 The inner-barrier heights E_A, isomeric energies E_{II} and second barrier heights E_B of ^{240}Pu assuming axial and parity symmetry obtained with the SkM* interaction with different BCS pairing strengths (G_n, G_p). 51

4.6 Comparison of the calculated band heads energies (in keV) at the ground state of ^{239}Pu with the SIII and SkM* interactions for a basis size defined by $N_0 = 14$ and $N_0 = 16$. 54

4.7 The inner-barrier E_A, fission-isomeric energy (E_{II} for even-even nucleus and E_{IS} for odd-mass nucleus) and outer-barrier E_B heights of ^{239,240}Pu with axial and parity symmetry in different basis sizes calculated with the SkM* interaction. The energies are given in MeV. 56

4.8 Similiar to Table 4.7 but for the barrier heights of the $5/2^+$ blocked configuration of ^{239}Pu obtained with the SLy5* interaction. 56

5.1 Calculated intrinsic charge quadrupole moment of even-even core nuclei 63

5.2 Calculated spectroscopic charge quadrupole moment of odd-mass nuclei 63

5.3 The calculated total magnetic moment μ_{tot} for ^{235}U, ^{239}Pu, ^{237}Np and ^{241}Am nuclei obtained with the different Skyrme parametrizations. 65

5.4 Excitation energies $\Delta E_{\alpha K\pi}$ without rotational correction of band-head states with respect to the lowest-energy solution in the ground-state well of ^{235}U, ^{239}Pu, ^{237}Np and ^{241}Am. . . . 68

5.5 Moment of inertia and the decoupling parameter of odd-neutron nuclei in the fission-isomeric well calculated with the three considered Skyrme parametrizations taken into account the Thouless-Valatin correction term. 75

5.6 The fission-isomeric energy E_{II} being the energy difference between the lowest-energy solutions at the fission-isomeric and the ground-state wells are given for three different cases with regards to the evaluation of the rotational correction. 75
5.7 The calculated intrinsic quadrupole moments in the isomeric well of ^{235}U and ^{239}Pu obtained with the three considered Skyrme parametrizations. 76
5.8 Ground state band heads energy of odd-neutron nuclei with the SkM* and the SIII parametrizations in the *full time-odd* scheme 77
5.9 Band heads energy of odd-neutron nuclei within the equal-filling approximation 78

6.1 The inner-barrier heights E_A, the fission-isomeric energy E_{II} and the outer-barrier height E_B of the neighbouring even-even nuclei obtained with the SkM*, the SLy5* and the SIII parametrizations assuming parity symmetry without and with the rotational correction. . . 85
6.2 The inner-barrier heights E_A, the fission-isomeric energy with respect to the same K^π ground-state solution E_{IS} and the outer-barrier height E_B of the odd-neutron nuclei obtained from HF+BCS calculations. 91
6.3 The fission-barrier heights calculated with the SkM* parametrization and evaluted within the Bohr-Mottelson unified model. 107
6.4 The specialization energies defined as the difference in the fission-barrier heights of the odd-mass nucleus with respect to the average values of the two neighouring even-mass nuclei is listed for the four blocked configurations of ^{239}Pu (in MeV). The results were obtained with the SkM* parametrization with a reduction factor of 50% for the rotational correction calculated using the Belyaev formula. 108
6.5 The inner and outer-barrier heights obtained from empirical data or from other calculations to be compared with the present results. 112
6.6 The inner and outer-barrier heights which have been either simultaneously fitted or fitted independent to one another to yield the best agreement to the neutron-induced fission cross-sections in the work of Ref. [19] 113

A.1 Values of the Skyrme parameters as a function of the Skyrme interaction. 129
A.2 The values of the coupling constants for each Skyrme interaction. 129

LIST OF FIGURES

2.1 Some samples of neutron induced fission cross-sections taken from the *Evaluated Nuclear Data File* [31] website for ^{232}Th, ^{234}U and ^{235}U. 6

2.2 Neutron-induced fission cross-sections of ^{232}Th from 0.5 MeV to 5.9 MeV taken from Ref. [33]. 7

2.3 A close-up of the neutron-induced fission cross-sections of ^{232}Th for incident neutron energy from 1 to 2.5 MeV taken from Ref. [33]. 8

2.4 This diagram extracted from Ref. [42] illustrate the calculation of the fission transmission coefficient for a four-humps barrier. The number of the barrier is denoted as h while the number of the well is denoted by w, whereby $w = 1$ refers to the ground-state well. $T_d(h,h')$ refers to the direct transmission coefficient from the h^{th}-hump to the h'^{th}-hump, while $T_a(w,w')$ refers to the absorption coefficient from the w^{th}-well to the w^{th}-well. . . . 12

2.5 Figure taken from Ref. [32]: Class I and class II states at the ground-state and fission-isomeric wells, respectively, together with the transition states at the top of the barriers. . 13

2.6 Five-dimensional shape parametrization used for the calculations of the potential-energy in the macroscopic-microscopic model. Figure extracted from Ref. [39]. 15

3.1 The single-particle states as a function of energy in ^{238,239}Pu to illustriate the lifting of the Kramers degeneracy of the single-particle states when the time-reversal symmetry is broken due to the presence of an odd numbers of neutron in ^{239}Pu. 22

4.1 The ground state neutron and proton single-particle spectra of ^{240}Pu obtained with the SIII and SkM* interactions in the default *minimal time-odd* scheme, while the SLy5* in the *full time-odd* scheme. The Fermi levels for each Skyrme interaction are indicated by the thick dashed lines. 45

4.2 Plot of the three point mass difference formula for a series of isotopes, calculated within the HFBCS approach using SkM* parametrization of the Skyrme force in basis size of $N_0 = 14$. 48

4.3 Similar to Fig. 4.2 but for a series of isotones. 48

4.4 Deformation energy curves (in MeV) of ^{240}Pu as a function of quadrupole moment (in barns) calculated with the SkM* interaction with different values of the BCS neutron pairing strength, G_n, as indicated on the figure. 51

4.5 Effect of basis size N_0 parameter on the deformation energy curve for the ^{252}Cf nucleus obtained with the SkM* parametrization. The plot is taken from the work of Ref. [60]. . . 55

4.6 Diagram extracted from Ref. [99] showing the location of local minima and maxima when using the modified Broyden's method 58

4.7 A portion of the deformation energy curve of ^{239}Pu calculated with a blocked $7/2^-$ state from the normally deformed ground state up to around the top of the inner-barrier to illustrate the location of the saddle point using Broyden's method. 60

5.1 Partial band-heads of ^{235}U and ^{239}Pu calculated with the SkM* and SIII interactions without rotational correction in the *minimal time-odd* scheme and the SLy5* in the *full time-odd* scheme with comparison to the experiments. 69
5.2 Partial band-heads of ^{237}Np and ^{241}Am calculated with the SkM* and SIII interactions without rotational correction in the *minimal time-odd* scheme while the SLy5* interaction in the *full time-odd* scheme with comparison to the experiments. 70
5.3 Band-head energy spectra of ^{239}Pu calculated with the SLy5*, SkM* and SIII parametrizations in the isomeric well with the inclusion of the rotational correction. 73
5.4 Band-head energy spectra of ^{235}U calculated with the SLy5*, SkM* and SIII parametrizations in the isomeric well, similar to Figure 5.3. The fission-isomeric energies have been calculated taking as reference the lowest-energy solution in the ground state deformation in which the K^{π} quantum numbers are given in parentheses for the respective Skyrme parametrizations. 74
5.5 Comparison of the ground state rotational band-head spectra for the two odd-neutron nuclei obtained with the SkM* and the SIII parametrizations in both the *minimal (default)* and *full time-odd* schemes. The moment of inertia and decoupling parameter are calculated in their respective *time-odd densities* scheme. 77

6.1 Deformation energy curves as a function of quadrupole moment of the neighbouring even-even nuclei calculated using the SkM* parametrization. The results obtained after taking into account the rotational correction are plotted in dashed lines. 81
6.2 Similar to Figure 6.1 for the SLy5* parametrization. 82
6.3 Similar to Figure 6.1 for the SIII parametrization 83
6.4 Rotational energy correction $E_{rot} = \frac{\hbar^2}{2\mathcal{I}}\langle \hat{J}^2 \rangle$ for the even-even neighbouring nuclei obtained with the SkM* and SLy5* parametrizations. The values of the moment of inertia $\mathcal{I}$ used for this plot were obtained from the calculations using the Belyaev formula. 84
6.5 Deformation energy curves starting from the ground-state up to beyond the second fission-barrier of the even-even neighbouring nuclei with the SkM* parametrization obtained with various approximation to the rotational correction. 86
6.6 Deformation energy curves (with the ground state energy taken as the reference) as a function of quadrupole moment Q_{20} (given in barns) of the different blocked configurations with K^{π} quantum numbers in ^{235}U obtained with the SkM* parametrization. 88
6.7 Similar to Figure 6.6 for ^{239}Pu nucleus obtained with the SkM* and the SLy5* parametrizations. 89
6.8 Deformation energy curves of the different blocked configurations with K^{π} quantum numbers in ^{235}U nucleus obtained with the SIII parametrization up to the fission-isomeric well. 90
6.9 Similar to Figure 6.8 for ^{239}Pu with the SIII parametrization. 91
6.10 The energy differences between various terms obtained from calculations in the default *minimal time-odd* scheme as opposed to the results obtained in the *full time-odd* scheme of ^{239}Pu with the SkM* parametrization. 94
6.11 Similar to Figure 6.10 but for the blocked configurations of ^{239}Pu with the SIII parametrization. 95
6.12 Deformation energy curves of ^{239}Pu as a function of deformation Q_{20} with parity symmetry breaking calculations obtained with the SkM* and the SLy5* parametrizations. 97
6.13 A cut in the potential energy surface around the top of the second barrier as a function of octupole moment Q_{30} (given in $barns^{3/2}$) of the 5/2 blocked configuration of ^{239}Pu obtained with the SkM* parametrization. 98

6.14 The hexadecapole moment Q_{40} as a function of Q_{20} in ^{239}Pu obtained with the SkM* and SLy5* parametrizations are plotted for solutions corresponding to a conserved and a broken parity symmetry. 99
6.15 Deformation energy curves of ^{235}U as a function of quadrupole moment obtained with the SkM* parametrization for the 1/2 blocked configuration for both parity symmetric and asymmetric solutions. 100
6.16 Deformation energy curves of ^{235}U as a function of quadrupole moment obtained with the SkM* parametrization for the 7/2 blocked configurations. The parity asymmetric solutions were obtained by blocking a single-particle state with $\Omega = 7/2$ nearest to the Fermi level at each deformation. 100
6.17 (Top): The evolution of the energies of the single particle states near the BCS chemical potential with $\Omega = 7/2$ quantum number as a function of quadrupole moment Q_{20} obtained in the parity asymmetric calculations of ^{235}U. (Bottom): The average parity of the blocked single-particle states as a function of deformation. 102
6.18 A portion of the deformation energy curves of the blocked $K = 7/2$ configurations in ^{235}U from the fission-isomeric well up to beyond the top of the second barrier. 103
6.19 Predicted effect of parity projection calculations on the outer-barrier of the 7/2 blocked configuration of ^{235}U 104
6.20 The deformation energy curves with a conserved parity symmetry of the considered plutonium isotopes within the Bohr-Mottelson unified model whereby the values of the rotational correction calculated using the Belyaev formula have been reduced by a factor 2. 106
6.21 The locations of the inner-barrier heights, fission-isomeric energy (for a fixed K^π) and the outer-barrier heights of the four considered K^π configurations of ^{239}Pu nucleus are plotted with respect to the deformation energy curves of the ^{238,240}Pu nuclei with a conserved parity symmetry and with the inclusion of rotational correction. 109
6.22 The discrete transition states at the top of the inner-barrier of ^{239}Pu with the SkM* parametrization shown as rotational bands build on top of the different band-heads, presented in the *Fission Experiments and Theoretical Advances Fission School and Workshop* (2014). . . . 114

D.1 Excitation energy of the rotational bands in ^{236}U and ^{240}Pu nuclei extracted from the calculations of Ref. [77] and compared to the experiments. 138

Chapter 1

INTRODUCTION

A scientist is not a person who has the right answers, but the one who asks the right questions.
- Claude Lévi-Strauss -

From the discovery of fission to fission barriers

Nuclear fission was first discovered by Hahn and Strassmann in 1939 and it immediately received much attention from both physicists and chemists alike since such a phenomena were unheard of at that time. Meitner and Frisch [1] coined the term fission to describe this phenomenon, whereby the nucleus is likened to a liquid drop which breaks into two smaller droplets. The existing semi-empirical mass formula (also known as the Bethe-Weizacker mass formula) was used to explain the fission process as a competition between the Coulomb repulsion and the surface tension of the nucleus. This idea was later on taken up and further developed by Bohr and Wheeler [2] for a more systematic description of fission. The liquid drop model was successful in describing the general trend of the nucleus as a function of deformation, i.e. the potential-energy landscape from the ground state up to the saddle point and then towards the scission point. Nevertheless, the model falls short of explaining many nuclear properties, for example why some nuclei have a deformed shape in their ground state, or the fact that the deformation energy of some heavy nuclei has a double peak. Improvement were later made by Strutinsky [3] in 1967 who proposed the incorporation of shell effects to the liquid drop model, giving rise to the microscopic-macroscopic model. In the 1970's, the theoretical study of nuclear structure takes on a new direction when calculations of global nuclear properties were performed from a microscopic view point via the Hartree-Fock (HF) method using an effective nucleon-nucleon interaction of the Skyrme type by Vautherin and Brink [4, 5]. This approach was then extended to large deformations by Flocard and collaborators using the constrained Hartree-Fock method [6] and was then applied to the study of the ^{240}Pu nucleus [7]. In recent years, many static calculations of the fission barriers have been performed microscopically based on the Skyrme [8, 9, 10], Gogny [11, 12, 13] and relativistic mean-field [14, 15, 16, 17] energy functionals. In all these approaches, one obtains the

total binding energies as a function of nuclear deformations (deformation energy surfaces) from which the fission-barrier heights can be deduced.

Although fission-barrier heights are not observable quantities, they are still important for many reasons. From a nuclear reaction point of view, the fission-barrier heights play an important role in determining whether the excited compound nucleus deexcites through neutron evaporation or fission. In order to facilitate the occurence of fission, the information on the fission-barrier height can assists in determining the amount of excitation energy needed in the compound nucleus for fission to occur by adjusting the energy of the incident projectile. On the other hand, fission barriers are an input for the calculations of fission cross-sections whereby the latter are directly comparable to the experimental data. In cases when the intended compound nucleus is hard to produce from nuclear reactions, the fission cross-sections for this nucleus can be predicted using fission barriers obtained from theoretical predictions.

From a different point of view, the fission barriers play a role in describing the stability of a nucleus from spontaneous fission. The stability of a nucleus with respect to spontaneous fission is related to its fission half-life, the calculation of which involves fission barriers. With recent technological advances, more and more exotic superheavy nuclei are being produced. For such unstable nuclei, the probability for fission increases and fission becomes an important decay mode to achieve nuclear stability in competition with α decay. In this case, a reliable estimate of the fission-barrier heights is all the more important [1] due to the short-lived nature of these nuclei.

In view of the wide application of fission barriers in nuclear reactions and nuclear energy as well as the understanding of spontaneuous fission, it is therefore important to improve on the theoretical approaches from which the fission barriers are obtained. While many fission-barrier calculations have been performed for even-mass (with even numbers of protons and neutrons) nuclei, there are comparatively very few microscopic studies dedicated to odd-mass nuclei. The main reason is the complication caused by the breaking of time-reversal symmetry at the mean-field level for a nuclear system composed of odd numbers of nucleons (fermions).

Mean-field calculations of fission barriers of odd-mass nuclei

One of the earlier microscopic study of odd-mass actinides at large deformation was performed by Libert and collaborators in Ref. [18] for the band-head energy spectra in the fission-isomeric well of ^{239}Pu within the rotor-plus-quasi-particle approach. More recently, fission-barrier calculations were performed within the Hartree-Fock-Bogoliubov approach by Goriely and collaborators [19] for nuclei between between $88 \leqslant Z \leqslant 96$ (Z here referring to the atomic number). The resulting fission barriers were then used

[1] As was pointed out in Ref. [29], a variation of 1 MeV in the fission-barrier heights will translate into a change of approximately four order of magnitudes in the fission half-life.

for the neutron-induced fission cross-section calculations as part of the RIPL-3 project published in Ref. [20]. At around the same time, Robledo and collaborators have performed fission-barrier calculations of ^{235}U nucleus [21] and ^{239}Pu nucleus [22] within the equal-filling approximation (EFA) presented in Ref. [23]. In practice, the EFA allows one to "break" the odd-nucleon (unpaired) into half and place one half in a specific single-particle states and the other half in the time-reversed state. In this way, the time-reversal symmetry is not broken and the calculations are performed as in the ground state of an even-even nucleus. However, in the Bohr and Mottelson picture the total angular momentum (total spin) of the odd-mass nucleus corresponds to the projection of the total angular momentum on the nuclear symmetry axis K of the blocked single-particle state, i.e. $I = K$.

Although the EFA was found to be a good approximation [24], a proper microscopic description of odd-mass nuclei requires the consideration of all the effects brought upon by the unpaired nucleon. This nucleon gives rise to non-vanishing time-odd densities entering the mean-field Hamiltonian. The terms involving time-odd densities vanish identically in the ground-state of even-even nuclei but increase the computing task for odd-mass nuclei. As discussed for e.g. in Refs. [25, 26], the time-odd densities cause a spin polarisation of the even-even core nucleus which results in the removal of the Kramers degeneracy of the single-particle states. Moreover, the recent work of Ref. [27] shows that the magnetic properties of deformed odd-mass nuclei can be properly described when taking into account the effect of core polarisation due to the breaking of the time-reversal symmetry in the mean-field level. Therefore, it is expected to be more appropriate to take into account the time-reversal symmetry breaking in the study of fission-barrier calculations.

In this work, the mean-field treatment of odd-mass nuclei is based on the Hartree-Fock-plus-BCS (HF+BCS) approach with self-consistent blocking (SCB). The nuclear part of the resulting energy-density functional is parametrized in the two-body density-dependent Skyrme form for the particle-hole channel and the seniority form for the particle-particle channel. The exchange terms induced by the Coulomb interaction are treated in the Slater approximation, and the one-body (dominant) contribution to the center-of-mass correction is taken into account. Axial symmetry is assumed throughout this work. The resulting mean-field solution then serves as the intrinsic state in the Bohr and Mottelson unified model in which the parity π and the projection of the total angular momentum of the blocked single-particle state on the nuclear symmetry axis K is assumed to correspond to the experimental I^π quantum numbers. The blocked configuration corresponding to given K^π quantum numbers is obtained by setting to 1 the occupation of the K^π single-particle state closest to Fermi level and to 0 the occupation of the conjugate state. It should be stressed that the SCB treatment for odd-mass nucleus has, in addition to treating properly the time-reversal symmetry breaking, the advantage that there is no ambiguity in defining the even-even core nucleus while also having a correct average nucleon number. This was not the case in the one-quasi-particle approach for e.g. in the earlier work of Ref. [28].

Research aim and objectives

As mentioned above, one of the quantity of interest from theoretical calculations which can be compared to experiment is the fission cross section. For odd-mass nuclei, one could expect different cross sections corresponding to the different I^π quantum numbers of the fissioning compound nuclei. In order to calculate the fission cross sections, one needs as one of the input, the fission-barrier heights. This work focuses only on the latter quantity in odd-mass nuclei, whereby the fission-barrier heights for various I^π quantum numbers of the fissioning nucleus are calculated from a self-consistent blocking procedure assuming $I = K$. While the SCB and the time-reversal symmetry breaking formalism have been developed a long time ago, there are by far no published results on the simultaneous application of both aspects to the calculation of fission barriers and energy spectra of odd-mass nuclei, to the best of our knowledge.

The purpose of this work is then to obtain new results with regards to the fission-barrier heights and energy spectra of odd-mass nuclei with the SCB approach in the HF+BCS framework and taking the time-reversal symmetry breaking at the mean-field level into account. The main objectives of this work are as follows:

- to calculate the deformation energy curves of odd-mass nuclei with various blocked K^π configurations from which the fission-barrier heights can be deduced
- to describe the energy spectra of odd-mass nuclei at various deformations, namely at the ground-state and fission-isomeric wells as well as the discrete transition states at the top of the barrier (no intrinsic parity breaking at the mean-field level).

In addition to the above, the fission-barrier heights for different blocked K^π configurations will also be compared to its neighbouring even-even nuclei. It is expected that the fission-barrier of odd-mass nuclei to be higher and wider than in even-even nuclei as a consequence of having to follow specific K^π quantum numbers along the fission path. The extra barrier energy of odd-mass nuclei referred to as the "specialization energy" has been proposed to explain the relatively longer fission half-life of odd-mass nuclei (in, e.g., Ref. [29]).

Roadmap of the thesis

Before presenting mean-field calculations of fission barriers, a discussion of neutron-induced fission cross sections will be presented in Chapter 2 to give an overview of where this work stands in the wider scope of induced-fission studies. Chapter 3 will be devoted to the theoretical framework of the work, in particular the self-consistent blocking procedure within the HF+BCS formalism as well as the description of the Bohr-Mottelson unified model. Some technical and numerical details will be given in Chapter 4. Then, the results will be presented in two separate chapters. Chapter 5 will be devoted to the spectroscopic properties in the ground-state and fission-isomeric wells of some selected odd-mass nuclei, whereas the results on the fission barriers will be presented in Chapter 6. Finally, conclusions and possible extensions of the work will be given in Chapter 7.

Chapter 2

FISSION CROSS-SECTIONS CALCULATIONS

2.1 Experimental study of the fission phenomenon

2.1.1 Fission as a nuclear reaction

There are several ways in which the fission phenomenon could be studied experimentally. One of them is decay through spontaneous fission which occurs for very heavy nuclei. Another way is through a nuclear reaction process whereby the target nucleus is bombarded by a projectile, supplying the target nucleus with enough energy to fission. Typical reactions include through particle-induced fission, in particular the (n,xnf) reaction where x is the number of emitted neutrons before the actual fission of the nucleus, and the photofission (γ,f) reaction which allows for the study of the sub-barrier excitation energy region. In the case when the intended compound-nucleus for which fission is to be studied is hard to be produced, the surrogate fission reactions such as (^{3}He,tf) reaction can be alternately employed (see for e.g. the review paper Ref. [30] about surrogate reactions). This chapter will focus on neutron-induced fission.

2.1.2 Structures in the (n,f) cross-sections

Figure 2.1 shows some examples of neutron-induced fission cross-sections for the ^{232}Th, ^{234}U and ^{235}U nuclei. The fission cross-section for the ^{232}Th nucleus shows that fission does not occur at very low incoming neutron energy. The total excitation energy of a heavy compound-nucleus is the sum of the total kinetic energy of the incident neutron E_n and the neutron separation energy of the resulting compound-nucleus $S_n(CN)$ such that

$$E^* = E_n + S_n(CN) \tag{2.1}$$

For low-energy neutron, the total energy of the ^{233}Th compound-nucleus is very much lower than its fission-barrier height and thus, does not result in fission. It is only when the compound-nucleus excitation energy is comparable to the height of the fission-barrier (the higher peak), i.e. around the fission threshold energy, that the fission process starts to be a viable decay mode. On the other hand, the neutron separation energy

of ^{235}U and ^{236}U compound-nuclei are comparatively higher than the corresponding value of ^{233}Th. In this case, the compound-nucleus excitation energy is already within the height of the fission barrier, even at very low neutron energy. Hence, the neutron-induced fission cross-sections for the two uranium isotopes are much higher than that of ^{232}Th at low neutron energy.

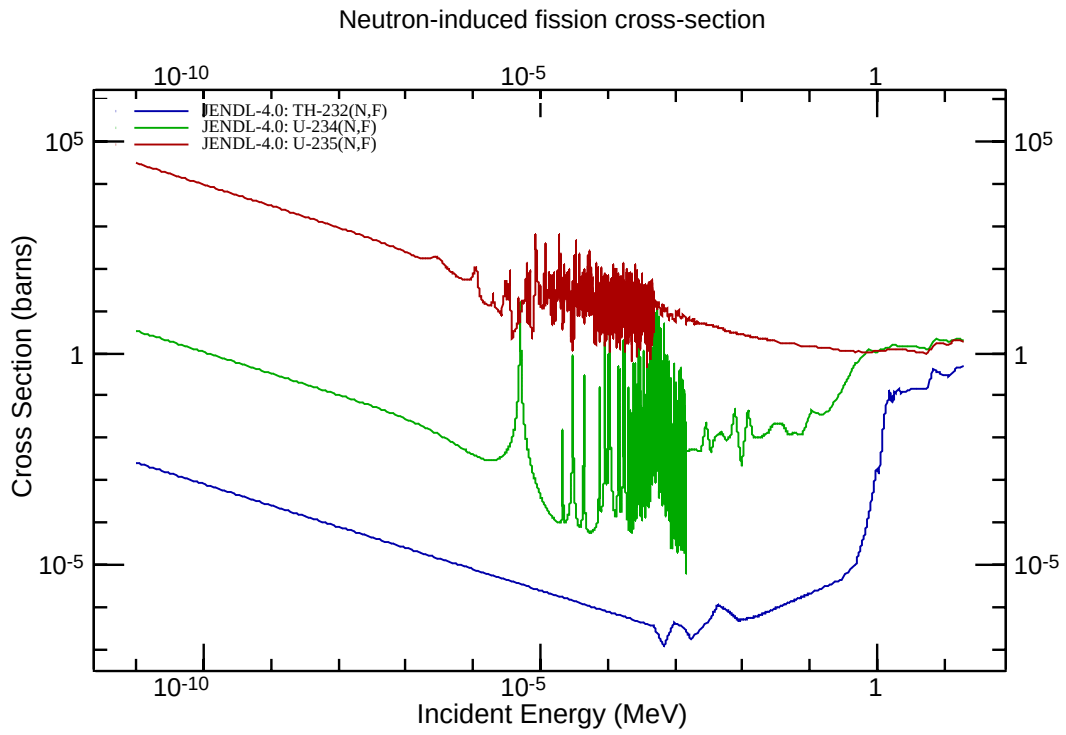

Figure 2.1: Some samples of neutron induced fission cross-sections taken from the *Evaluated Nuclear Data File* [31] website for ^{232}Th, ^{234}U and ^{235}U.

In the fission cross-sections of the uranium isotopes, the energy region from about 1 eV to about 1 keV is referred to as the resolved resonances region. In this energy region, the cross-sections are enhanced due to the existence of peaks in the nuclear level-density at well-defined energies. Above this energy region is the unresolved resonances region whereby the nuclear resonances are too close to each other that it could not be resolved properly by experiment. This gives rise to a smooth variation of the fission cross-sections as a function of increasing incident neutron energy. At even higher neutron energy of more than 0.1 MeV is the fast neutron region. In this energy region, there appears possibility of multi-chance fission. There are also other competing decay channels for the compound-nucleus. For example, one- or even two- neutron emissions are possible when the excitation energy of the compound-nucleus is higher than the corresponding threshold energies.

This work have considered odd-mass nuclei for the calculations of the fission barriers. These odd-mass compound-nuclei can be formed through neutron-induced reactions of its neighbouring even-mass nucleus as the target nucleus. In view of this, the energy region which is of interest is the energy region above the unresolved resonances, whereby the resulting compound-nucleus excitation energy is at least slightly higher than the height of the lower fission barrier. In this energy region one can consider that the so-called *statistical regime* of Ref. [32] is reached.

In order to show how the fission-barrier heights can be estimated from the neutron-induced fission cross-sections, the neutron-induced fission cross-sections for ^{232}Th for incident neutron energy from 0.5 to 5.9 MeV are shown in Figure 2.2 and a close-up of the fission cross-sections (in linear scale) from 1.0 to 2.5 MeV are shown in Figure 2.3. As was discussed in Ref. [33], the first change in the slope of the fission cross-sections appears around incident neutron energy of 1.1 MeV, suggesting that the first inner barrier height is about 5.9 MeV (the neutron separation energy for ^{233}Th is 4.78 MeV). A fission threshold energy at about 1.5 MeV incident neutron energy suggests an outer barrier height at about 6.3 MeV. These estimates of the fission-barrier heights require fission cross-sections modelling which will be briefly discussed in the next section.

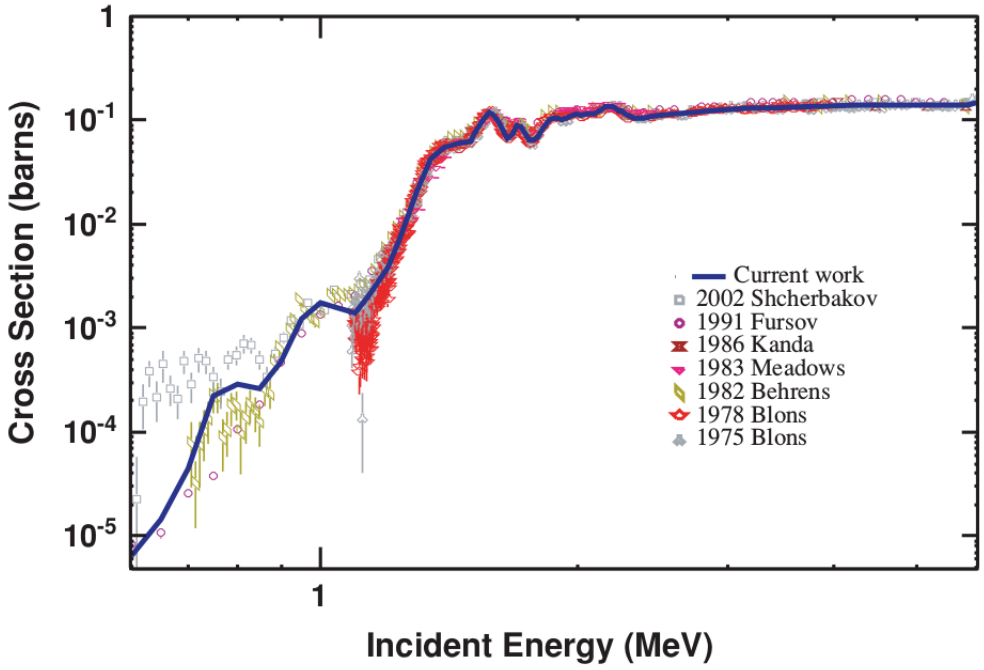

Figure 2.2: Neutron-induced fission cross-sections of ^{232}Th from 0.5 MeV to 5.9 MeV taken from Ref. [33].

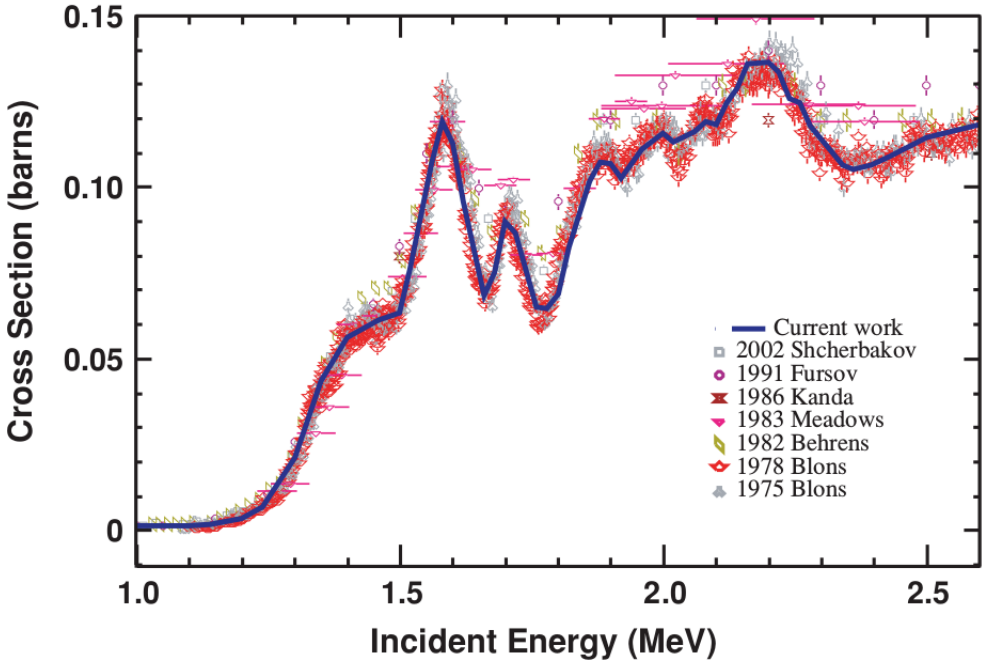

Figure 2.3: A close-up of the neutron-induced fission cross-sections of ^{232}Th for incident neutron energy from 1 to 2.5 MeV taken from Ref. [33].

2.2 Fission cross-section modeling

2.2.1 Fission reaction mechanism

The fission process is a many-body quantum mechanical process which involves the evolution of a nuclear system with strongly interacting nucleons over time. The phenomenon should in principal be described by solving exactly the Lippmann–Schwinger equation in the formal theory of nuclear reactions [34] for the nucleus (Z,N) whose many-body Hamiltonian is written, assuming a two-body nucleon-nucleon interaction $\hat{V}_{NN}$ as

$$\hat{H} = K_{intr} + \hat{V}_{NN} \tag{2.2}$$

where $\hat{K}_{intr}$ is the one-body-plus-two-body kinetic energy operator in the center-of-mass frame. This yields the full, interacting stationary reaction states from which one can deduce the T-matrix elements for the relevant entrance and exit channels and finally obtain the angular differential cross-section. This is a challenging task because all the nucleons participate to the fission dynamics and the corresponding reaction mechanism is a complicated process. To tackle this problem one has to approximate the solution to the Lippmann–Schwinger equation, which amounts to simplifying the reaction mechanism.

To do so we shall consider for a nuclear reaction only a *two-body arrangement channel* whereby the

particles participating in the reaction consists of two clusters of nucleons in bound states written as

$$x + A \longrightarrow y + B \tag{2.3}$$

where x, A are the clusters in the entrance channel (projectile and target nucleus) and y, B are those in the exit channel (the primary fission fragments in the fission channel). Each arrangement channel consisting of the two nuclei are characterized by some sets of quantum numbers for e.g. the total angular momentum with its projection on the $z-$ axis chosen to coincide with the fission direction, the spin and its projection on the $z-$ axis, as well as the parity quantum numbers, kinetic and intrinsic energies.

There are two extreme types of nuclear reaction mechanisms, namely the direct mechanism and the compound-nucleus mechanism. In the former only a few nucleons or excitation modes are involved, whereas many nucleons and transitory configurations participate in the latter. The major difference between both mechanisms is the time taken for the reaction to occur. The direct reaction occurs within a very short time interval, typically about 10^{-22} s, which allows for very few nucleon-nucleon collisions. The pickup (d, p) and stripping (p, d) reactions are examples of direct reactions.

In contrast, the compound-nucleus reaction occurs within a time generally between 10^{-19} s and 10^{-16} s which is relatively long on the nuclear time scale. The projectile shares its energy with the other nucleons through many nucleon-nucleon collisions, thus leading to a thermal equilibrium in the compound-nucleus. This mechanism happens when the projectile has a relatively low kinetic energy, typically a few MeV, and the target is a heavy nucleus. As this is precisely the energy range considered here for the incident neutron on an actinide target, the discussion will focus on this mechanism only.

In the compound-nucleus mechanism, we can rewrite the nuclear reaction shown above as

$$x + A \longrightarrow C^* \longrightarrow y + B \tag{2.4}$$

to reflect the formation of a compound-nucleus C^* before it decays through one of the many possible exit channels. The highly excited compound-nucleus can de-excite either through particle emissions or fission. Since the compound-nucleus exists for a relatively long time, it seems reasonable to postulate that the decay of this compound-nucleus should not depend on the formation of the compound-nucleus. This is reflected by the Bohr's independence hypothesis which states that *the formation and the decay of the compound-nucleus are independent of each other*.

As a consequence of this hypothesis, the nuclear reaction cross-section with the entrance channel e and the exit channel e' can be written as

$$\sigma_{ee'} = \sum_{J^\pi} \sigma_{ee'}^{J^\pi} = \sum_{J^\pi} \sigma_e^{J^\pi}(E_e)\, P_{e'}^{J^\pi}(E_{e'}) \tag{2.5}$$

where $\sigma_e^{J^\pi}(E_e)$ is the compound-nucleus formation cross-section at a given incident energy E_e and $P_{e'}^{J^\pi}(E_{e'})$ is the decay probability of the compound-nucleus with energy $E_{e'}$. The decay process, in this way, depends only on the total angular momentum J, parity π, excitation energy (in the center of mass frame), atomic and mass number of the compound-nucleus. Owing to the microreversibility principle the decay probability $P_{e'}^{J^\pi}(E_{e'})$ is related to the compound-nucleus formation cross-section from channel e through

$$P_{e'}^{J^\pi}(E_{e'}) = \frac{k_{e'}^2 \sigma_{e'}^{J^\pi}(E_{e'})}{\sum_{e''} k_{e''}^2 \sigma_{e''}^{J^\pi}(E_{e'})} \tag{2.6}$$

where k_e is the wave number associated with the relative kinetic energy E_e in the channel e such that

$$E_e = \frac{(\hbar k_e)^2}{2\mu_e}\,, \tag{2.7}$$

with μ_e the reduced mass of the two clusters in the channel e. The partial cross-section $\sigma_{ee'}^{J^\pi}$ is thus determined solely in terms of the compound-nucleus formation cross-sections in all channels.

Because of the numerous excited configurations of the compound-nucleus, the scattering matrix elements which enter the formal expression of the cross-section are strongly fluctuating (compound-nucleus resonance) as a function of the compound-nucleus excitation energy. The experimentally observed cross section is thus a quantity averaged over energy intervals which are large with respect to the typical spacing between overlaping compound-nucleus resonances, but small when compared to the experimental energy resolution. The resulting compound-nucleus formation cross section can thus be expressed as

$$\sigma_e^{J^\pi}(E_e) = \frac{\pi}{k_e^2}(2J+1)\, T_e^{J^\pi}(E_e) \tag{2.8}$$

where T_e is defined in terms of the energy-averaged scattering matrix elements and is called transmission coefficient in the channel e. The reaction cross-section (equation 2.5) can therefore be expressed purely in terms of transmission coefficients: this corresponds to the Hauser–Feshbach statistical model [35].

In the case of neutron-induced fission, the entrance channel is that of the incoming neutron particle and the target nucleus while the exit channel consists of the pair of fission fragments after scission. This exit channel is in competition with other decay channels, whereby the probability for fission P_f is given as

$$P_f^{J^\pi} = \frac{T_f^{J^\pi}}{T_f^{J^\pi} + \sum_d T_d^{J^\pi}} \tag{2.9}$$

with $T_f^{J^\pi}$ being the fission transmission coefficient for given angular momentum J and parity π of the compound-nucleus. The summation in the denominator is over other decay channels.

In all rigor, the decay of the compound-nucleus from a given initial state is a many-body, time-dependent

quantum mechanical problem. This difficult problem can be approximately solved by reducing it to a one-body, time-dependent problem within an adiabatic approach in which the collective and intrinsic degrees of freedom can be decoupled. This has been performed for example in Refs. [36, 37] in the framework of the time-dependent generator coordinate method with the gaussian overlap approximation. The collective motion of the nucleus is assumed to be described by a few collective variables which are the relevant shape degrees of freedom, and the intrinsic structure of the nucleus including pairing is treated using a self-consistent microscopic model. One is led to solve a Schrödinger equation with the Hamiltonian

$$\hat{H}|\Phi\rangle = i\hbar \frac{d|\Phi\rangle}{dt} \tag{2.10}$$

where in the deformation coordinate representation [37]

$$\hat{H} = -\frac{\hbar^2}{2} \sum_{i,j} \frac{\partial}{\partial q_i} B_{ij}(\{q_k\}) \frac{\partial}{\partial q_j} + V(\{q_k\}) \tag{2.11}$$

with $\{q_k\}$ being a set of collective degrees of freedom, which are the expectation values of the corresponding multipole moment operators $\hat{Q}_k$ in $|\Phi\rangle$. The kinetic term involves deformation-dependent inertia parameters B_{ij} while $V(\{q_k\})$ is the binding energy as a function of nuclear deformations with the inclusion of the the so-called zero-point-energy correction. In the calculations with axial symmetry before scission point, the quadrupole q_{20} and octupole q_{30} moments are usually chosen as the relevant shape degrees of freedom. When approaching scission, q_{40} becomes necessary to identify various valleys in the potential-energy surface (PES). In this way, the study of static nuclear properties as a function of deformation is required (see Section 2.3). Such an approach allows for the description of the evolution of the compound nucleus from a given initial state towards fission in a completely quantum-mechanical manner. From the knowledge of the nuclear state as a function of time one can then in principle compute the fission transmission coefficient $T_f^{J^\pi}$.

Even in the approximation made in the previous paragraph the computation of $T_f^{J^\pi}$ is challenging. In state-of-the-art fission cross-section modeling one has recourse to the so-called optical model for fission to calculate $T_f^{J^\pi}$.

2.2.2 Optical model for fission

When the wave function describing the collective variables is well localized in the deformation space at all times, one can simplify the problem into the time-evolution of the nucleus along a trajectory in the deformation space. Fission can then be viewed as a quantum tunnelling process through a potential barrier which corresponds to a one-dimensional fission path on a multi-dimensional potential-energy surface. Using the stationary-state formalism one can thus calculate fission-barrier penetrability, which is nothing else but the above introduced fission transmission coefficient. The actual fission path can be approximated by the least-action path [38] or the minimum-energy path as in the adiabatic approximation often considered. From the corresponding deformation-energy curve, one can deduce the fission-barrier heights. This has been done for instance in the macroscopic-microscopic approach in Ref. [39], and microscopic approaches using the

Skyrme and Gogny energy-density functionals [36, 37, 40, 41]. A further approximation of the fission path is often made by projecting the actual path onto the driving-coordinate axis, namely elongation. In practice, in microscopic approaches one chooses the quadrupole moment Q_{20} as the driving coordinate.

For nuclei in the actinide region, the fission barriers are known to have two humps. In this case, fission is viewed as a two-step process whereby the incoming waves representing the compound-nucleus are first transmitted across the first (inner) barrier. When encountering the inner barrier, a portion of the incident waves can be reflected back in the ground-state well, while the rest is transmitted through the barrier. From the transmitted flux a fraction can be absorbed into the second well whereby the wave then attempts to tunnel through the outer barrier leading to fission. A one-step fission process is valid only in cases when the excitation energy is too low or too high as compared to the fission-barrier heights. In these cases one can assume that there is no absorption in the second well (the so-called *no-damping* limit) and that the incident wave tunnels through the double-hump fission-barrier and exit beyond the outer saddle point [42].

The calculations of the fission transmission coefficient over a multi-humped barrier taking into account the incident-wave reflection by each barrier and the partial absorption of waves into each well have been performed in Ref. [42]. Figure 2.4, extracted from Ref. [42], illustrates the direct transmission and absorption coefficients in the calculation of the fission transmission coefficient for a four-humps barrier. The possibility for a partial absorption and reflection of the incident wave in the calculations of the fission transmission coefficient is important when the excitation energy of the compound-nucleus is lower than the heights of both the inner and outer barriers. At this excitation energy, the coupling between class I and class II states, which are energy levels dominantly located in the ground-state and fission-isomeric wells, respectively, (see Figure 2.5 in the double-hump case) brings a substantial impact on T_f.

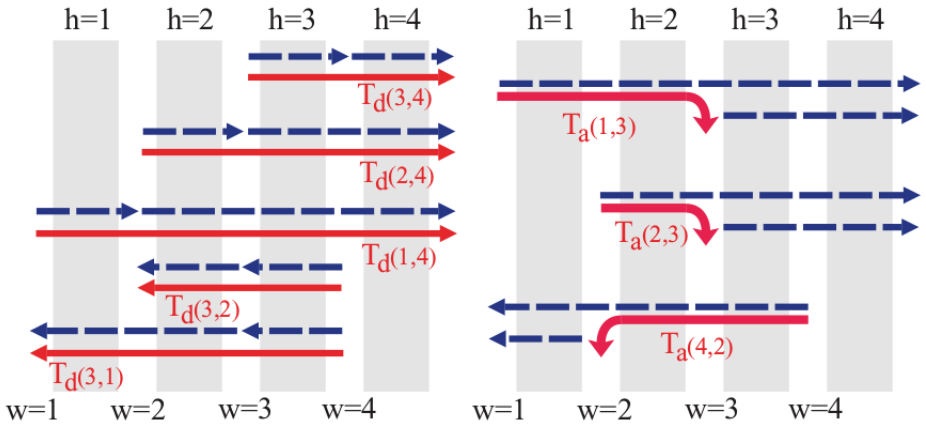

Figure 2.4: This diagram extracted from Ref. [42] illustrate the calculation of the fission transmission coefficient for a four-humps barrier. The number of the barrier is denoted as h while the number of the well is denoted by w, whereby $w = 1$ refers to the ground-state well. $T_d(h,h')$ refers to the direct transmission coefficient from the h^{th}-hump to the h'^{th}-hump, while $T_a(w,w')$ refers to the absorption coefficient from the w^{th}-well to the w^{th}-well.

When the excitation energy of the compound-nucleus is higher than the lower of the two barriers (in the *statistical regime*), one can assume that all the incoming waves impinging on the inner barrier is fully absorbed into the second well. In this *full-damping* limit [42], the fission transmission coefficient T_f is given by

$$T_f^{J^\pi} = \frac{T_A(E,J^\pi)\,T_B(E,J^\pi)}{T_A(E,J^\pi)+T_B(E,J^\pi)} \tag{2.12}$$

where $T_A(E,J^\pi)$ and $T_B(E,J^\pi)$ are the transmission coefficient through the inner and outer barrier, respectively.

The transmission coefficient across a barrier for specific J^π quantum numbers is the sum of the barrier penetrabilities of all the transition states at the top of the barrier (see Figure 2.5) having the same J^π quantum numbers.

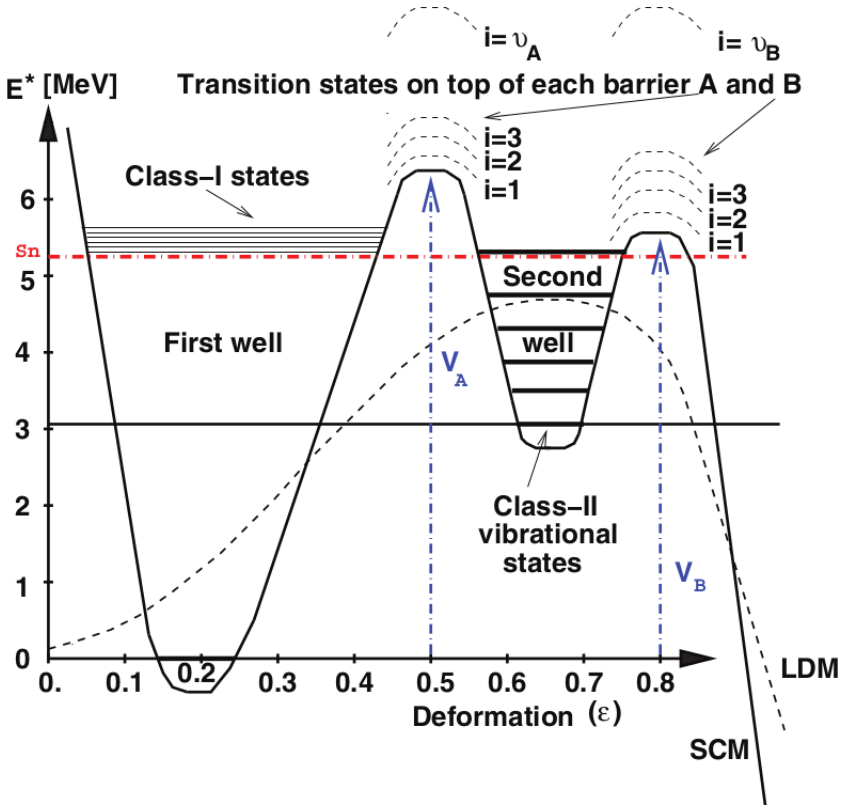

Figure 2.5: Figure taken from Ref. [32]: Class I and class II states at the ground-state and fission-isomeric wells, respectively, together with the transition states at the top of the barriers.

The transition states above barriers can be separated into discrete states and continuum states. The transmission coefficients for these transition states were calculated in Ref. [19] using the expression

$$T_j(E,J^\pi) = \sum_d \mathscr{P}_j(E,V_{jd}^{J^\pi}) + \int_{E_d}^{E^*_{max}} \mathscr{P}(E,V_j^{J^\pi}(\varepsilon))\,\rho(\varepsilon,J,\pi)d\varepsilon \tag{2.13}$$

where the index $j = A$ and B refers to the inner and outer barrier, respectively. The sum is taken over all

discrete transition states with the same J^π quantum numbers[1] as the decaying compound-nucleus with their barrier heights given by $V_{j_d}^{J^\pi}$. In the continuum region where the nuclear levels are very close to one another, the summation of the discrete states is replaced by an integration involving the level-density ρ over an energy range with an associated barrier height denoted by $V_j^{J^\pi}(\varepsilon)$, starting from the energy below which it is appropriate to consider the discrete part of the transition states, to a maximum energy E^*_{max} defined as $E^*_{max} = E^* + B_f$ in Ref. [43] where E^* is the compound-nucleus excitation energy and B_f is the lowest-energy fission-barrier height.

The barrier penetrabilities should in principal be obtained from integrating over the fission-barrier curve as a function of the one dimensional fission path along the multi-dimensional potential-energy surface, with the expression for $\mathscr{P}(E, V_{j_d}^{J^\pi})$ given within the Wentzel—Kramers—Brillouin (WKB) approximation [38] as

$$\mathscr{P}_j(E, V_{j_d}^{J^\pi}) \;=\; \frac{1}{1 + \exp(2\,K_j^{(d)})} \tag{2.14}$$

where

$$K_j^{(d)} \;=\; \pm \int_{a_j}^{b_j} \Big[\frac{2\,B_{eff}(s)}{\hbar^2}\Big(E - V_{j_d}^{J^\pi}(s)\Big)\Big]^{1/2} ds \tag{2.15}$$

is the action integral, and B_{eff} is the effective nuclear inertia along the fission path and s is the curve linear abscissa along this path. The boundaries a_j and b_j refer to the intercepting points of the fission path with the constant energy E. The negative sign in the integral is taken when the excitation energy E^* is higher than the barrier height and conversely, the positive sign is taken when E^* is lower than the barrier height. In the former case, the WKB approximation is valid for an energy which is at least slightly higher than the top of the barrier [19, 33].

The calculation of the barrier penetrabilities can be simplified even further by assuming the double-humped barrier as consisting of two independent inverted parabolas. In this case, the penetrability through each single barrier is given by the exact Hill-Wheeler expression

$$\mathscr{P}_j^{HW}(E, V_{j_d}^{J^\pi}) \;=\; \Big[1 + \exp\Big(2\pi \frac{V_{j_d}^{J^\pi} - E}{\hbar\,\omega_{j_d}^{J^\pi}}\Big)\Big]^{-1} \quad , \tag{2.16}$$

where the curvature of the parabolic barrier is driven by the quantity $\hbar\omega_j^{J^\pi}$.

2.3 Nuclear structure input

2.3.1 Potential-energy surface

As was discussed in the previous section, fission cross-section calculations require nuclear-structure input. One of such information is related to the potential-energy surface which is the binding energy as a

[1] In practice, the summation is usually taken for the discrete transition states with the projection of the total angular momentum on intrinsic symmetry axis, K, quantum number having the same J quantum number as the compound-nucleus.

function of deformation. There are two main approaches in which one can calculate the potential-energy surface. One can follow, as done in the present work, a fully microscopic approach by implementing a self-consistent mean-field model. The coordinates for the potential-energy surface usually considered in the mean-field approach are the quadrupole, octupole and hexadecapole moments. The quadrupole moment describes the elongation of the nucleus as it goes towards fission. When a heavy nucleus becomes more and more elongated, there may appear a situation in which a pear-shaped nucleus is more energetically favored. This shape degree of freedom is described by the octupole moment. The hexadecapole moment, on the other hand, provides an indication of the formation of a neck as one approaches the scission point. Another approach which is more phenomenological, relies on the liquid drop model with shell corrections and including pairing. This is the so-called macroscopic-microscopic model in which the potential-energy surface is parametrized for example in terms of five-dimensional shape degrees of freedom (see, e.g., [39, 44]) illustrated in Figure 2.6.

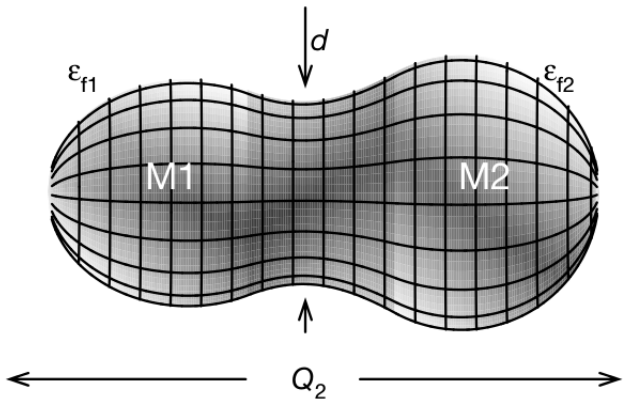

Figure 2.6: Five-dimensional shape parametrization used for the calculations of the potential-energy in the macroscopic-microscopic model. Figure extracted from Ref. [39].

2.3.2 Nuclear spectra

Another important piece of information for the fission cross-section calculations is related to the energy spectra at the ground-state deformation (class I states), in the fission-isomeric well (class II states) and at the saddle points where the corresponding states are called transition states. This information can be provided by microscopic calculations. For an odd-mass nucleus, the low-lying discrete states in the class I and class II states as well as the discrete transition states can be obtained using for e.g. the quasi-particle approach of Ref. [28], or through self-consistent blocking calculations (as performed herein). One can then

build rotational and vibrational bands on top of the nuclear band heads as a mean to obtain the low-lying discrete states.

At higher excitation energy, even below the neutron emission threshold, the nuclear states are so narrowly spaced that one can consider a continuum of states characterized by a nuclear level-density, instead of discrete states. The nuclear level-density calculations have been usually performed using analytical-Fermi-gas type formulas (for e.g. Refs. [45, 46]). On the other hand, when moving away from experimentally known regions, a more reliable and physically sound microscopic approach is preferred. Global microscopic models of the nuclear level densities have been developed and refined over the years. The combinatorial approach (see for e.g. Refs. [47, 48]) is one of such example, and it has been applied to the calculations of the neutron-induced fission cross-section calculations in Ref. [19].

2.3.3 Inertia parameters

As discussed in the previous section, the calculations of barrier penetrabilities require the evaluation of the effective inertia parameter (also known as *mass parameter* in some references) B_{eff} in equation (2.15). A microscopic determination of this quantity allows one to take into account its deformation dependence. According to Ref. [38], the expression for the effective inertia parameter is

$$B_{eff}(s) \;=\; \sum_{i,j} B_{ij}(\{q_k\})\,\frac{dq_i}{ds}\,\frac{dq_j}{ds} \tag{2.17}$$

where at first order perturbation theory

$$B_{ij} \;=\; 2\hbar^2 \sum_{m} \frac{\langle 0|\frac{\partial}{\partial q_i}|m\rangle\,\langle m|\frac{\partial}{\partial q_j}|0\rangle}{E_0 + E_m} \tag{2.18}$$

where $|0\rangle$ and $|m\rangle$ denote ground and excited states of a nucleus with corresponding energies E_0 and E_m.

Because of the complexity of the calculation of B_{eff}, this quantity is approximated by the empirical expression

$$B_{eff} \;\approx\; 0.054\,A^{5/3}\,\mathrm{MeV}^{-1} \tag{2.19}$$

which depends only on the mass number A, based on a fit procedure to the spontaneous fission half-lives of some superheavy nuclei [49] in the work of Refs. [19, 33] where the fission path is projected on the Q_{20} axis.

Chapter 3

THEORETICAL FRAMEWORK

This chapter is devoted to the theoretical models employed in this study. It is not meant to be an exhaustive review, but a rather brief discussion on the major topics that are related to the present work. It is divided into five main sections as follows. A major portion is devoted to Section 3.1 focusing on the Hartree-Fock method supplemented with a presentation of the Skyrme effective nucleon-nucleon interaction. The pairing correlations, described within the Bardeen-Cooper-Schrieffer (BCS) method will be discussed in Section 3.2. One of the correction to the mean-field approach comes from the breaking of the translational invariance due to the fact that the mean-field wave-function is not of a plane-wave type. This results in an approximate correction to the center-of-mass motion which will be treated in Section 3.3. The last section, 3.4, will be devoted to the derivation of equations relating the intrinsic mean-field solution to the lab frame solution within the collective Bohr-Mottelson unified model. Such an approach is meant to translate the mean-field calculation results obtained in the intrinsic state onto laboratory frame quantities before comparing the results to any experimental data when available.

3.1 The mean-field approach

3.1.1 The Skyrme approximation to the effective nucleon-nucleon interaction

The effective internucleon interactions entering the many-body Hamiltonian consist of two parts. There is the strong nuclear force which binds nucleons together, and the repulsive Coulomb force which acts between protons. The strong nuclear force part of the effective interaction is hereby approximated with a phenomenological two-body density-dependent Skyrme interaction [50] of the form:

$$V(\mathbf{r}_1,\mathbf{r}_2) = V_c(\mathbf{r}_1,\mathbf{r}_2) + V_{DD}(\mathbf{r}_1,\mathbf{r}_2) + V_{s.o}(\mathbf{r}_1,\mathbf{r}_2) \tag{3.1}$$

whereby the central V_c, density-dependent V_{DD} (to approximate the in medium effects in an effective way), and the spin-orbit $V_{s.o}$ contributions have the following expressions:

$$\begin{aligned} V_c(\mathbf{r}_1,\mathbf{r}_2) &= t_0(1+x_0P_\sigma)\delta(\mathbf{r}_1-\mathbf{r}_2) \\ &+\frac{1}{2}(t_1+x_1P_\sigma)[\delta(\mathbf{r}_1-\mathbf{r}_2)\mathbf{k}^2+\mathbf{k}^{\dagger 2}\delta(\mathbf{r}_1-\mathbf{r}_2)] \\ &+t_2(1+x_2P_\sigma)\mathbf{k}^\dagger\delta(\vec{\mathbf{r}_1}-\vec{\mathbf{r}_2})\mathbf{k} \end{aligned} \tag{3.2}$$

$$V_{DD}(\mathbf{r}_1,\mathbf{r}_2) = \frac{1}{6}t_3(1+x_3P_\sigma)\rho^\alpha\delta(\vec{\mathbf{r}_1}-\vec{\mathbf{r}_2}) \tag{3.3}$$

$$V_{s.o}(\mathbf{r}_1,\mathbf{r}_2) = iW_0(\sigma^{(1)}+\sigma^{(2)})\cdot\mathbf{k}^\dagger\times\delta(\vec{\mathbf{r}_1}-\vec{\mathbf{r}_2})\mathbf{k} \tag{3.4}$$

In the above equation, the notation ρ and $P_\sigma = \frac{1}{2}[1+\vec{\sigma}_1\cdot\vec{\sigma}_2]$ refers to the density and the spin-exchange operator respectively while $\mathbf{k}^\dagger$ is the conjugate of the momentum operator, $\mathbf{k}$, of the form:

$$\mathbf{k} = \frac{1}{2i}\left(\vec{\nabla}_1-\vec{\nabla}_2\right) \tag{3.5}$$

The symbols t_i, x_i with $i=1,2,3$ and W_0 are parameters whose values were obtained from a fit to some set of experimental nuclear data.

3.1.2 The Hamiltonian density in the case of time-reversal symmetry breaking

By employing the effective internucleon interaction of the Skyrme type, the total energy of the nucleus, E, being an expectation value of the Hamiltonian operator in the normalized Slater determinant $|\Psi_{HF}\rangle$ can be written as an integral of a Hamiltonian density, $\mathscr{H}$, such that:

$$\begin{aligned} E = \langle\Psi_{HF}|\hat{H}|\Psi_{HF}\rangle &= \int \mathscr{H}(\mathbf{r})\,d\mathbf{r} \\ &= \int \left(\mathscr{H}_{kin}(\mathbf{r})+\mathscr{H}_c(\mathbf{r})+\mathscr{H}_{DD}(\mathbf{r})+\mathscr{H}_{s.o}(\mathbf{r})+\mathscr{H}_{Coul}(\mathbf{r})\right)d\mathbf{r} \end{aligned} \tag{3.6}$$

The Hamiltonian densities namely $\mathscr{H}_{kin}$, $\mathscr{H}_c$, $\mathscr{H}_{DD}$, $\mathscr{H}_{s.o}$ and $\mathscr{H}_{Coul}(\mathbf{r})$ are the kinetic energy, central, density-dependent, spin-orbit and Coulomb energy density contributions respectively, with the following expressions [51, 52]:

$$\mathscr{H}_{kin}(\mathbf{r}) = \left(1-\frac{1}{A}\right)\frac{\hbar^2}{2m}\tau \tag{3.7}$$

$$\begin{aligned} \mathscr{H}_c(\mathbf{r}) &= B_1\rho^2+B_{10}\mathbf{s}^2+B_3(\rho\tau-\mathbf{j}^2)+B_{14}(\overleftrightarrow{J}^2-\mathbf{s}\cdot\mathbf{T})+B_5\rho\triangle\rho \\ &+B_{18}\mathbf{s}\cdot\triangle\mathbf{s}+\sum_q\{B_2\rho_q^2+B_{11}\mathbf{s}_q^2+B_4(\rho_q\tau_q-\mathbf{j}_q^2) \\ &+B_{15}\left(\overleftrightarrow{J}_q^{\,2}-\mathbf{s}_q\cdot\mathbf{T}_q\right)\}+B_6\rho_q\triangle\rho_q+B_{19}\mathbf{s}_q\cdot\triangle\mathbf{s}_q \end{aligned} \tag{3.8}$$

$$\tag{3.9}$$

$$\mathscr{H}_{DD}(\mathbf{r}) = \rho^{\alpha}\Big[B_7\rho^2 + B_{12}\mathbf{s}^2 + \sum_q (B_8\rho_q^2 + B_{13}\mathbf{s}_q^2)\Big] \tag{3.10}$$

$$\mathscr{H}_{s.o}(\mathbf{r}) = B_9\Big[\rho\nabla\cdot\mathbf{J} + \mathbf{j}\cdot\nabla\times\mathbf{s} + \sum_q \big(\rho_q\nabla\cdot\mathbf{J}_q + \mathbf{j}_q\cdot\nabla\times\mathbf{s}_q\big)\Big] \tag{3.11}$$

$$\mathscr{H}_{Coul}(\mathbf{r}) \approx \frac{1}{2}\rho_p(\mathbf{r})V_{CD}(\mathbf{r}) - \frac{3}{4}e^2\Big(\frac{3}{\pi}\Big)^{\frac{1}{3}}\rho_p^{\frac{4}{3}}(\mathbf{r}) \tag{3.12}$$

The factor $(1-\frac{1}{A})$ appearing in the kinetic energy density is a corrective term introduced to approximately eliminate the center-of-mass motion spuriously introduced by the breaking of the translational invariance inherent to the mean-field approach. A more detailed discussion on this corrective term will be made in Section 3.3.

The Coulomb energy density consists of two terms whereby the direct term is given as the first term on the r.h.s of equation (3.12) with

$$V_{CD} = e^2\int d\mathbf{r}'\,\frac{\rho_p(\mathbf{r}')}{||\mathbf{r}-\mathbf{r}'||} \tag{3.13}$$

Further discussion on the calculation of the direct Coulomb term can be found for e.g. in Ref. [5, 53, 54]. The exchange part given by the second term of equation (3.12) has been approximated here as usually done, with a Slater approximation [55]. The effect of using such an approximation as opposed to performing rather time-consuming exact Coulomb exchange calculations have been previously investigated (see Ref. [56, 57, 58]). It has been found that the appropriateness of the Slater approximation is directly proportional to the proton single-particle level density near the Fermi level, being less good for a spherical (close shell) nucleus as compared to a well deformed nucleus. More importantly and of interest to the present study is that the Slater approximation was found to underestimate the first fission-barrier by 0.31 MeV and the fission-isomer energy by 0.28 MeV in ^{238}U upon using the SkM* parametrization of the Skyrme interaction, when compared to calculations incorporating exact Coulomb exchange terms [58]. This effect will be taken into account later when comparing the present results with the experimentally derived fission-barrier heights.

All the above Hamiltonian densities are time-even functionals of the local densities that are further categorized into time-even and time-odd densities with respect to the action of the time-reversal operator. The time-even densities are the particle density $\rho(\mathbf{r})$, the kinetic energy density $\tau(\mathbf{r})$ and the spin-current density $J_{\mu\nu}(\mathbf{r})$ of the following form [51, 52]:

$$\rho(\mathbf{r}) = \sum_k v_k^2[\phi_k]^{\dagger}(\mathbf{r})[\phi_k](\mathbf{r}) \tag{3.14}$$

$$\tau(\mathbf{r}) = \sum_k v_k^2\Big(\nabla[\phi_k]^{\dagger}(\mathbf{r})\Big)\cdot\nabla[\phi_k](\mathbf{r}) \tag{3.15}$$

$$J_{\mu\nu}(\mathbf{r}) = \frac{1}{2i}\sum_k v_k^2\Big\{[\phi_k]^{\dagger}(\mathbf{r})\sigma_\nu\nabla_\mu[\phi_k](\mathbf{r}) - \Big(\nabla_\mu[\phi_k]^{\dagger}(\mathbf{r})\Big)\sigma_\nu[\phi_k](\mathbf{r})\Big\} \tag{3.16}$$

For each of the time-even densities, there exists a time-odd counterpart, namely the spin density $\mathbf{s}(\mathbf{r})$, the spin kinetic density, $\mathbf{T}_\mu(\mathbf{r})$ and the current density $\mathbf{j}(\mathbf{r})$ [51, 52]:

$$\mathbf{s}(\mathbf{r}) = \sum_k v_k^2 [\phi_k]^\dagger(\mathbf{r}) \sigma [\phi_k](\mathbf{r}) \tag{3.17}$$

$$\mathbf{T}_\mu(\mathbf{r}) = \sum_k v_k^2 \Big(\nabla [\phi_k]^\dagger(\mathbf{r}) \Big) \cdot \sigma_\mu \nabla [\phi_k](\mathbf{r}) \tag{3.18}$$

$$\mathbf{j}(\mathbf{r}) = \frac{1}{2i} \sum_k v_k^2 \Big\{ \Big(\nabla [\phi_k]^\dagger(\mathbf{r}) \Big) [\phi_k](\mathbf{r}) - [\phi_k]^\dagger(\mathbf{r}) \nabla [\phi_k](\mathbf{r}) \Big\} \tag{3.19}$$

These densities are time-odd only by construction and are non-vanishing in cases where the time-reversal symmetry is broken. They contribute to the single-particle Hamiltonian in such a way that the expectation value of the energy is a time-even quantity as it should. For the corresponding mean-field Hamiltonian (as explicited in Eq. 3.21 below), one will observe when the solution is not even under time-reversal, a lifting of the Kramers degeneracy of its eigenvalues. Such situations occur, for instance, in the case of odd-mass nuclei and even-mass nuclei with odd numbers of both protons and neutrons, as well as in the case of rotating nuclei treated semi-quantally within the so-called Routhian approach. Figure 3.1 shows a comparison of the single-particle energy levels in ^{239}Pu exhibiting the lifting of the Kramers degeneracy with the degenerate case corresponding to the ^{238}Pu nucleus.

The notation v_k^2 entering the expressions of the local densities refers to the partial occupation probablity of the single-particle states due to pairing correlations which are described within the Bardeen-Cooper-Schrieffer (BCS) approach discussed in a later section. The coupling constants B_i are given in terms of the parameters t_i, x_i and W_0 from the phenomenological Skyrme interaction. The values of the interaction parameters together with the resulting coupling constants which depend on the type of Skyrme forces in use are listed in Appendix A.

3.1.3 The Hartree-Fock equations

The Hartree-Fock equations are obtained by varying the total energy given in equation (3.6) with respect to the single-particle wavefunctions ϕ_k.

$$\frac{\delta}{\delta\phi_j(\mathbf{r})}\left(E[\phi_k] \;-\; \sum_{k,\tau,\sigma} e_k \int d\mathbf{r}\,|\phi_k(\mathbf{r})|^2\right) \;=\; 0 \tag{3.20}$$

to obtain the one-body Hamiltonian $\hat{h}_{HF}$ of the following form in coordinate representation [51, 52]:

$$\begin{aligned}\langle\mathbf{r}|\hat{h}^{(q)}_{HF}|\phi_k\rangle = &-\nabla\cdot\Big(\frac{\hbar^2}{2m^*_q(\mathbf{r})}\nabla[\phi_k](\mathbf{r})\Big)+\Big(U_q(\mathbf{r})+\delta_{qp}U_{Coul}(\mathbf{r})\Big)[\phi_k](\mathbf{r})\\ &+i\mathbf{W}_q(\mathbf{r})\cdot\Big(\sigma\times\nabla[\phi_k](\mathbf{r})\Big)-i\sum_{\mu,\nu}\Big\{\Big(W^{(J)}_{q,\mu\nu}(\mathbf{r})\sigma_\nu\nabla_\mu[\phi_k](\mathbf{r})\Big)\\ &+\nabla_\mu\Big(W^{(J)}_{q,\mu\nu}(\mathbf{r})\sigma_\nu[\phi_k](\mathbf{r})\Big)\Big\}-\frac{i}{2}\Big\{\mathbf{A}_q(\mathbf{r})\cdot\nabla[\phi_k](\mathbf{r})+\nabla\cdot\Big(\mathbf{A}_q[\phi_k](\mathbf{r})\Big)\Big\}\\ &+\mathbf{S}_q(\mathbf{r})\cdot\sigma[\phi_k](\mathbf{r})-\nabla\cdot\Big(\big(\mathbf{C}_q(\mathbf{r})\cdot\sigma\big)\nabla[\phi_k](\mathbf{r})\Big)\end{aligned} \tag{3.21}$$

The time-even fields m^*, U_q, U_{Coul}, $\mathbf{W}_q$ and $W^{(J)}_{q,\mu\nu}$ are the effective mass, the central-plus-density-dependent field, the Coulomb field, the spin-orbit field and the spin-current field respectively. The notation q labels the nuclear charge state, with $q = n$ referring to neutron and $q = p$ for proton charge state. These time-even fields are complemented by the time-odd fields; $\mathbf{S}_q$, $\mathbf{A}_q$ and $\mathbf{C}_q$ which vanish in the cases when there exists a time-reversal symmetry for e.g. in the case of a nucleus with an even number of protons and neutrons (see e.g. Ref. [5]).

These fields are given as follows [51, 52] in terms of the various densities by:

$$\frac{\hbar^2}{2m^*_q} = \frac{\hbar^2}{2m_q} + B_3\rho + B_4\rho_q \tag{3.22}$$

$$\begin{aligned}U_q = &\,2\big(B_1\rho+B_2\rho_n\big)+B_3\tau+B_4\tau_q+2\big(B_5\Delta\rho+B_6\Delta\rho_q\big)+(2+\alpha)B_7\rho^{1+\alpha}\\ &+B_8\big(\alpha\rho^{(\alpha-1)}\big(\rho_n^2+\rho_p^2\big)+2\rho^\alpha\rho_q\big)+B_9\big(\nabla\cdot\mathbf{J}+\nabla\cdot\mathbf{J_q}\big)\\ &+\alpha\rho^{\alpha-1}\big(B_{12}\mathbf{s}^2+B_{13}\big(\mathbf{s}_n+\mathbf{s}_p^2\big)\big)\end{aligned} \tag{3.23}$$

$$U_{Coul} = V_{dir} - e^2\,\big(\frac{3}{\pi}\rho_p\big)^{1/3} \tag{3.24}$$

$$\mathbf{W}_q = \,-B_9\big(\nabla\rho+\nabla\rho_q\big) \tag{3.25}$$

$$W_{q,\mu\nu} = B_{14}J_{\mu\nu}+B_{15}J_{q,\mu\nu} \tag{3.26}$$

$$\mathbf{S}_q = 2\big(B_{10}+B_{12}\rho^{\alpha}\big)\mathbf{s}+2\big(B_{11}+B_{13}\rho^{\alpha}\big)\mathbf{s}_q - B_9\nabla\times\big(\mathbf{j}+\mathbf{j}_q\big) - B_{14}\mathbf{T} - B_{15}\mathbf{T}_q + 2\big(B_{18}\Delta s + B_{19}\Delta s_q\big) \tag{3.27}$$

$$\mathbf{A}_q = -2\big(B_3\,\mathbf{j}+B_4\,\mathbf{j}_q\big)+B_9\nabla\times\big(\mathbf{s}+\mathbf{s}_q\big) \tag{3.28}$$

$$\mathbf{C}_q = -\Big(B_{14}\,\mathbf{s}+B_{15}\,\mathbf{s}_q\Big) \tag{3.29}$$

The local densities for each charge state q are shown explicitly, while the sum of the local density for both charge state is given without any indices (e.g. $\rho = \rho_n + \rho_p$).

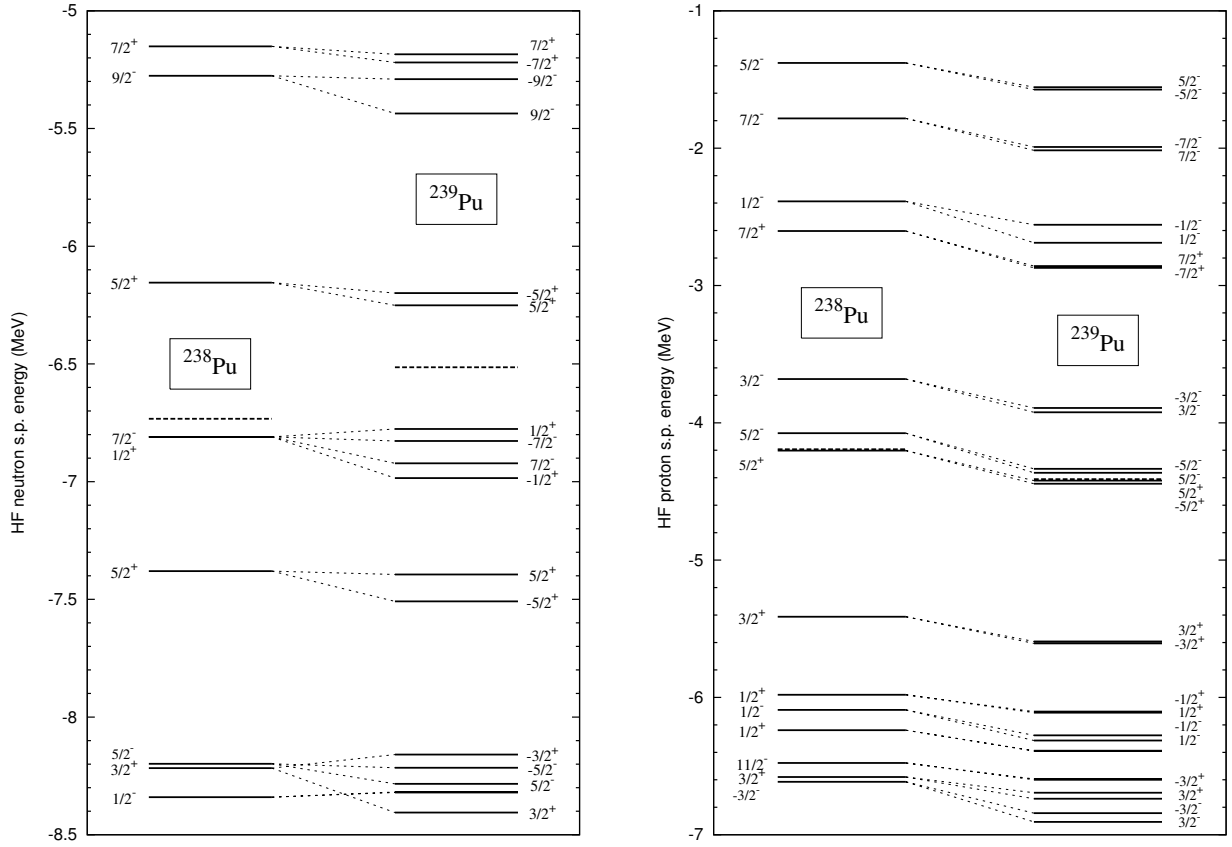

Neutron single-particle spectra Proton single-particle spectra

Figure 3.1: The single-particle states as a function of energy in ^{238,239}Pu to illustriate the lifting of the Kramers degeneracy of the single-particle states when the time-reversal symmetry is broken due to the presence of an odd numbers of neutron in ^{239}Pu.

3.1.4 Self-consistent blocking calculation (SCB)

For the description of odd-mass nuclei, only seniority-one states have been considered whereby the *seniority* quantum number [59] refers to the number of unpaired nucleons, i.e which thus do not participate in the

pairing treatment. The ground state of an even-even nucleus is a *seniority*-0 state, with subsequent excited states of seniority 2,4,6,...,etc. The projection Ω_k of the total angular momentum onto the axial symmetry $z-$axis, $\hat{J}_z$, of the single-particle state $|k\rangle$

$$\langle k|\hat{J}_z|k\rangle = \Omega_k \tag{3.30}$$

and its parity π_k are assumed to be good quantum numbers. In general, the lowest nuclear K^π state corresponds to an unpaired nucleon blocked in the single-particle state which is the nearest to the Fermi level with $\Omega_k^\pi = K^\pi$. The single-particle states in the Ω^π blocks are sorted as a function of an increasing energies and is labelled by *rank*. The *rank* of the single-particle state reflects the number of single-particle states with the desired Ω^π quantum numbers. In practice, the single-particle state nearest to the Fermi level is systematically chosen to be populated by the last unpaired nucleon. The Fermi energy e_F in this case is defined as the average energy of the last occupied single-particle state and the next unoccupied state, given by

$$e_F \;=\; \frac{1}{2}(e_{N_q} + e_{(N_q+1)}) \tag{3.31}$$

where N_q is the total number of nucleons of a given charge state q. In so-called *self-consistent blocking* (SCB) calculations, the occupation probability v_k^2 of this chosen blocked state is then set to 1 at each step of the iterative process.

Having decided which single-particle state is to be blocked, one then needs to define a pair conjugate state which is indeed its time-reversed state when the time-reversal symmetry is preserved. Denoting such a true time-reversed state by $|\overline{\phi}^{(k)}_{K,\pi}\rangle$, such that:

$$|\overline{\phi}^{(k)}_{K,\pi}\rangle = \hat{T}|\phi^{(k)}_{K,\pi}\rangle \equiv |\phi^{(k)}_{-K,\pi}\rangle \tag{3.32}$$

The action of the time-reversal operator $\hat{T}$ on the single-particle state yields a change in the sign of the K quantum number. In the case where the time-reversal symmetry is broken, the Kramers degeneracy is lifted. One does not have thus a straightforward correspondence to define $(K,-K)$ partner states. In this work, a pair partner of the $|\phi^{(k)}_{K,\pi}\rangle$ state is considered within the eigen-solutions of the mean-field Hamiltonian denoted as $|\tilde{\phi}^{(k)}_{K,\pi}\rangle$. It is to be distinguished from the previous partner state $|\overline{\phi}^{(k)}_{K,\pi}\rangle$ which is not an eigen-solution of the mean-field Hamiltonian.

In practice, the pair partner state is selected by calculating the overlap $\chi^{(k)}_{K,\pi}$ between two eigenstates $|\phi^{(k)}_{K,\pi}\rangle$ and $|\tilde{\phi}^{(k)}_{-K,\pi}\rangle$, such that:

$$\chi^{(k)}_{K,\pi} = \langle\phi_{K,\pi}|\left(\hat{T}|\tilde{\phi}_{-K,\pi}\rangle\right) \tag{3.33}$$

These partner states $|\phi^{(k)}_{K,\pi}\rangle$ and $|\tilde{\phi}^{(k)}_{-K,\pi}\rangle$ form a so-called *pseudo-pair*. The value of this overlap would be exactly 1 when time-reversal symmetry is observed. As a fact assessed by actual calculations the breaking of the time-reversal symmetry modifies slightly the wave function $|\tilde{\phi}^{(k)}_{-K,\pi}\rangle$ as compared with $|\overline{\phi}^{(k)}_{K,\pi}\rangle$. Thus, if the above value of $|\chi^{(k)}_{K,\pi}|^2$ is close to 1 when the time-reversal symmetry is broken, it can be safely as-

sumed that this state originates from the same Kramers degenerate pair as $|\phi^{(k)}_{K,\pi}\rangle$. However, there may *a priori* exist several single-particle states with the same K and π quantum numbers within some small energy range. In order to define the pseudo-pairs in such a case, the partner state of $|\phi^{(k)}_{K,\pi}\rangle$ is assigned to be the state with the largest overlap value of $|\chi^{(k)}_{K,\pi}|^2$.

3.1.5 Self-consistent symmetries

In performing any mean-field calculation, one has to define a variational space in which the lowest energy solution is searched. By using the most general variational space, one would in principal obtain the exact variational solution. However, this would require unavailable computing resources and makes such a study impossible. One is thus compelled to perform the variation in a truncated ensemble. A further restriction arises when one imposes a certain number of symmetry conditions reducing the variational ensemble whether these conditions are of physical or numerical origins.

If one have a many-body Hamiltonian which possesses a certain symmetry represented here by the symmetry operator $\hat{S}$, then by definition, these two operators will commute:

$$[\hat{H}, \hat{S}] = 0 \tag{3.34}$$

Then if one starts from a mean-field solution $\hat{\rho}$ which also possess this symmetry, the corresponding one-body reduction of the many-body Hamiltonian (e.g. the Hartree-Fock Hamiltonian $\hat{h}[\hat{\rho}]$) also possesses this symmetry

$$[\hat{h}[\rho], \hat{S}] = 0 \tag{3.35}$$

In that way, the solutions to $\hat{h}[\hat{\rho}]$ will also be symmetric under the action of $\hat{S}$. Due to the self-consistent procedure, one finds that by starting from a mean-field solution which obeys certain symmetries as mentioned above, this set of symmetries will be conserved in the rest of the self-consistent iterative process. These symmetries are then referred to as the self-consistent symmetries [59].

3.1.6 Constrained Hartree-Fock

Solving the Hartree-Fock secular equation as it is would yield the nuclear properties at a local extremum, in practice a local minimum, for instance describing the nuclear ground state. In order to obtain information at a specific nuclear deformation $\langle\hat{Q}_{lm}\rangle$, an external field may be included to a constrained Hamiltonian introducing some Lagrange multiplier λ. As discussed in Ref. [6] one may equivalently consider the variation quantity written as:

$$\hat{H}' = H + f(\mu_l, \langle\hat{Q}_{lm}\rangle) \tag{3.36}$$

for instance with quadratic constraint [6]

$$f(\mu_l, \langle \hat{Q}_{lm} \rangle) = \frac{1}{2} C_l (\langle \hat{Q}_{lm} \rangle - \mu_l)^2 \tag{3.37}$$

where C_l is a curvature parameter and μ_l is the center of a parabolic shape which is adjusted in order to obtain the desired value for the expectation value of the operator $\hat{Q}_{lm}$:

$$\langle \hat{Q}_{lm} \rangle = \int d\mathbf{r}\, \rho(\mathbf{r})\, q_l(\mathbf{r}) \tag{3.38}$$

Applying the variational procedure with the above constrained Hamiltonian, one would have

$$\frac{\delta}{\delta \phi_j(\mathbf{r})} \left(E[\phi_k] \, + \, f(\mu_l, \langle \hat{Q}_{lm} \rangle) - \sum_{k,\tau,\sigma} e_k \int d\mathbf{r}\, |\phi_k(\mathbf{r})|^2 \right) = 0 \tag{3.39}$$

whereby the variation of the external constraint with respect to the single-particle state would be written as:

$$\frac{\delta}{\delta \phi_j(\mathbf{r})} f(\mu_l, \langle \hat{Q}_{lm} \rangle) \, = \, C_l \, (\langle \hat{Q}_{lm} \rangle - \mu_l) \, \frac{\delta \langle \hat{Q}_{lm} \rangle}{\delta \phi_j(\mathbf{r})} \tag{3.40}$$

with

$$\frac{\delta \langle \hat{Q}_{lm} \rangle}{\delta \phi_j(\mathbf{r})} = \frac{\delta}{\delta \phi_j(\mathbf{r})} \Big(\int d\mathbf{r} \sum_k \phi_k(\mathbf{r})\, \phi_k^*(\mathbf{r})\, Q_{lm}(\mathbf{r}) \Big) \, = \, \phi_j^*(\mathbf{r})\, q_l(\mathbf{r}) \tag{3.41}$$

The Hamiltonian density is then modified to include this constraint and is written as:

$$\mathscr{H}'(\mathbf{r}) \, = \, \mathscr{H}(\mathbf{r}) \, + \, C_l \, (\langle \hat{Q}_{lm} \rangle - \mu_l)\, Q_{lm}(\mathbf{r})\, \rho(\mathbf{r}) \tag{3.42}$$

yielding a constraint in the Hartree-Fock mean-field given by:

$$\hat{V}_{constr} \, = \, C_l \, (\langle \hat{Q}_{lm} \rangle - \mu_l)\, q_l(\mathbf{r}) \tag{3.43}$$

Starting from an axially symmetric shape for the ground state, the leading multipole moment to be considered as the nucleus undergoes fission is the quadrupole moment corresponding to $Q_{20}(\mathbf{r}) = 2z^2 - r^2$ (with $r = x^2 + y^2$) so that

$$Q_{20} \, = \, \langle \hat{Q}_{20} \rangle \, = \, \int d\mathbf{r}\, \rho(\mathbf{r}) (2z^2 - r^2) \tag{3.44}$$

Around the top of the inner-barrier of actinide nuclei, the nucleus is unstable with respect to triaxial shape. The non-axial quadrupole deformation is defined as the expectation value of the $\hat{Q}_{22}$ operator corresponding to $Q_{22}(\mathbf{r}) = x^2 - y^2$ so that

$$Q_{22} \, = \, \langle \hat{Q}_{22} \rangle \, = \, \int d\mathbf{r}\, \rho(\mathbf{r}) (x^2 - y^2) \tag{3.45}$$

Although the breaking of the axial symmetry plays a role in decreasing slightly the inner-barrier height, this will not be considered in the present study. The reduction in the inner-barrier height would instead be taken from a previous study [60] and is estimated to be about 0.5 MeV for instance in the three actinide nuclei

(^{234,236}U and ^{240}Pu) using the SkM* parametrization of the Skyrme interaction.

Another constraint of interest would be the hexadecapole moment corresponding to $Q_{40}(\mathbf{r}) = r^4\, Y_4^0(\theta,\varphi)$ so that:

$$Q_{40} \;=\; \langle \hat{Q}_{40} \rangle \;=\; \int d\mathbf{r}\, \rho(\mathbf{r})\, r^4\, Y_4^0(\theta,\varphi) \tag{3.46}$$

In the case when the constrained Hartree-Fock calculation is performed with a constraint only on the quadrupole moment, the fission path may be slightly different, away from stationary points, from the *true* fission valley (see the discussion of Ref. [6]). However, this is of minimal consequence as the focus of this study is placed on the height of the barriers.

Moving away from the superdeformed isomeric well and towards the outer-barrier, the nucleus is known to explore left-right asymmetric shapes. This extra degree of freedom lowers coincidentally the second fission-barrier height. For that purpose, one should consider non-vanishing octupole moments corresponding to $Q_{30}(\mathbf{r}) = r^3\, Y_3^0(\theta,\varphi)$ so that

$$Q_{30} \;=\; \langle \hat{Q}_{30} \rangle \;=\; \int d\mathbf{r}\, \rho(\mathbf{r})\, r^3\, Y_3^0(\theta,\varphi) \tag{3.47}$$

This symmetry breaking entails a significant complication of the numerical calculations. When performing calculations with a conserved intrinsic parity symmetry the integration over the $z-$ coordinates may be simplified by considering merely

$$2\int_0^\infty f(r,z)\, dz \tag{3.48}$$

due to the condition that $f(r,z) = f(r,-z)$. This no longer holds of course when the parity symmetry is broken. In this case, the integration must be performed over the full $z-$ space

$$\int_{-\infty}^{\infty} f(r,z)\, dz \tag{3.49}$$

In practice, parity breaking calculations of the fission-barrier are performed by constraining the quadrupole moment to some relevant value, while leaving the octupole moment unconstrained so as to obtain the most energetically favored solution in the Q_{30} direction. One should then, of course, guarantee that the center-of-mass of the solution is fixed at the origin point $\langle z \rangle = 0$ to preserve a consistent meaning for the calculated multipole moments.

In addition to the commonly used quadratic constraint, a procedure has been developed employing an automatic readjustment of linear constraints so as to converge at the desired deformation points. The derivation of the readjustment of the linear constraints is detailed in the Appendix B and only the main point shall be highlighted here.

When using a linear constraint, the one-body Hartree-Fock Hamiltonian can be written as:

$$\hat{h}'_{HF} = \hat{h}_{HF} - \sum_l \lambda_l \hat{q}_l \tag{3.50}$$

where λ_l are Lagrange multipliers. The readjustment of the constraints is made such that at each of the n^{th} iteration of the Hartree-Fock process, the λ_l value is adjusted by a small amount of $d\lambda_l^{(n)}$ so that the Hamiltonian to be diagonalized in the next iteration would be

$$\hat{h}_{HF}^{(n+1)} = \hat{h}_{HF}^{(n)} - \sum_l \left(\lambda_l^{(n)} + d\lambda_l^{(n)}\right)\hat{q}_l \tag{3.51}$$

with

$$d\lambda_l^{(n)} = \sum_j \left(\chi^{-1}\right)_{lj} \cdot \left(Q_{lm} - \langle\Phi_0^{(n)}|\hat{Q}_{lm}|\Phi_0^{(n)}\rangle\right) \tag{3.52}$$

where Q_{lm} is the desired deformation point.

3.2 Treatment of pairing correlation

The most important ground-state correlations to be considered beyond the Skyrme Hartree-Fock mean-field scheme are due to the pairing part of the residual interaction. The wavefunction in the HF approximation is a Slater determinant which is good for the description of a doubly magic nuclei, whereby the occupation factors of the single particle states is $v_k^2 \in \{0,1\}$. However, for non-magic nuclei which have a high single-particle level density at the Fermi surface, the residual interaction will allow for a partial population of these single-particle states in the many-body ground state so that the occupation factors of the single particle states should no longer correspond to empty or occupied states.

In such cases, the treatment of pairing correlation comes into play. The description of pairing beyond the mean field scheme is usually carried out using the Bardeen-Cooper-Schrieffer (BCS) approximation [61]. The BCS ansatz is an approximation to the Hartree-Fock-Bogoliubov (HFB) approximation. On the other hand, the manner in which the Skyrme forces are usually fitted does not enable such an approach with it and therefore a different interaction is often needed to treat adequately pairing correlations (see e.g. the discussion of Ref. [62]).

The BCS pairing treatment in nuclei via the BCS method is usually restricted to the $|T_z = 1|$ (neutron-neutron and proton-proton) isospin channel. Such a restriction is justifiable in view of the current scope of the study which focuses on heavy nuclei in the stability valley or close to it. This is due to the fact that the pairing between neutrons and protons which contributes to both the T=1 and T=0 channel has a significant impact only for nuclei with about equal numbers of protons and neutrons. Among the many single-particle states available for pairing, the states near the Fermi level are the ones to contribute the most. However, for stable or not too unstable heavy nuclei with much more neutrons than protons, the wave functions of the occupied single-particle states of both charge states near the Fermi level may be very different in structure. Coupled with the fact that the pairing interaction is a short-range interaction which could be approximated by a delta contact interaction

$$\hat{V}_p(\mathbf{r},\mathbf{r'}) \approx \delta(\mathbf{r}-\mathbf{r'}) \tag{3.53}$$

the overlap of the two differing single-particle charge states in that case would be very small, thus yielding vanishing neutron-proton pairing correlations in such heavy nuclei.

3.2.1 The BCS approximation

The ground state of an even-even nucleus (namely even with respect to the number of protons and neutrons) is written using the second quantization notation as:

$$|BCS\rangle = \prod_{\Omega_k>0} \left(u_k + v_k a_k^+ a_{\bar{k}}^+\right)|0\rangle \tag{3.54}$$

where u_k and $v_k \in \Re$, a_k^+ and $a_{\bar{k}}^+$ are the particle creation operators in the state k and its time-conjugate state, $\bar{k}$ respectively, while the null vector $|0\rangle$ denotes the particle vacuum state. The occupation probablility of the state k is given by v_k^2 while its non-occupation probability is given by u_k^2 such that $v_k^2 + u_k^2 = 1$.

Using a restricted Bogoliubov canonical transformation known as the Bogoliubov-Valatin transformation, one could transform the description of a system of paired-interacting particles in terms of a state of non-interacting quasi-particles where the relations between the particle and quasi-particle creation operators are given as

$$\alpha_k^\dagger = u_k a_k^\dagger - v_k a_{\bar{k}} \tag{3.55}$$

$$\alpha_{\bar{k}}^\dagger = u_k a_{\bar{k}}^\dagger + v_k a_k \tag{3.56}$$

with the following phase convention:

$$u_{\bar{k}} = u_k > 0 \text{ and } \mathrm{v_{\bar{k}}} = -\mathrm{v_k} < 0 \tag{3.57}$$

for $\Omega_k > 0$.

A blocked BCS wave function for odd-mass nuclei is defined in the following way. One adds to a BCS state representing the even-even core, a specific single-particle state denoted here by the index i, such that

$$|BCS^{(i)}\rangle = a_i^\dagger |BCS^{(core)}\rangle = a_i^\dagger \prod_{\substack{k\neq i \\ \Omega_k>0}} \left(u_k + v_k a_k^+ a_{\tilde{k}}^+\right)|0\rangle \tag{3.58}$$

In this case, one defines quasi-pairs (k and $\tilde{k}$) as defined in Section 3.1.4 where one of the quasi-pair partners is no longer the time-reversed state of the other. The single-particle state i will always be occupied ($v_i^2 = 1$) while its quasi-pair partner $\tilde{i}$ state will be always empty ($u_{\tilde{i}}^2 = 0$). Owing to the Pauli principle, the quasi-pairs to which the blocked state belongs would not participate in the scattering of the quasi-pair excitations due to the pairing residual interaction. This would in effect reduce the number of available quasi-pair states, and thus, lowering the effective single-particle level density near Fermi surface. As a consequence, one have a quenching of pairing due to the blocking procedure. For a nucleus with high enough single-particle level density, the BCS pairing treatment for a valence space which is reduced by one quasi-pair is of little consequence. A problem would occur for the case when the blocking procedure is applied to a situation where we have a weak-pairing regime characterized by

$$\tilde{g}|G| \ll 1 \tag{3.59}$$

with G representing a typical pairing matrix element and $\tilde{g}$ denoting the average single-particle level density near the Fermi surface. Then the quenching of the pairing correlations would be unduly strong.

As a way to circumvent the potential problem due to the inappropriateness of the BCS pairing treatment

in the case of low single-particle level density near the Fermi level, one could consider a different pairing treatment called the Highly Truncated Diagonalization approach (HTDA) [63]. This alternative pairing treatment is akin to the shell model -like calculations which has the essential benefit in that this method conserves the particle number as opposed to the BCS approach (the violation of which is known to cause the inadequacy of the BCS approximation in the low pairing correlation regime).

Since the BCS wave function given in equation (3.54) clearly mixes Slater determinants corresponding to different particle numbers, one makes use, as discussed e.g. in Ref. [64], of a Lagrange multiplier, λ (also referred to as the BCS chemical potential), to constrain the particle number on the average, whereby the particle number operator is given as

$$\hat{N} = \sum_{\mu} a_{\mu}^{+} a_{\mu} \tag{3.60}$$

For an odd-mass nucleus with N_{total} particles, our blocked BCS wave function is thus constrained to have a particle number equal to N_{total}. Denoting by N_{even} the particle number of its neighbouring $N-1$ (even-even) nucleus, one has thus

$$\langle BCS^{(i)}|\hat{N}|BCS^{(i)}\rangle \;=\; N_{total} \;=\; N_{even}+1 \tag{3.61}$$

with $\langle BCS^{(core)}|\hat{N}|BCS^{(core)}\rangle = N_{even}$. The even-even core $|BCS^{(core)}\rangle$ defined in equation (3.58) to be distinguished from the wave function considered in equation (3.54) in that one is now dealing with a polarized even-even core where the Bogoliubov-Valatin transformation is now connecting the pair members $|i\rangle, |\tilde{i}\rangle$ of a quasi-pair.

3.2.2 The BCS approximation with a seniority force

Let us first start with the many-body Hamiltonian, $\hat{H}$, which consists of the (one-body) kinetic energy operator, $\hat{K}$, and a two-body interaction, $\hat{V}^{(2b)}$

$$\hat{H} = \hat{K} + \hat{V}^{(2b)} \tag{3.62}$$

The present approach made use of an approximation reducing the many-body problem to a one-body approach. One realization of this program is the Hartree-Fock approximation. The Hartree-Fock Hamiltonian which is one possible one-body reduction of $\hat{H}$ associated with a self-consistent Hartree-Fock density matrix $\hat{\rho}_{HF}$ denoted here as $\hat{h}_{HF}$ and can be written as

$$\hat{h}_{HF} = \hat{K} + \hat{U}_{HF} \tag{3.63}$$

where $\hat{U}_{HF}$ is the one-body reduction of the two-body interaction $\hat{V}^{(2b)}$ associated with $\hat{\rho}_{HF}$.

Consider a functional of the density operator $\hat{\rho}$ defined with respect to a two-body Hermitian operator,

$\hat{V}^{(2b)}$,

$$V^{(2b)}[\hat{\rho}] = \frac{1}{2}\sum_{mnpq} \hat{\rho}_{nm}\,\hat{\rho}_{qp}\langle mp|\hat{V}^{(2b)}|\widetilde{nq}\rangle \tag{3.64}$$

where the indices *m,n,p,q* denote the single-particle states of a complete single-particle basis and $\widetilde{|nq\rangle}$ is an anti-symmetrized wavefunction given by

$$\widetilde{|nq\rangle} = |nq\rangle - |qn\rangle \tag{3.65}$$

The one-body reduction of $\hat{V}^{(2b)}$ is a one-body operator whose matrix elements are given by

$$\langle m|\hat{U}_{HF}|n\rangle = \frac{\delta}{\delta\hat{\rho}_{nm}}\hat{V}^{(2b)} = \sum_{pq}\langle mp|\hat{V}^{(2b)}|\widetilde{nq}\rangle\hat{\rho}_{qp} \tag{3.66}$$

In the Hartree-Fock case, the density operator $\hat{\rho}_{HF}$ associated with the Slater determinant $|\Psi\rangle$ has {0,1} as a spectrum.

The part of $\hat{V}^{(2b)}$ which is not accounted for in the $\hat{U}_{HF}$ potential is referred to as the residual interaction $\hat{V}_{res}$ where

$$\hat{V}_{res} = \hat{V}^{(2b)} - \hat{U}_{HF} \tag{3.67}$$

so that the many-body Hamitonian may be now written as

$$\hat{H} = \hat{h}_{HF} + \hat{V}_{res} \tag{3.68}$$

We now make an approximation for $\hat{V}_{res}$ by considering it to be a seniority force. Given a one-body density matrix $\hat{\rho}$ and a spectrum $\{e_i\}$ associated to its eigensolutions $|i\rangle$, we perform a BCS calculation with this pairing interaction. This defines a new many-body wave function $|\Psi_{BCS}\rangle$ from which one would obtain a BCS density matrix $\hat{\rho}_{BCS}$ with occupation probability lying between 0 and 1. At this point, the one-body reduction of the two-body interaction called now $\hat{U}_{mf}$ (with *mf* standing for *mean-field*) is no longer associated with $\hat{\rho}_{HF}$ as before, but with $\hat{\rho}_{BCS}$. Using $\hat{\rho}_{BCS}$ as an input, one then defines a new one-body Hamiltonian called $\hat{h}_{mf}$. Diagonalizing $\hat{h}_{mf}$ one yields the density operator $\hat{\rho}_{mf}$ defining a new canonical basis to which a new energy spectrum is associated. The BCS pairing treatment is then performed on this basis states to obtain a new $\hat{\rho}_{BCS}$ which will be the input to define $\hat{h}_{mf}$ in the next iteration. These steps are then repeated until self-consistency is achieved. Self-consistency was considered to be reached when the variations of the total binding energy and the quadrupole moment from one iteration to the next are lesser than 10 eV and 0.010 fm^2, respectively.

The seniority force which is used to approximate the pairing interaction $\hat{V}_p$ assumes the constancy of so-called pairing matrix elements between all the single-particle states belonging to a restricted single-particle configuration space. This pairing matrix element between two pair-conjugate states is written as

$$\langle k\tilde{k}|\hat{V}_p^{(q)}|\widetilde{l\tilde{l}}\rangle \;=\; f_k f_{\tilde{k}} f_l f_{\tilde{l}}\,\hat{v}^{(q)}_{k\tilde{k}l\tilde{l}} \tag{3.69}$$

with

$$\hat{v}^{(q)}_{k\tilde{k}l\tilde{l}} = -\frac{G_q}{11.0+N_q}(MeV) \tag{3.70}$$

being dependent on the total number of nucleon N_q, of a particular charge state, q. The values for the pairing strengths G_q are obtained herein from a fit to the odd-even mass differences of some sets of nuclei. This will be the subject of the discussion in Section 4.2.1. The functions f_k is written as

$$f_k = \frac{1}{1+e^{(|e_k-e_F-X|-Y)/\mu}} \tag{3.71}$$

where

$$X = (E_{max}-E_{min})/2 \tag{3.72}$$

$$Y = (E_{max}+E_{min})/2 \tag{3.73}$$

E_{min} and E_{max} being the minimum and maximum energies, respectively, within which the single-particle states (with single-particle energy e_k) are considered. In the present work, all the single-particle states below the Fermi level ($E_{min} = -\infty$) up to a maximum energy of 6 MeV above the Fermi level ($E_{max} = 6$ MeV) are allowed for pairing. In order to avoid a sudden transition in the single-particle states from being an occupied to an unoccupied state, a gradual single-particle energy cut-off (instead of a sharp cut-off) is allowed by taking a diffuseness parameter $\mu = 0.20$ MeV.

The gap equation to be solved takes on the form [59]

$$\Delta_k = \sum_{\Omega_l>0} \hat{v}^{(q)}_{k\tilde{k}l\tilde{l}} \frac{\Delta_l}{[(e^{'}_l-\lambda)^2+\Delta^2_l]^{1/2}} \tag{3.74}$$

where $e^{'}_l$ is the average single-particle energy for the pair-conjugate $(l,\tilde{l})$ states, such that

$$e^{'}_l = \frac{1}{2}(e_l+e_{\tilde{l}}) \tag{3.75}$$

Due to the constancy of the pairing matrix element, one gets the same gap for all single-particle states belonging to the retained configuration space.

$$\forall\, k\,; \qquad \Delta_k = \Delta \tag{3.76}$$

Similiarly, due to equation (3.75) one has

$$\forall\, k\,; \qquad v^2_k = v^2_{\tilde{k}} \tag{3.77}$$

The constraint on the particle number requires that the sum of the occupation probability of all occupied states is equal to the total particle number of a specific nuclear charge state:

$$2\sum_{\Omega_k>0} v^2_k = N_q \tag{3.78}$$

As mentioned above, the particle number would corresponds to the neighbouring $N-1$ even-even nucleus when performing a BCS calculation for an odd-mass nucleus.

The occupation probability v_k^2 of the single-particle state k, and its complement, u_k^2 are given by:

$$v_k^2 = \frac{1}{2}\Big\{1 - \frac{e_k^{'} - \lambda}{[(e_k^{'} - \lambda)^2 + \Delta^2]^{1/2}}\Big\} \tag{3.79}$$

$$u_k^2 = \frac{1}{2}\Big\{1 + \frac{e_k^{'} - \lambda}{[(e_k^{'} - \lambda)^2 + \Delta^2]^{1/2}}\Big\} \tag{3.80}$$

After obtaining the converged solution, the two-body quantity which is of interest is the total binding energy. It is defined in this case as the expectation value of the Hamiltonian in the blocked BCS wave function, given as:

$$\langle BCS^{(i)}|\hat{H}|BCS^{(i)}\rangle = \int \mathscr{H}^{Skyrme}(\mathbf{r})\, d\mathbf{r} + G \sum_{\substack{k,l\neq i \\ \Omega_k,\Omega_l>0}} u_k v_k u_l v_l \tag{3.81}$$

where the Hamiltonian densities contributing to the term $\mathscr{H}^{Skyrme}$ is given in equation (3.7) to (3.12) using of course the one-body density $\hat{\rho}_{BCS}$ while the last term on the *r.h.s* is the contributing term coming from the pairing correlations (with $G \equiv \hat{v}^{(q)}_{k\tilde{k}l\tilde{l}}$).

3.3 The center-of-mass correction

The many-body nuclear Hamiltonian can be written in terms of relative coordinates $\hat{r}_i$ (with momentum operator $\hat{\pi}_i$ and reduced mass μ_i) and the center-of-mass coordinate $\hat{X} = \sum_i \frac{\hat{x}_i}{A}$ with its conjugate momentum operator $\hat{P} = \sum_i \hat{p}_i$ such that (see e.g. [65]):

$$\hat{H} = \frac{\hat{P}^2}{2mA} + \sum_i^{A-1} \frac{\hat{\pi}_i^2}{2\mu_i} + \hat{V}(\hat{r}_1, \hat{r}_2, ...\hat{r}_i) \tag{3.82}$$

The many-body kinetic energy of A nucleons may be splitted into two parts.

$$\begin{aligned} \hat{K} &= \hat{K}^{(cm)} + \hat{K}^{(rel)} \\ &= \frac{\hat{P}^2}{2mA} + \hat{K}^{(rel)} \end{aligned} \tag{3.83}$$

where $\hat{P}$ is the center of mass momentum. In this work, the $\hat{K}^{(cm)}$ term is approximated by

$$\hat{K}^{(cm)} = \sum_i^A \frac{\hat{p}_i^2}{2mA} \tag{3.84}$$

i.e. neglecting its two body contribution. This introduces a renormalization term $\left(1 - \frac{1}{A}\right)$ to the kinetic energy operator as seen in equation (3.7).

Such an approach has been noted to overestimate the contribution from the center-of-mass correction [66]. Nevertheless, the approximate treatment of the correction term is consistent with the manner in which the adopted Skyrme parametrizations were fitted which is assumed to cure approximately this defect. A study on the various approximations used to include the center-of-mass correction term in the mean-field approach and also its effects on nuclear properties as well as deformation energy surface has been performed in Ref. [67]. Of particular interest is the consequence of the center-of-mass correction to the deformation energy of heavy nuclei. Comparison between the deformation energy curves obtained with the SLy4 and SLy6 parametrizations of the Skyrme force shows that the former parametrization results in a wider and higher fission-barrier [67]. This was attributed to the different treatment for the center-of-mass correction term, and consequently reflected in the value of surface coefficient a_{surf} for the respective interaction. Effective interactions with small value of a_{surf} were reported to yield lower deformation energy, with $a_{surf} = 17.4$ MeV for SLy6 as compared to $a_{surf} = 18.2$ MeV for SLy4. The surface coefficient for the SkM* parametrization frequently used for fission-barrier calculations was reported to be 17.6 MeV and this value has been constrained in the earlier fit of the interaction.

3.4 From HF+BCS energies to nuclear energies

3.4.1 The case of even-mass nuclei

We will first limit our discussion to the case of even-mass nuclei.

The HF+BCS energies cannot be associated in general with the nuclear energies since they incorporate a spurious component due to the breaking of the rotational symmetry. For deformed nuclei, these microscopically calculated energies corresponds, as well known, to the energy of intrinsic states. Due to the Heisenberg uncertainty principle, the imposition of a definite angular position for the intrinsic state entails a mixing of angular momenta in the lab frame. The ground state energy in the lab frame will thus correspond to the energy of a superposition of states having *a priori* all possible values of the angular momentum compatible with the symmetries. If the intrinsic solution is axially symmetrical and possesses left-right reflection symmetry, it is thus a mixture of 0^+, 2^+, 4^+ ... states. If it is a reasonably well-deformed it will correspond to a mixture of states belonging to the rotational ground state band. In such a case, a simple approach yielding the ground state energy out of the microscopically calculated HF+BCS energy have been proposed and will be detailed as follows.

Starting from a mean-field solution whose wave-function is noted as $|\Psi^{\alpha}_{K\pi}\rangle$ where α refers to a particular solution, the projection onto normalized good angular momentum states $|\Phi^I\rangle$ would yield:

$$|\Psi^{\alpha}\rangle \;=\; \sum_{I\geqslant K} X^{\alpha}_{I}\;|\Phi^{I}_{\alpha}\rangle \tag{3.85}$$

The expectation value of the Hamiltonian in this wave-function is assumed to provide a rotational spectra (as proposed by Lipkin [65]) such that:

$$\langle\Phi^{I}_{\alpha}|\hat{H}^{Skyrme}|\Phi^{I}_{\alpha}\rangle \;=\; E^{(I=0)}_{\alpha} \;+\; \frac{\hbar^2}{2\,\mathcal{I}_L} I(I+1) \tag{3.86}$$

with $E^{(I=0)}_{\alpha}$ being the energy of the contribution to $|\Phi^{I}_{\alpha}\rangle$ of the $I=0$ component, while $\mathcal{I}_L$ plays the role of a moment of inertia. Subsequently, one could write:

$$\langle\Psi^{\alpha}|\hat{H^{Skyrme}}|\Psi^{\alpha}\rangle \;=\; \sum_{I=0}^{\infty} |X^{\alpha}_{I}|^2 \Big[E^{(I=0)}_{\alpha} \;+\; \frac{\hbar^2}{2\,\mathcal{I}_L}\, I(I+1)\Big] \tag{3.87}$$

and thus

$$E^{(I=0)}_{\alpha} \;=\; \langle\Psi^{\alpha}|\hat{H}^{Skyrme}|\Psi^{\alpha}\rangle \;-\; \frac{1}{2\,\mathcal{I}_L}\,\langle\Psi^{\alpha}|\hat{\mathrm{J}}^2|\Psi^{\alpha}\rangle \tag{3.88}$$

The evaluation of the spurious rotational energy content of $|\Psi^{\alpha}\rangle$ will thus imply the calculations of the expectation value of the $\hat{\mathrm{J}}^2$ operator for this state as well as an estimate of the moment of inertia $\mathcal{I}_L$. The former quantity is calculated as recalled in Appendix C. The determination of the moment of inertia is somewhat more difficult.

The usual way to handle it is to use the Inglis-Belyaev formula [68]. It is not satisfactory for at least three reasons. It corresponds to the adiabatic limit of the Routhian Hartree-Fock-Bogoliubov approach. The Routhian approach is, as well known, only a semi-quantal prescription to describe the rotation of a quantal object. Moreover, it is not clear, as we will see, that the corresponding collective motion is adiabatic. Finally, the Belyaev formula corresponds to a well-defined approximation to the Routhian-Hartree-Fock-Bogoliubov approach. As discussed in Ref. [69], the Belyaev moment of inertia ought to be renormalized to take into account the so-called Thouless-Valatin corrective terms [70]. These corrective terms have been studied in detail in Ref. [69]. They come about due to the fact the that response of the self-consistent fields with respect to the time-odd density (as e.g. current and spin vector densities) generated by the rotation of the nucleus is neglected in the Belyaev formula. In order to incorporate these corrective terms in our current approach, the moment of inertia yielded by the Belyaev formula $\mathcal{I}_{Bel}$ could be scaled by a factor α whose value is taken to be 0.32 following the prescription of Ref. [71]:

$$\mathcal{I}' = \mathcal{I}_{Bel}\,(1+\alpha) \tag{3.89}$$

As a result, one should diminish by the same percentage the rotational correction evaluated upon using the Belyaev moment of inertia.

Projecting after variation the 0^+ state out of a HF+BCS solution, corresponds, of course, in principle to a better approach to the determination of the ground-state energy. This has been performed in Ref. [72] for the fission-barrier of ^{240}Pu upon using two Skyrme force parametrizations (SLy4 and SLy6 [73, 74]). These authors clearly show that using the Inglis-Belyaev leads to an overestimation of the rotational correction by about 10 - 20% in the region of inner-barrier and fission-isomeric state and by more than 80% close to the outer-barrier. A word of caution on the specific values listed above should be made, however, since these calculations yield a first 2^+ energy in the ground-state band which is about twice its experimental value (83 keV instead of 43 keV).

Moving now to a third theoretical estimate which belongs to the family of phenomenological approaches known as Variable Moment of Inertia models. It describes the evolution of rotational energies in a band by consideration of the well known Coriolis Anti-Pairing (CAP) effect [75] in terms of intrinsic vortical currents (see e.g. Ref. [76]). The Belyaev treatment to the moment of inertia corresponds to a global nuclear rotation which is adiabatic, i.e. corresponding to a low angular velocity Ω, or equivalently to a rather small value of the total angular momentum (also referred to as spin). One can compute the average value of the total angular momentum I_{av} spuriously included in the mean-field solution $|\Psi^{\alpha}_{0^+}\rangle$ computed as described in Appendix C as

$$I_{av}(I_{av}+1)\,\hbar^2 = \langle\,\hat{\mathbf{J}}^2\,\rangle \tag{3.90}$$

where $\hat{\mathbf{J}}$ is the total angular momentum operator. It cannot even, at ground-state deformation, be considered as being small (one finds there that $I_{av} \approx 13$). Consequently, the moment of inertia entering the rotational

correction term should reflect the fact the average Ω is large.

Recently, a polynomial expression for the moment of inertia as a function of Ω denoted as $\beth(\Omega)$ has been proposed [77] according to this approach to CAP. This model shall be referred to as the Intrinsic Vorticity Model (IVM) in the discussion herein. The IVM was found to work well for the rotational bands in the ground-state deformation for some actinide nuclei, for instance a very good agreement for ^{240}Pu for a value of I as high as $I_{av} \approx 30$ (where it predicts a rotational energy differing by only 70 keV from the experimental value). A more detailed discussion on the model and the comparison of the calculated rotational bands to the experiments will be made in Appendix D. A brief description will be given in the following as to how this model will be applied in the context of fission-barrier heights calculations. The IVM uses merely two inputs for each nuclei in order to describe up to 16 rotational energies, namely the experimental values of the charge quadrupole moment and the 2^+ energy of the ground-state band. As such, it is limited to describe only the rotational mode for the ground-state, and thus the corresponding spurious rotational energy correction.

Table 3.1 lists the spurious rotational energy obtained using the Belyaev formula as compared to the IVM rotational energy for a given value of the total angular momentum I_{av} in the ground-state of the even-even nuclei. In all cases, the spurious rotational energy evaluated using the Belyaev formula is larger by about a factor 2 with respect to the values obtained in the IVM approach. Therefore, the rotational energy obtained using the Belyaev formula should be reduced by approximately 50%. The same amount of correction is assumed to apply as well to all other deformations, and therefore possibly include this 50% reduction in the calculations of the fission-barrier heights.

Table 3.1: Rotational energy (given in MeV) calculated from Belyaev formula (IB) and the Intrinsic Vorticity Model (IVM) at the ground-state deformation as a function of the total angular momentum I_{av} with $I_{av}(I_{av}+1) = \langle \hat{\mathbf{J}}^2 \rangle$.

Nucleus	I_{av}	IB	IVM
^{234}U	12.988	2.371	1.232
^{236}U	12.905	2.423	1.255
^{238}Pu	13.146	2.441	1.266
^{240}Pu	13.143	2.408	1.232

To conclude this subsection, it appears that the evaluation of the spurious rotational energy content of the intrinsic wavefunction $|\Psi^\alpha\rangle$ is very significantly overestimated upon using Belyaev's moments of inertia. On the other hand, as will seen later, it corresponds to energies that can amount over a fission-barrier to a few MeV which is by far a fairly large correction. Since this correction varies with deformation, its exact estimate is of paramount importance for an accurate calculations of the fission-barrier heights.

In the current situation when a reliable prescription could not be made, the present results for fission barriers may be obtained by using four prescriptions for the rotational energy correction:

- upon using the Belyaev's moment of inertia
- reducing the above moments by 32% (i.e. correcting for the omission of some Thouless-Valatin self-consistent terms)
- using the reduction factors from the Belyaev approach for all considered even-mass nuclei, as found (as a function of the deformation) for ^{240}Pu with the SLy4 Skyrme force
- using at all deformations the reduction factors found at the ground-state of the considered nuclei within the so-called Intrinsic Vorticity model.

3.4.2 The case of odd-mass nuclei

An adequate description of the nuclear energy of states corresponding to a rigid deformation implies the treatment of both the single-particle dynamics and the collective rotational mode. This is achieved here according to the so-called Bohr-Mottelson model [78] within the rotor-plus-particle approach. The Bohr-Mottelson Hamiltonian given as

$$\hat{H}^{(BM)} = \hat{H}^{(intr)} + \frac{(\hat{\mathrm{I}}-\hat{\mathrm{j}})^2}{\mathcal{I}_C} \tag{3.91}$$

where the first part of $\hat{H}^{(BM)}$ corresponds to the intrinsic degrees of freedom and the second part is the rotational energy of the core (whose moment of inertia is noted by $\mathcal{I}_C$ and angular momentum by $\hat{R} = \hat{\mathrm{I}}-\hat{\mathrm{j}}$). Note that whereas the core is made of an even number of nucleons, $\mathcal{I}_C$ is not the moment of inertia of the corresponding even-even nucleus alone since the presence of an odd particle will increase its value due to the pair quenching induced by the blocking of the level which the odd particle occupies.

The eigenstates of $\hat{H}^{(intr)}$ corresponding to an intrinsic frame solution $|\Psi^{\alpha}_{K\pi}\rangle$ are written as

$$|IM\alpha K\pi\rangle = \sqrt{\frac{2I+1}{16\pi}}\Big(D^{I}_{M\,K}|\Psi^{\alpha}_{K\pi}\rangle + (-)^{(I+K)}D_{M\,-K}\,\hat{T}|\Psi^{\alpha}_{K\pi}\rangle\Big) \tag{3.92}$$

The intrinsic energy

The eigenvalue of $\hat{H}^{(intr)}$ is not given as the expectation value of $\hat{H}^{Skyrme}$ for the state $|\Psi^{\alpha}_{K\pi}\rangle$ in that this intrinsic frame wave function includes a spurious rotational component. Similarly to what is the case for even nuclei, it is assumed that

$$\langle IM\alpha K\pi|\hat{H}^{(intr)}|IM\alpha K\pi\rangle = \langle\Psi^{\alpha}_{K\pi}|\hat{H}^{(Skyrme)}|\Psi^{\alpha}_{K\pi}\rangle - \frac{1}{2\,\mathcal{I}_L(\alpha K\pi)}\Big[\langle\Psi^{\alpha}_{K\pi}|\hat{\mathrm{J}}^2|\Psi^{\alpha}_{K\pi}\rangle - K(K+1)\hbar^2\Big] \tag{3.93}$$

One can split the one-body part of $\hat{\mathrm{J}}^2$ into core plus odd particle contributions and similarly for its two-body part to which however one should add a cross term, so that with an obvious notation, one has

$$\langle\Psi^{\alpha}_{K\pi}|\hat{\mathrm{J}}^2|\Psi^{\alpha}_{K\pi}\rangle \;=\; \langle\Psi^{\alpha}_{K\pi}|\hat{\mathrm{J}}^2_{core}|\Psi^{\alpha}_{K\pi}\rangle \;+\; \langle\Psi^{\alpha}_{K\pi}|\hat{\mathrm{j}}^2_{odd}|\Psi^{\alpha}_{K\pi}\rangle \;+\; 2\,\langle\Psi^{\alpha}_{K\pi}|\hat{\mathrm{J}}_{core}\cdot\hat{\mathrm{j}}_{odd}|\Psi^{\alpha}_{K\pi}\rangle \tag{3.94}$$

Within the blocked BCS approach, it is easy to show that only the one-body part of $\hat{\mathrm{j}}^2_{\mathrm{odd}}$ contributes to the relevant matrix element so that

$$\langle\Psi^{\alpha}_{K\pi}|\hat{\mathrm{j}}^2_{odd}|\Psi^{\alpha}_{K\pi}\rangle \;=\; \langle\alpha K\pi|\hat{\mathrm{j}}^2|\alpha K\pi\rangle \tag{3.95}$$

where $|\alpha K\pi\rangle$ is the single-particle state corresponding to the odd-particle and $\hat{\mathrm{j}}^2$ a one-body operator.

For the cross-term involving the two-body separable operator $\hat{\mathrm{J}}_{core}\cdot\hat{\mathrm{j}}_{odd}$, one obtains readily due to the axial symmetry that

$$\langle\Psi^{\alpha}_{K\pi}|\hat{\mathrm{J}}_{core}\cdot\hat{\mathrm{j}}_{odd}|\Psi^{\alpha}_{K\pi}\rangle \;=\; -2\sum_{\substack{c,\\ K_c=K_\alpha+1}} v^2_c|\langle c|\hat{\mathrm{j}}_+|\alpha K\pi\rangle|^2 \tag{3.96}$$

where c are all the canonical basis states satisfying the matching condition $K_c = K_\alpha + 1$. This contribution is assumed to be negligible and thus

$$\langle\Psi^{\alpha}_{K\pi}|\hat{\mathrm{J}}^2|\Psi^{\alpha}_{K\pi}\rangle \;\approx\; \langle\Psi^{\alpha}_{K\pi}|\hat{\mathrm{J}}^2_{core}|\Psi^{\alpha}_{K\pi}\rangle \;+\; \langle\alpha K\pi|\hat{\mathrm{j}}^2|\alpha K\pi\rangle \tag{3.97}$$

To compute, in practice, the expectation value of $\hat{\mathrm{J}}^2_{core}$ one perform the calculations of the expectation value of the corresponding one-body and two-body operators for a restricted single-particle space where the state occupied by the odd particle together with its quasi-pair partner have been removed. In particular, one may note that this calculation corresponds to a BCS calculation for even numbers of particles with pairing correlations diminished from what it is expected to be present in the core nucleus alone (i.e. without a polarizing odd particle). One thus gets for the intrinsic energy eigenvalue

$$\begin{aligned}\langle IM\alpha K\pi|\hat{H}^{(intr)}|IM\alpha K\pi\rangle \;=\; &\langle\Psi^{\alpha}_{K\pi}|\hat{H}^{(Skyrme)}|\Psi^{\alpha}_{K\pi}\rangle \;-\; \frac{1}{2\,\mathcal{I}_L(\alpha K\pi)}\Big[\langle\Psi^{\alpha}_{K\pi}|\hat{\mathrm{J}}^2_{core}|\Psi^{\alpha}_{K\pi}\rangle \\ &+\; \langle\alpha K\pi|\hat{\mathrm{j}}^2|\alpha K\pi\rangle \;-\; K(K+1)\hbar^2\Big]\end{aligned} \tag{3.98}$$

The core rotational energy

Since any band coupling through the so-called Coriolis interaction term is neglected, one will merely consider here the diagonal term

$$\begin{aligned}\langle IM\alpha K\pi|\hat{H}^{(core)}|IM\alpha K\pi\rangle \;=\; &\frac{1}{2\,\mathcal{I}_C(\alpha K\pi)}\Big[I(I+1)\hbar^2 \;+\; \langle\Psi^{\alpha}_{K\pi}|\hat{\mathrm{j}}^2|\Psi^{\alpha}_{K\pi}\rangle \\ &-\,2K^2 \;+\; \delta_{K,\frac{1}{2}}\,a\,(-1)^{I+1/2}\,(I+\frac{1}{2})\Big]\end{aligned} \tag{3.99}$$

with the so-called decoupling parameter a defined as

$$a \;=\; \langle \Psi^{\alpha}_{\frac{1}{2}\pi} | \hat{\mathrm{j}}_{+} \hat{T} | \Psi^{\alpha}_{\frac{1}{2}\pi} \rangle \tag{3.100}$$

Some remark is in order here. In the spirit of the rotor-plus-particle approach, the one-body operator $\hat{\mathrm{j}}$ is acting only in the space of the odd particle. Consequently, as was seen before and with the same notation as above

$$\langle \Psi^{\alpha}_{K\pi} | \hat{\mathrm{j}}^2 | \Psi^{\alpha}_{K\pi} \rangle \;=\; \langle \alpha K\pi | \hat{\mathrm{j}}^2 | \alpha K\pi \rangle \tag{3.101}$$

and similiarly

$$\langle \Psi^{\alpha}_{\frac{1}{2}\pi} | \hat{\mathrm{j}}_{+} \hat{T} | \Psi^{\alpha}_{\frac{1}{2}\pi} \rangle \;=\; \langle \alpha \, \frac{1}{2} \, \pi | \hat{\mathrm{j}}_{+} | \overline{\alpha \, \frac{1}{2} \, \pi} \rangle \tag{3.102}$$

noting that here one considers not the conjugated state $|\widetilde{\alpha \, \tfrac{1}{2} \, \pi}\rangle$ of $|\alpha \, \tfrac{1}{2} \, \pi\rangle$ in the sense of the quasi-pairs in use in the approach but its time-reversed state. However, in view of the closeness of $|\langle \overline{\alpha \, \frac{1}{2} \, \pi} | \widetilde{\alpha \, \frac{1}{2} \, \pi} \rangle|$ to 1 and the weak impact on the total energy of the corresponding term, this difference may be neglected.

The total Bohr-Mottelson energy

A final assumption is made, namely identifying $\mathcal{I}_L(\alpha \; K \; \pi)$ with $\mathcal{I}_C(\alpha \; K \; \pi)$ for each configuration defining the Bohr-Mottelson eigenstate. It is to be noted in that respect, that both are affected by the same pairing quenching due to the blocking effect. One may remark that the former ($\mathcal{I}_L$) corresponds to a number A (odd) of particles while the second ($\mathcal{I}_C$) to a number $A \pm 1$ (even). The bulk effect (scaling as $A^{5/3}$) of this mass discrepancy for $A \sim 240$ is rather small anyway (less than 0.7%).

As a result of the above, the $\langle \alpha K\pi | \hat{\mathrm{j}}^2 | \alpha K\pi \rangle$ terms cancel in the total energy to yield

$$\begin{aligned} \langle IM\alpha K\pi | \hat{H}^{(BM)} | IM\alpha K\pi \rangle = \langle \Psi^{\alpha}_{K\pi} | \hat{H}^{(Skyrme)} | \Psi^{\alpha}_{K\pi} \rangle \;+\; \frac{\hbar^2}{2\,\mathcal{I}_C(\alpha K\pi)} \Big\{ [I(I+1) - K(K-1)]\hbar^2 \\ -\; \langle \Psi^{\alpha}_{K\pi} | \hat{\mathrm{j}}^2_{core} | \Psi^{\alpha}_{K\pi} \rangle \;+\; \delta_{K,\frac{1}{2}} \, a \, (-1)^{I+1/2} \, (I + \frac{1}{2}) \Big\} \end{aligned} \tag{3.103}$$

Limiting only to the lowest-energy ground-state of the rotational band for each configuration (the so-called band heads), one gets

$$\begin{aligned} E^{(BM)}(\alpha K\pi) \;= \langle \Psi^{\alpha}_{K\pi} | \hat{H}^{(Skyrme)} | \Psi^{\alpha}_{K\pi} \rangle \;+\; \frac{1}{2\,\mathcal{I}_C(\alpha K\pi)} \Big\{ 2K\hbar^2 \;-\; \langle \Psi^{\alpha}_{K\pi} | \hat{\mathrm{j}}^2_{core} | \Psi^{\alpha}_{K\pi} \rangle \\ +\; \delta_{K,\frac{1}{2}} \, a \, (-1)^{I+1/2} \, (I + \frac{1}{2}) \hbar^2 \Big\} \end{aligned} \tag{3.104}$$

One may note *en passant* that the corrective term to the HF+BCS energy for even-mass nuclei may also be obtained from the formula obtained for odd-mass nuclei upon setting $K = 0$.

As it was the case for even nuclei, a specific evaluation of the above corrective term to $\langle\Psi^{\alpha}_{K\pi}|\hat{H}^{(Skyrme)}|\Psi^{\alpha}_{K\pi}\rangle$ depends on the choice made to estimate the moment of inertia $\mathcal{I}_C(\alpha K\pi)$. Three different approaches are considered, namely

- upon using the Belyaev's moment of inertia
- reducing the above moment by 32% (i.e. correcting for the omission of some Thouless-Valatin self-consistent terms)
- making an estimate of $\mathcal{I}_C(\alpha K\pi)$ from the data at ground-state deformation to define a reduction factor to be used at all deformations as it will be discussed below.

The latter estimate of $\mathcal{I}_C(\alpha K\pi)$ will follow these lines. From the calculated values of $\langle\Psi^{\alpha}_{K\pi}|\hat{\mathrm{J}}^2_{core}|\Psi^{\alpha}_{K\pi}\rangle$ we define an average spin value through

$$R_{av}(\alpha K\pi)\Big[R_{av}(\alpha K\pi)+1\Big]\hbar^2 \;=\; \langle\Psi^{\alpha}_{K\pi}|\hat{\mathrm{J}}^2_{core}|\Psi^{\alpha}_{K\pi}\rangle \tag{3.105}$$

From the energy sequence in a rotational band $(\alpha K\pi, I)$, one deduce the rotational core energy. For that purpose, for instance for the $7/2^-$ ground-state band of ^{235}U, $R=0$ is assigned for the $I=7/2$ state, $R=2$ for the $I=11/2$ state and so on. The core dynamical moment of inertia as a function of R is deduced through the formula currently used by experimentalists

$$\mathcal{I}_C(R) \;=\; \frac{4\hbar^2}{E(R+2\rightarrow R)-E(R\rightarrow R-2)} \tag{3.106}$$

where $E(R_0+2\rightarrow R_0)$ is the transition energy from the state with $R=R_0+2$ to the state with $R=R_0$. The value of $\mathcal{I}_C(R_{av})$ is then computed by interpolation.

In Table 3.2, a comparison is made between the values of the rotational correction for 4 configurations in ^{235}U and the $1/2^+$ configuration in ^{239}Pu at ground-state deformation obtained with the method using the R_{av} spin value and the Inglis-Belyaev moments of inertia.

Table 3.2: Rotational energy (given in MeV) calculated from Belyaev formula (IB) and those using the moment of inertia deduced from R_{av} spin value at the ground-state deformation for ^{235}U and ^{239}Pu nuclei. The $1/2^+$ configuration in ^{235}U is not included for comparison due to the possible influence of the Coriolis coupling.

Nucleus	K^π	R_{av}	IB	E($\mathcal{I}(R_{av})$)
^{235}U	$7/2^-$	12.26	2.335	0.718
	$3/2^+$	12.33	2.257	0.686
	$5/2^+$	12.47	2.265	0.668
	$5/2^-$	12.12	2.247	0.710
^{239}Pu	$1/2^+$	12.91	2.147	0.890

It was found that the reduction factor of the rotational correction is about 65% when using the R_{av} values with respect to the Inglis-Belyaev approach, which is slightly larger as compared to the estimated reduction factor obtained with the IVM approach in even-mass nuclei. In order to be consistent with what was done for even-even nuclei, the same 50% reduction to the rotational energy calculated using the Belyaev formula will be applied to the case of odd-mass nuclei.

Consequences for fission barriers

The net results is that one should correct microscopically evaluated (HF+BCS) energies (at a given deformation β for a given configuration ($\alpha K\pi$) called $E^{mf}(\alpha K\pi,\beta)$) by a rotational correction $E^{corr}(\alpha K\pi,\beta)$. The latter may have two origins. For all nuclei, it comes as an approximate correction for a spurious content of rotational energy. In odd-mass nuclei, it comes as an estimate of a dynamical contribution to the energy for the rotation of the core. Clearly when dealing with relative energies, such as deformation energies for a given configuration (which is exactly what is needed to construct a fission-barrier), one should add to the HF+BCS deformation energy

$$\Delta E^{def}(\alpha K\pi,\beta_1\beta_2) \;=\; E^{mf}(\alpha K\pi,\beta_2) \;-\; E^{mf}(\alpha K\pi,\beta_1) \tag{3.107}$$

the corresponding rotational correction energy

$$E^{corr}(\alpha K\pi,\beta_1\beta_2) \;=\; E^{corr}(\alpha K\pi,\beta_2) - E^{corr}(\alpha K\pi,\beta_1) \tag{3.108}$$

which will depend in general (beyond the deformation in β_1 and β_2) on the configuration ($\alpha K\pi$).

Note that as discussed in subsection 3.4.1 and the previous subsection, various ways will be considered to define in practice this correction when presenting fission-barrier heights.

Chapter 4

TECHNICAL ASPECTS OF THE CALCULATIONS

Some technical aspects of the calculations will be discussed in this chapter. Section 4.1 will be devoted to the discussions of the choice of Skyrme parametrizations employed in the study. For each choice of the Skyrme parametrization, the pairing strengths entering the BCS pairing treatment have been fitted to the odd-even mass differences of some actinide nuclei. The results from such a fit procedure will be discussed in Section 4.2. The discussion on the choice of numerical parameters will be made in Section 4.3 and the Broyden's method for the determination of the extremum points in the deformation energy curves will be made in Section 4.4. The last Section 4.5 will be devoted to the implementation of blocking procedure in the code and issues arising in the course of the work.

4.1 Choice of the Skyrme parametrization

In the domain of the microscopic calculation of fission barriers, the SkM* parametrization of the Skyrme force have proved to be a reliable yardstick. This set of parameters have been fitted to the liquid drop fission-barrier of ^{240}Pu [79] and seen wide applicaton in the studies of fission-barrier properties for example in Ref. [60, 80] performed within the HF framework and Ref. [81, 82] in the Hartree-Fock-Bogoliubov calculations.

On the other hand, another set of Skyrme parameters of the SIII type which have been fitted to the nuclear properties of even-mass spherical nuclei [83] is known to perform better in the domain of nuclear spectroscopy. The validity of the SIII force has been tested in many instances. In particular, it gives good single-particle spectra when compared to the experimental ones [28] and it reproduces fairly well the N-Z dependence of the binding energy [84]. It is imperative then, to consider the SIII parametrization for the spectroscopic study of odd-mass nuclei.

Although the SIII and SkM* parameter sets perform rather well in the intended fields of studies in which

they have been fitted for, both sets of Skyrme parameters are rather old in that they have been fitted over 30 years ago. There are currently many types of Skyrme parametrizations such as the TIJ [85], SLyIII.0.8 [86] and SLy5* [87], to name a few.

The SLy5* in particular, is interesting because of some similiarities to the SkM* parametrization. Both SkM* and SLy5* have a density dependence of 1/6 (see Appendix A for the sets of parameters of the considered Skyrme forces) to simulate a density dependent interaction. The center-of-mass correction is approximated by its one-body part while the Coulomb exchange interaction is treated using the Slater approximation in both cases. One difference between these two Skyrme parameters sets are the manner in which they deal with the time-even spin-current density $J_{\mu\nu}$ term entering the Hamiltonian density. The spin-current density was taken into account in the fit of the SLy5* parametrization whereas it is absent in the fit of the earlier SkM* interaction. On a different aspect of the fit procedure, the SLy5 interaction being the initial version of the SLy5* set is fitted without adjusting the surface coefficient [88, 73], in constrast to what was done for the case of the SkM* interaction. In view of the above, it is meaningful and interesting to compare some limited yet relevant results obtained using the SLy5* parametrization with those obtained with the SIII and SkM* parametrizations.

We shall now take a rather different point of view with regards to our choice of Skyrme parametrizations for the study. The older generation of Skyrme forces were fitted with respect to the nuclear properties of even-mass nuclei. As such, some terms entering the Hamiltonian density are non-contributing during the fit due to the vanishing time-odd densities. When performing calculations for cases where the time-odd densities are not vanishing, as it is the case with odd-mass nuclei, the unconstrainted coupling constants are contigent upon on the values of the Skyrme parameters (in an uncontrollable fashion) which were obtained in the fit of the even-mass nuclei [89]. One is then forced to decide on the course of action with regards to the terms which were not considered during the fitting procedure. To this end, one could decide to either adopt the *interaction* or a *functional* point of view.

From the *interaction* point of view, all the cumulative terms involving the Skyrme parameters entering the expression of the Hamiltonian density (equations (3.7) to (3.12)) have to be taken into account. In doing so, the coupling constants will depend on the values obtained in the original fit of the Skyrme force. On the other hand, adopting the *functional* point of view would allow for a choice of the coupling constants of the time-odd terms independent of what has been done for the time-even ones. In addition, some terms in the Hamitonian densities can be omitted by setting the corresponding coupling constants to zero. However, the term $(\rho\tau - \mathbf{j}^2)$ which ensures the Galilean invariance property of the Skyrme functional [51] should be either cancelled or maintained as a whole in such an approach.

The *interaction* point of view has been adopted while respecting the original fit of the Skyrme parametrizations as a default approach for the study. In this way, the coupling constants of B_{14}, B_{15}, B_{18} and B_{19} are set to zero when employing the SIII and SkM* parameters sets. By setting these coupling constants to zero,

the only terms related to time-odd densities which are not vanishing are those of the form $\mathbf{s}^2$, $(\rho\tau - \mathbf{j}^2)$ and $(\mathbf{j}\cdot\nabla\times\mathbf{s})$. This shall be referred herein as the *minimal time-odd* scheme.

The *full time-odd* scheme would refer to the case when all the time-odd densities appearing in the Hamiltonian density are taken into account when solving the Hartree-Fock equations. This would indeed be the default scheme for the SLy5* parameters set. The contributions from unconstrainted coupling constant terms in the *full time-odd* scheme when employing the SIII and the SkM* parametrizations will be investigated for some relevant cases. Figure 4.1 shows as an example the single-particle energy spectra in the ground-state of ^{240}Pu obtained with the SIII and SkM* (in the *minimal time-odd* scheme) and the SLy5* (in the *full time-odd* scheme).

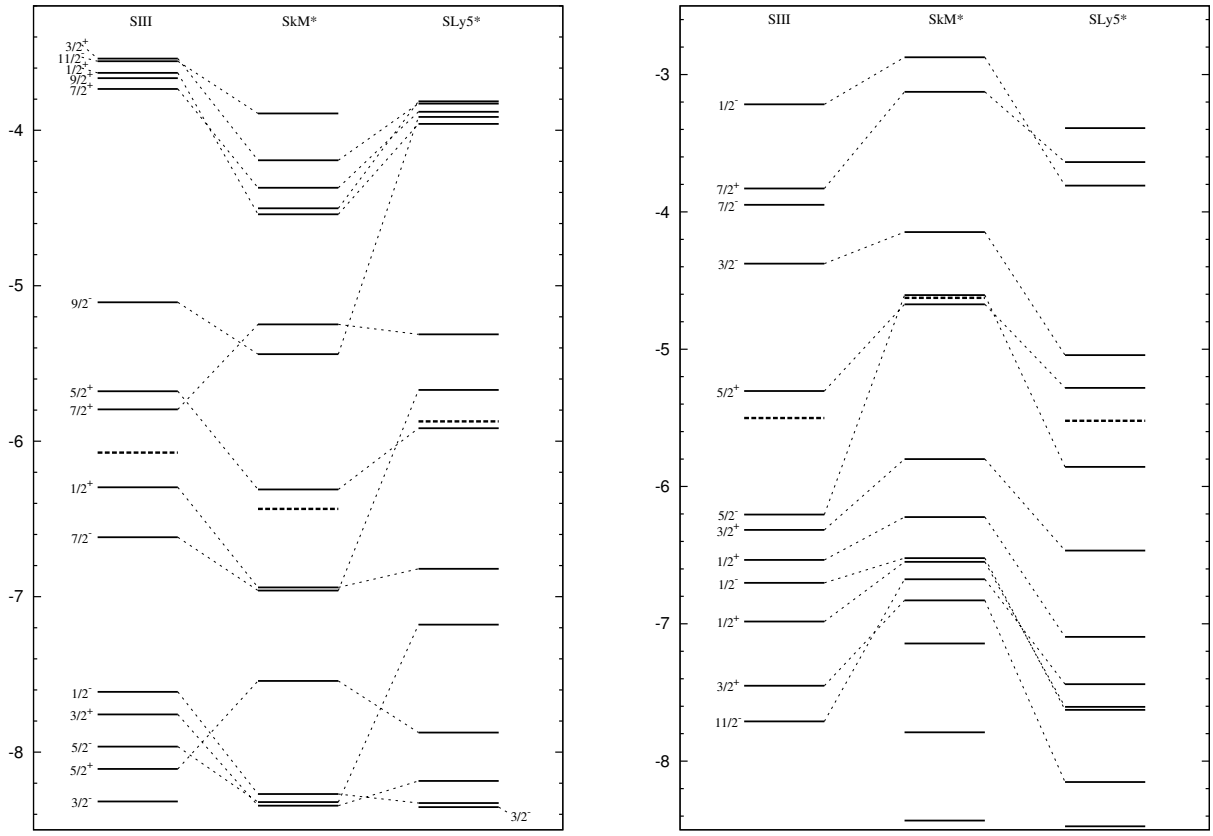

Figure 4.1: The ground state neutron and proton single-particle spectra of ^{240}Pu obtained with the SIII and SkM* interactions in the default *minimal time-odd* scheme, while the SLy5* in the *full time-odd* scheme. The Fermi levels for each Skyrme interaction are indicated by the thick dashed lines.

4.2 Pairing strengths in the BCS framework

4.2.1 Determining the neutron and proton pairing strengths

It is well known that the amount of nuclear pairing will affect the fission-barrier heights substantially. For example, the study of fission-barrier heights of ^{240}Pu in the relativistic mean-field approach with the BCS pairing scheme [90] shows that an increase of 20% in pairing strengths would decrease the inner-barrier height by about 2 MeV, while the asymmetric outer-barrier would be reduced by about 1 MeV. Similarly, the work of Ref. [91] in the Hartree-Fock-Bogoliubov framework in some actinide nuclei, assuming axial symmetry, gives an estimate of an increase of the inner and outer-barrier height by 2 MeV and 3 MeV, respectively, with a 15% decrease in pairing strength. An identical pattern of the effect on the inner-barrier height due to pairing was also reported in Ref. [92].

In view of the importance of nuclear pairing on the barrier heights, it is thus necessary to perform a good estimate of the pairing strengths entering the BCS scheme. This was achieved by means of a fit of the odd-even staggering of the nuclear masses for some actinide nuclei, using the three-point mass formula (see Refs. [93, 94] for a more detailed discussion on the odd-even staggering calculations):

$$\Delta_q^{(3)}(N) = \frac{(-)^N}{2}\big[E(N+1) - 2E(N) + E(N-1)\big] \tag{4.1}$$

with q referring to the charge state of the odd number of nucleon, N, entering the equation above. Although the five-point mass formula, $\Delta^{(5)}$, has been reported to be better at projecting out the pairing contribution as compared to $\Delta^{(3)}$ [95], such an approach has not been pursued here. It should be noted that a recent work [96] utilized a similiar fit of the pairing force in the study of fission barriers of Thorium and Uranium isotopes.

The sets of nuclei chosen for the fit of the pairing strengths were selected on the basis of two criteria. The chosen nuclei have to be of a rigidly deformed shape in order to minimize the effect of nuclear vibration invalidating a single configuration description of the ground state. It is also important to ensure that the BCS approximation in the intended nuclei is satisfactory and therefore avoid cases of low pairing regime whereby the BCS scheme is known to be less appropriate. This was checked by comparing the calculated pairing gap of the neighbouring even-even nuclei to be within the range of 200 keV from the standard average value of $\frac{12.5\,\text{MeV}}{\sqrt{A}}$, where A is the nuclear mass number.

In view of these considerations, the calculations of the mass differences were performed for the following nuclei

(i) $^{231}_{90}$Th, $^{235}_{92}$U, $^{239}_{94}$Pu, $^{241}_{94}$Pu, $^{245}_{96}$Cm and $^{249}_{98}$Cf to determine the neutron pairing strength G_n

(ii) $^{229}_{89}$Ac, $^{237}_{93}$Np, $^{239}_{93}$Np, $^{241}_{95}$Am and $^{249}_{97}$Bk to determine the proton pairing strength G_p

The mass differences were calculated with two sets of pairing strengths (G_n, G_p) for the SkM* interaction entering the BCS scheme such that

$$\hat{v}^{(q)}_{k\bar{k}l\bar{l}} = -\frac{G_q}{11.0+N_q}(MeV) \tag{4.2}$$

where N_q is the number of nucleons of the charge state q. In some nuclei, the calculated lowest energy solution at ground state deformation may have K^π quantum numbers which may not correspond to the experimental I^π quantum numbers. In such cases, the mass differences were calculated for both blocked K^π configurations (i.e. blocked state corresponding the lowest-energy solution and the blocked state corresponding to the experimental I^π). The plot of the mass differences as a function of nucleon numbers are shown in Figure 4.2 and Figure 4.3 for the fit of neutron and proton pairing strengths, respectively. In both diagrams, the results corresponding to the experimental I^π quantum numbers are plotted with filled squares and circles, while the unfilled ones corresponds to the calculated lowest-energy solutions.

It is quite evident from the diagrams that the set of the pairing strengths (16.0, 16.0) yields a better agreement of the mass differences with the experimental ones, with some minimal exceptions in $^{245}_{96}$Cm and $^{249}_{97}$Bk. For a direct comparison of the mass differences obtained in the two sets of pairing strengths, we have tabulated only the calculated values for the blocked states corresponding to the experimental I^π quantum numbers in Table 4.1. The agreement between the calculated values with pairing strengths (16.0, 16.0) were found to be comparatively better, with a root-mean-square deviation of 118 keV for $\Delta_n^{(3)}$ and 119 keV for $\Delta_p^{(3)}$. These are to be compared with the root-mean-square deviations obtained with the pairing strengths (14.5,14.6) at 208 keV and 173 keV for the neutron and the proton charge states, respectively. In view of the better agreement with the experimental data when using the set of pairing strengths (16.0,16.0), these values were retained for the present work.

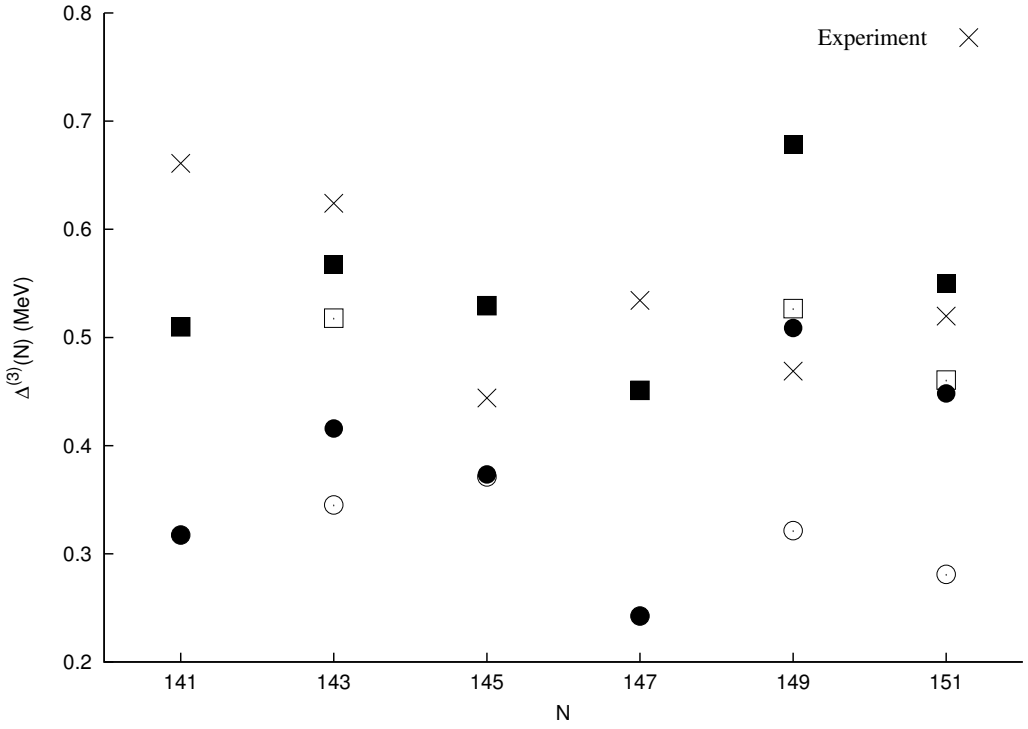

Figure 4.2: Plot of the three point mass difference formula for a series of isotopes, calculated within the HFBCS approach using SkM* parametrization of the Skyrme force in basis size of $N_0 = 14$. Data plotted in boxes and circles were calculated with pairing strengths (G_n , G_p) of (16.0 , 16.0) and (14.5 , 14.6) MeV respectively. In both cases, the filled squares (circles) corresponds to experimental K^π states while the unfilled ones correspond to the K^π configurations with the lowest calculated energy.

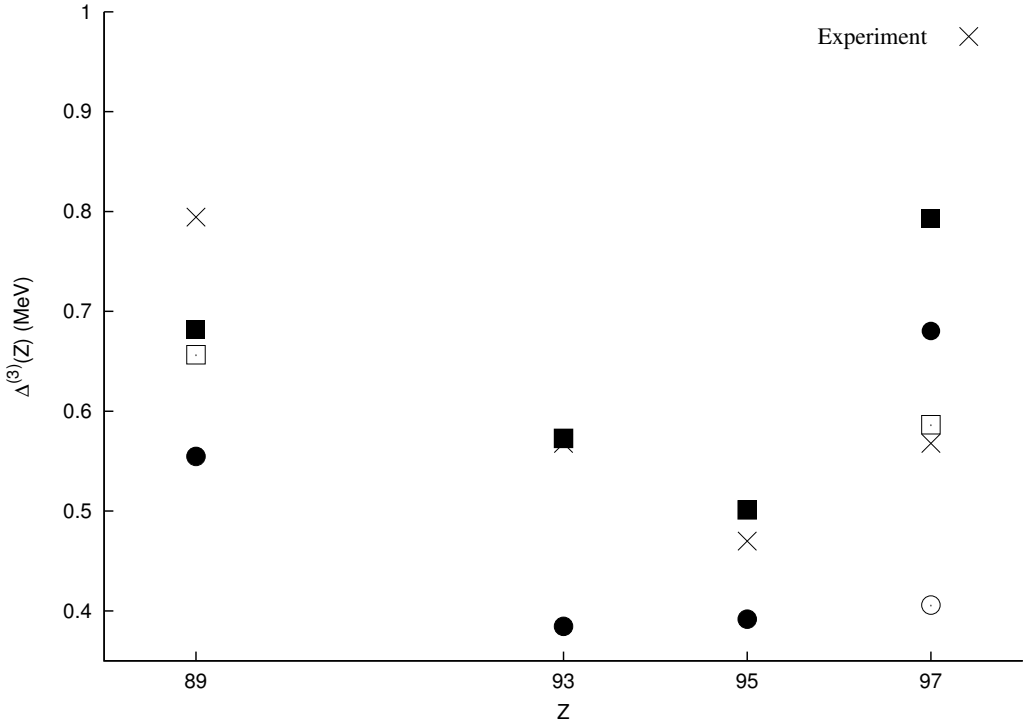

Figure 4.3: Similar to Fig. 4.2 but for a series of isotones.

Table 4.1: Calculated values of the odd-even mass difference $\Delta_q^{(3)}$ (in keV) with the SkM* parametrization for two pairs of pairing strengths (G_n, G_p) in comparison with experimental data (exp). The quoted values for the blocked state corresponds to the experimental I^π quantum numbers.

Nucleus	(16.0,16.0)	(14.5,14.6)	Exp
^{231}Th	510	317	661
^{235}U	567	416	624
^{239}Pu	525	373	444
^{241}Pu	452	242	534
^{245}Cm	678	509	469
^{249}Cf	550	448	520
^{229}Ac	681	555	794
^{237}Np	573	385	568
^{239}Np	568	391	594
^{241}Am	502	392	470
^{249}Bk	806	680	568

Table 4.2: Root-mean-square energy deviation of the calculated $\Delta_q^{(3)}$ quantities (in keV) with corresponding data given in Table 4.1. These results are presented for three groups: considering the sets of nuclei for (I) neutron pairing only, (II) proton pairing only and (III) both proton and neutron pairing strengths.

Group	(16.0,16.0)	(14.5,14.6)
(I)	118	207
(II)	119	174
(III)	119	193

The pairing strengths when employing the SIII interaction were fitted in similar manner leading to the retained pairing strengths of $G_n = 17.15$ MeV and $G_p = 14.0$ MeV [97]. A lesser version of the fit was performed for the pairing strengths when utilizing the SLy5* parametrization. The pairing strengths were obtained in this case by reproducing the BCS gap parameter of the ^{236}U and ^{240}Pu obtained earlier with the SkM* parametrization. The retained values of the pairing strengths with the SLy5* interaction are $G_n = 18.0$ MeV and $G_p = 17.0$ MeV. Using these pairing strengths, the $\Delta_n^{(3)}$ values corresponding to the calculated lowest-energy state and the blocked state yielding the experimental I^π quantum numbers are tabulated for the ^{239,241}Pu nuclei in Table 4.3 and compared with the data.

To sum up the discussion in this section on the determination of the BCS pairing strengths, the retained values are tabulated in Table 4.4 for each type of Skyrme parametrizations considered herein.

Table 4.3: Odd-even mass difference $\Delta_n^{(3)}$ (in keV) calculated with the SLy5* parametrization with pairing strengths $G_n = 18.0$ MeV and $G_p = 17.0$ MeV. The results for both solutions corresponding to the calculated and experimental ground states are given.

Nucleus	Calculated GS	Experimental GS	Exp
^{239}Pu	504	748	444
^{241}Pu	502	502	534

Table 4.4: The retained pairing strengths for the three considered Skryme parametrizations.

Skyrme force	G_n (MeV)	G_p (MeV)
SkM*	16.0	16.0
SIII	17.15	14.0
SLy5*	18.0	17.0

4.2.2 Effect of pairing on fission-barrier heights

Having obtained an optimal estimate of the pairing strengths, it would then be interesting to investigate the effect on the fission-barrier heights by changing their values. The test was made on the ^{240}Pu nucleus assuming axial and parity symmetry. The deformation energy as a function of quadrupole moment obtained with a lowering of the neutron pairing strength by 1 MeV is plotted on Figure 4.4. The corresponding fission-barrier heights are tabulated in Table 4.5. It appears that the decreasing the neutron pairing strength by 1 MeV would increase the inner and outer-barrier heights by about 0.6 MeV and 0.9 MeV, respectively. The fission-isomeric energy is less affected, with an increase of about 50 keV for the same amount of reduction in neutron pairing strength.

In order to assess the effect of proton pairing strength, a similar study were done by decreasing the proton strength by 1 MeV. The effect brought about due to the reduction of the proton pairing strength on the inner and outer-barrier heights are lesser when compared to the case of neutron pairing. It was found that the inner-barrier increases by 0.35 MeV and the outer-barrier by 0.26 MeV when decreasing the proton pairing strength by 1 MeV. However, the fission-isomeric energy is much affected (see Table 4.5) when the proton pairing strength is reduced. The fission-isomeric energy was found to increase by nearly 0.3 MeV when decreasing the proton pairing strength, in contrast to the case of neutron pairing whereby the fission-isomeric energy increases by an average of 0.06 MeV for the same amount of decrement in the pairing strength.

Through this assessment of the fission-barrier heights it points out that while the inner and symmetric outer-barrier are much affected by the pairing strength of both charge states, the isomeric energy is much

more sensitive to the proton pairing strength.

Table 4.5: The inner-barrier heights E_A, isomeric energies E_{II} and second barrier heights E_B of ^{240}Pu assuming axial and parity symmetry obtained with the SkM* interaction with different BCS pairing strengths (G_n, G_p). The energies are given in MeV. The locations of the global and second minimum, as well as the saddle points were determined using the modified Broyden's method (see Section 4.4).

Pairing strengths	E_A	E_{II}	E_B
(14.0,16.0)	9.40	2.65	12.02
(15.0,16.0)	8.79	2.60	11.11
(16.0,16.0)	8.18	2.53	10.18
(16.0,15.0)	8.53	2.81	10.44

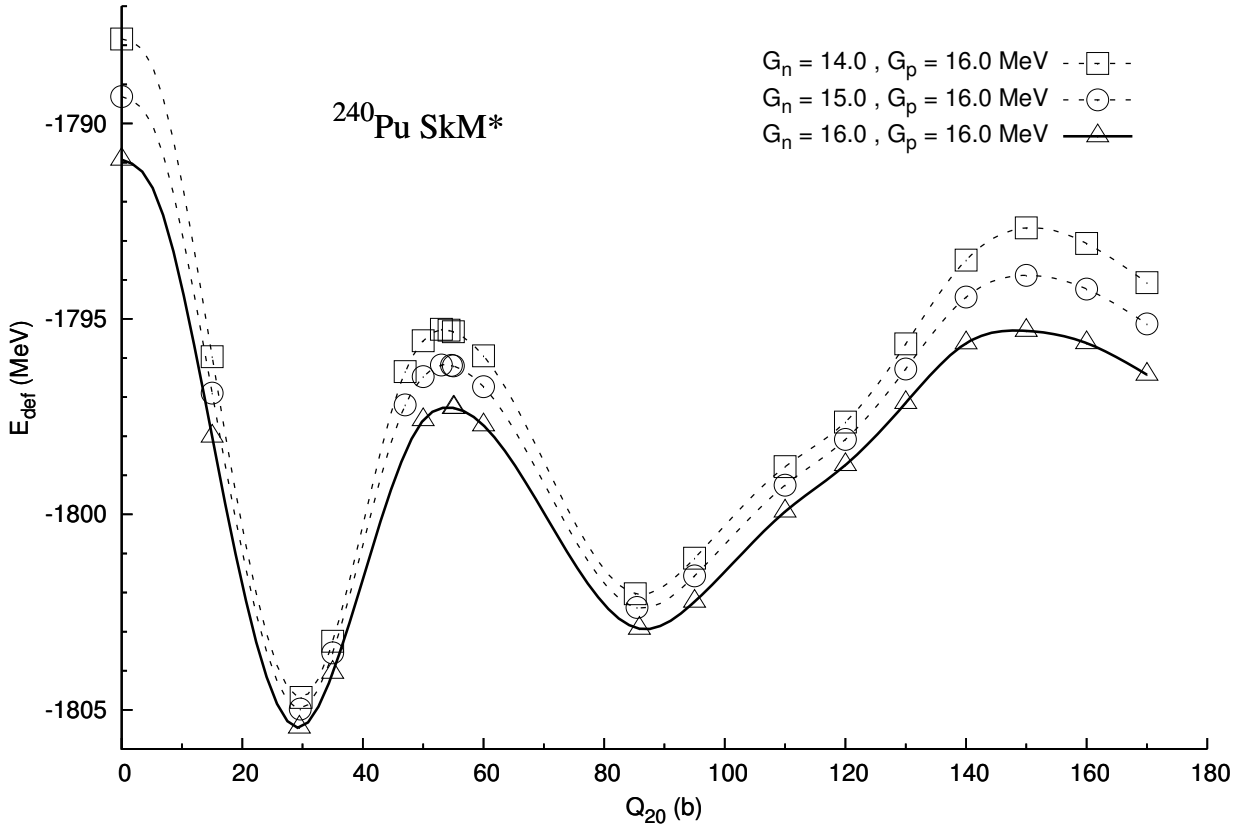

Figure 4.4: Deformation energy curves (in MeV) of ^{240}Pu as a function of quadrupole moment (in barns) calculated with the SkM* interaction with different values of the BCS neutron pairing strength, G_n, as indicated on the figure.

4.3 Some numerical aspects

4.3.1 Expansion of the single-particle wavefunctions on an axially symmetrical harmonic oscillator basis

In solving the one-body hamitonian $\hat{h}_{HF}$ by means of an iterative diagonalization process,

$$\hat{h}_{HF}|k\rangle = e_k|k\rangle \tag{4.3}$$

the single-particle states $|k\rangle$ were chosen to be represented in terms of an axially symmetrical harmonic oscillator basis states defined as

$$\phi_k(\mathbf{r},\sigma,q) = \chi_q \sum_\alpha C_\alpha^{(k)}\ \varphi_\alpha(\mathbf{r},\sigma) \tag{4.4}$$

in which χ_q is a function specifying the isospin state and the $\{C_\alpha^{(k)}\}$ set stands for the expansion coefficients of the eigenvector associated with the eigenvalue e_k. The notation α represents the various quantum numbers of the harmonic oscillator states. For an axially deformed harmonic oscillator Hamiltonian we have $\alpha \equiv \{n_z, n_r, l_z, s_z\}$ where n_z and n_r are the number of nodes in the z- direction and perpendicular direction respectively while l_z and s_z are the third component of the orbital angular momentum and spin quantum numbers, respectively. The harmonic oscillator wavefunctions in the cylindrical coordinate $\{\mathbf{r} = r, z, \varphi\}$ are written as:

$$\varphi_\alpha(\mathbf{r},\sigma) = \Gamma_{s_z}(\sigma)\ \psi_{n_z}(z)\ \psi_{n_r}^{l_z}(r)\ \frac{e^{il_z\varphi}}{\sqrt{2\pi}} \tag{4.5}$$

where the wavefunctions in the z- and perpendicular direction are written in terms of the Hermite polynomial $H_{n_z}(\xi)$ and the associated Laguerre $L_{n_r}^{l_z}(\eta)$ with

$$\xi = \beta_z z \qquad ; \qquad \eta = \beta_\perp^2 r^2 \tag{4.6}$$

such that:

$$\psi_{n_z}(z) = N_{n_z}\beta_z^{1/2} e^{-\xi^2/2} H_{n_z}(\xi) \tag{4.7}$$

and

$$\psi_{n_r}^{l_z}(r) = N_{n_r}^{l_z}\beta_\perp\sqrt{2}\ \eta^{l_z/2} e^{-\eta/2} L_{n_r}^{l_z}(\eta) \tag{4.8}$$

The normalization factors [98] are given as

$$N_{n_z} = \Big(\frac{1}{\sqrt{\pi}\ 2^{n_z} n_z!}\Big)^{1/2} \qquad ; \qquad N_{n_r}^{l_z} = \Big(\frac{n_r!}{(n_r+l_z)!}\Big)^{1/2} \tag{4.9}$$

while the oscillator parameters are written as

$$\beta_z = \sqrt{m\omega_z/\hbar} \qquad ; \qquad \beta_\perp = \sqrt{m\omega_\perp/\hbar} \tag{4.10}$$

In our approach, the total angular momentum Ω of the single-particle state written as

$$\Omega = l_z + s_z \tag{4.11}$$

and parity (when the parity symmetry is observed) given by

$$\pi = (-1)^{(n_z + l_z)} \tag{4.12}$$

are good quantum numbers. The single-particle states are divided into blocks categorized by Ω and π. As was discussed in Section 3.1.4, the single-particle states are sorted according to an increasing single-particle energies and are labelled by *rank*.

4.3.2 Optimization of basis parameters

Solving the one-body Hamiltonian in the single-particle states expanded on the deformed harmonic oscillator basis states requires in practice that the expansion to be truncated. The truncation is performed according to the prescription of Ref. [6] such that

$$\hbar\omega_\perp\left(n_\perp + 1\right) + \hbar\omega_z\left(n_z + \frac{1}{2}\right) \leq \hbar\omega_0\left(N_0 + 2\right) \tag{4.13}$$

One defines a spherical angular frequency, ω_0 in terms of the frequencies ω_z and $\omega_\perp$ defining the oscillator potential by $\omega_0 = \omega_\perp^2\,\omega_z$.

The oscillator parameter, $\beta_0 = \sqrt{\frac{m\omega_0}{\hbar}}$ and the deformation parameter, $q \equiv \frac{\omega_\perp}{\omega_z}$ are optimized to obtain the lowest energy at each deformation points in a chosen basis size,N_0. For computational time reasons, and also for the purpose of extracting out, within reasonable numerical effort, interesting physics with regards to the odd-mass nuclei, it has been deemed sufficient that calculations are restricted to the basis size of $\mathrm{N}_0 = 14$. Such a choice of deformed oscillator basis size corresponds to 15 spherical major shells. The b and q parameters for the calculations involving the SIII and SkM* interactions in odd-mass nuclei are optimized by minimizing the binding energy for its neighbouring even-even nuclei in this basis size at each deformation points. It was then checked that the same values obtained from the SkM* interaction are applicable for the SLy5* parameters sets, with a minimal variation in the binding energy of the order of tens of keV.

Some investigations on the truncation effect have been performed for some cases of the energy spectra and the fission-barrier heights. Table 4.6 shows the band heads energies calculated in two basis sizes with the SIII and SkM* interactions. The results between solutions for the two basis size differ only by some tens of keV. Therefore, the choice of the basis size $\mathrm{N}_0 = 14$ is appropriate and sufficient for comparison with the experimental data when values are of the order of hundreds of keV.

Table 4.6: Comparison of the calculated band heads energies (in keV) at the ground state of ^{239}Pu with the SIII and SkM* interactions for a basis size defined by $N_0 = 14$ and $N_0 = 16$.

K^π	$N_0 = 14$		$N_0 = 16$	
	SkM*	SIII	SkM*	SIII
$1/2^+$	0	0	0	0
$5/2^+$	121	359	134	367
$7/2^-$	27	95	38	97
$7/2^+$	1022	260	1010	265

The investigation of the basis size effect on fission-barrier heights was first performed for the even-even core ^{240}Pu considered as a test nucleus with the assumption of axial and parity symmetry along the whole fission path. Calculations were performed with the SkM* interaction for three basis sizes (N_0= 14, 16, 18). While it is desirable to optimize the b and q parameters for each basis size, the work of Ref. [60] comparing solutions which has been optimized in their respective basis size, has shown that the impact of the optimization process on the barrier heights is rather small. Furthermore, since the present purpose is only to test the accuracy of results as the function of the basis size, all other things kept constant, the same b and q parameters obtained earlier in the optimization process in $N_0 = 14$ are used. The locations of the saddle points as well as the ground state and second minima in the deformation energy surface were obtained by using the modified Broyden's method (kindly refer to Section 4.4 for further discusssions).

The fission-barrier heights obtained for the various basis sizes are shown in Table 4.7. From this table, we have an estimate of the basis size correction when comparing the barrier heights obtained in the basis size of $N_0 = 14$ and $N_0 = 16$. The truncation effect are shown to increase with deformation with a value of about 0.2 MeV for the inner-barrier and isomeric energy, and about twice the amount for the outer-barrier. The same amount of basis size effect was also to be expected for the odd-mass nuclei, as was shown in Table 4.7 for the blocked $5/2^+$ configuration of ^{239}Pu with the SkM* interaction. A rather similar estimate was obtained when computing the barrier heights with the SLy5* parametrization with a slightly larger correction of 0.1 MeV more than the corresponding values in the case of SkM* interaction for the second barrier height (refer Table 4.8).

It should be noted that a more thorough study of the deformation energy curves and the fission-barrier heights as a function of basis size have been performed in the work of Refs. [60, 54] for the ^{252}Cf nucleus with the SkM* parametrization (replicated here in Figure 4.5). The increase in the basis size translates into a downward shift of the deformation energy curves in terms of energy, with an optimal basis size of $N_0 = 16$.

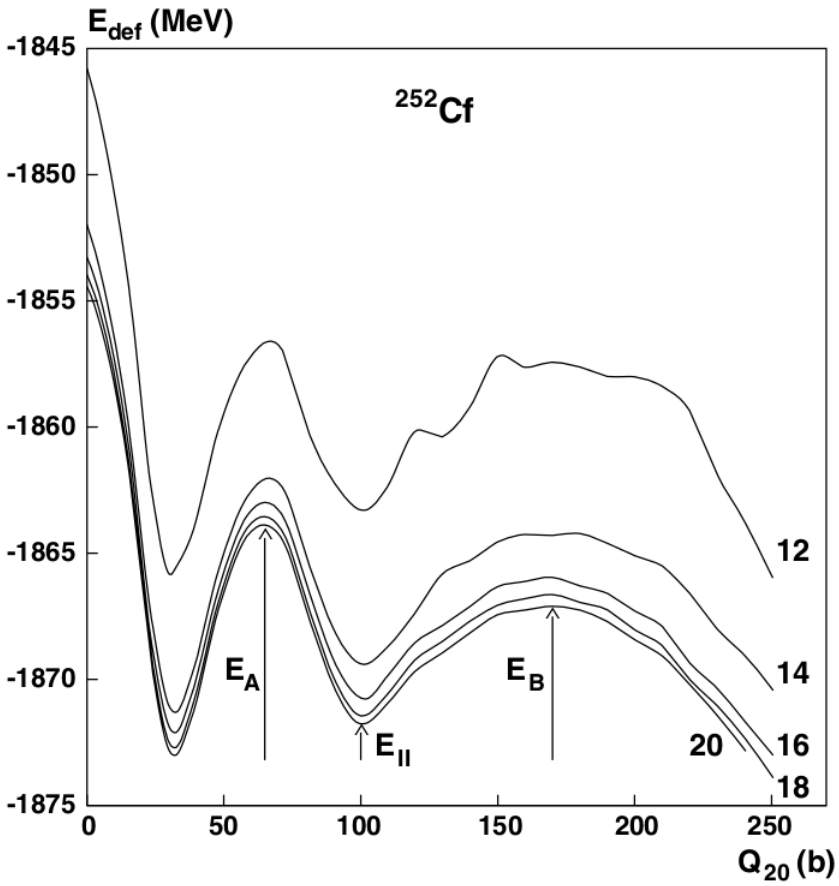

Figure 4.5: Effect of basis size N_0 parameter on the deformation energy curve for the ^{252}Cf nucleus obtained with the SkM* parametrization. The plot is taken from the work of Ref. [60].

As a short summary, the test of the basis size truncation effect provides a useful information on the convergence of the results with regards to the basis size in use. Firstly, it shows that the calculated band-head energy spectra are reasonably well converged when performing calculation in the basis size of $\mathrm{N}_0 = 14$. This provides a justification for performing the other calculations of the energy spectra with a similar choice of the basis size. Secondly, we have obtained estimates of the basis corrections to the fission-barrier heights for two Skyrme forces considered here.

Table 4.7: The inner-barrier E_A, fission-isomeric energy (E_{II} for even-even nucleus and E_{IS} for odd-mass nucleus) and outer-barrier E_B heights of ^{239,240}Pu with axial and parity symmetry in different basis sizes calculated with the SkM* interaction. The energies are given in MeV.

Nucleus	N_0	E_A	E_{IS} /E_{II}	E_B
^{239}Pu $(5/2^+)$	14	8.14	2.42	11.25
	16	7.97	2.22	10.83
	18	7.93	2.12	10.80
^{240}Pu	14	8.18	2.53	10.18
	16	8.00	2.31	9.76
	18	7.96	2.22	9.71

Table 4.8: Similiar to Table 4.7 but for the barrier heights of the $5/2^+$ blocked configuration of ^{239}Pu obtained with the SLy5* interaction.

Nucleus	N_0	E_A	E_{II}	E_B
^{239}Pu $(5/2^+)$	14	8.81	4.35	15.47
	16	8.62	4.15	14.93

4.3.3 Numerical integration

In solving the Hartree-Fock equation, one will need to evaluate matrix elements (equation (3.21)) which involve an integration over space. When representing the single-particle states in the deformed harmonic oscillator basis states, such an integration over the space coordinates could be written in a general form

$$\int\int e^{-\xi^2}\, e^{-\eta}\, g(\xi,\eta)\, d\xi\, d\eta \tag{4.14}$$

The numerical integration is performed by using the Gauss-Hermite and Gauss-Laguerre quadrature methods, such that

$$\int\int e^{-\xi^2}\, e^{-\eta}\, g(\xi,\eta)\, d\xi\, d\eta \;\approx\; \sum_{i=1}^{N_G^{(z)}} \sum_{j=1}^{N_G^{(r)}} w_i\, w_j\, f(\xi_i)\, f(\eta_j) \tag{4.15}$$

where the weighting factors $\{w_i\}$ and $\{w_j\}$ are given as [98]

$$w_i = \frac{2^{(N_G^{(z)}-1)}\, N_G^{(z)}!\, \sqrt{\pi}}{{N_G^{(z)}}^2 [H_{N_G^{(z)}-1}(\xi_i)]^2} \tag{4.16}$$

$$w_j = \frac{\eta_j}{(N_G^{(r)}+1)^2 [L_{N_G^{(r)}+1}(\eta_j)]^2} \tag{4.17}$$

The integration is performed at the roots of the Hermite polynomials, $H_n(\xi)$ and the Laguerre polynomials, $L_n(\eta)$ with the number of Gauss-Hermite and Gauss-Laguerre integration points given by $N_G^{(z)}$ and $N_G^{(r)}$ respectively.

An extensive evaluation of the impact of the number of Gauss-Hermite and Gauss-Laguerre points on the inner and outer-barrier of ^{252}Cf was done in the work of Ref. [60, 54]. It was found that at very large deformation where the basis parameter $q >> 1$, one would include basis states with higher number of n_z nodes. The number of Gauss-Hermite integration points $N_G^{(z)}$ should then be adjusted to accommodate the maximal value of n_z. For the basis size of $\mathrm{N}_0 \leq 20$, the value of $N_G^{(z)} = 50$ was reported to be a reasonable choice for a study of the deformation energy up to a point far beyond the top of the second fission-barrier. In the case where the parity symmetry is conserved, the integration is performed for $z > 0$ and this would involve 25 Gauss-Hermite integration points. In the perpendicular direction, the Gauss-Laguerre points of $N_G^{(r)} = 16$ was used.

4.4 Locating the top of the barrier using the modified Broyden's method

In the calculation of fission-barrier heights, one usually relies on the interpolation of some points around the barrier top in the deformation energy curves in order to estimate the top of the barrier. However, it was reported recently in the work of Ref. [99] that the modified Broyden's method was able to locate the exact maxima, in addition to the local minima, in the deformation energy curve of ^{212}Ra (as shown in Figure 4.6). It was also shown that the Broyden's method results in a faster convergence of the iterative process as compared to the usually used linear mixing. In view of the success of this method, the modified Broyden's method was incorporated and tested in the present calculations of odd-mass nuclei when parity is conserved.

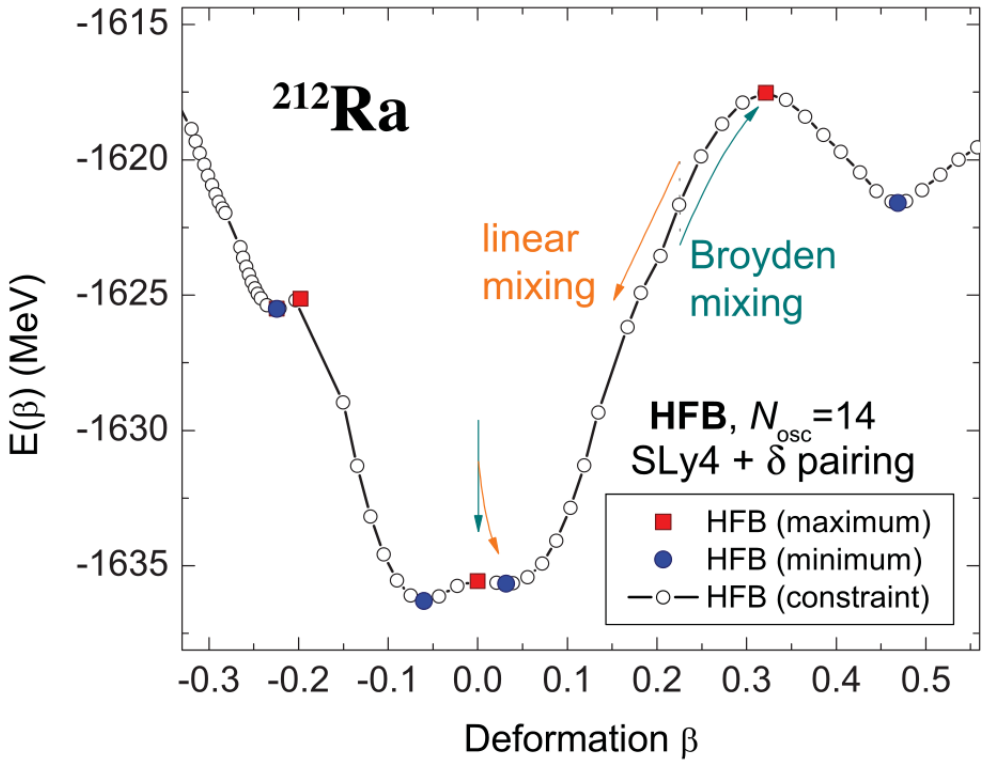

Figure 4.6: Location of local minima and maxima when using the modified Broyden's method. Extracted from Broyden's method in nuclear structure calculations by Baran *et al.* (2008) [99].

In solving self-consistent equations, one usually used as an input for iteration $m+1$ in the linear mixing method, a mixing of input and output at iteration m with mixing parameter α with $\alpha \in [0,1]$, such that

$$\begin{aligned} \mathbf{V}_{in}^{(m+1)} &= \alpha\,\mathbf{V}_{out}^{(m)} + (1-\alpha)\,\mathbf{V}_{in}^{(m)} \\ &= \mathbf{V}_{in}^{(m)} + \alpha\,\mathbf{R}^{(m)} \qquad ; \qquad \mathbf{R}^{(m)} = \mathbf{V}_{out}^{(m)} - \mathbf{V}_{in}^{(m)} \end{aligned} \tag{4.18}$$

where the input $\mathbf{V}_{in}^{(m)}$ at iteration m denotes, in our case here, a set of Hartree-Fock fields. With a proper choice of α, one may obtained converged solutions but the rate of convergence is rather slow in most cases. The modified Broyden's method which has been widely used in quantum chemistry was implemented in

nuclear structure calculations, and was reported to improve vastly the convergence rate as reported in Ref. [99], in addition to the fact that this method could be used to locate extremum points in the energy curve. The modified Broyden's mixing procedure is given by the expression [99, 100]

$$\mathbf{V}_{in}^{(m+1)} = \mathbf{V}_{in}^{(m)} + \alpha\,\mathbf{R}^{(m)} - \sum_{n=\tilde{m}}^{m-1} w_n\,\gamma_{mn}\,\mathbf{u}^{(n)} \tag{4.19}$$

with $\tilde{m} = \max(1, \mathrm{m} - \mathrm{M})$ where $M = 7$ was chosen in this work, while

$$\gamma_{mn} = \sum_{k=\tilde{m}}^{m-1} c_k^m\,\beta_{kn} \tag{4.20}$$

$$\mathbf{u}^{(n)} = \alpha\,\Delta\mathbf{R}^{(n)} + \Delta\mathbf{V}^{(n)} \tag{4.21}$$

where

$$\beta_{kn} = (w_0^2\,\mathbf{I} + \mathbf{a})_{kn}^{-1} \quad ; \quad \mathbf{a}_{kn} = w_k\,w_n\left(\Delta\mathbf{R}^{(n)}\right)^{\dagger}\Delta\mathbf{R}^{(k)} \tag{4.22}$$

$$c_k^m = w_k[\Delta\mathbf{R}^{(k)}]^{\dagger}\,\mathbf{R}^{(m)} \tag{4.23}$$

$$\Delta\mathbf{V}^{(n)} = \frac{\mathbf{V}_{in}^{(n+1)} - \mathbf{V}_{in}^{(n)}}{|\mathbf{R}^{(n+1)} - \mathbf{R}^{(n)}|} \tag{4.24}$$

$$\Delta\mathbf{R}^{(n)} = \frac{\mathbf{R}^{(n+1)} - \mathbf{R}^{(n)}}{|\mathbf{R}^{(n+1)} - \mathbf{R}^{(n)}|} \tag{4.25}$$

The weights associated with each previous iteration $w_n (n = 1, 2, 3..., M)$ was set to 1, while $w_0 = 0.01$ was chosen. When employing the modified Broyden's convergence method, the mixing parameter was chosen to be $\alpha = 0.5$. Starting with an initial input $\mathbf{V}_{in}^{(0)}$, one performs the calculation to obtain the first output solution $\mathbf{V}_{out}^{(0)}$. The input for the next iteration $m = 1$, is a linear mixing between $\mathbf{V}_{in}^{(0)}$ and $\mathbf{V}_{out}^{(0)}$. It is only at iteration $m = 2$ and above that the Broyden correction term is contributing to determine the input for the next iteration.

In order to locate the extrema in the energy curve, the calculations are performed as described below. The deformation energy curve as a function of the quadrupole moment is first obtained with the usual constrained HF-BCS calculation with axial symmetry. This would give an estimate of the location of the top of the barrier. Starting from the converged solution within the vicinity of the barrier top, one then obtain the maxima point by performing an unconstrained HF-BCS calculation with Broyden mixing. It was found that the Broyden's method is able to locate the lowest-energy solution at the top of the barrier in the (Q_{20}, Q_{40}) planes.

In some cases, the location of the top of the barrier using Broyden's method may differ from the usual way of estimating the barrier top from interpolation of the total energy as a function of Q_{20} only. This was found to be the case, for example in the $7/2^-$ blocked state of ^{239}Pu calculated with the SkM* interaction (refer to Figure 4.7). When considering the constrained HF-BCS solution along the Q_{20} direction assuming

axial symmetry, one would find that the height of the inner-barrier is about 9.4 MeV whereas the Broyden's solution is about 400 keV lower. In order to investigate the appropriateness of the Broyden's solution at the top of the barrier, calculations constraining on the hexadecapole moment Q_{40} with a fixed value $Q_{20} = 50b$ were performed. The plot of the total energy as a function of Q_{40} is plotted as an inset of Figure 4.7. The results shows that there exists a solution with lower energy at a different Q_{40} value as compared to the initial calculation without a constraint on Q_{40}. When considering the local minima solution in the Q_{40} direction, it is found that the Broyden's solution does correspond to the actual top of the inner-barrier, confirming that the modified Broyden method is appropriate and efficient to locate the top of the barrier in our calculations. Moreover, the comparison between the results obtained with and without constraint on Q_{40} seems to suggest that constraining on Q_{20} alone may not be sufficient and that an extra constraint is needed to obtain the lowest-energy solution for a given Q_{20}.

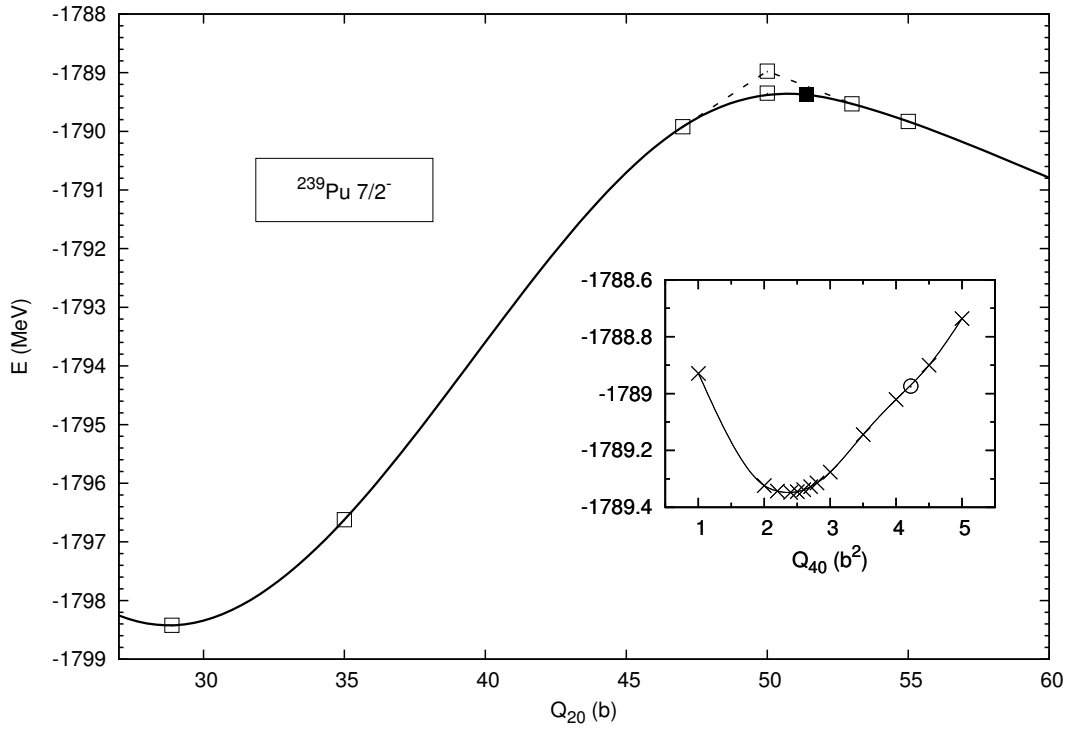

Figure 4.7: A portion of the deformation energy curve of ^{239}Pu calculated with a blocked $7/2^-$ state from the normally deformed ground state to around the top of the inner-barrier. The top of the inner-barrier obtained by using the Broyden's method is shown by the filled square. Inset: Plot of the energy as a function of the hexadecapole moment Q_{40} with a value $Q_{20} = 50$b. The result at $Q_{20} = 50$b obtained without constraint on Q_{40} corresponds to a solution with higher binding energy as shown here by a circle.

4.5 Implementation of the blocking procedure

As previously mentioned, only a *seniority-one* state is considered for the description of odd-mass nuclei in this thesis work. This is achieved by blocking one single-particle state $|\phi^{(k)}_{K,\pi}\rangle$ with the desired $\Omega^\pi = K^\pi$ quantum numbers nearest to the Fermi level. For self-consistent blocking (SCB) calculations, the occupation probability for the single-particle state to be blocked is set to 1, while its conjugate state $|\tilde{\phi}^{(k)}_{K,\pi}\rangle$ is set to 0. On the other hand, the *equal filling approximation* which is also considered herein to study the impact of the time-reversal symmetry breaking in some cases was performed by setting the occupation probabilities of both single-particle states to 0.5.

The choice of the single-particle state to be blocked was automated in the code based on the energy distance from the Fermi level. In this way, the *rank* of the blocked single-particle state may changed from one iteration to another. This was indeed the case when there are more than one single-particle state with the same Ω^π quantum numbers near the Fermi level. The oscillation from one blocked single-particle state to another may prevent one from arriving at a converged solution. When this problem occurs, we are then forced to perform two sets of calculations, one for each blocked single-particle state with fixed rank and then to choose among them, the solution which corresponds to the lowest total binding energy.

It has also been found for some isolated cases that blocking the single-particle state closest to the Fermi level whereby the Fermi level is as defined in equation (3.31) may not yield the lowest-energy HF+BCS solution. In order to obtain the lowest-energy solution, one needs to block instead the single-particle state with the desired Ω^π quantum numbers nearest to the BCS chemical potential (denoted by λ in equation (3.74)). In the present work, we verify that the solution is indeed the lowest-energy HF+BCS solution by manually inspecting the single-particle energy spectra obtained from a converged solution. A second calculation is then performed by specifying specifically the *rank* of the single-particle state to be blocked, if the automated selection of the blocked state does not yield the single-particle state nearest to the BCS chemical potential.

Chapter 5

SPECTROSCOPIC PROPERTIES OF ODD-MASS ACTINIDES

This chapter shall be devoted to the spectroscopic properties at the ground-state and fission-isomeric wells. Two odd-neutron (odd-mass nucleus with an odd numbers of neutron) nuclei namely ^{235}U and ^{239}Pu and two odd-proton (odd-mass nucleus with an odd numbers of proton) nuclei namely ^{237}Np and ^{241}Am are considered at the ground-state well, whereas only the two odd-neutron nuclei were considered for the fission-isomeric well. We shall first discussed the static moments, namely the charge quadrupole moments and the magnetic moments in the ground-state deformation obtained from the mean-field calculations in Section 5.1. This section serves in someway as an assessment of the mean-field solutions before comparing the calculated band-head energies with the experiment. The band-head energies evaluated from the Bohr-Mottelson unified model will be presented in Section 5.2 for the ground-state well and in Section 5.3 for the fission-isomeric well. The last two sections will be devoted to technical details of the mean-field approach. In Section 5.4, we shall discussed the effect on the band-head energies of the ground-state well when the calculations employing the SkM* and the SIII parametrizations were performed in a different manner from which they were initally fitted with respect to the time-odd densities. Finally, we shall briefly discussed the effect of performing calculations with a conserved time-reversal symmetry within the so-called equal filling approximation (EFA) on the ground-state band-head energies in Section 5.5.

5.1 Static moments in the ground state well

The intrinsic charge quadrupole moment of the neighbouring even-even core nuclei calculated with the SIII, SkM* and SLy5* parametrizations are shown in Table 5.1. The root-mean-square (r.m.s) deviation of the charge quadrupole moment obtained with the SkM* and SIII parametrizations are 0.19 and 0.26 barn, respectively. The intrinsic charge moment obtained with the SLy5* parametrization agree best with the experiment among the three Skyrme forces with a r.m.s deviation of 0.11 barn. Having shown good agreement between the calculated and experimental intrinsic charge quadrupole moment of the even-even core nuclei, similar comparison is also made for the odd-mass nuclei.

Table 5.1: Intrinsic charge quadrupole moment (in barn) of the even-even core nuclei calculated with the SkM* and SIII parametrizations in the *minimal time-odd* scheme and the SLy5* in the *full time-odd* scheme. The experimental values deduced from the $B(E2)$ value of Ref. [101] are shown. The numbers in parentheses represents the uncertainty in the last digits.

Nucleus	SkM*	SIII	SLy5*	Exp
^{234}U	10.48	10.14	10.26	10.35(10)
^{236}U	10.79	10.37	10.62	10.80(7)
^{238}Pu	11.49	11.16	11.34	11.26(8)
^{240}Pu	11.71	11.27	11.51	11.44(13)

Comparison between the intrinsic Q_0 and spectroscopic charge quadrupole moment $Q^{(s)}$ of the odd-mass nuclei can made using the relation:

$$\mathrm{Q^{(s)}} = \frac{3\mathrm{K}^2 - \mathrm{I(I+1)}}{(\mathrm{K}+1)(2\mathrm{I}+3)}\mathrm{Q_0} \tag{5.1}$$

where K is the projection of the total angular momentum on the z- axis. The spectroscopic charge quadrupole moment $Q^{(s)}$ for the odd-mass nuclei obtained with the three Skyrme parametrizations are tabulated in Table 5.2. At the moment, there is no known experimental data on spectroscopy charge quadrupole moment of ^{239}Pu available for comparison. However, three out of the four band-heads available for comparison shows that the calculated spectroscopic quadrupole moments differ, at most, by 0.2 barn when compared to the experimental data. The experimental data of ^{241}Am is less well established. The calculated values, nevertheless, lies within the error bars of two of the three experimental values.

Table 5.2: Calculated values of the spectroscopic (charge) quadrupole moment (in barns) of odd-mass nuclei obtained with the SkM* and the SIII parametrizations in the *minimal time-odd* scheme while the SLy5* in the (*full time-odd densities scheme*). The experimental data compiled in [102] are shown for comparison.

Nucleus	K^π	SkM*	SIII	SLy5*	Exp.
^{235}U	$7/2^-$	4.98	4.78	4.92	4.936(6)
					4.55(9)
^{237}Np	$5/2^+$	4.01	3.90	3.97	+3.866(6)
	$5/2^-$	3.96	3.89	3.92	+3.85(4)
^{241}Am	$5/2^-$	4.30	4.24	4.25	+3.81(1.2)
					+3.14(5)
					+4.20(13)

We now present the total magnetic moment for the considered odd-mass nuclei. The total magnetic moment $\mu_{\rm tot}$ is given by the sum of the intrinsic magnetic moment $\mu_{\rm intr}$ and the collective magnetic moment $\mu_{\rm coll}$ given by:

$$\mu_{\rm tot} \;=\; \mu_{\rm intr} \;+\; \mu_{\rm coll} \tag{5.2}$$

The intrinsic magnetic moment is obtained by evaluating the expectation value of the magnetic dipole moment operator projected on the symmetry axis (chosen to be the z-axis here), $\hat{\mu}_z$ written as:

$$\mu_{\rm intr} = \frac{K}{K+1}\langle\Psi_{BCS}|\hat{\mu}_z|\Psi_{BCS}\rangle \tag{5.3}$$

The one-body operator $\hat{\mu}_z$ is defined as

$$\hat{\mu}_z \;=\; g_l^{(q)}\,\hat{l}_z \;+\; g_s^{(q)}\,\hat{s}_z \tag{5.4}$$

with $\hat{l}_z$ and $\hat{s}_z$ being the projection of the single-particle orbital and spin angular momentum on the symmetry z- axis. The spin gyromagnetic ratios are given by $g_s^{(n)} = -3.826085$ and $g_s^{(p)} = 5.585695$ while the corresponding orbital gyromagnetic ratios are $g_l^{(n)} = 0$ and $g_l^{(p)} = 1.0$ for neutrons and protons, respectively.

The collective magnetic moment is related to the collective gyromagnetic ratio g_R given by:

$$\mu_{\rm coll} = \frac{K}{K+1}\,g_R \tag{5.5}$$

with

$$g_R \;=\; \frac{\sum_{k,l}\langle l|\hat{\mu}_-|k\rangle\langle k|\hat{j}_+|l\rangle(u_k v_l - u_l v_k)^2/(E_k+E_l)}{\sum_{k,l}\langle l|\hat{j}_-|k\rangle\langle k|\hat{j}_+|l\rangle(u_k v_l - u_l v_k)^2/(E_k+E_l)} \tag{5.6}$$

where u_k and v_k are the BCS probability amplitudes of the single-particle state $|k\rangle$ to be empty and occupied, respectively with quasi-particle energy E_k. The operators $\hat{j}_\pm = \hat{j}_x \pm i\,\hat{j}_y$ are the angular momentum raising and lowering operators, with similar expression for $\hat{\mu}_\pm$. The g_R value have been calculated for a polarized even-even $(A-1)$ core nucleus, whose self-consistent fields were obtained from the blocking calculations of the odd-mass nucleus with mass number A.

The calculated intrinsic, collective and total magnetic moments are tabulated in Table 5.3 together with experimental values taken from Ref. [102]. It should be noted that such a study on the magnetic moments have been reported in Ref. [27]. The results obtained with the SIII parametrization herein are slightly different than the corresponding values reported in Ref. [27] due to the difference in the BCS pairing strengths and also possibly due to the harmonic-oscillator basis parameters. From the small sample of nuclei considered here, the results obtained with the SIII parametrization gives better agreement to the experimental data. The root-mean-square deviation for the SIII parametrization is 0.47, as compared to 0.59 and 0.61 for the SLy5* and the SkM* parametrizations, respectively (with values given in units of nuclear magneton μ_N).

Table 5.3: The calculated total magnetic moment μ_{tot} (in units of nuclear magneton μ_N), is a sum of the intrinsic magnetic moment μ_{intr} and the collective magnetic moment μ_{coll} which are shown for each Skyrme parametrization in used, and compared to the experimental data [102]. The collective gyromagnetic ratios denoted as $g_R^{(pol)}$ so as to reflect that this quantity was calculated from the underlying polarized even-even core.

Nucleus	μ_{intr}			$g_R^{(pol)}$			μ_{coll}			μ_{tot}			μ_{exp} [102]
	SkM*	SIII	SLy5*	SkM*	SIII	SLy5*	SkM*	SIII	SLy5*	SkM*	SIII	SLy5*	
^{235}U ($7/2^-$)	-0.665	-0.763	-0.988	0.385	0.529	0.355	0.300	0.412	0.276	-0.365	-0.351	-0.712	-0.38(3)
^{239}Pu ($1/2^+$)	0.148	0.262	0.334	0.338	0.540	0.349	0.113	0.180	0.116	0.261	0.442	0.450	0.203(4)
($5/2^+$)	-0.298	-0.810	-0.950	0.341	0.557	0.336	0.244	0.398	0.240	-0.054	-0.412	-0.570	-1.3(3)
^{237}Np ($5/2^+$)	2.661	2.666	2.878	0.259	0.363	0.248	0.185	0.259	0.177	2.846	2.925	3.055	3.14(4)
($5/2^-$)	0.909	0.829	0.619	0.263	0.453	0.254	0.188	0.324	0.181	1.097	1.153	0.800	1.68(3)
^{241}Am ($5/2^-$)	0.895	0.833	0.617	0.258	0.465	0.277	0.184	0.332	0.198	1.079	1.165	0.815	1.58(1)

5.2 Band-head spectra at the ground state deformation

Since the present approach considers a one quasi-particle blocked state (seniority one), band-head at higher excitation energy which may involve a more complicated many-body structure (i.e. higher seniority states) are not considered herein. Therefore, only the states found within 650 keV excitation energy in the experimental spectrum are considered for the blocked HF+BCS calculations. The results obtained from the HF+BCS calculations have been interpreted within the Bohr-Mottelson unified model without taking into account the contribution from the rotational energy term. In doing so, we assume that the effect of the rotational correction on the band-head excitation energies corresponding to the same deformation could be neglected. However, the rotational correction will be taken into account when calculating the fission-barrier heights where such a correction is known to have an important effect.

As explicitly shown in equation (3.104), the total energy in the Bohr-Mottelson model requires the evaluation of the moment of inertia at specific nuclear deformation for each band-head characterized by the K^{π} quantum numbers. Two sets of the moment of inertia have been considered in the present calculations. On one hand, we have considered the moment of inertia obtained with the Belyaev formula with a renormalization of 32% due to the omission of the Thouless-Valatin terms. On the other hand, we have also considered the empirical moment of inertia obtained from Ref. [103] in which the study of the rotational bands in this mass region has been carefully performed some years ago.

Both sets of moment of inertia have been used to calculate the excitation energy of the odd-mass nuclei, taking as reference the state having the same quantum numbers as the experimental ground-state. The excitation energies are tabulated in Table 5.4 whereby the results obtained with the empirical moment of inertia are given in parentheses. The negative excitation energies are due to the fact that the calculated lowest-energy solution may not necessary corresponds to the same quantum numbers as the experimental ground-state. Comparison of the results in Table 5.4 shows that the excitation energies calculated with the two sets of moment of inertia differ only by some tens of keV. This is despite of the relatively large difference of about a factor 2 between the calculated and the empirical moment of inertia.

The excitation energies of the two odd-neutron nuclei obtained with the calculated moment of inertia are plotted in Figure 5.1. The spectra calculated using the SIII interaction appears to be qualitatively more consistent with the experimental data, with the spectra from the SLy5* interaction being the least good among the three considered Skyrme parametrizations. This has been assessed by calculating the root-mean-square (r.m.s) energy deviation from the data for the six excited states in ^{235}U and the three excited states in ^{239}Pu. The r.m.s. energy deviation was found to be about 250 keV, 350 keV and 650 keV for the SIII, the SkM* and the SLy5* interactions, respectively. It should be noted that some Coriolis inter-band coupling between the $I = 5/2^{+}$ and $I = 7/2^{+}$ states in the 350-500 keV range in ^{235}U cannot be *a priori* ruled out, which may potentially perturbed our direct comparison of the calculated results with the experimental data.

The band-head energy spectra of the odd-proton nuclei are plotted in Figure 5.2. The agreement of the

calculated results to the experiments are slightly worse in this case for the SIII and SkM* parametrizations. The r.m.s energy deviation for the seven excited states considered in ^{237}Np and ^{241}Am were found to be about 450 keV and 500 keV for the SIII and the SkM* parametrizations. On the other hand, the agreement to the experimental band-head energies was found to be better for the odd-proton nuclei as compared to the odd-neutron nuclei when using the SLy5* interaction, with a r.m.s energy deviation of about 460 keV for the former.

An explanation for the difference in quality of our evaluation of the odd-neutron and odd-proton nuclei especially for the case when using the SIII and SkM* parametrizations could possibly be due to the used of the Slater approximation to treat the Coulomb exchange term. As noted in earlier papers (e.g. Refs. [56, 57]) and explained in Ref. [58], there is a systematic and significant bias in the single-particle proton spectra brought by this approximation: the occupied states are unevenly shifted upwards and the unoccupied states downwards, which perturbs in an uncontrolled fashion the relative ordering of nuclear levels. Some exact calculations of the Coulomb two-body interaction would be required in order to assess the effect of this approximation on the odd-proton nuclear spectra. This would require a significant numerical effort for such very heavy nuclei in general and even more so upon breaking the time-reversal symmetry, and is therefore not attempted for the current work. Finally, we would like to note that the spectroscopy results presented in this section have been submitted for publication in Ref. [97].

Table 5.4: Excitation energies $\Delta E_{\alpha K\pi}$ (without rotational correction) of band-head states with respect to the ground state, energy parameters $A = \frac{\hbar^2}{2\alpha\mathcal{J}}$ (where $\alpha = 1.32$ is the Thouless–Valatin correction factor from Ref. [71]) and decoupling parameters a calculated within our approach (SIII, SkM* and SLy5* columns) and compared with experimental values (exp) for which A and a are taken from the study of Jain and collaborators [103]. The band-head energies in parenthesis and italic are obtained using the values of A and a from Ref. [103]. The values obtained with the SkM* and SIII parametrizations are obtained in the *minimal time-odd* scheme while those from the SLy5* were obtained in the *full time-odd* scheme.

Nucleus	K^π	$\Delta E_{\alpha K\pi}$ (keV)				A (keV)				a (keV)			
		SkM*	SIII	SLy5*	exp	SkM*	SIII	SLy5*	exp	SkM*	SIII	SLy5*	exp
^{235}U	$7/2^-$	0	0	0	0	12.60	10.88	12.14	5.1	-	-	-	
	$1/2^+$	−123 (*−78*)	93 (*124*)	-899 (*−860*)	0.076	11.00	9.51	11.35	6.0	−0.26	−0.65	-0.61	−0.28
	$5/2^+$	−24 (*0*)	630 (*628*)	-464 (*−443*)	129.30	11.44	10.21	11.76	6.0	-	-	-	-
	$5/2^+$	422 (*439*)	614 (*650*)	-285 (*−269*)	332.84	11.69	10.05	11.69	4.9	-	-	-	-
	$3/2^+$	644 (*680*)	528 (*557*)	195 (*229*)	393.20	11.85	10.40	11.65	6.6	-	-	-	-
	$7/2^+$	1191 (*1217*)	597 (*612*)	217 (*229*)	445.70	10.78	10.53	12.35	7.1	-	-	-	-
	$5/2^-$	640 (*657*)	626 (*639*)	-684 (*−675*)	632.90	12.13	10.70	13.38	5.4	-	-	-	-
^{239}Pu	$1/2^+$	0	0	0	0	11.06	9.06	11.86	6.3	−0.40	−0.74	-0.70	−0.58
	$5/2^+$	141 (*121*)	368 (*359*)	-208 (*−222*)	285.50	11.29	9.23	11.15	6.4	-	-	-	-
	$7/2^-$	77 (*27*)	126 (*95*)	-9 (*−52*)	391.60	12.46	10.08	12.45	4.8	-	-	-	-
	$7/2^+$	1054 (*1022*)	280 (*260*)	320 (*290*)	511.80	11.20	9.44	11.64	5.9	-	-	-	-
^{237}Np	$5/2^+$	0	0	0	0	11.08	10.83	10.74	4.7	-	-	-	-
	$5/2^-$	59 (*66*)	−251 (*−237*)	-320 (*−312*)	59.5	10.90	9.32	10.67	6.2	-	-	-	-
	$1/2^-$	1091 (*1149*)	463 (*522*)	1026 (*1084*)	281.35	11.08	9.87	11.16	6.9	1.69	2.08	1.80	-1.67
	$1/2^+$	908 (*981*)	360 (*410*)	538 (*624*)	332.40	10.50	8.82	10.91	6.2	5.09	3.29	6.15	1.08
	$3/2^-$	367 (*385*)	970 (*988*)	175 (*192*)	514.20	10.69	10.19	10.70	6.3	-	-		-
^{241}Am	$5/2^-$	0	0	0	0	10.18	9.02	10.78	5.9	-	-		-
	$5/2^+$	52 (*40*)	−705 (*−723*)	-185 (*−197*)	205.90	10.76	10.59	11.45	4.2	-	-		-
	$3/2^-$	53 (*63*)	1 (*6*)	-122 (*−111*)	471.80	10.18	9.52	10.88	6.5	-	-		-
	$1/2^+$	1255 (*1298*)	363 (*390*)	995 (*1075*)	623.10	9.65	8.45	10.80	6.0	3.03	2.08	5.98	0.67

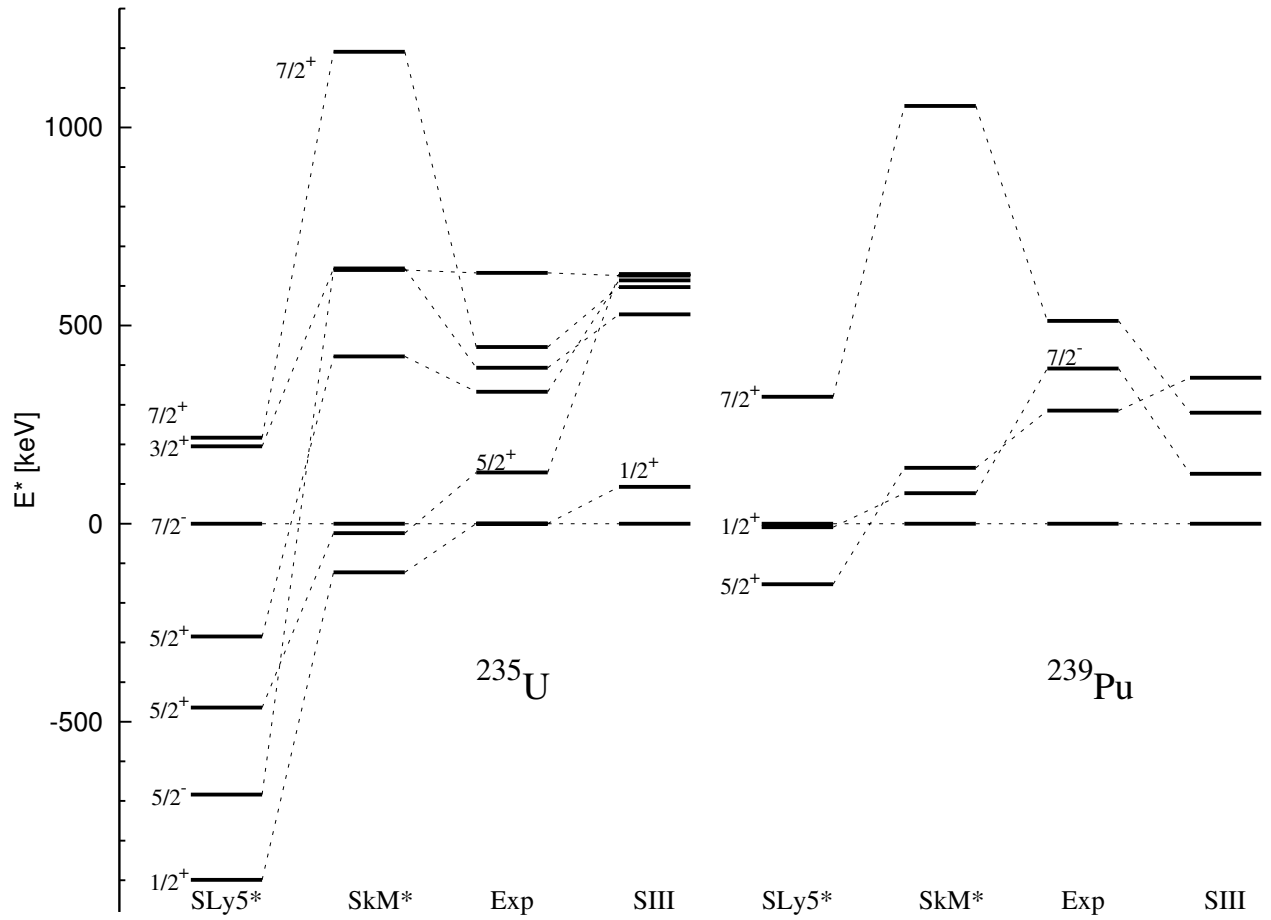

Figure 5.1: Partial band-heads of ^{235}U and ^{239}Pu calculated with the SkM* and SIII interactions without rotational correction in the *minimal time-odd* scheme and the SLy5* in the *full time-odd* scheme with comparison to the experiments.

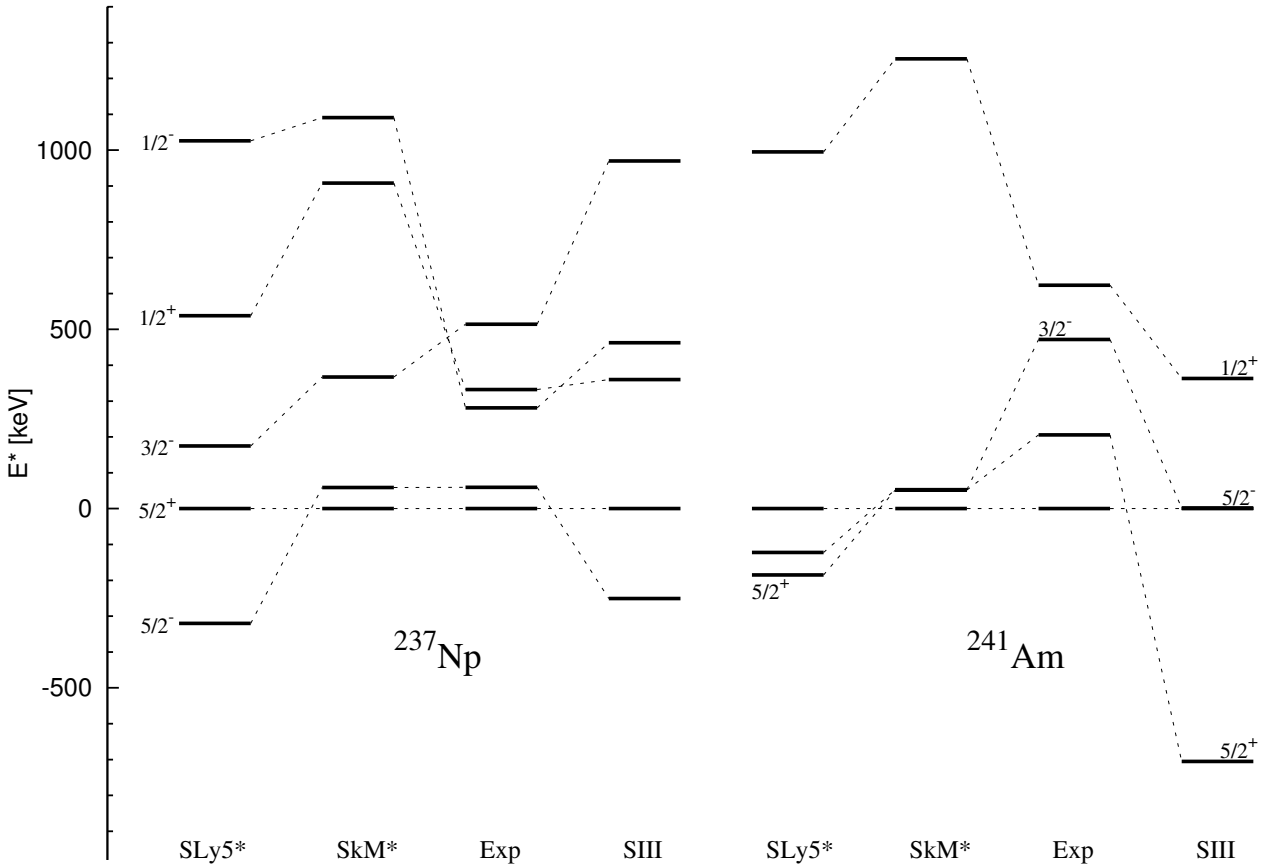

Figure 5.2: Partial band-heads of ^{237}Np and ^{241}Am calculated with the SkM* and SIII interactions without rotational correction in the *minimal time-odd* scheme while the SLy5* interaction in the *full time-odd* scheme with comparison to the experiments.

5.3 Spectroscopic properties in the isomeric well

Moving now to the discussion on the results obtained in the fission-isomeric well for the ^{235}U and ^{239}Pu nuclei. A quantity of interest is the the fission-isomeric energy E_{II} which is defined as the energy difference between the lowest-energy solutions denoted here as E_0, irrespective of the K^π quantum numbers at the ground-state (GS) and the fission-isomeric well (IS) such that

$$E_{II} = \left(E_0\right)_{IS} - \left(E_0\right)_{GS} \tag{5.7}$$

On top of the lowest-energy solution at the fission-isomeric well are the band-head excited states similar to the band-heads in the ground-state deformation well. These two informations have been sketched in Figure 5.3 and Figure 5.4 for the ^{239}Pu and ^{235}U nuclei, respectively. These results have been obtained with the inclusion of rotational correction whereby the approximate Thouless-Valatin corrective term have been taken into account in the calculations of the moment of inertia. The moment of inertia for the various blocked K^π configurations in the fission-isomeric well are listed in Table 5.5.

Let us first discuss the energy spectra for the ^{239}Pu nucleus for which a comparison with the experimental data of Ref. [104, 105] are available. As shown in Figure 5.3, the experimental ground state quantum numbers at the normal-deformed well is a $1/2^+$ state while it is a $5/2^+$ state in the fission-isomeric well. These exact sequence of states was reproduced by the SkM* and the SIII parametrizations. On the contrary, the solutions obtained with the SLy5* interaction shows a $5/2^+$ state in the normal-deformed solution and a $1/2^+$ lowest-energy state in the fission-isomeric well. The E_{II} value obtained with the SkM* interaction is much too compressed when compared to the experiment, while the corresponding value obtained with the SLy5* interaction appears to be within a more reasonable range when compared to the experimental value.

The rather good agreement of the E_{II} obtained with the SLy5* interaction is watered-down immediately when comparing the experimental first excited state ($K^\pi = 9/2^-$) in the fission-isomeric well to the calculated results. The $K^\pi = 9/2^-$ state appears at a much higher energy at 549 keV above the fission-isomer ground-state $K^\pi = 1/2^+$ solution. The excited $9/2^-$ state appears at 139 keV for the SkM* interaction and 127 keV for the SIII interaction, above the ground-state $5/2^+$ solution in the fission-isomeric well. These values can be expected to be favorably improved when comparing the effect of Coriolis coupling, as suggested from the work of Ref. [18] for the calculations of band-heads energies in the fission-isomeric well of ^{239}Pu using the SIII parametrization. In addition, a $11/2^+$ excited state was predicted at 151 keV, 129 keV and 299 keV with the SLy5*, the SkM* and the SIII parametrizations, respectively. The $11/2^+$ state was predicted at 44 keV excitation energy in the work of Ref. [22].

The rotational bands built on the $5/2^+$ band-head were also compared to the available experimental data. The calculated rotational energies for the first two excited states evaluated within our Bohr-Mottelson unified model were found to be rather similiar when going from one Skryme force to another, and they compares well with the experiment.

Let us now move to the results for the ^{235}U nucleus as sketched in Figure 5.4. To the best of our knowledge, there were no experimental data available for comparison with our calculated values in the superdeformed well of ^{235}U. There is, however, some calculations performed with the Gogny force in the work of Ref. [21] which predicted a $5/2^+$ ground state with a first excited state at 120 keV in the isomeric well of this nucleus. The same level sequence of a $5/2^+$ ground-state followed by a $11/2^+$ excited state was also obtained with the SkM* and the SLy5* interactions, although the $11/2^+$ state is located at a much higher energy in the latter Skyrme parametrization. The calculations with the SIII interaction yields the opposite level sequence, with a $5/2^+$ state at 66 keV above the $11/2^+$ ground-state.

We shall now return to the discussion on the fission-isomeric energy E_{II} with emphasis on the effect of rotational correction. As discussed before, the rotational correction calculated using the Belyaev formula was found to be too large, resulting in an underestimation of the fission-barrier heights. Another way to improve on the overestimation of the rotational correction is to reduced the amount obtained from the Belyaev formula by 50%. The resulting E_{II} values are listed in Table 5.6. It has been checked that the band-head energy spectra in the fission-isomeric well are only affected by some tens of keV from the values shown in Figure 5.3 and Figure 5.4, when applying a 50% reduction to the rotational correction calculated using the Belyaev formula. The K^π quantum numbers of the lowest-energy solutions in all cases remained unchanged except for ^{235}U with the SkM* interaction. In this case, we have a changed in the level ordering of the ground-state and first excited state, whereby the quoted value of $E_{II} = 2.20\,\text{MeV}$ is for the $K^\pi = 11/2^+$ blocked configuration.

Finally, the calculated intrinsic quadrupole moments for some relevant K^π configurations in the fission-isomeric well are listed in Table 5.7. The only experimental value available for comparison is in ^{239}Pu [106, 107], whereby our calculated values falls within the range of the quoted error bars.

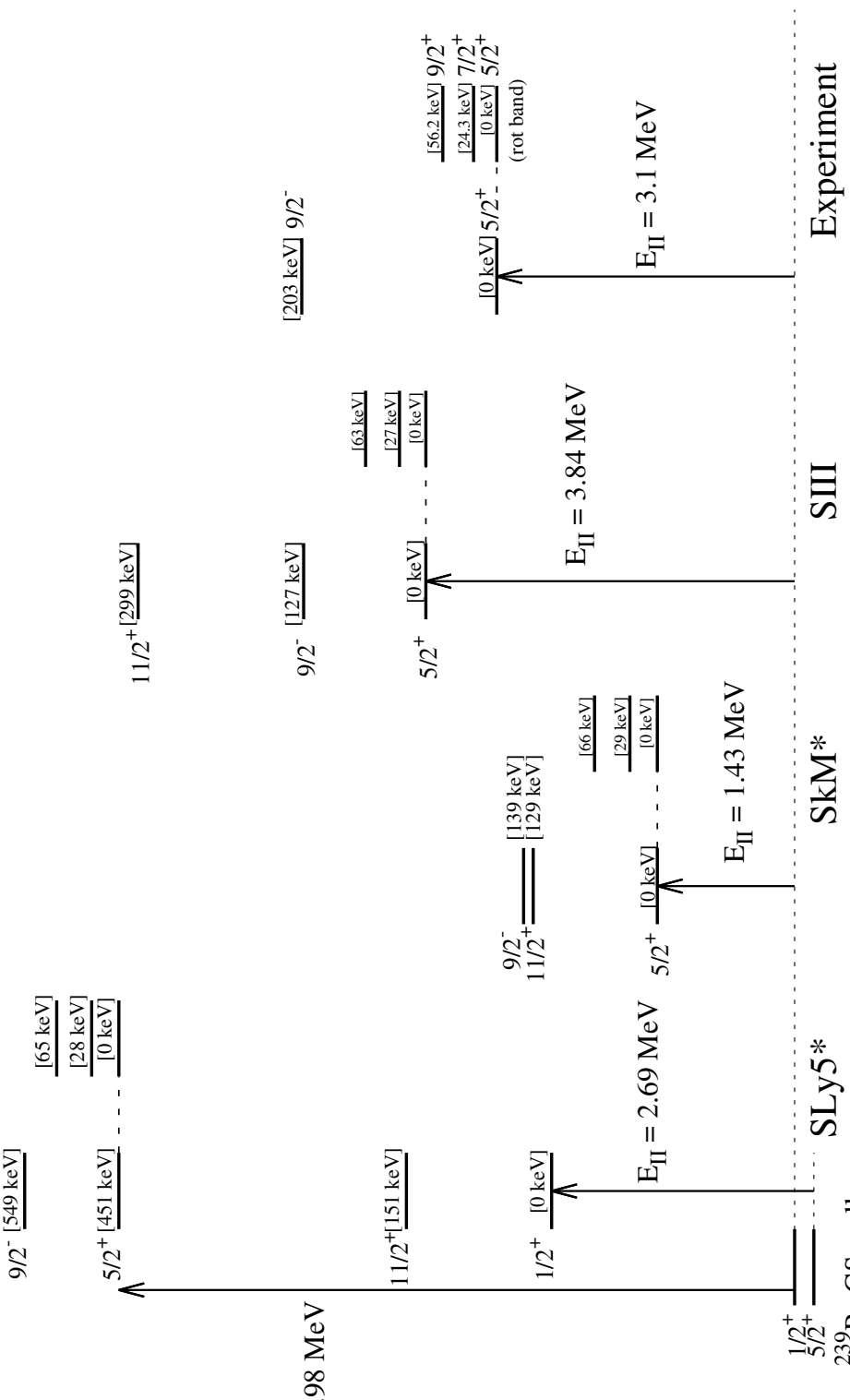

Figure 5.3: Band-head energy spectra of ^{239}Pu calculated with the SLy5*, SkM* and SIII parametrizations in the isomeric well with the inclusion of the rotational correction. The Thouless-Valatin correction have been taken into account for the moment of inertia calculated for each band heads. The rotational spectra built upon the lowest-energy $5/2^+$ state *(rot band)* are also shown on the second column of each Skyrme force. The experimental data was taken from Ref. [104, 105]. The fission-isomeric energy defined as the energy difference between the lowest-energy solution in the ground state and the fission-isomeric well is denoted by E_{II}.

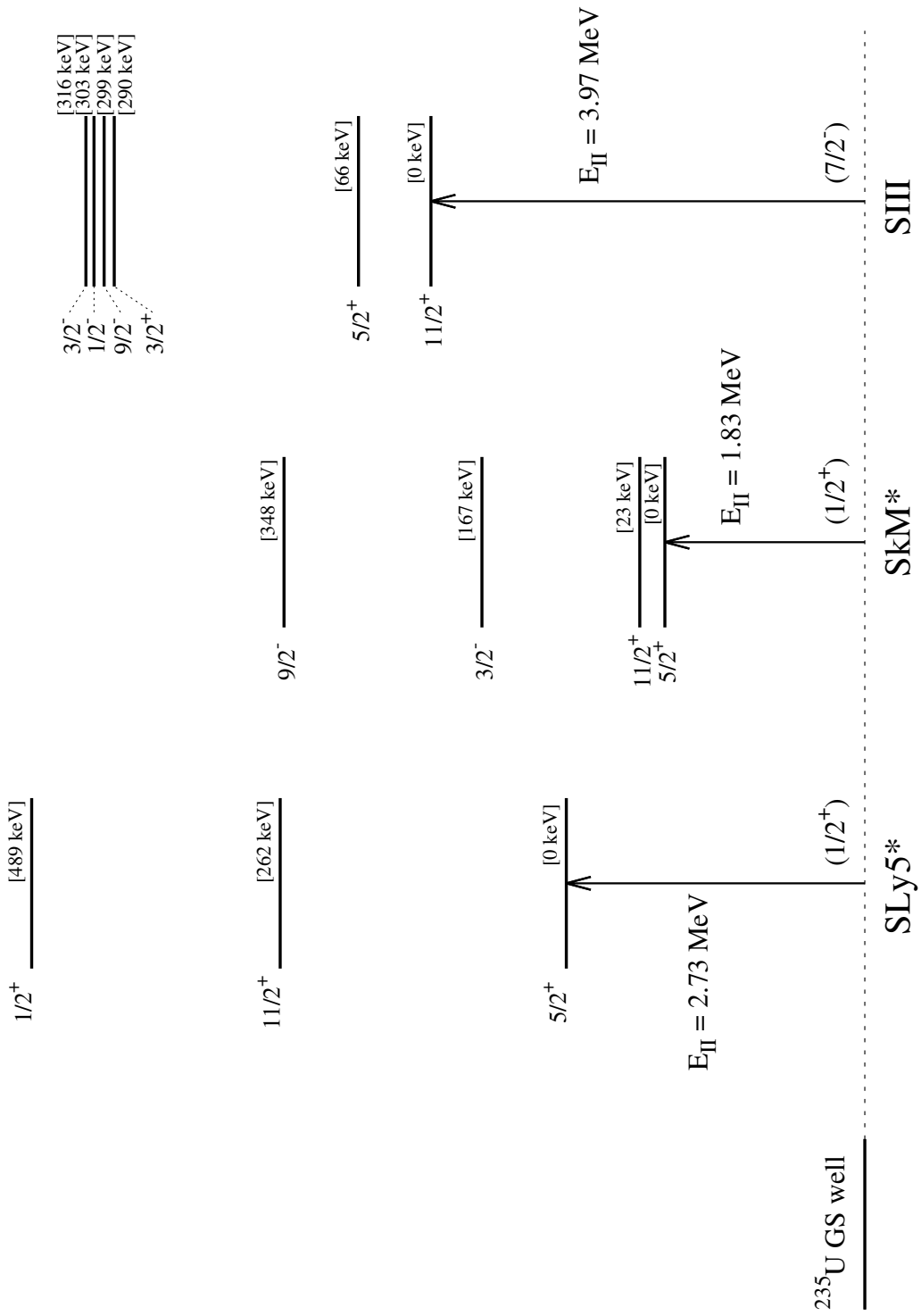

Figure 5.4: Band-head energy spectra of ^{235}U calculated with the SLy5*, SkM* and SIII parametrizations in the isomeric well, similar to Figure 5.3. The fission-isomeric energies have been calculated taking as reference the lowest-energy solution in the ground state deformation in which the K^{π} quantum numbers are given in parentheses for the respective Skyrme parametrizations.

Table 5.5: Moment of inertia ($A = \hbar^2/2\,\mathscr{J}$) and the decoupling parameter a of odd-neutron nuclei in the fission-isomeric well calculated with the SkM* and SIII parametrizations in the *minimal time-odd* scheme, and the SLy5* in the *full time-odd* scheme. The moment of inertia have been corrected for by taking into account the so-called Thouless-Valatin correction term.

Nucleus	K^π	A (keV)			a (keV)		
		SkM*	SIII	SLy5*	SkM*	SIII	SLy5*
^{235}U	$5/2^+$	4.17	4.03	4.05	-	-	-
	$11/2^+$	4.00	3.82	3.94	-	-	-
	$9/2^-$	4.19	4.10	4.06	-	-	-
	$3/2^-$	4.11	3.94	4.13	-	-	-
	$1/2^-$	4.17	3.96	4.13	0.82	1.29	1.06
^{239}Pu	$5/2^+$	4.09	3.92	4.04	-	-	-
	$11/2^+$	3.86	3.69	4.05	-	-	-
	$9/2^-$	4.02	3.86	4.16	-	-	-
	$1/2^+$	-	-	3.90	-	-	-1.08

Table 5.6: The fission-isomeric energy E_{II} being the energy difference between the lowest-energy solutions at the fission-isomeric and the ground-state wells are given for three different cases (in MeV) with regards to the evaluation of the rotational correction. The first case denoted by the index IB refers to results obtained with the moments of inertia obtained using the Belyaev formula. The second case denoted by IB-TV are obtained from the scaling of the Belyaev moment of inertia by a factor $(1+\alpha)$ with α chosen to be 0.32. The results obtained with the reduction of the rotational correction obtained from the Belyaev formula by 50% are denoted as IB-50%. Going from one rotational correction scheme to another, the excitation energy of the band-heads with respect to the lowest-energy solution in the fission-isomeric well have been checked to be affected only by some tens of keV. The K^π quantum numbers of the ground-state solution in the fission-isomeric well remains unchanged from the ones shown in Figure 5.3 and 5.4, except for case of ^{235}U with the SkM* interaction and a reduction of the rotational correction obtained using the Belyaev formula by 50% (IB-50%), whereby the $E_{II} = 2.20\,\text{MeV}$ was obtained for a $K^\pi = 11/2^+$ blocked configuration.

Nucleus	SLy5*			SkM*			SIII			Exp
	IB	IB-TV	IB-50%	IB	IB-TV	IB-50%	IB	IB-TV	IB-50%	
^{235}U	2.36	2.73	3.11	1.46	1.83	2.20	3.62	3.97	4.35	-
^{239}Pu	2.30	2.69	3.10	1.08	1.43	1.80	3.42	3.84	4.30	3.1

Table 5.7: The calculated intrinsic quadrupole moments (in barn) in the isomeric well are reported for the two lowest-energy states in ^{235}U and the two states corresponding to the experimental K^{π} quantum numbers in ^{239}Pu. In addition, the values obtained for the $11/2^{+}$ state in ^{239}Pu were also reported since this state was found to be the lowest-energy solution in the calculation performed with the SLy5* interaction. The experimental value for ^{239}Pu was taken from the work of Ref. [106, 107].

Nucleus	K^{π}	SkM*	SIII	SLy5*	Exp
^{235}U	$5/2^{+}$	32.93	31.81	33.41	-
	$11/2^{+}$	32.52	31.79	32.26	-
^{239}Pu	$5/2^{+}$	34.08	33.22	34.83	36 ± 4
	$9/2^{-}$	34.10	33.18	34.54	-
	$11/2^{+}$	34.51	33.86	34.31	-

5.4 Effect of the neglected time-odd densities in the fit of the Skyrme forces

The excitation energy $\Delta E_{\alpha K\pi}$ for the two odd-neutron nuclei have also been calculated in the *full time-odd* scheme whereby all the coupling constants entering the Hamiltonian density were considered (see discussions in Section 4.1). The moment of inertia and decoupling parameter used for the calculations of $\Delta E_{\alpha K\pi}$ have been calculated in their respectively time-odd schemes, with the values obtained in the *full time-odd* scheme being listed in Table 5.8.

The energy spectra in both time-odd schemes are plotted in Figure 5.5 for comparison. In going from one time-odd scheme to another, we see that unconstrained coupling constants affects the band-heads spectra in an uncontrollable fashion. Therefore, it is important that the Skyrme interactions should be employed in the same manner in which they have been fitted with respect to the time-odd densities entering the Hamiltonian density.

Table 5.8: The band-head energies ($\Delta E_{\alpha K\pi}$ in keV) similiar to Table 5.4 calculated with the SkM* and the SIII parametrizations within the *full time-odd* scheme are listed together with the moments of inertia ($A = \hbar^2/2\mathscr{J}$) after taking into account the Thouless-Valatin correction, and the decoupling parameter a. The excitation energy $\Delta E_{\alpha K\pi}$ obtained within the two *time-odd densities* schemes are plotted in Figure 5.5 for easier comparison of the spectra.

Nucleus	K^π	$\Delta E_{\alpha K\pi}$		A		a	
		SkM*	SIII	SkM*	SIII	SkM*	SIII
^{235}U	$7/2^-$	0	0	12.83	11.62	-	-
	$1/2^+$	-492	-236	11.60	10.46	-0.42	-0.78
	$5/2^+$	-139	750	12.06	10.90	-	-
	$5/2^+$	-110	304	12.07	11.04	-	-
	$3/2^+$	437	243	11.97	11.35	-	-
	$7/2^+$	696	-84	12.13	11.35	-	-
	$5/2^-$	-85	-4	13.36	12.13	-	-
^{239}Pu	$1/2^+$	0	0	11.68	9.47	-0.54	-0.82
	$5/2^+$	-40	364	11.46	9.59	-	-
	$7/2^-$	-23	63	12.72	10.33	-	-
	$7/2^+$	684	53	11.90	9.63	-	-

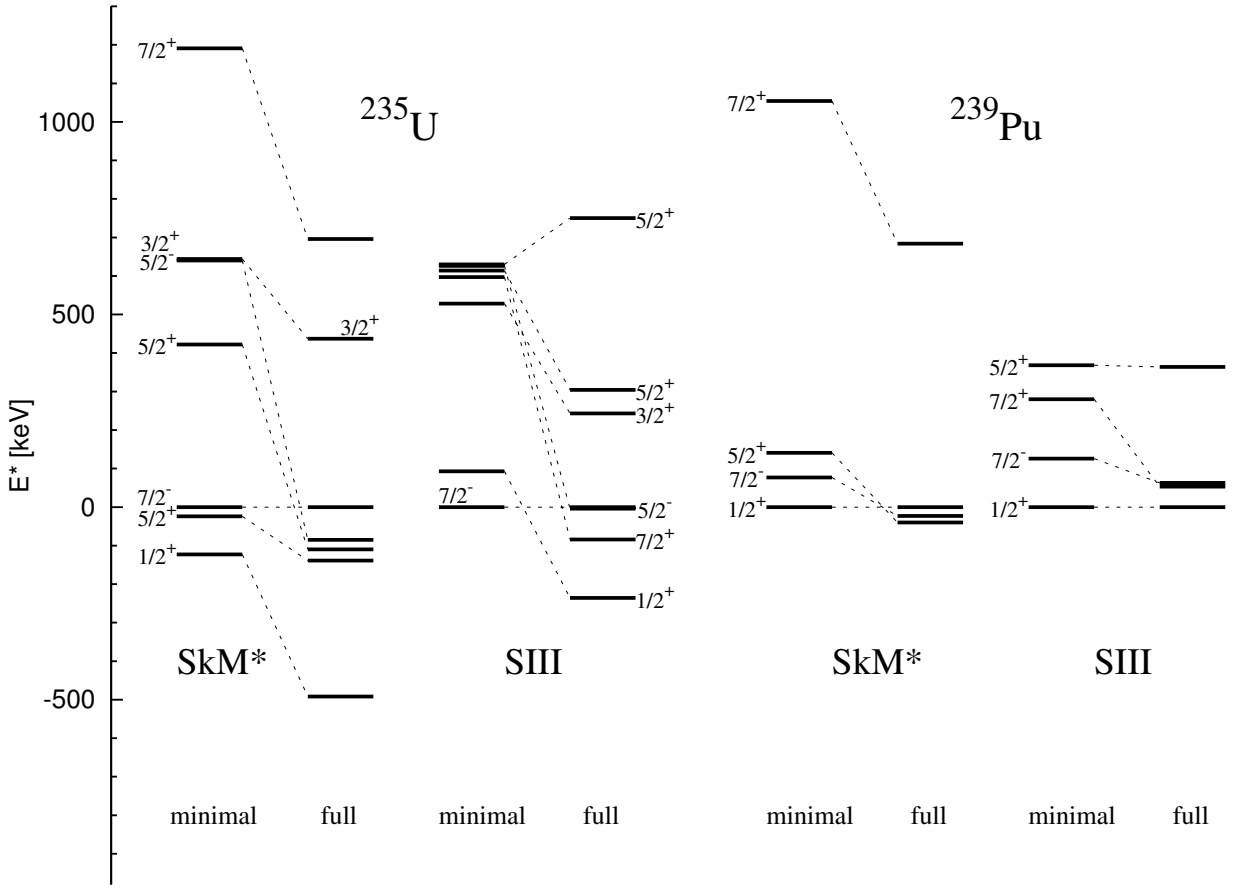

Figure 5.5: Comparison of the ground state rotational band-head spectra for the two odd-neutron nuclei obtained with the SkM* and the SIII parametrizations in both the *minimal (default)* and *full time-odd* schemes. The moment of inertia and decoupling parameter are calculated in their respective *time-odd densities* scheme.

5.5 Effect of time-reversal symmetry breaking on the ground-state band heads energy

Taking the two odd-neutron nuclei again as a testing ground, the calculations of the band-head energies $\Delta E_{\alpha K\pi}$ have been performed within the so-called equal-filling approximation (EFA) scheme. In the EFA scheme, for a specific K^π configuration, the occupation number is divided equally between a single-particle state and its time-reversed state. In doing so, the various time-odd densities entering the Hamiltonian density vanishes and the time-reversal symmetry is again established. The difference in the total binding energy within the EFA scheme and our blocking calculations were found to be of the order of 100 keV at most. This translates to an effect of one order less in the relative energies, of about tenths of keV (see Table 5.9). The rather small differences stems from the perturbative character of the time-odd density terms.

Table 5.9: Energy differences ($\Delta E_{\alpha K\pi}$ in keV) of a given band head K with respect to the ground state within the equal-filling approximation without rotational correction. The moments of inertia ($A = \hbar^2/2\,\mathscr{J}$) and the decoupling parameter (a) are taken from the study of Jain and collaborators [103]. The energy difference (in keV) between the solutions of equal-filling approximation (EFA) and the self-consistent blocking (SCB) procedure are shown in the last three columns for each Skyrme interaction.

Nucleus	K^π	$\Delta E_{\alpha K\pi}$			$\Delta E^{(EFA)}_{\alpha K\pi} - \Delta E^{(SCB)}_{\alpha K\pi}$		
		SkM*	SIII	SLy5*	SkM*	SIII	SLy5*
^{235}U	$7/2^-$	0	0	0	0	0	0
	$1/2^+$	-69	124	-857	9	0	3
	$5/2^+$	15	642	-451	15	14	-8
	$5/2^+$	455	658	-271	16	8	-2
	$3/2^+$	686	549	216	6	-8	-13
	$7/2^+$	1228	631	231	11	19	2
	$5/2^-$	652	636	-682	-5	-3	-7
^{239}Pu	$1/2^+$	0	0	0	0	0	0
	$5/2^+$	130	366	-230	9	7	-8
	$7/2^-$	21	97	-55	-6	2	2
	$7/2^+$	1031	279	291	9	19	1

Chapter 6

FISSION BARRIERS OF ACTINIDE NUCLEI

From the study of the ground-state band-head energy spectra presented in Chapter 5 we take stock of a better agreement between the calculated results of odd-neutron nuclei with the experiments as compared to odd-proton nuclei. In view of this, calculations of the fission-barrier heights have been considered only for the two odd-neutron nuclei, namely ^{235}U and ^{239}Pu, and their neighbouring even-even nuclei. The calculations of the total energy as a function of deformations, with a conserved parity symmetry, were first performed for even-even nuclei. The converged fields were then used as starting points for the calculations of the odd-mass nuclei. The SkM* parametrization has been employed for the calculations of both the uranium and plutonium isotopes up to a point beyond the top of the second fission-barrier. On the other hand, calculations using the SIII parameters set were performed only up to the fission-isomeric well. We have also considered the ^{239}Pu nucleus and its neighbouring even-even nuclei as a testing ground for the SLy5* parametrization.

In Section 6.1, we will present the results for the neighbouring even-even nuclei obtained from parity-conserving calculations. The spurious rotational energy correction to the binding energy evaluated using the Belyaev formula for the moment of inertia will be presented first in Section 6.1.1. Then, in Section 6.1.2, a sensitivity study of the fission-barrier heights to the moment of inertia is made. The Section 6.2 will be devoted to the fission barriers of odd-mass nuclei. For the odd-mass nuclei, the discussions have been separated into four subsections whereby the first three will be devoted to the results obtained from our mean-field calculations. We shall first discuss the fission barriers of the odd-mass nucleus with a conserved parity symmetry in Section 6.2.1. The effect of the unconstrained coupling-constant terms in the Hamiltonian density when utilizing the SIII and the SkM* parametrizations on the fission-barrier heights will be presented in Section 6.2.2. The results obtained with parity symmetry breaking around the outer fission-barrier for some relevant cases will be discussed in Section 6.2.3. Finally, the fission-barrier heights obtained with the SkM* parametrization and evaluated within the Bohr-Mottelson unified model will be presented in Section 6.2.4. In Section 6.3, we compare the deformation energy curves of the considered plutonium isotopes to illustrate the concept of "specialization energy". Finally, we shall compare our results with other calculations or empirical fission-barrier heights in Section 6.4, together with a short discussion on how our results could be of use in fission cross-sections calculations.

6.1 Even-even nuclei

6.1.1 Results with a conserved parity symmetry

The deformation energy curves for ^{234}U, ^{236}U, ^{238}Pu and ^{240}Pu nuclei obtained with the SkM* are plotted in Figure 6.1. Similar plots obtained with the SLy5* parametrization for the ^{238}Pu and ^{240}Pu nuclei are displayed in Figure 6.2 while those obtained with the SIII parametrization are shown in Figure 6.3. In all these plots, the solid lines correspond to mean-field solutions while the dashed lines show the downward shift in energy after taking the rotational energy correction into account. The rotational energy correction in these cases have been obtained using the Belyaev formula. Further refinements to the moment of inertia thus obtained will be discussed in the next section. The inner-barrier height E_A, the fission-isomeric energy E_{II} and the outer-barrier height E_B deduced from these deformation energy curves are tabulated in Table 6.1.

Let us first discuss the results obtained from our mean-field solutions. The deformation energy curves exhibit the well-known double-hump fission barriers. A striking feature of the deformation energy curves comes from those obtained with the SLy5* parametrization, around the top of the second barrier. A comparison of the total energy E obtained with the SkM* parametrization around this saddle point shows that the corresponding values of E obtained with the SLy5* parametrization are too high in energy. This in turn gives rise to an unphysically high value of the second fission-barrier height. In addition, we observe that the total binding energy does not decrease as smoothly as is seen for the curves obtained with the SkM* parameter set at very large deformations. On the other hand, a comparison of the inner-barrier heights and the fission-isomeric energies of ^{238}Pu and ^{240}Pu nuclei as obtained with the SLy5* and the SIII parametrizations, shows that the SLy5* parametrization performs better as compared to SIII.

We shall now turn our discussion to the results including the rotational energy correction. The variation of the rotational energy calculated with the Belyaev moment of inertia as a function of deformation is plotted in Figure 6.4, limiting ourselves to those obtained with the SkM* and SLy5* parametrizations. At each deformation point, the magnitude of the rotational correction obtained with the SkM* parametrization is about the same for all considered even-even nuclei. This translates to a lowering of E_A and E_{II} by about 1.2 MeV and 1.4 MeV, respectively, while the correction to E_B is much larger and reaches 2.5 MeV with the SkM* parametrization. The effect of the rotational correction on the fission-barrier heights obtained with the SLy5* is slightly larger as compared those obtained with the SkM*, by about 0.2 MeV for E_A, and about 0.5 MeV for E_B.

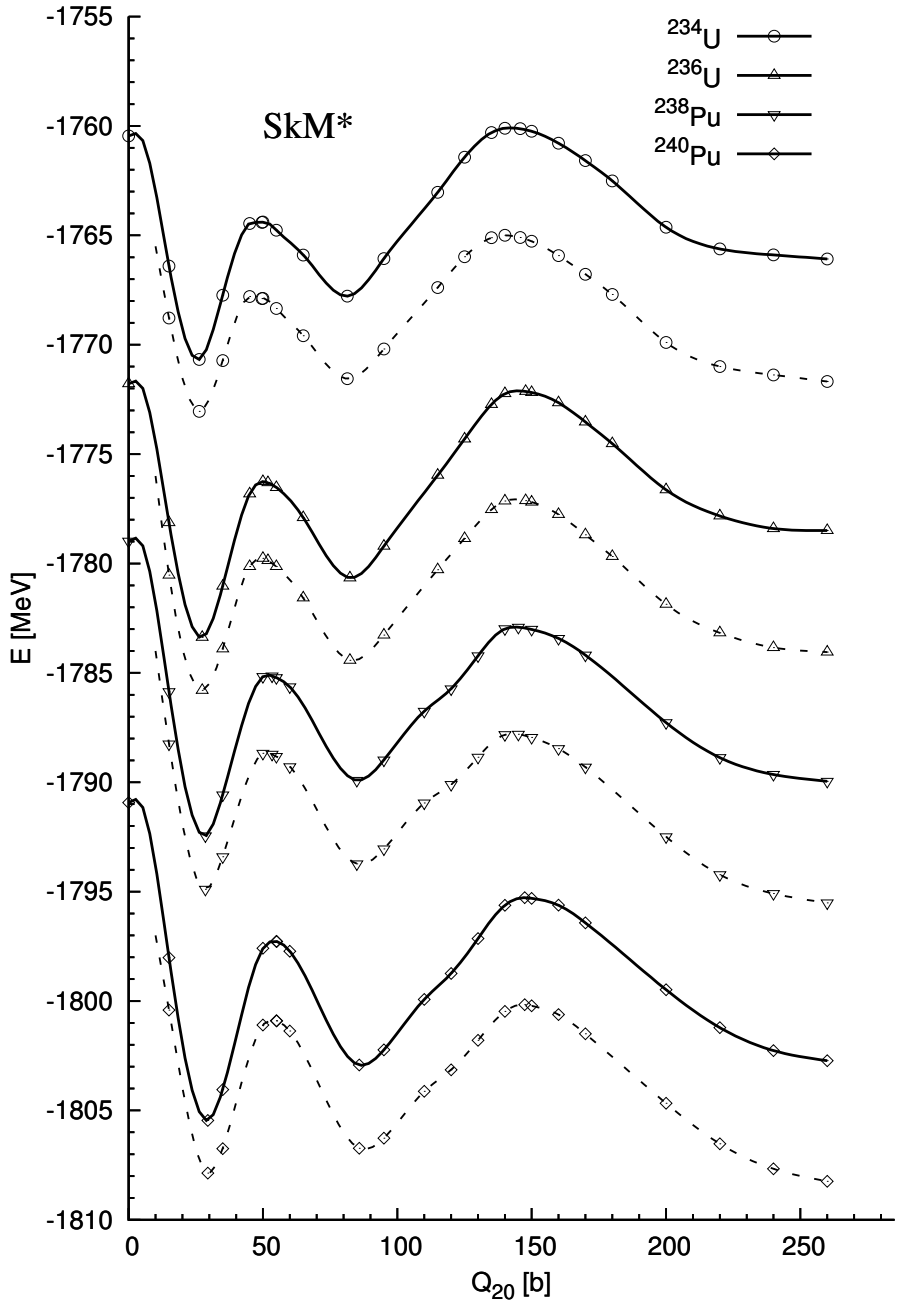

Figure 6.1: Deformation energy curves as a function of quadrupole moment of the neighbouring even-even nuclei calculated using the SkM* parametrization. The results obtained after taking into account the rotational correction are plotted in dashed lines.

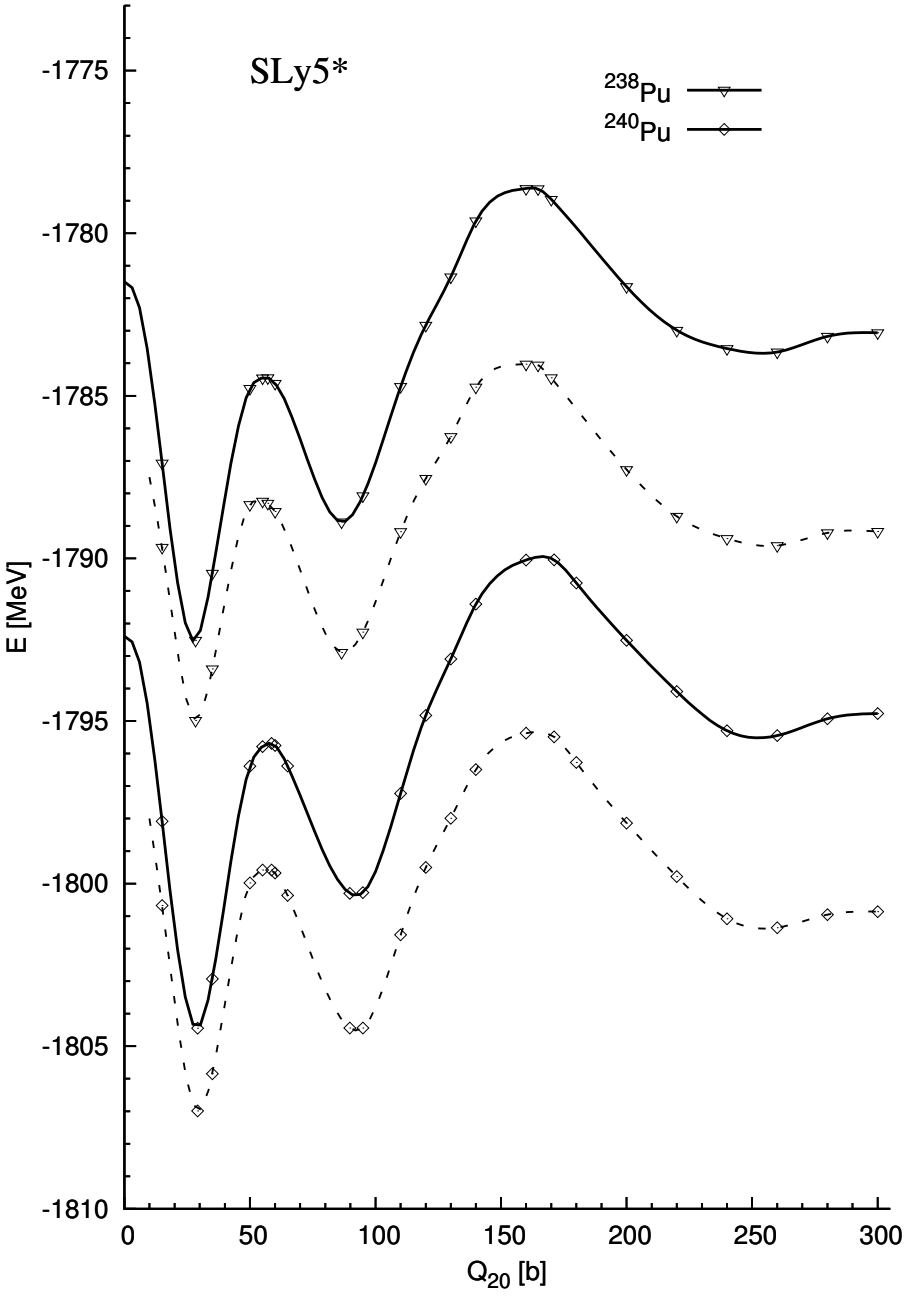

Figure 6.2: Similar to Figure 6.1 for the SLy5* parametrization.

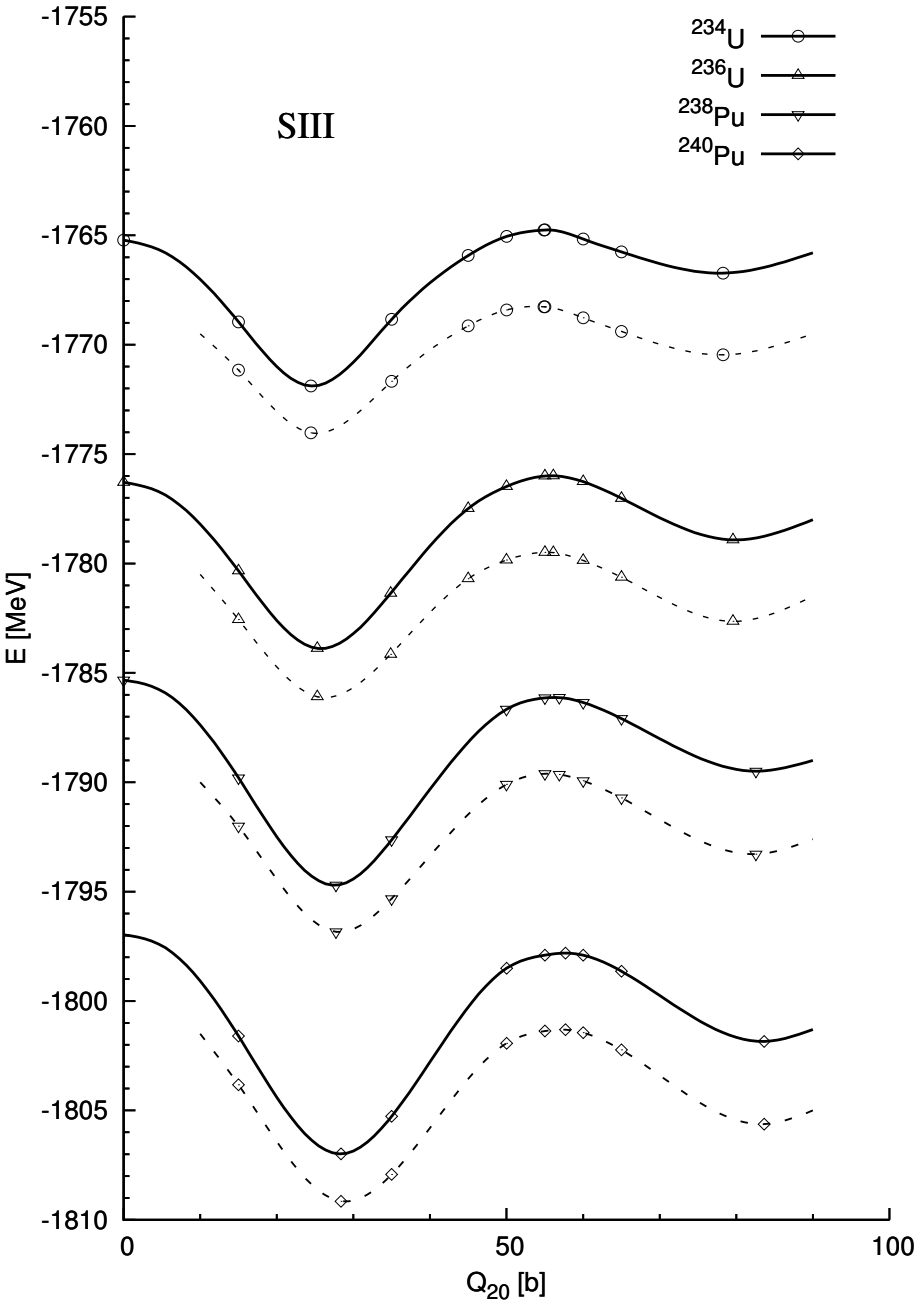

Figure 6.3: Similar to Figure 6.1 for the SIII parametrization

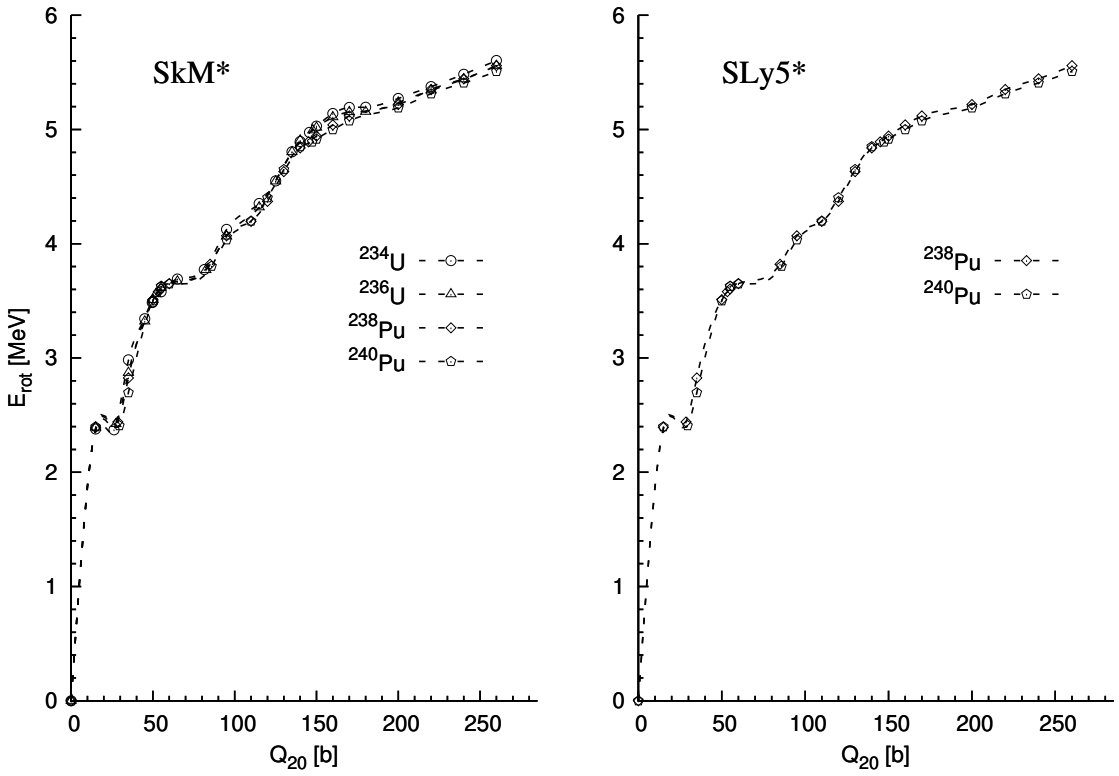

Figure 6.4: Rotational energy correction $E_{rot} = \frac{\hbar^2}{2\mathcal{I}}\langle \hat{J}^2 \rangle$ for the even-even neighbouring nuclei obtained with the SkM* and SLy5* parametrizations. The values of the moment of inertia $\mathcal{I}$ used for this plot were obtained from the calculations using the Belyaev formula.

6.1.2 Sensitivity of the fission-barrier heights of even-even nuclei to the moment of inertia

As was discussed in Section 3.4.1, the rotational energy calculated using the Belyaev formula was found to be too large, resulting in an underestimation of the fission-barrier heights. Three ways of improvement to the rotational energy have been considered. The first approach is to include the so-called Thouless-Valatin corrective term which translates into a scaling of the Belyaev moment of inertia by a multiplicative factor $(1+\alpha)$ with $\alpha = 0.32$. The second approach was to consider a reduction of the rotational energy obtained from the Belyaev formula by 50%, as indicated from the test of the intrinsic vorticity model. The third approach is to employ the amount of rotational energy obtained from the angular momentum projection calculations in ^{240}Pu of Ref. [72] and use the same values for the other nuclei.

Table 6.1 lists the resulting fission-barrier heights of the considered even-mass nuclei obtained from the four different approaches to the rotational correction. The inner-barrier height and fission-isomeric energy obtained from the scaling of the rotational energy calculated using the Belyaev formula by 50% were found to be rather close to those obtained when using the rotational correction deduced from Ref. [72]. The values of the rotational correction and as a consequence, the outer-barrier height, between these two approaches was found to differ by about 0.3 MeV. It is also worth noting that a more reasonable fission-isomeric

Table 6.1: The inner-barrier heights E_A, the fission-isomeric energy E_{II} and the outer-barrier height E_B of the neighbouring even-even nuclei obtained with the SkM*, the SLy5* and the SIII parametrizations assuming parity symmetry without and with the rotational correction. The contribution from the rotational energy have been included in four ways, namely by using the Belyaev formula (IB), the scaling of the Belyaev moment of inertia by a factor $(1+\alpha)$ with $\alpha = 0.32$ to treat approximately the Thouless-Valatin corrective term (IB+TV), a reduction of the rotational correction calculated using the Belyaev formula by 50% (IB-50%) as indicated from the test of the intrinsic vorticity model, and the values of rotational energy at various deformations from the angular momentum projection calculations (ang. mom. proj.) in ^{240}Pu by Ref. [72].

Nucleus		E_A (MeV)			E_{II} (MeV)			E_B (MeV)		
		SkM*	SLy5*	SIII	SkM*	SLy5*	SIII	SkM*	SLy5*	SIII
^{234}U	without	6.27	-	7.13	2.89	-	5.16	10.55	-	-
	IB	5.15	-	5.77	1.49	-	3.57	7.95	-	-
	IB+TV	5.42	-	6.10	1.83	-	3.95	8.58	-	-
	IB-50%	5.71	-	6.45	2.19	-	4.36	9.25	-	-
	ang. mom. proj.	5.77	-	6.63	2.09	-	4.36	9.05	-	-
^{236}U	without	7.07	-	7.89	2.72	-	4.96	11.24	-	-
	IB	5.93	-	6.59	1.38	-	3.45	8.68	-	-
	IB+TV	6.21	-	6.91	1.90	-	3.81	9.30	-	-
	IB-50%	6.50	-	7.24	2.05	-	4.20	9.96	-	-
	ang. mom. proj.	6.57	-	7.39	1.92	-	4.16	9.74	-	-
^{238}Pu	without	7.31	8.07	8.58	2.54	3.64	5.21	9.54	13.89	-
	IB	6.17	6.67	7.20	1.16	2.09	3.55	7.09	10.92	-
	IB+TV	6.45	7.01	7.53	1.49	2.46	3.96	7.68	11.64	-
	IB-50%	6.74	7.37	7.89	1.85	2.87	4.38	8.31	12.41	-
	ang. mom. proj.	6.81	7.57	8.08	1.74	2.84	4.41	8.04	12.39	-
^{240}Pu	without	8.18	8.76	9.18	2.53	4.15	5.14	10.18	14.40	-
	IB	6.96	7.41	7.84	1.14	2.55	3.52	7.70	11.50	-
	IB+TV	7.25	7.74	8.17	1.47	2.94	3.92	8.30	12.21	-
	IB-50%	7.57	8.08	8.51	1.83	3.35	4.33	8.94	12.95	-
	ang. mom. proj.	7.68	8.26	8.68	1.73	3.35	4.34	8.68	12.90	-

energies were obtained when reducing the rotational correction by 50%. The fission-isomeric energies listed in Table 6.1 could be compared to the empirical values of (2.3 ± 0.2), (2.7 ± 0.2) and (2.4 ± 0.2) MeV for ^{236}U, ^{238}Pu and ^{240}Pu, respectively, of Ref. [108]. Figure 6.5 shows the effect of rotational correction on the deformation energy curves of the four considered even-even mass nuclei, only for the SkM* interaction. We can see from the plots that the rotational energy, in general, plays a significant role in the lowering of the deformation energies, especially more so around and beyond the second fission-barrier.

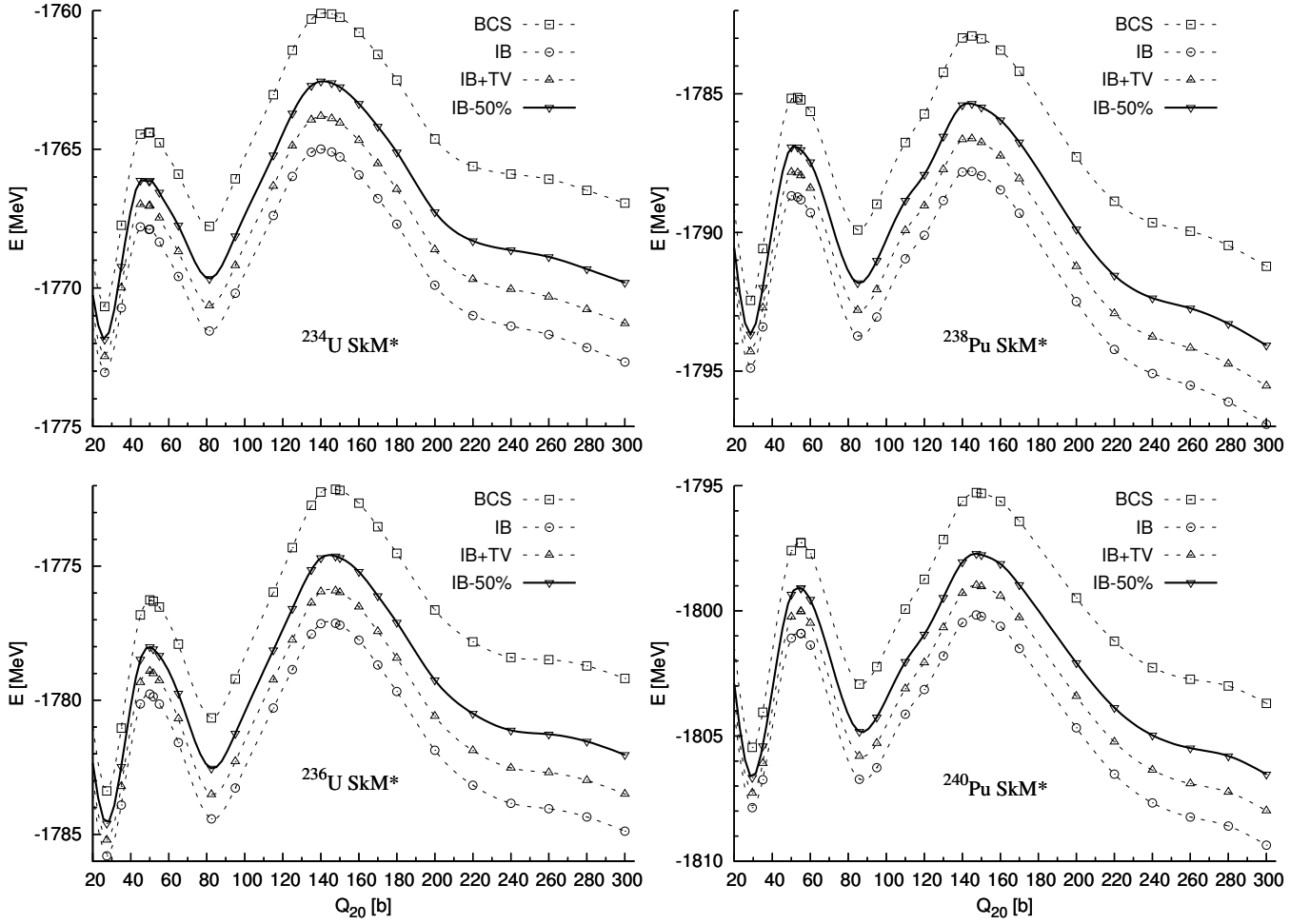

Figure 6.5: Deformation energy curves starting from the ground-state up to beyond the second fission-barrier of the even-even neighbouring nuclei with the SkM* parametrization obtained with various approximation to the rotational correction. The line denoted as BCS refers to the mean-field results obtained without the rotational correction, while IB refers to the inclusion of the rotational energy calculated using the Belyaev formula. The inclusion of the so-called Thouless-Valatin correction to the moment of inertia is referred to as IB+TV. The reduction of the rotational energy calculated using the Belyaev formula by 50% is denoted as IB-50%.

6.2 Odd-mass nuclei

6.2.1 HF+BCS results with a conserved parity symmetry

We shall now turn to the calculations of deformation energies of odd-mass nuclei, confining ourselves first to the mean-field results (i.e. without rotational correction term). The calculations of the deformation energies for odd-mass nuclei are performed for the blocked K^π configurations considered in the band-head energy spectra discussed in Chapter 5. The deformation energy as a function of the quadrupole moment Q_{20} has been calculated for the two considered odd-neutron nuclei with the SkM* parametrization up to some deformation beyond the top of the second fission-barrier. The deformation-energy curves, with the corresponding K^π ground-state energy as the energy reference, obtained with the SkM* parameter set are shown in Figure 6.6 for the ^{235}U nucleus and in Figure 6.7 for the ^{239}Pu nucleus. The corresponding inner-barrier heights E_A, fission-isomeric excitation energies E_{IS} and outer-barrier heights E_B are tabulated in Table 6.2. It should be noted that fission-isomeric excitation energy denoted here as E_{IS} is to be distinguished from the relative energy E_{II} discussed in Chapter 5. Indeed E_{II} refers to the energy difference between the lowest-energy configuration in the fission-isomeric and ground-state wells, whereas E_{IS} is the energy difference for a particular K^π blocked configuration between the lowest-energy solution in the two wells, such that;

$$E_{IS} = E^{(K^\pi)}_{IS\,well} - E^{(K^\pi)}_{GS\,well} \tag{6.1}$$

The fission-barrier heights are found to vary from one blocked configuration to another between 7 and 9 MeV for both nuclei.

A further lowering of the inner-barrier height is to be expected when allowing for axial-symmetry breaking shapes. Triaxial calculations performed with the SkM* parametrization for the ^{234}U, ^{236}U, ^{240}Pu and ^{252}Cf nuclei in Ref. [60] show a reduction of the inner-barrier height by about 0.5 MeV for the three lighter nuclei, and by as much as about 2 MeV for the ^{252}Cf nucleus. We can thus assume that performing triaxial calculations for odd-mass nuclei would also yields a correction to the inner-barrier heights of about the same order of magnitude as the one reported in Ref. [60]. In this work, we have rather focussed on the effect of parity symmetry breaking which is expected to have a larger impact on the outer fission-barrier height. This shall be discussed in the Section 6.2.3.

We have also performed calculations of the deformation energies of the ^{239}Pu nucleus with the SLy5* parametrization. The deformation-energy curves has been plotted in Figure 6.7 for comparison with those obtained with the SkM* parametrization. The SLy5* parametrization is found to describe well the variation of the binding energy with quadrupole deformation up to a point beyond the top of the inner-barrier. The deformation energy curves obtained with the SIII parametrization are plotted in Figure 6.8 and 6.9 for the two considered nuclei up to the fission-isomeric well. Despite the limited number of results available for comparison between the three Skyrme parametrizations considered herein, namely in ^{239}Pu only, we note that the SIII parametrization gives for all retained K^π configurations higher inner-barriers than SkM*, as

already known for even-even nuclei, and that SLy5* yields inner-barrier heights slightly smaller than SIII but overall significantly larger than SkM*.

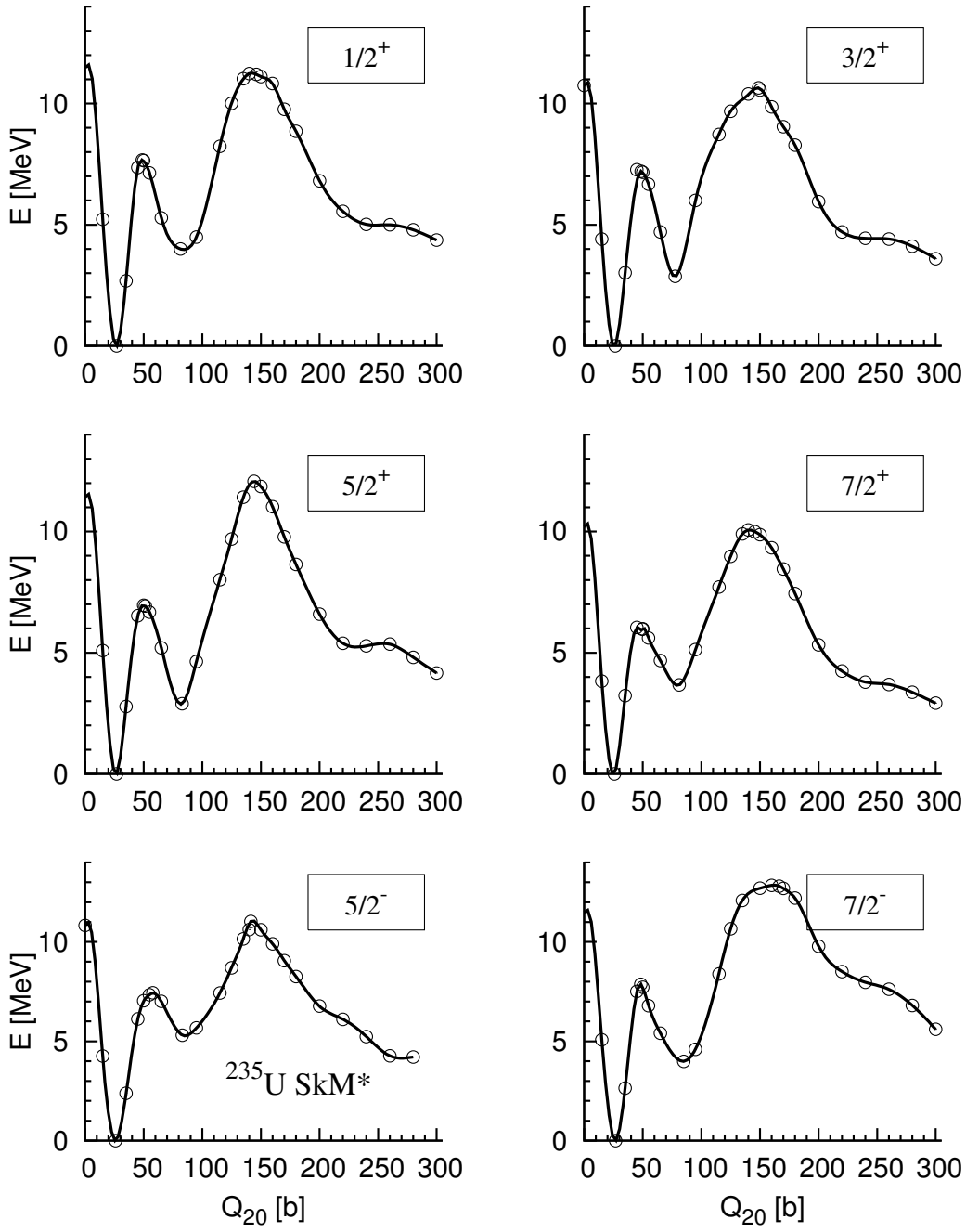

Figure 6.6: Deformation energy curves (with the ground state energy taken as the reference) as a function of quadrupole moment Q_{20} (given in barns) of the different blocked configurations with K^{π} quantum numbers in ^{235}U obtained with the SkM* parametrization.

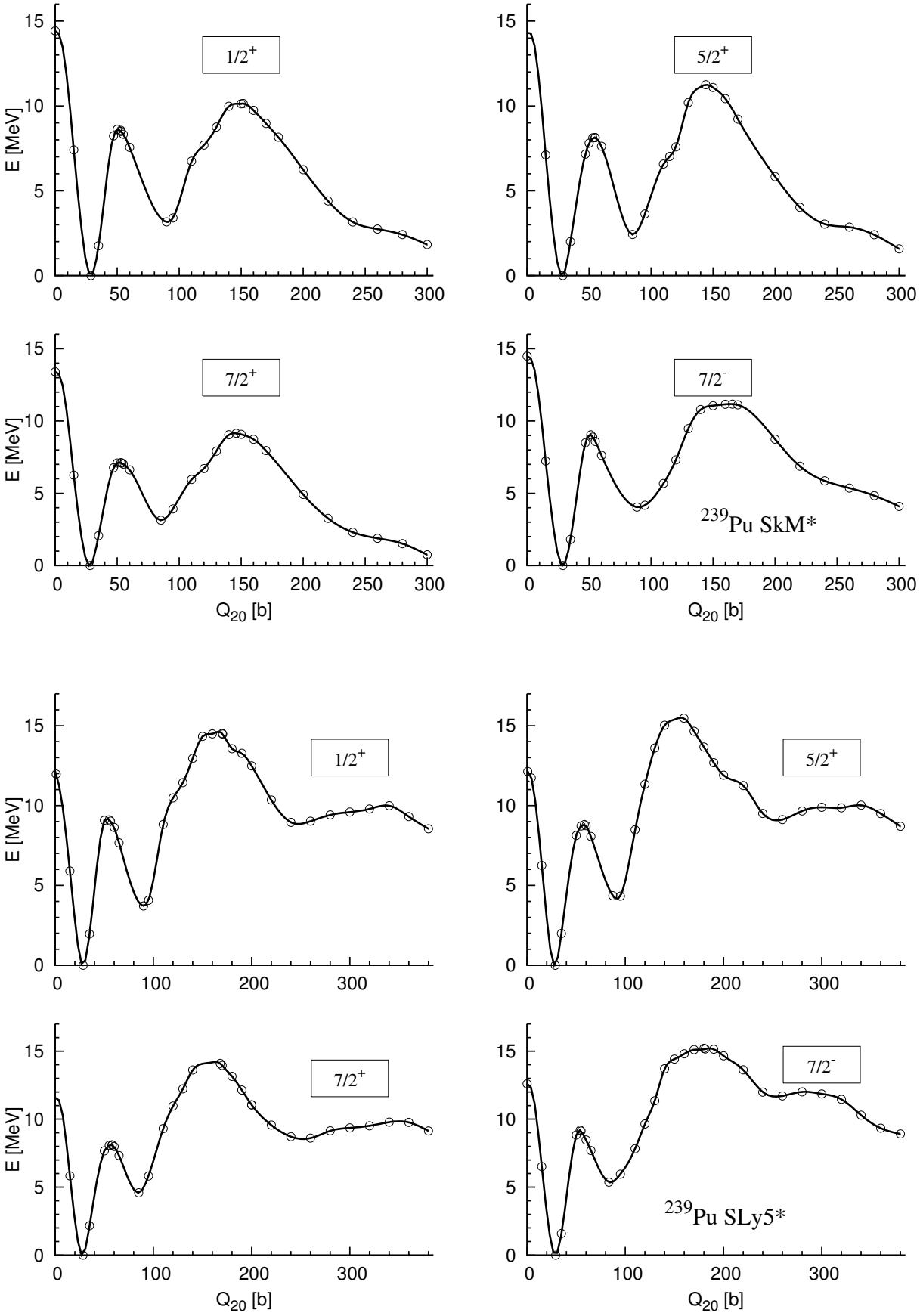

Figure 6.7: Similar to Figure 6.6 for ^{239}Pu nucleus obtained with the SkM* (top two rows) and the SLy5* (bottom two rows) parametrizations.

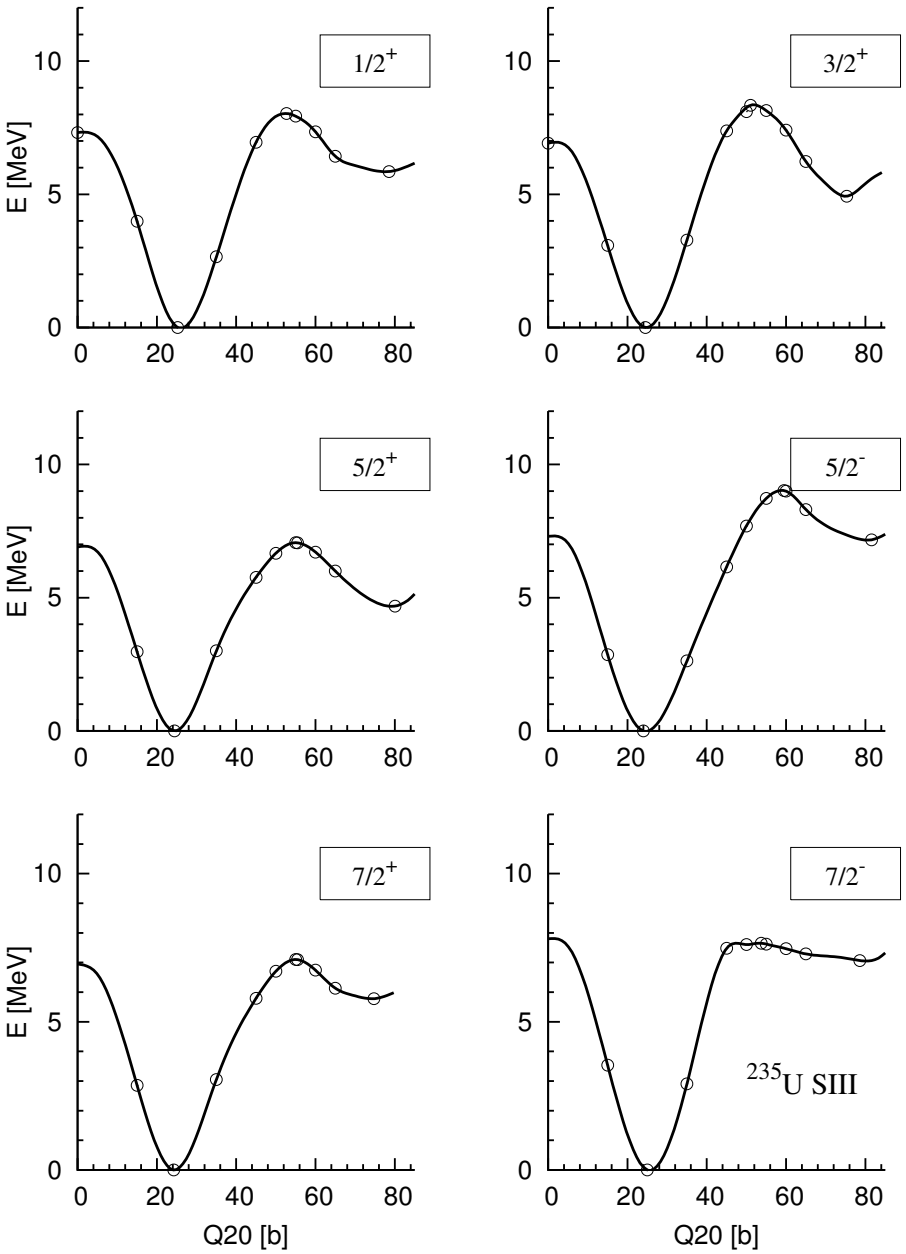

Figure 6.8: Deformation energy curves of the different blocked configurations with K^{π} quantum numbers in ^{235}U nucleus obtained with the SIII parametrization up to the fission-isomeric well.

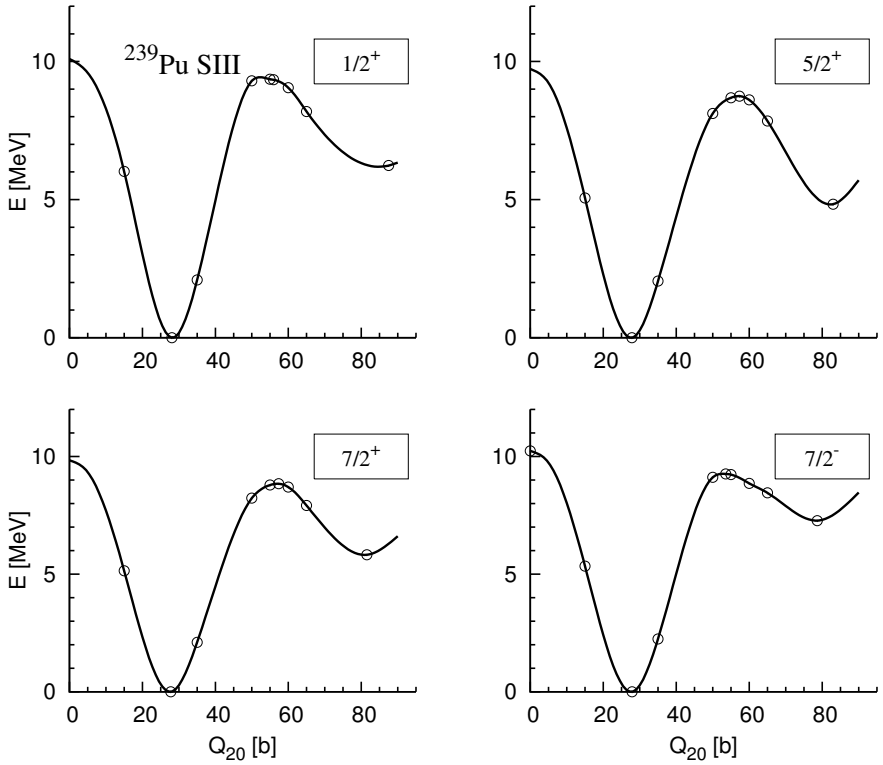

Figure 6.9: Similar to Figure 6.8 for ^{239}Pu with the SIII parametrization.

Table 6.2: The inner-barrier heights E_A, the fission-isomeric energy with respect to the same K^π ground-state solution E_{IS} and the outer-barrier height E_B of the odd-neutron nuclei obtained with the SkM*, the SLy5* and the SIII parametrizations. The outer-barrier height obtained from a parity breaking calculations are given in parentheses for the selected blocked configurations. Results shown were obtained from mean-field calculations without rotational correction.

Nucleus	K^π	E_A (MeV)			E_{IS} (MeV)			E_B (MeV)	
		SkM*	SLy5*	SIII	SkM*	SLy5*	SIII	SkM*	SLy5*
^{235}U	1/2$^+$	7.67	-	8.03	4.00	-	5.85	11.20 (7.5)	-
	7/2$^-$	7.87	-	7.65	3.99	-	7.07	12.81 (7.4)	-
	5/2$^+$	6.93	-	7.06	2.89	-	4.69	12.07	-
	3/2$^+$	7.21	-	8.34	2.87	-	4.93	10.64	-
	7/2$^+$	5.97	-	7.10	3.67	-	5.78	9.99 (6.2)	-
	5/2$^-$	7.44	-	9.02	5.31	-	7.17	10.75	-
^{239}Pu	1/2$^+$	8.56	9.02	9.34	3.17	3.71	6.23	10.14 (6.3)	14.47 (9.9)
	7/2$^-$	9.05	9.19	9.26	4.05	5.37	7.28	11.17	15.16
	7/2$^+$	7.09	8.11	8.84	3.14	4.59	5.82	9.15	14.10
	5/2$^+$	8.14	8.81	8.75	2.42	4.35	4.83	11.25 (6.6)	15.47 (9.9)

6.2.2 Effect of neglected time-odd terms on the fission barriers

Calculations of the total binding energies as a function of deformation with parity symmetry have also been performed from the normal-deformed ground-state well up to the fission-isomeric well for the two odd-mass nuclei with the SkM* and the SIII parametrizations in the *full time-odd* scheme. In this scheme, the B_{14}, B_{15}, B_{18} and B_{19} coupling-constants are not set to zero, as was done for the default *minimal time-odd* scheme. From the converged solutions, the energy contributions to the inner-barrier height E_A and fission-isomeric energy E_{IS} stemming from the kinetic energy, the Coulomb energy, the pairing energy as well as the various coupling-constant terms appearing in the expression of the Hamiltonian density are calculated in both schemes.

For each energy contribution, we take the difference between the values obtained in both *time-odd* schemes. Restricting our discussion here to the inner-barrier height, the above corresponds to taking the energy difference for example, for the term related to B_1 coupling-constant, such that

$$\Delta E'_{B_1} = \Delta E^{(\mathrm{full})}_{B_1} - \Delta E^{(\mathrm{min})}_{B_1} \tag{6.2}$$

where $\Delta E^{(\mathrm{full})}_{B_1}$ and $\Delta E^{(\mathrm{min})}_{B_1}$ refers to the inner-barrier height in the *full time-odd* and the *minimal time-odd* schemes, respectively. The sum of all the energy differences except for the those related to the B_{14}, B_{15}, B_{18} and B_{19} terms between the two *time-odd* schemes are denoted as $\Delta E'_{even}$ such that

$$\Delta E'_{even} = \Delta E'_{kin} + \Delta E'_{B_x} + \Delta E'_{pairing} + \Delta E'_{Coulomb} \quad ; \quad x \neq 14, 15, 18, 19 \tag{6.3}$$

The contribution of the B_{14} and B_{15} terms to the difference in the inner-barrier height between the two *time-odd* schemes are denoted as $E_{B_{14,15}}$ while those from B_{18} and B19 terms are denoted as $E_{B_{18,19}}$. The difference in the inner-barrier height in the two *time-odd* schemes is then given as

$$\Delta E'_A = \Delta E'_{even} + \Delta E'_{B_{14,15}} + \Delta E'_{B_{18,19}} \tag{6.4}$$

and the same applies also to case of the fission-isomeric energy E_{IS}.

Comparing both Figure 6.10 and Figure 6.11, we see that the inner-barrier heights, in general, decreases when going from a *minimal* to a *full time-odd* scheme. This is reflected by the negative values of $\Delta E'_A$ in the histogram. The difference in the inner-barrier height between both time-odd schemes is overall a competition between the $\Delta E'_{even}$ and $\Delta E'_{B_{14,15}}$ terms, while the $\Delta E'_{B_{18,19}}$ term has a negligible effect. The $\Delta E'_{B_{14,15}}$ term is related to the local densities in the form of $(\overleftrightarrow{J}^2 - \mathbf{s}\cdot\mathbf{T})$. It was checked that the contribution of the $(s\cdot T)$ component was rather unconsequential and that the bulk of it comes from the $\overleftrightarrow{J}^2$ component. When both $\Delta E'_{even}$ and $\Delta E'_{B_{14,15}}$ contributions are of the same magnitude but with opposite sign, then we do not have a change in the inner-barrier height, as is the case for the $7/2^+$ blocked configuration obtained with the SkM* parametrization.

The effect of the time-odd scheme on fission-isomeric energy E_{IS} is less clear-cut. However, we could still observe an interplay between the *even* and the B_{14}, B_{15} terms in determining the overall effect on ΔE_{IS}. The effect of the time-odd scheme is generally less in the fission-isomeric energy as compared to the inner-barrier height, with the notable exceptions for the the $1/2^+$ configuration with the SkM* and the $5/2^+$ configuration with the SIII parametrizations.

This study shows that the coupling-constant terms which are not constrained in the earlier fits of the Skyrme force can impact the fission-barrier heights. This suggests that the effect of the unconstrained terms cannot be absorbed into the variational procedure. This could provide a constraint of some coupling constants in the fit of the Skyrme parametrizations in a functional point of view.

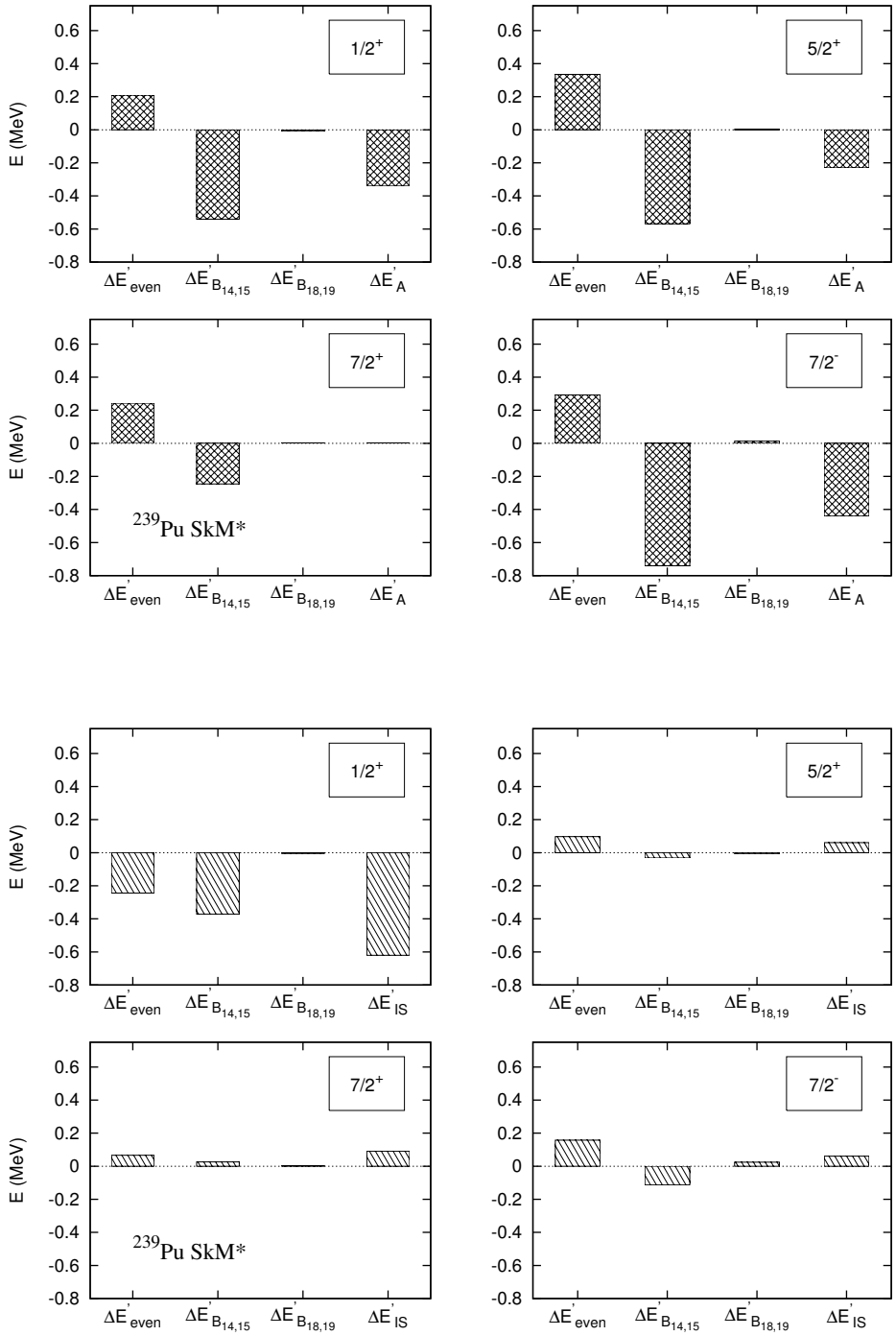

Figure 6.10: The plot shows the energy differences between various terms obtained from calculations in the default *minimal time-odd* scheme as opposed to the results obtained in the *full time-odd* scheme of ^{239}Pu with the SkM* parametrization. All the terms in the Hamiltonian density which contributes to the total binding energy in the case of an even-even nucleus are grouped and denoted to as $\Delta E'_{even}$. The energy contributions coming from the B_{14} and B_{15} terms are denoted as $\Delta E'_{B_{14,15}}$ while those related to the B_{18} and B_{19} terms are denoted as $\Delta E'_{B_{18,19}}$. The difference in the inner-barrier heights $\Delta E'_{\rm A}$ and the fission-isomeric energy $\Delta E'_{\rm IS}$ between the two schemes are also given for each blocked configurations.

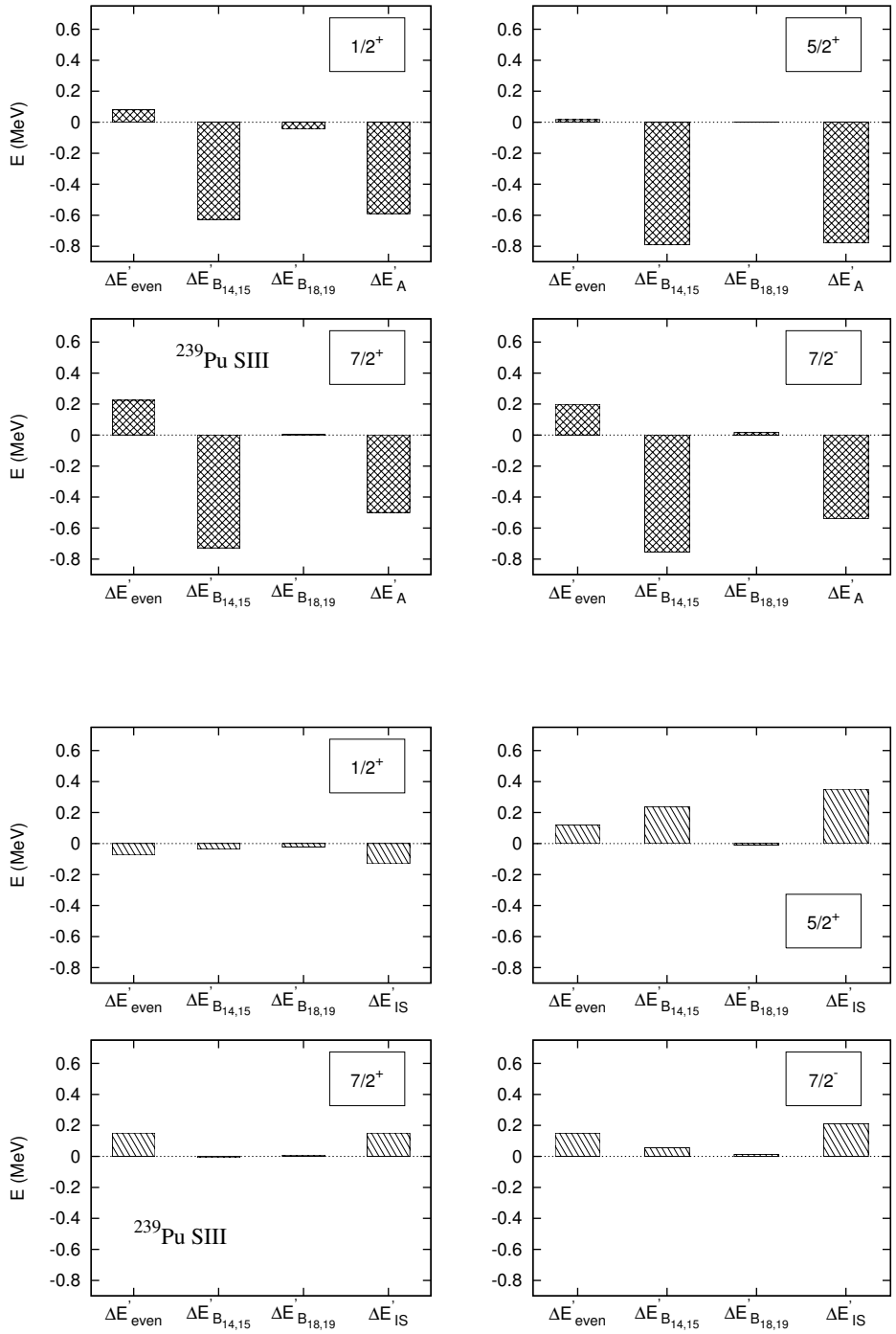

Figure 6.11: Similar to Figure 6.10 but for the blocked configurations of ^{239}Pu with the SIII parametrization.

6.2.3 HF+BCS results with parity symmetry breaking

Parity symmetry breaking calculations have been performed for the experimental lowest two band heads in the normal-deformed ground-state well of the ^{235}U and ^{239}Pu nuclei. In the ^{235}U ground-state well, the first and second band-head states correspond to the $K^{\pi} = 1/2^{+}$ and $K^{\pi} = 7/2^{-}$, respectively, while in ^{239}Pu, they correspond to $K^{\pi} = 1/2^{+}$ and $K^{\pi} = 5/2^{+}$. When breaking the intrinsic parity symmetry, we have always considered the blocking of the single-particle state nearest to the Fermi level corresponding to the desired K quantum number. The parity symmetry breaking calculations have been started from a converged left-right symmetric field with a constraint on Q_{30} for a limited number of iterations so as to allow for the nucleus to explore left-right asymmetric shapes. Subsequently, the constraint on Q_{30} has been released so that the calculation converges to a local minimum at fixed elongation.

Let us first discuss the results for the ^{239}Pu nucleus. The deformation energies corresponding to the parity asymmetric solutions obtained with the SkM* and SLy5* parametrizations have been plotted in Figure 6.12 in dashed lines. As well known, the parity symmetry breaking calculations do yield a substantial effect on the deformation energies around the outer fission-barrier. The asymmetrical outer-barrier height for the $K = 1/2$ configuration with SkM* is lowered by about 3.9 MeV with respect to the symmetrical solution, which yields a barrier height $E_B = 6.3$ MeV. For the $K = 5/2$ configuration with the same Skyrme parameters we find an outer-barrier height of 6.6 MeV including a reduction of about 4.7 MeV with respect to the left-right symmetric solution.

In contrast to the parity-breaking deformation energy curves obtained with the SkM*, those obtained with the SLy5* parameters are much flatter with a very slow decrease of E with Q_{20} even up to about $Q_{20} = 300$ b. This shows that the SLy5* parametrization has unsatisfactory surface properties as compared to SkM*. The left-right asymmetric outer fission-barrier heights obtained with these two Skyrme parameter sets are tabulated in Table 6.2 in parentheses.

A cut in the potential energy surface along the Q_{30} direction at fixed Q_{20} values was performed for the $K = 5/2$ blocked configuration with the SkM* parametrization around the top of the second fission-barrier. The results are plotted in Figure 6.13. The figure clearly illustrates the transition from a symmetrical equilibrium solution at $Q_{20} = 95$b to increasingly asymmetrical solutions as a function of Q_{20}. The top of the barrier around $Q_{20} = 115$b for the 5/2 blocked configuration corresponds to a rather large value of Q_{30}. It is worth mentioning here that in the work of Ref. [80] in the ^{240}Pu nucleus within the Highly Truncated Diagonalization approach, the parity-projection calculation was found to have no effect on the total binding energy at the top of the outer fission-barrier, where the value of Q_{30} was also found to be large. In contrast, projecting on a positive parity state causes a lowering of the total binding energy in the fission-isomeric well. In view of this, we expect that restoring the parity symmetry may not have a large impact, if any, on calculated outer-barrier heights with respect to the normal-deformed ground-state well in odd-mass actinides.

Another shape degree of freedom of interest in this fission context is the hexadecapole moment Q_{40}. This quantity provides an indication of the formation of a neck as one approaches the scission point, where the fissioning nucleus splits into two smaller nuclei. In this situation a sudden decrease occurs in the value of Q_{40}. It has been checked that the results obtained here correspond to the same fission valley, without any drastic change in Q_{40}. An example of variation of Q_{40} as a function of Q_{20} around the top of the outer-barrier is shown in Fig. 6.14 for the lowest-energy $K = 1/2$ and $K = 5/2$ solutions in ^{239}Pu with SkM* and SLy5* parametrizations. A smooth variation is obtained in each case when asymmetric shapes are allowed. However, a shoulder appears when restricting to left-right symmetric shapes with SkM*, with the inflexion point located near the top of the outer barrier. With SLy5* this deviation from a smooth variation is actually accentuated and turned into a shallow local minimum, again around the top of the outer saddle point. It has been checked that this is not an artifact that arises, for example, when jumping from one fission valley to another.

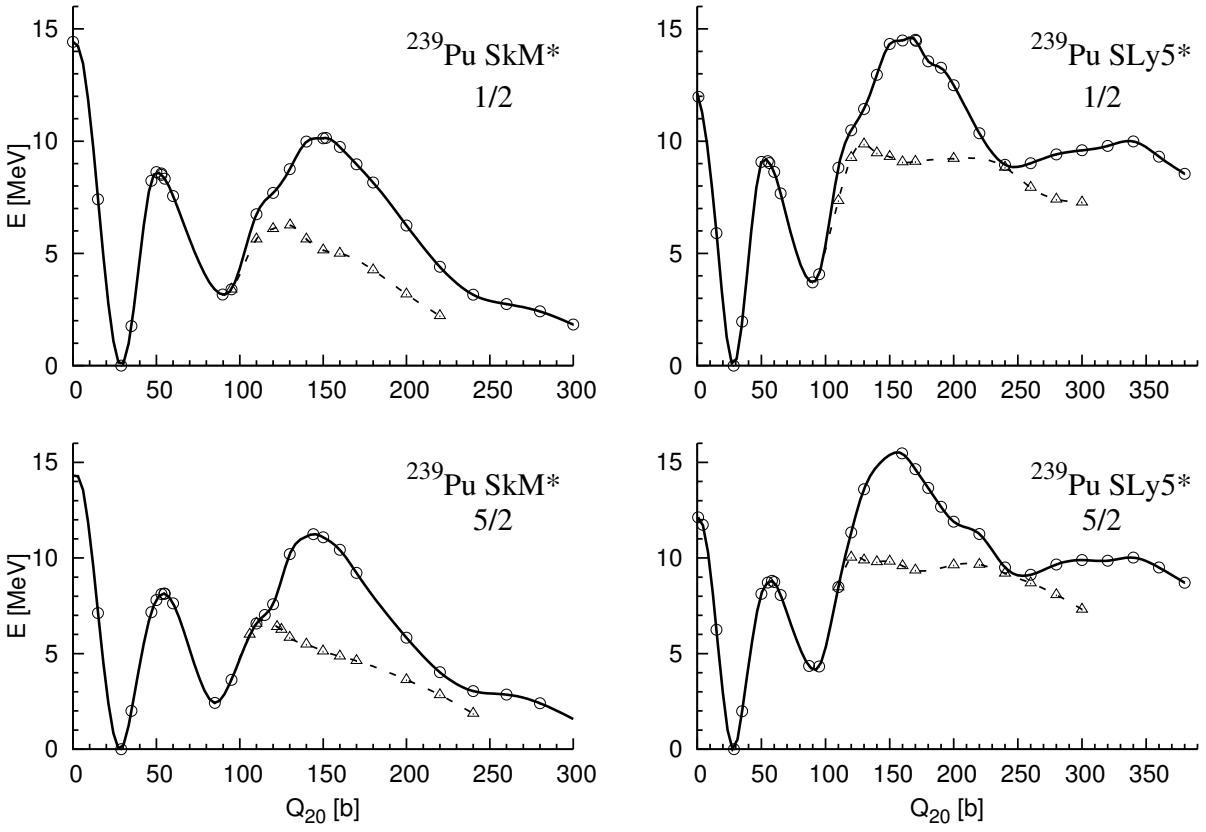

Figure 6.12: Deformation energy curves of ^{239}Pu as a function of deformation Q_{20} with parity symmetry breaking calculations obtained with the SkM* and the SLy5* parametrizations.

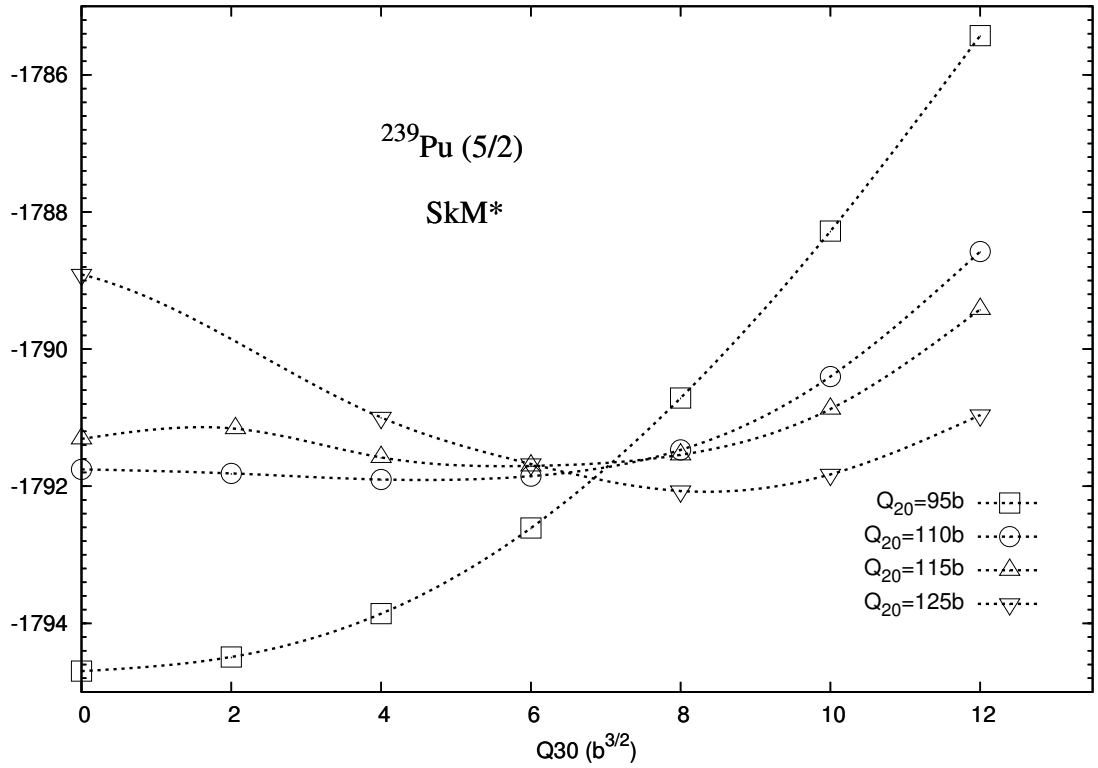

Figure 6.13: A cut in the potential energy surface around the top of the second barrier as a function of octupole moment Q_{30} (given in $barns^{3/2}$) of the 5/2 blocked configuration of ^{239}Pu obtained with the SkM* parametrization.

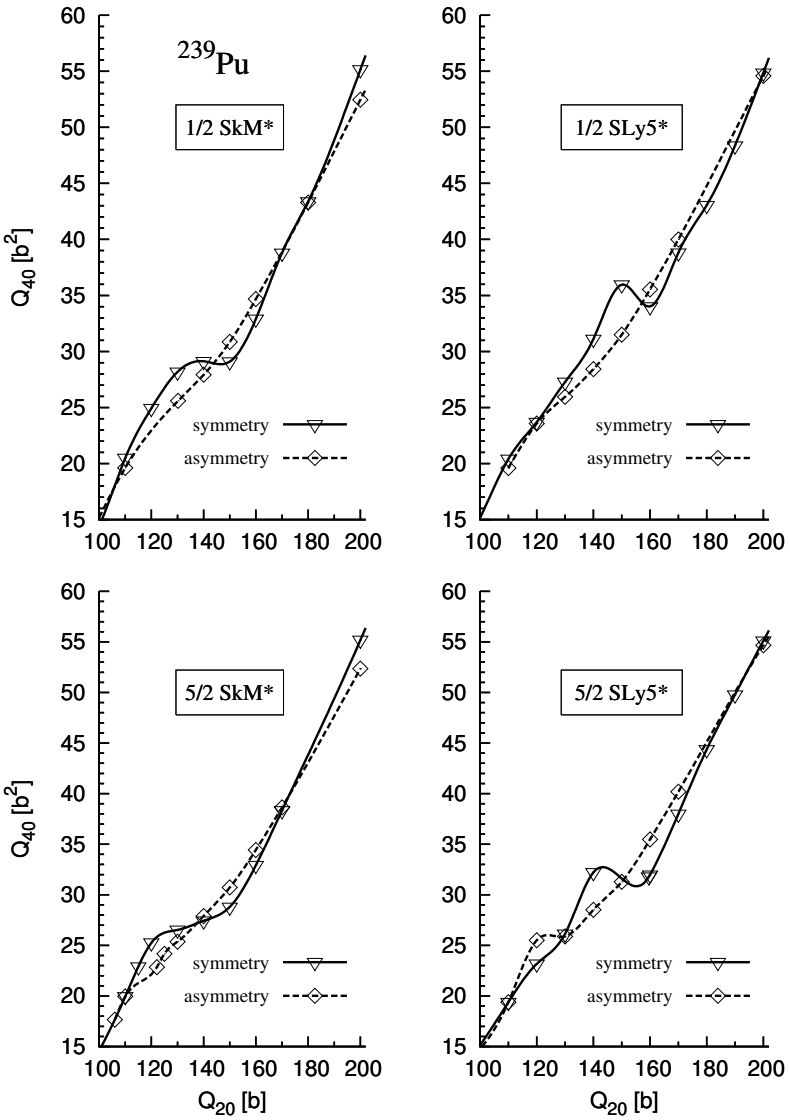

Figure 6.14: The hexadecapole moment Q_{40} as a function of Q_{20} in ^{239}Pu obtained with the SkM* and SLy5* parametrizations are plotted in solid lines for the solutions corresponding to a conserved parity symmetry. The solutions for the 1/2 and 5/2 blocked configurations with a broken parity are plotted in dashed lines.

We now move to the results of the parity symmetry breaking calculations for the ^{235}U nucleus with the SkM* parametrization. As mentioned before, the blocked configurations considered for the parity asymmetric calculations correspond to $K = 1/2$ and $K = 7/2$. As was done for the ^{239}Pu nucleus, the Hartree–Fock–BCS solutions for both configurations were obtained by blocking the single-particle state with $\Omega = K$ nearest to the Fermi level at each Q_{20} deformation. The deformation-energy curve for the $K = 1/2$ blocked configuration is plotted in Figure 6.15. The parity-asymmetric outer-barrier height for this blocked configuration is found to be 7.5 MeV, which is 3.7 MeV less than the left-right symmetric barrier height.

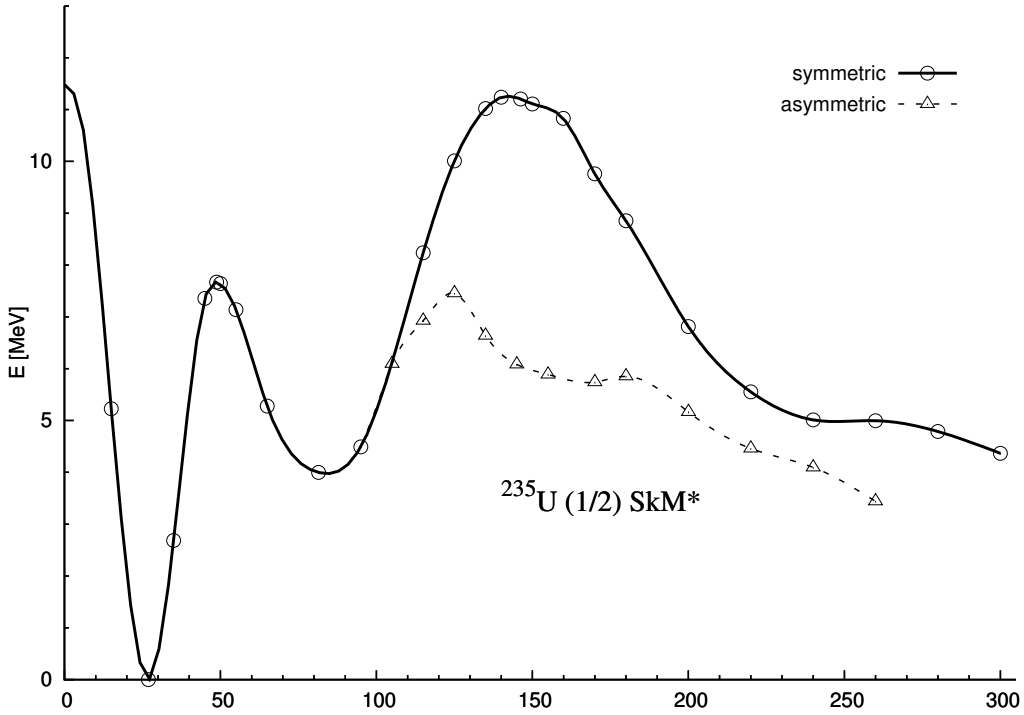

Figure 6.15: Deformation energy curves of ^{235}U as a function of quadrupole moment obtained with the SkM* parametrization for the 1/2 blocked configuration. The parity symmetric solutions are plotted in solid line while the asymmetric solutions are plotted in dashed line.

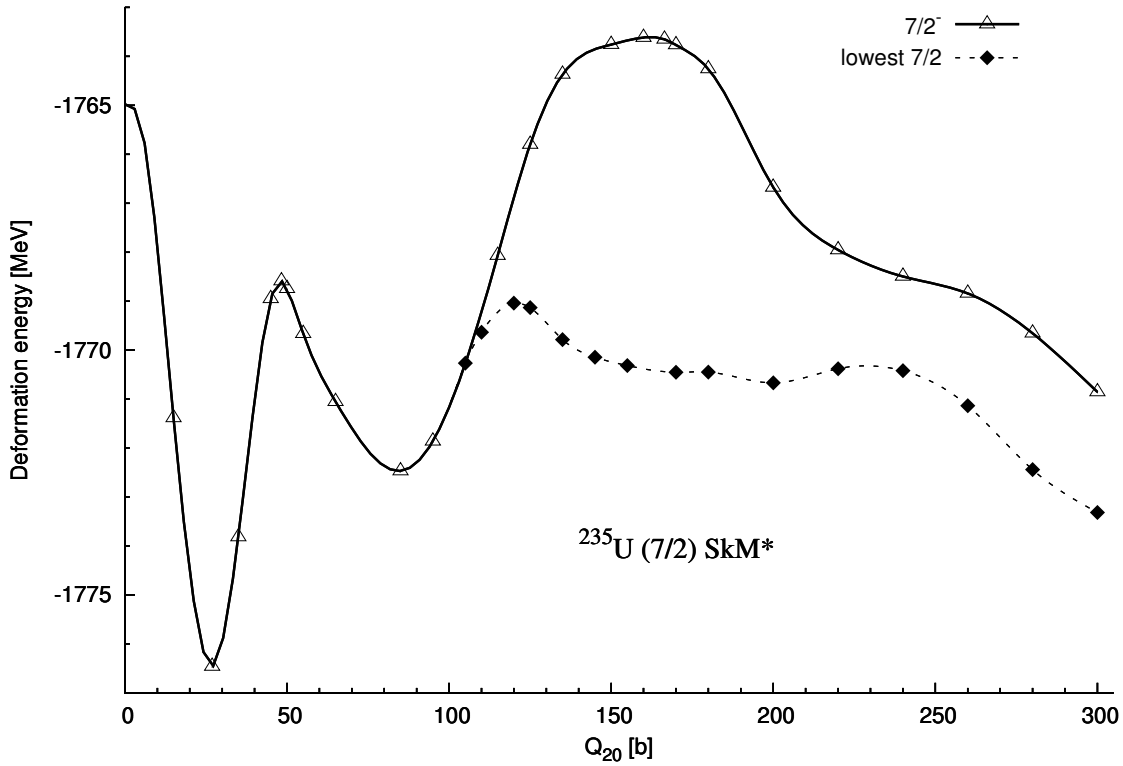

Figure 6.16: Deformation energy curves of ^{235}U as a function of quadrupole moment obtained with the SkM* parametrization for the 7/2 blocked configurations. The parity asymmetric solutions obtained with the blocking of a single-particle state with $\Omega = 7/2$ nearest to the Fermi level at each deformation are connected by a dashed line.

Similarly the deformation-energy curve for the $K = 7/2$ blocked configuration is plotted in Figure 6.16. In this case the decrease of the outer-barrier height obtained by the release of the parity-symmetry constraint is about 5.4 MeV, which is much more than the above 1/2 case.

Because in the ground-state well, experiments have found a $7/2^+$ state only 445 keV above the $7/2^-$ ground-state, we have to make sure that the obtained curve for the $K = 7/2$ blocked configuration does represent a continuous fission-path. To do so we first analyze the structure of the $\Omega = 7/2$ single-particle states near the Fermi level as a function of the quadrupole moment Q_{20} from the superdeformed well (where $Q_{20} \approx 85$ b) to higher elongations. The upper panel of Figure 6.17 shows the variation of the single-particle energies for the two $\Omega = 7/2$ states nearest to Fermi level as a function of Q_{20}, whereas the lower panel shows the expectation value of the parity operator (average parity) in theses two states as a function of Q_{20}. As expected the average parity is equal to -1 for solutions of left-right asymmetric calculations performed at elongations slightly larger than the one of the superdeformed minimum and decreases in absolute value as Q_{20} increases. Up to $Q_{20} = 110$ b the lowest $7/2$ blocked configuration is found to has a negative average parity. The corresponding fission-path is then continuous up to this elongation value. For Q_{20} values equal to and larger than 120 barns the average parity is found to be positive with a large value slowly decreasing as a function of Q_{20}. We might then suspect a possible discontinuity in the fission-path between 110 and 120 barns. Indeed in this interval two $7/2$ single-particle states above the Fermi level seem to become almost degenerate as is visible from the upper panel of Figure 6.17. However, according to the "no-crossing rule", the curves corresponding to the variation with a continuous quantity (here the quadrupole moment) of the energy of two single-particle states with the same good quantum number (here the projection of the angular momentum on the z axis) do not cross. Therefore the energy of the many-body solution obtained by blocking the single-particle state nearest to Fermi level remains a continuous function of Q_{20} in the 110-120 barns interval despite the jump of the average parity (see solid line in lower panel of Figure 6.17).

Figure 6.18 summarizes the various solutions obtained as a function of the quadrupole moment between the isomeric well and $Q_{20} = 200$ b. The dashed line connecting the open symbols correspond to left-right symmetric calculations for the $7/2^+$ (circles) and the $7/2^-$ (triangles) blocked configurations. It is worth keeping in mind that the solutions resulting from these calculations are not necessarily local minima as functions of left-right asymmetric deformations. In contrast filled symbols represent equilibrium solutions resulting from left-right asymmetric calculations for two blocked configurations: circles correspond to a positive average-parity solution whereas triangles correspond to the other 7/2 configuration (of negative average parity up to 110 barns). When these symbols lie on the dashed line one has a local minimum at $Q_{30} = 0$ as a function of the octupole moment Q_{30} for a fixed value of the quadrupole moment. Finally the solid line in Figure 6.18 connects the lowest-energy solutions as a function of Q_{20}. From this figure and the above "no crossing rule" we deduce that following a fission-path along which the structure of the blocked state remains continuous from the left-right symmetric $7/2^+$ and $7/2^-$ soutions in the isomeric well give different and erroneous fission barriers. The actual mean-field, left-right asymmetric fission barrier is the one represented as a solid line in Figure 6.18.

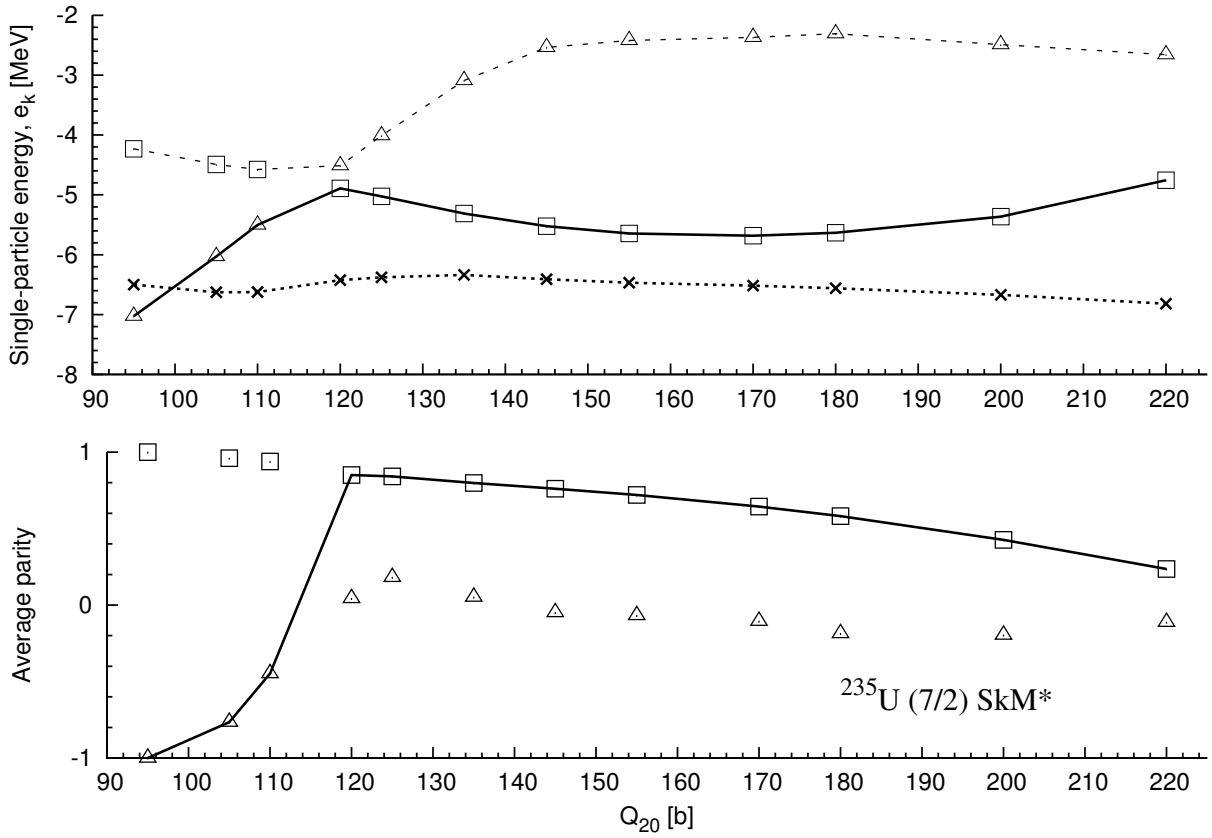

Figure 6.17: (Top): The evolution of the energies of the single particle states near the BCS chemical potential (marked with crosses) with $\Omega = 7/2$ quantum number as a function of quadrupole moment Q_{20} obtained in the parity asymmetric calculations of ^{235}U. The solid line connects the blocked single-particle states as a function of deformation. (Bottom): The average parity of the blocked single-particle states as a function of deformation.

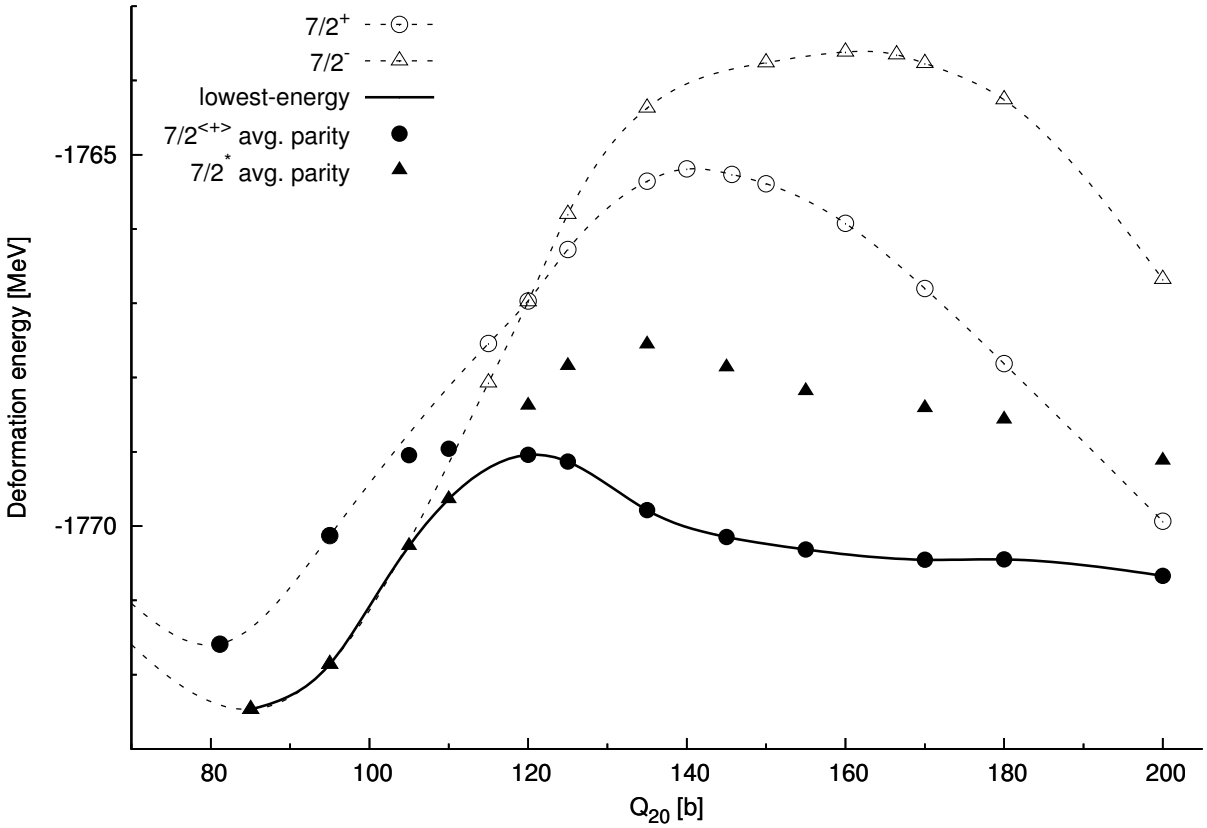

Figure 6.18: A portion of the deformation energy curves of the blocked $K = 7/2$ configurations in ^{235}U from the fission-isomeric well up to beyond the top of the second barrier. The filled symbols refer to the local minima as functions of Q_{30} for fixed elongation Q_{20} while the unfilled symbols refer to the solutions obtained by constraining the nucleus to have a left-right symmetry. The solid line connects the lowest-energy solutions when the left-right symmetry is broken.

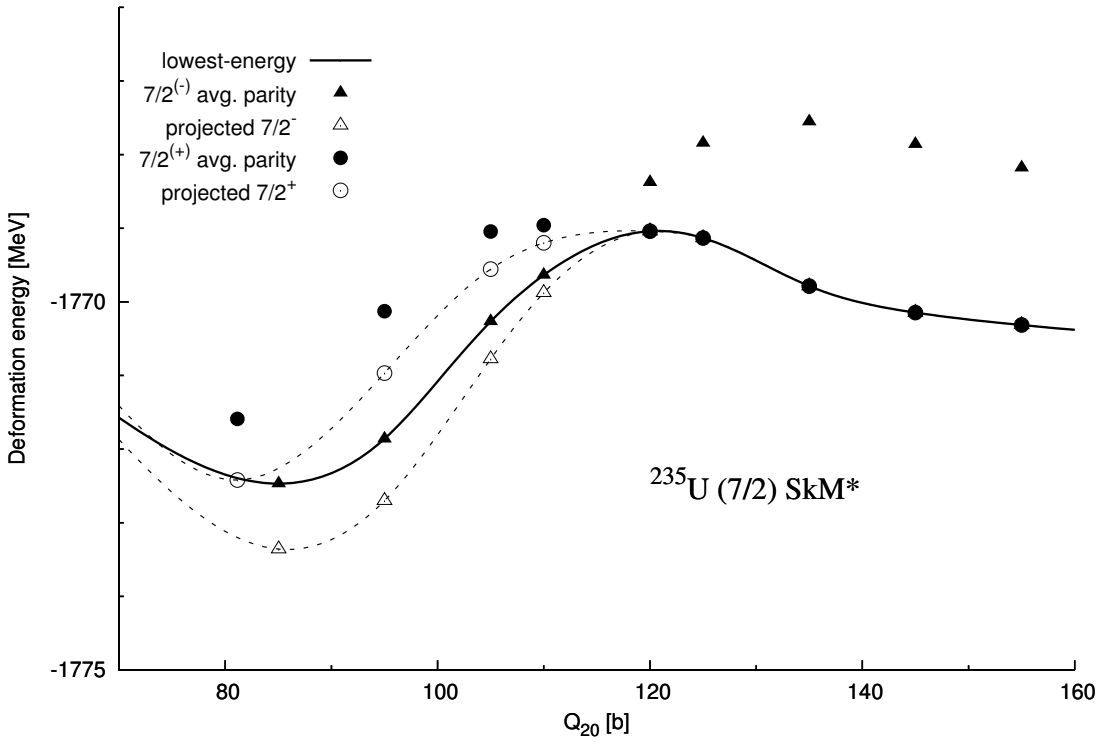

Figure 6.19: A portion of the deformation energy curves for the two 7/2 blocked configurations around the top of the outer-barrier. The lowest-energy mean-field solutions are connected by a solid line. The unfilled symbols refer to the predicted solution when the parity projection calculations are performed by projecting the mean-field solutions on a good parity state of similar (positive or negative) sign. The effect of parity projection on the total energy are estimated from the values obtained for ^{240}Pu in Ref. [80].

As known from Refs. [91, 80], the effect on the total energy of parity projection after variation of left-right asymmetric mean-field solutions is the larger in the isomeric well and decreases as one approaches the top of the outer-barrier. In Figure 6.19 we estimate this effect as follows. As in the previous figure the filled symbols represent left-right asymmetric equilibrium solutions for two 7/2 blocked configurations and the solid line connect the lowest ones as a function of the quadrupole moment. The corresponding unfilled symbols connected by dashed lines are estimates of parity projected solutions assuming the same gain in energy as found for ^{240}Pu as a function of Q_{20} in Ref. [80]. More precisely open circles correspond to positive parity projection of the positive average parity mean-field solution represented by the filled circles, whereas open triangles correspond to negative parity projection of the other blocked mean-field solution represented by the filled circles. Beyond 115 barns the effect of parity projection is assumed to be negligible, hence the merge of the two dashed curves with the solid curve for $Q_{20} \geq 120$ b. With the above assumptions the barrier tops for the $K^\pi = 7/2^-$ and the $K^\pi = 7/2^+$ band heads are predicted to coincide at about $Q_{20} = 120$ b. Therefore the barrier-height difference for these two states is expected to be entirely due to the their binding-energy difference in the ground-state well.

6.2.4 Fission-barrier heights within the Bohr-Mottelson unified model

From the earlier discussions in this section up to this point, we have investigated at how the different Skyrme parametrizations perform in the calculations of the deformation energies at the mean-field level. In order to evaluate our mean-field solutions within the Bohr-Mottelson unified model, we will need to take into account the core rotational correction. The rotational correction calculated using the Belyaev formula were evaluated from three different ways. The values obtained from pure Belyaev formula are denoted as IB, those which take into account the approximate Thouless-Valatin correction term to the moment of inertia are denoted as IB+TV and the reduction of rotational correction calculated using the Belyaev formula by 50% are denoted as IB-50%. In all three cases, the $\langle \hat{J}^2_{\rm core} \rangle$ term was calculated for its polarized even-even $(A-1)$ core nucleus, where A is the mass number of the odd-mass nucleus, by excluding the blocked state and its conjugate state from the expression of $\langle \hat{J}^2_{core} \rangle$ of Ref. [109].

In this section, we shall limit the evaluation of the fission barriers within the Bohr-Mottelson model to the mean-field solutions obtained with the SkM* parametrization. The SIII and SLy5* parametrizations have been shown to give higher fission barriers as compared to SkM* at the mean-field level, and this remains true even with the inclusion of the rotational correction. The fission-barrier heights for the various K^π blocked configurations in the two considered odd-neutron nuclei are listed in Table 6.3. Both the parity symmetric and asymmetric outer-barrier heights are tabulated for completeness. The parity asymmetric outer-barrier heights obtained for other blocked configurations are also given in the table. It can be seen that the rotational correction calculated using the Belyaev formula gives too low an outer fission-barrier in some cases as compared to the empirical values found to be within the range of 5.5 - 6.0 MeV (see Table 6.5). From the study of fission-isomeric energy E_{II} presented in Section 5.3 for the odd-mass nuclei and Section 6.1.2 for even-mass nuclei, it has been found that the calculated values compares more reasonably to the experiment when considering a 50% reduction to the rotational correction calculated using the Belyaev formula. In view of this, we shall make use of the fission-barrier heights obtained from this rotational correction scheme for comparison with empirical values and values obtained from other work in a later section. The inner-barrier heights, fission-isomeric energy for a fixed K^π configuration E_{IS}, and asymmetric outer-barrier heights obtained with this rotational correction scheme were found to differ by about 0.50, 0.70 and 1.0 MeV, respectively, from the results obtained with the Belyaev moment of inertia. Figure 6.20 shows the deformation energy curves evaluated within the Bohr-Mottelson model for the four blocked configurations in ^{239}Pu as compared to its neighbouring even-mass nuclei. The rotational correction used for the plot were the values obtained using the Belyaev values with a reduction by 50%.

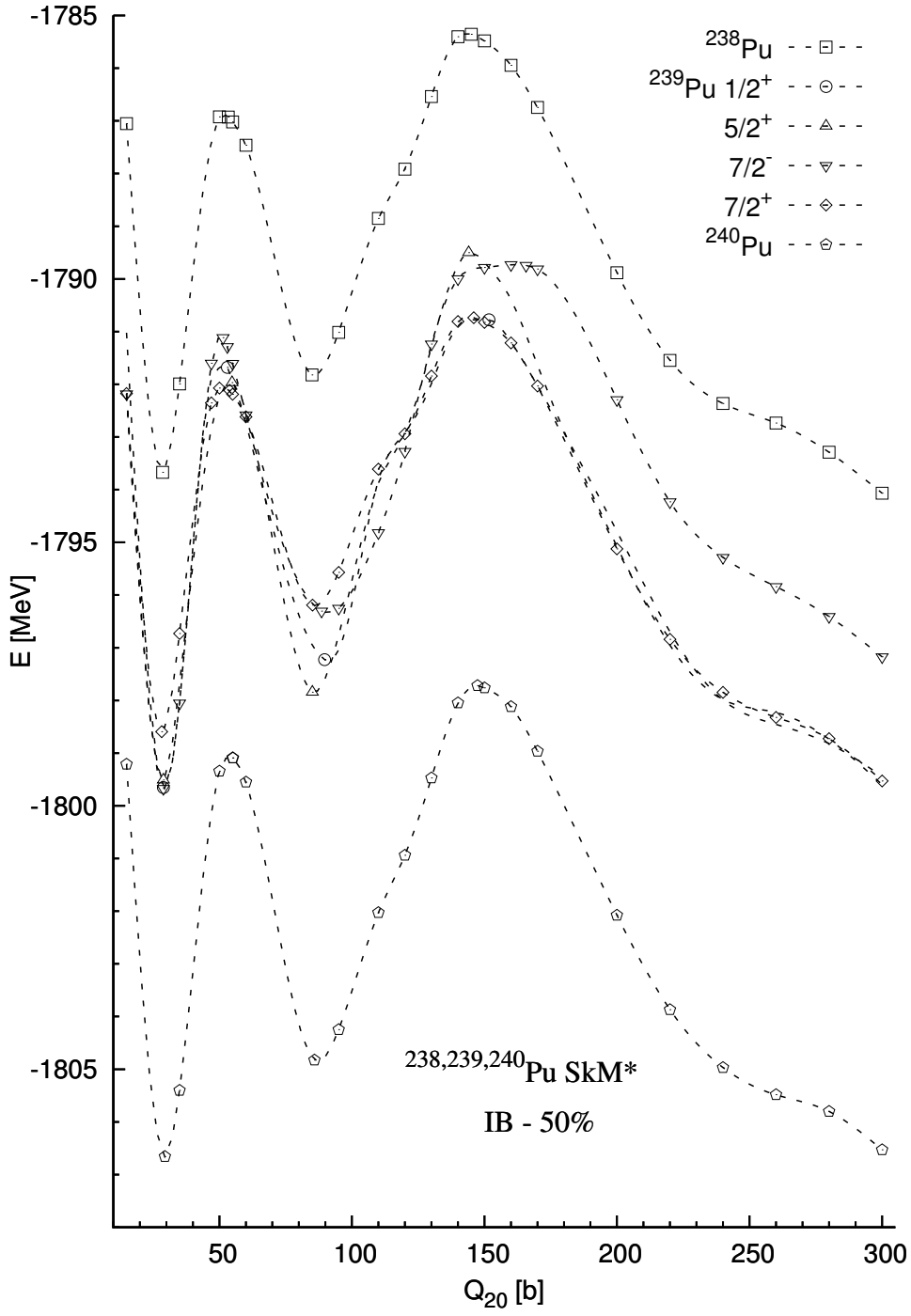

Figure 6.20: The deformation energy curves with a conserved parity symmetry of the considered plutonium isotopes within the Bohr-Mottelson unified model whereby the values of the rotational correction calculated using the Belyaev formula have been reduced by a factor 2.

Table 6.3: The inner-barrier heights E_A, the fission-isomeric energy with respect to the respective ground state E_{IS} and the outer-barrier height E_B of the odd-neutron nuclei within the Bohr-Mottelson unified model. The mean-field results were obtained with the SkM* parametrization. Three values (in MeV) were given for each barrier corresponding to the manner in which the rotational correction is calculated. The calculations using the Belyaev formula is denoted as IB, while the scaling of the Belyaev moment of inertia to account for the so-called Thouless-Valatin correction is denoted as IB+TV. The IB-50% refers to the reduction of the rotational correction calculated using the Belyaev formula by 50%.

Nucleus	K^π	E_A			E_{IS}			E_B (symmetric)			E_B (asymmetric)		
		IB	IB+TV	IB-50%	IB	IB+TV	IB-50%	IB	IB+TV	IB-50%	IB	IB+TV	IB-50%
^{235}U	$1/2^+$	6.57	6.83	7.11	2.60	2.94	3.30	8.60	9.23	9.90	5.31	5.83	6.38
	$7/2^-$	6.97	7.18	7.41	2.70	3.00	3.32	10.25	10.85	11.49	5.49	5.94	6.42
	$5/2^+$	5.83	6.09	6.37	1.44	1.78	2.15	9.57	10.17	10.80	4.90	5.36	5.84
	$3/2^+$	6.19	6.43	6.69	1.48	1.81	2.16	8.12	8.72	9.37	3.82	4.33	4.88
	$7/2^+$	4.75	5.04	5.35	2.21	2.55	2.91	7.29	7.93	8.61	4.03	4.54	5.09
	$5/2^-$	6.32	6.59	6.87	3.97	4.28	4.62	8.21	8.81	9.46	4.24	4.70	5.18
^{239}Pu	$1/2^+$	7.43	7.71	7.98	1.70	2.05	2.43	7.63	8.24	8.88	4.15	4.66	5.20
	$7/2^-$	8.10	8.32	8.56	2.74	3.05	3.37	8.75	9.32	9.93	4.70	5.12	5.57
	$7/2^+$	5.90	6.18	6.48	1.72	2.05	2.40	6.63	7.22	7.86	3.53	4.00	4.49
	$5/2^+$	6.97	7.25	7.54	0.96	1.30	1.67	8.83	9.40	10.00	4.68	5.13	5.62

6.3 The specialization energy of odd-mass nucleus

Figure 6.21 shows the fission-barrier heights with a conserved parity symmetry evaluated within the Bohr-Mottelson unified model of the various blocked K^π configurations of ^{239}Pu with respect to those of the neighbouring even-even nuclei. We see that the inner and outer-barrier heights of some blocked configurations (the $7/2^-$ configuration being an excellent example) are higher than the even-even nucleus as a consequence of following fixed K^π quantum numbers. On the other hand, the $7/2^+$ blocked configuration appears to have lower fission-barrier heights as compared to the even-even nucleus. This is so because the $7/2^+$ configuration is found at much higher energy in the ground-state deformation well (see Section 5.2), but with a lower energy solution at the saddle points as compared to the other blocked configurations (refer to Figure 6.20).

We define here the specialization energy as the difference in the fission-barrier heights of the various blocked configurations of odd-mass nucleus with respect to the average fission-barrier heights of its neighbouring even-mass nuclei. Table 6.4 list the specialization energies denoted as $E^{spec}_{A,B}$ (with *A* and *B* referring to the inner and outer-barrier, respectively) for the four considered blocked configurations in ^{239}Pu. The negative values reported for the $7/2^+$ state reflect that the inner and outer fission-barrier heights for this blocked configuration are lower than the average fission-barrier heights of ^{238}Pu and ^{240}Pu nuclei.

Table 6.4: The specialization energies defined as the difference in the fission-barrier heights of the odd-mass nucleus with respect to the average values of the two neighouring even-mass nuclei is listed for the four blocked configurations of ^{239}Pu (in MeV). The results were obtained with the SkM* parametrization with a reduction factor of 50% for the rotational correction calculated using the Belyaev formula.

	K^π			
	$1/2^+$	$5/2^+$	$7/2^+$	$7/2^-$
E^{spec}_A	0.83	0.39	-0.68	1.41
E^{spec}_B	0.26	1.38	-0.77	1.31

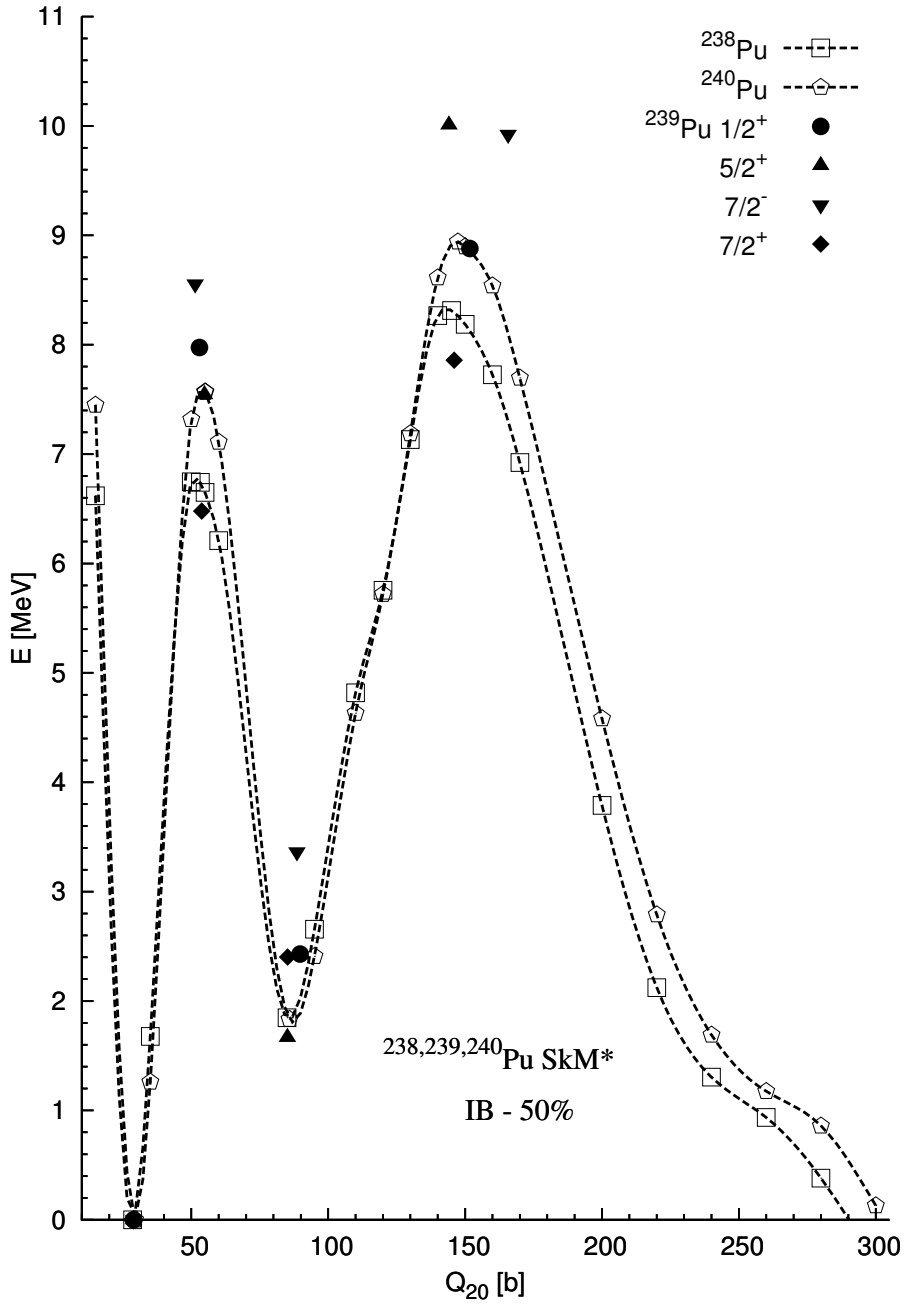

Figure 6.21: The locations of the inner-barrier heights, fission-isomeric energies (for a fixed K^{π}) and the outer-barrier heights of the four considered K^{π} configurations of ^{239}Pu nucleus (with a conserved parity symmetry) are plotted with respect to the deformation energy curves of the ^{238,240}Pu nuclei. The results used for the plot were obtained with the SkM* parametrization and including the reduction factor of 50% for the rotational correction calculated using the Belyaev formula.

6.4 Connection with fission cross sections

6.4.1 Comparison of barrier heights with empirical values and other calculations

It is to be noted that some corrections should be taken into account before comparing our fission-barrier heights within the Bohr-Mottelson unified model listed in Table 6.3 with barrier heights obtained in other calculations or those deduced from experiment. We shall discuss first the corrections to be made for the inner-barrier heights. As discussed in Section 4.3.2, the inner-barrier height is estimated to be lowered by about 0.2 MeV when increasing the basis size parameter N_0 from 14 to 16. Secondly, the correction due to the Slater approximation for the Coulomb exchange interaction was found to increase the inner-barrier height by about 0.3 MeV in ^{238}U [58] and we shall assume a similar amount of correction for the two considered nuclei herein.

On top of that, one should also consider the impact of breaking the axial symmetry especially around the top of the inner-barrier where this symmetry breaking have been shown to lower the inner-barrier height, especially so for superheavy nuclei. When breaking the axial symmetry, K is no longer a good quantum number and this may pose a problem in the blocking procedure for an odd-mass nucleus. One may expect that the single-particle states would contain mixtures of K quantum numbers. By following a blocked single-particle state as a function of deformations, there may arise situations where the "transition" from one blocked solution to another occur for single-particle states with differing K content. We would rather consider the impact of the axial symmetry breaking on the inner-barrier of odd-mass nuclei by using the estimates obtained in the calculations for even-mass nuclei in the work of Ref. [60]. Assuming that the effect of triaxiality to be the same for all considered blocked configurations, we expect a reduction in the inner-barrier height by about 0.5 MeV. This translates into a total reduction (including the two corrective terms discussed above) of the inner-barrier height by about 0.4 MeV.

A note is to be made here with regards to the effect of triaxiality. As was reported in Ref. [110], the effect of triaxiality in dynamical calculations depends on the manner in which the inertia parameter is calculated. When using the non-perturbative cranking approximation for the inertia parameter, the fission-path of ^{264}Fm was found to be closer to the triaxial fission-path obtained from static (minimum-energy) calculations, with a slightly higher barrier height for the former as compared to the latter. On the other hand, the dynamical fission-path is closer to axially symmetric fission-path when the inertia parameter is calculated from a perturbative cranking approximation. In view of this, the triaxial correction as mentioned above is thus an upper limit of this effect on the inner-barrier height.

Moving now to the outer-barrier, the correction due to the Slater approximation have not been tested due to the rather heavy computing task, in particular when breaking the parity symmetry. We need to rely on a rough estimate for this purpose. In Ref. [58], exact calculations were found to increase the fission-isomeric energy by about 0.28 MeV. Since the Slater approximation is supposed to work well for cases where the single-particle level density near the Fermi level is high, as is the case at the outer-barrier, we

may then assume that the amount of correction to the outer fission-barrier height is about 0.25 MeV at most. This amount of correction due to the Slater approximation partly compensates for the lowering of the outer-barrier due to the basis size truncation effect estimated to be around 0.40 MeV. The total effect of the corrective terms to the outer-barrier is therefore a lowering of the barrier height by about 0.1 - 0.2 MeV.

When taking the total corrections to the fission-barrier heights as mentioned above, the inner-barrier heights for the different blocked configurations obtained with the SkM* parametrization and including the (IB-50%) rotational correction scheme ranges from about 5.0 to 7.0 MeV for ^{235}U, and about 6.1 to 8.2 MeV for ^{239}Pu. The left-right asymmetric outer-barrier heights lies within the range of about 4.7 to 6.2 MeV for the ^{235}U nucleus, while it range from about 4.3 to 5.4 MeV for the ^{239}Pu nucleus.

Some sets of fission-barrier heights of the two considered odd-neutron nuclei obtained from other calculations or from empirical means are tabulated in Table 6.5 for comparison. Three sets of values were obtained from calculations, namely the calculations by Robledo and collaborators [21, 22], the fission-barrier heights fitted to reproduce the neutron-induced fission cross-sections by Goriely and collaborators [19], and the macroscopic-microscopic calculations by Möller [44]. In the the RIPL-3 [20] database, another set of fission-barrier heights are given apart from those of Ref. [19]. This set of data which is also listed in the table is taken from the empirical estimates compiled by Maslov *et al.* [111]. The last set of data is the empirical fission-barrier heights of Bjørnholm and Lynn [108] obtained from the lowest energy solution at the saddle points irrespective of the nuclear angular momentum and parity quantum numbers.

Out of these values, only those obtained from Refs. [21, 22] using the Gogny D1S force within the Hartree-Fock-Bogoliubov-EFA framework (listed in the third column of Table 6.5) are directly comparable to our results. Their fission-barrier heights assuming axial symmetry are much higher when compared to our calculated results. However, the values obtained in Refs. [21, 22] are consistent with the rather high fission-barrier heights obtained for the even-even ^{240}Pu nucleus in the earlier work of Ref. [36]. It should be stressed that the rather large differences between our results and those reported in Refs. [21, 22] should not be interpreted as an effect due to the treatment of the time-reversal symmetry breaking. In fact, it has been checked that equal-filling approximation (EFA) calculations affects the total binding energies by a few hundreds keV at most for the parity symmetric case. A test calculation performed for the parity asymmetric case of ^{239}Pu also leads to the same conclusion, that the effect of time-reversal symmetry breaking is approximately constant with deformation.

The comparison with the other sets of data in Table 6.5 are less straight forward and we could not established a one-to-one comparison between our calculated values with the empirical data. As was mentioned in Ref. [82], since the uncertainty in the empirical fission-barrier heights is about 1 MeV, it is then deemed reasonable if the fission-barrier heights are reproduced within 1-2 MeV from the empirical values. In our case, the fission-barrier heights calculated with the SkM* parametrization and after taking into account the various corrective terms as discussed above, falls within the 2 MeV range from the empirical values.

For comparison, the values of the fission-barrier heights corresponding to the experimental ground-state K^{π} quantum numbers, obtained after corrections are listed in the last column of Table 6.5. The calculated outer-barrier heights compares favorably with the RIPL-3 empirical data. However, the agreement is less good for the inner-barrier and this could be due to the approximate correction to the effect of triaxiality.

Interestingly, the calculated inner-barrier heights for all blocked configurations in ^{235}U and ^{239}Pu were found to be higher than their respective outer-barrier. This pattern is consistent with the results of Ref. [21, 22] and the empirical values provided by Ref. [108]. On the other hand, the macroscopic-microscopic calculations of Ref. [44] and the fission-barrier heights supplied by Ref. [20] suggest a higher outer-barrier as compared to its inner-barrier in ^{235}U .

Finally, it is to be noted that the inner and outer-barrier heights supplied by Ref. [19] in the RIPL-3 database, and listed in Table 6.5 have been independently optimized so as to reproduce at best the neutron-induced fission cross-sections. The simultaneous optimization of the inner and outer-barrier heights have also been attempted (with the resulting fission-barrier heights given in Table 6.6) but such a procedure was found to yield a poorer agreement to the fission cross-sections as compared to the independent optimization of the two barriers.

Table 6.5: The inner E_A and outer-barrier E_B heights (given in MeV) of the two considered odd-neutron nuclei obtained from other calculations as well as the values deduced from experiments. The EFA results were extracted from Ref. [21] and [22]. The RIPL-3 [20] values consists of two sets of data; one by Ref. [19] whereby the barrier heights have been fitted independently of one another to best reproduce the experimental neutron-induced fission cross section, while the other set consists of empirical values compiled by Maslov *et al.* [111]. The fission-barrier heights obtained from the macroscopic-microscopic model of Ref. [44] and the empirical values of Bjørnholm and Lynn [108] are also tabulated for comparison. The calculated fission-barrier heights corresponding to the experimental ground-state K^{π} quantum numbers are listed in the last column, whereby these values have been obtained after taking the various corrections into account.

Nucleus	K	EFA		Ref. [19]		Ref. [111]		Ref. [108]		Ref. [44]		present work	
		E_A	E_B	E_A	E_B	E_A	E_B	E_A	E_B	E_A	E_B	E_A	E_B
^{235}U	1/2	9.0	8.0	5.54	5.80	5.25	6.00	5.9	5.6	4.20	4.87	-	-
	7/2	8.5	7.2									7.01	6.22
^{239}Pu	1/2	11.0	8.5	5.96	5.86	6.20	5.70	6.2	5.5	5.73	4.65	7.58	5.00
	5/2	11.5	9.0									-	-
	7/2	11.0	8.5									-	-

Table 6.6: The values (given in MeV) are extracted from Table I of Ref. [19]. The inner E_A and outer E_B barrier heights were obtained from independent fit of the fission-barrier heights of RIPL-2 [46] to best reproduce the neutron-induced fission cross-sections. The values of E'_A and E'_B were obtained when fitting both the inner and outer-barrier heights simultaneously but the resulting fission cross-sections obtained with these values of the fission-barrier heights were found to be in less good agreement to the experimental data.

Nucleus	E_A	E_B	E'_A	E'_B
^{235}U	5.54	5.80	4.80	5.58
^{239}Pu	5.96	5.86	6.02	5.38

6.4.2 Transition states at the top of the inner-barrier

As was discussed in Chapter 2, the calculations of the neutron-induced fission cross sections requires the knowledge of the transition states. The transition states are further categorized into discrete states and a continuum. Some of the discrete transition states can be obtained by performing self-consistent blocking calculations as was done for the band-heads energy spectra in the ground-state and fission-isomeric wells spectra presented in Chapter 5. They describe multi-quasiparticle configuration and the rotational band built upon them. Other excitation modes exist at higher energies and have to be described with an appropriate nuclear-structure model.

Figure 6.22 shows a sample of the transition states above the inner saddle point of ^{239}Pu obtained with the SkM* parametrization. Calculations have been performed first by blocking several single-particle states corresponding to different Ω^π quantum numbers near to the Fermi level. Such solutions corresponds to the different K^π band-head energies. The rotational bands are then build on top of these band-heads using the usual expression:

$$E^{(I)}_{K\pi} = E^{(I=K)}_{K\pi} + \frac{\hbar^2}{2\mathcal{J}}\Big[I(I+1) - K(K+1)\Big] \tag{6.5}$$

where $E^{(I=K)}_{K\pi}$ is the band-head energy while $I = K, K+1, K+2$, ... etc.

Such an approach to obtain the discrete transition states can be extended to other nuclei, as well as to the outer saddle point. The calculations of the discrete transition states at the outer saddle points are however more involved as one will need to perform parity-breaking calculations for several K quantum numbers. In addition to the rotational states thus obtained, one could also apply the highly truncated diagonalization approach (HTDA) model [63] to build multi-particle-multi-hole excited states above the saddle points.

6.4.3 Additional nuclear structure ingredients for fission transmission coefficients

As was discussed in Section 2.2.2, one would need to calculate the barrier penetrabilities $\mathscr{P}_j(E, V^{J^\pi}_{j_d})$ in order to obtain the fission transmission coefficients for a compound nucleus with specific J^π quantum numbers

and excitation energy E. Apart from the above two ingredients which could be supplied by our microscopic model, namely the fission barriers and the transition states at the saddle points, one would need at least three more kinds of nuclear structure input for the calculations of the barrier penetrabilities.

The first one is the fission-barrier profile for each discrete transition states. In the neutron-induced fission cross sections calculations of Ref. [19], the shape of the fission barriers are assumed to be the same for all Bohr transition states. One can now improve on this approximation by making use of the approach discussed in Section 6.4.2 to obtain a unique fission-barrier profile for each of the considered discrete state. This can be done by building rotational bands on top of each band-heads at different Q_{20} deformations. The solutions corresponding to the same J^π quantum numbers originating from the same band-heads along Q_{20} can then be connected to obtain the deformation energy curves.

The second piece of information is related to the inertia parameter as a function of deformation (see Section 2.3.3) and to be computed for each considered K^π quantum numbers. Finally, one would need the nuclear level density at high excitation energy and this could be supplied by an appropriate nuclear-structure model.

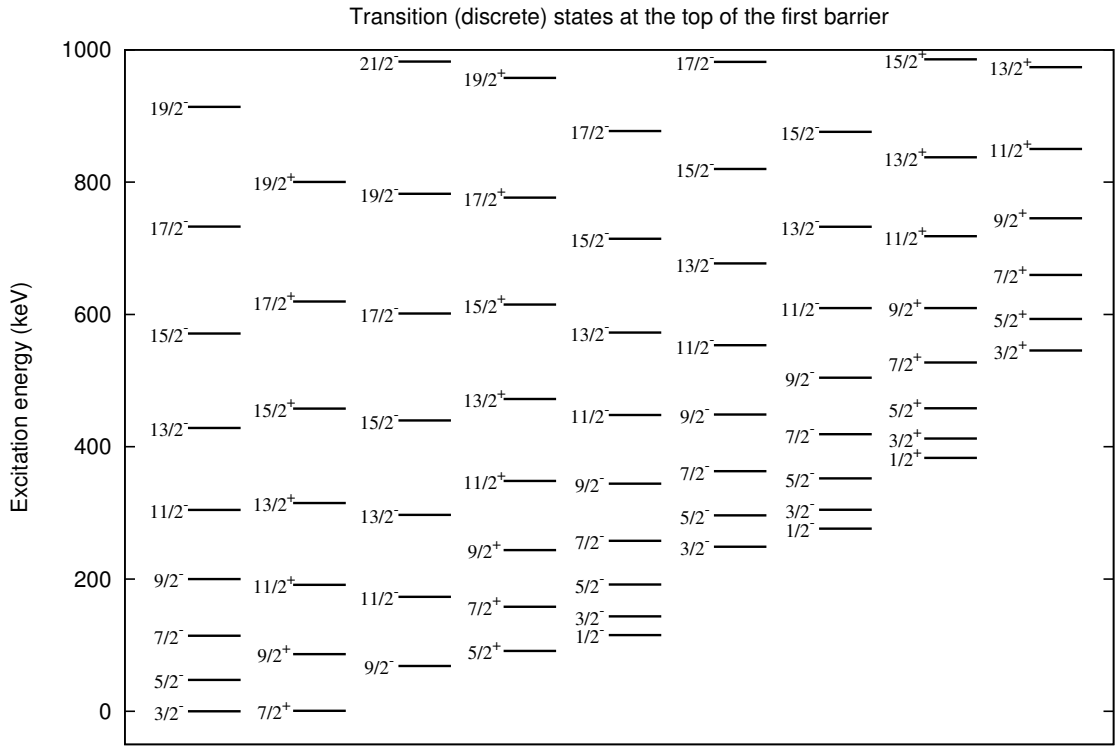

Figure 6.22: The discrete transition states at the top of the inner-barrier of ^{239}Pu with the SkM* parametrization shown as rotational bands build on top of the different band-heads, presented in the *Fission Experiments and Theoretical Advances Fission School and Workshop* (2014).

Chapter 7

CONCLUSION & PERSPECTIVES

Spectroscopic properties and fission-barrier heights of odd-mass nuclei have been calculated within the Skyrme-Hartree-Fock-plus-BCS (HF+BCS) framework, assuming axial symmetry, for various blocked K^π configurations taking into account the effect of time-reversal symmetry breaking. For each set of quantum numbers K^π, the lowest energy solution is obtained by blocking the $\Omega_i^{\pi_i} = K^\pi$ single-particle state $|i\rangle$ closest to Fermi level. The SIII, SkM* and SLy5* parametrizations were used. The HF+BCS results were interpreted within the Bohr-Mottelson unified model in the laboratory frame with some due attention made to the core rotational energy in fission-barrier calculations. The moment of inertia entering the rotational energy is usually calculated using the Belyaev formula. However, it has been reported in an earlier work that the rotational correction thus obtained is overestimated resulting in underestimation of the fission-barrier heights. Two improvements have been considered herein. First is the scaling of the moment of inertia by a factor (1+α) with $\alpha = 0.32$ to account for the omission of some Thouless-Valatin corrective term in the Belyaev formula. The second is to reduce the rotational energy calculated with Belyaev formula by 50%. In this way, the various approaches to the rotational correction allows for a sensitivity study of the fission-barrier heights to the moment of inertia.

Since the fission-barrier heights are related to the energies at the saddle points with respect to the ground-state solution, the study of the band-head energies in the normal-deformed (ground-state) well of some odd-mass nuclei was first performed as a test of the quality of our approach. The calculations were restricted to the experimental band-heads of ^{237}Np, ^{241}Am, ^{235}U and ^{239}Pu nuclei up to 650 keV excitation energy. An overall good qualitative agreement with experimental data was found for the odd-neutron ^{235}U and ^{239}Pu nuclei when using the SIII and SkM* parametrizations with root-mean-square (r.m.s) energy deviation of about 250 keV and 350 keV, respectively. The agreement with experimental data was however less good for the odd-proton ^{237}Np and ^{241}Am nuclei when using these two Skyrme parametrizations with the r.m.s energy deviation at about 450 keV for the SIII and 500 keV for the SkM* parametrizations. A possible reason for the poorer agreement in odd-proton nuclei is the use of the Slater approximation in the treatment of the Coulomb exchange term. On the other hand, the band-head energies obtained with the SLy5* parametrization were found to give a better agreement with experimental data for the odd-proton nuclei with an r.m.s energy deviation of about 460 keV as compared to 650 keV for the odd-neutron nuclei. In general, the SIII

parametrization give a better agreement with experimental band-head energies than the other two Skyrme parametrizations.

The static moments of the four considered odd-mass nuclei in their ground-state deformation have also been investigated. Out of the three odd-mass nuclei (namely ^{235}U, ^{237}Np and ^{241}Am) for which the experimental spectroscopic charge quadrupole moment are available for comparison, the calculated values were found to differ at most by 0.2 barn. The charge quadrupole moment of the neighbouring even-mass nuclei namely ^{234}U, ^{236}U, ^{238}Pu and ^{240}Pu were best reproduced when using the SLy5* parametrization, with a r.m.s of about 0.1 barn. For the total magnetic moments of the four odd-mass nuclei, the r.m.s deviation when using the SIII parameters set was found to be about 0.5 μ_N (μ_N being the nuclear magneton) while the corresponding value for the other two Skyrme parametrizations is about 0.6 μ_N. The collective gyromagnetic ratio g_R entering the expression of the total magnetic moment have been calculated for the neighbouring $(A-1)$ polarized even-even core (where A is the mass number of the odd-mass nucleus).

In the fission-isomeric well, there are two kinds of quantities which could be compared to the experiment namely the fission-isomeric energy, which is defined as the energy difference of the lowest-energy solution between the fission-isomeric and the ground-state wells, and band-head energies. The experimental data available for comparison in this region of nuclear deformation exists only for the ^{239}Pu nucleus, out of the two considered odd-neutron nuclei. Overall, the fission-isomeric energy was found to be much more sensitive to the various rotational correction schemes implemented herein as opposed to the band-head energies in the isomeric well. The three rotational correction schemes mentioned above have been considered. Between the first (Belyaev) and the latter (with 50% reduction) scheme, the fission-isomeric energy was found to vary by about 800 keV, while the band-head energies in the isomeric well, in general, were only affected by some tens of keV. The experimental level sequence of a $5/2^+$ ground-state with a $9/2^-$ excited state in the isomeric well of ^{239}Pu was reproduced when using the SIII parametrization. The intrinsic quadrupole moment for the $5/2^+$ state in the isomeric well of ^{239}Pu calculated with the three Skyrme parametrizations was found to be within the error bar of the experimental value.

The K^π quantum numbers of the band-heads in the ground-state well of ^{235}U and ^{239}Pu nuclei were considered for the calculations of the deformation energies as a function of deformation. The heights and shape of fission barriers were found to be dependent on the blocked K^π configurations. Both the SIII and SLy5* parametrizations give much higher fission barriers as compared to the SkM* parametrization usually used for fission-barrier calculations. In particular, the width of the outer-barrier obtained with the SLy5* parametrization are too large as compared to those obtained with SkM*. As expected, allowing the nucleus to explore left-right asymmetrical shapes in the region of the outer fission-barrier considerably lowers the barrier height. It was conjectured that restoration of the broken parity symmetry through parity projection calculations would yield for the case of two blocked configurations with the same K quantum number but of opposite parity, the same energy solution at the top of the outer barrier. Therefore, the difference between the outer-barrier heights would solely be due to their energy difference in the ground-state deformation.

While the fission-barrier heights are not observable quantities, one usually compares the calculated results with the empirical values derived from experimental fission cross sections to serve as a guide on the appropriateness of the theoretical approach. We could only made a qualitative comparison since a direct comparison between the calculated fission-barrier heights for the various blocked configurations with existing empirical data is not possible since the empirical values were obtained by taking the lowest-energy solution at each deformation irrespective of the K quantum number. As expected, the rotational correction calculated from the usual Belyaev formula was found to give too low a value for the fission-isomeric energy, E_{II}, and parity asymmetric outer-barrier heights of some blocked K configurations. From the study of E_{II} of odd-mass and even-mass nuclei with the SkM* parametrization, the reduction of the rotational correction calculated using the Belyaev formula by 50% was found to give reasonable E_{II} values as compared to the experiment. This rotational correction scheme was found to increase the inner-barrier heights, fission-isomeric energy for a fixed K^{π} configuration E_{IS}, and asymmetric outer-barrier heights by about 0.50, 0.70 and 1.0 MeV, respectively, from the ones obtained with the Belyaev moment of inertia.

When using the 50% reduction scheme to the rotational correction with the SkM* parametrization, it was found that the lower range of the inner-barrier and the higher range of the asymmetric outer-barrier in both nuclei agree best with the empirical values. The inner-barrier heights for the various blocked configurations are within the range of 5.0 to 7.0 MeV for ^{235}U nucleus and from 6.1 to 8.2 MeV for ^{239}Pu nucleus. Recent dynamical calculations using non-perturbative cranking approach show that static calculations overestimates somewhat the impact of triaxility and thus underestimate the height of the inner-barrier. As such, a slight increase in the inner-barrier height is to be expected. The asymmetrical outer-barrier heights were found to be between 4.7 and 6.2 MeV for ^{235}U, and from 4.3 to 5.4 MeV for ^{239}Pu. In all cases, these values are within 2 MeV away from the empirical data. Interestingly, the inner-barrier heights of all the considered blocked configurations in both nuclei were found to be higher than the outer-barrier heights. This is at variance with the recent empirical values for the ^{235}U nucleus published in RIPL-3 database, whereby the inner-barrier was reported to be lower than its outer-barrier.

Two technical aspects of the work have also been investigated. The first is regarding the effect of the missing terms in the Skyrme energy-density functionals on the fission-barrier heights. This have been studied for the inner-barrier height, E_A, and fission-isomeric energy for a fixed K^{π}, E_{IS}, with the SIII and SkM* parametrizations with a conserved parity symmetry. Both E_A and E_{IS} were found to be sensitive to the $\overleftrightarrow{J}^2$ term and this term yields an uncontrolablle effect on the fission-barrier heights. As such, the Skyrme parametrizations should only be employed in the same manner in which they have been fitted. Secondly, the consequence of the time-reversal symmetry breaking has been investigated by comparing the results obtained from SCB calculations with the EFA. It was found that the difference in absolute energies between those two approaches to be less than 200 keV and even smaller, of the order of tens of keV, for relative energies.

A possible extension from this work would be to restore the parity and rotation symmetries to obtain deformation energy curves with good J^{π} quantum numbers. The framework of the angular momentum projection calculations have been recently extended to include odd-mass nuclei in Ref. [112]. When projecting on good total angular momentum states, the problem of whether the K quantum number is a conserved quantity or not along the fission path would not arise. One should also consider a better pairing treatment using for example the HTDA approach which allows also to treat vibrational correlations on the same footing [113]. From the preliminary study published in Ref. [114], the particle-number symmetry breaking as in BCS approach tends to underestimate fission-barrier heights. Finally, the present work could be extended to a wider range of odd-mass as well as odd-odd nuclei.

Bibliography

[1] L. Meitner and O. R. Frisch (1939). Disintegration of Uranium by neutrons : a new type of nuclear reaction. *Nature*. 143, 239

[2] N. Bohr and J. A. Wheeler (1939). The mechanism of nuclear fission. *Phys. Rev.* 56, 426

[3] V. M. Strutinsky (1967). Shell effects in nuclear masses and deformation energies. *Nucl. Phys. A*. 95, 420

[4] D. Vautherin and D. M. Brink (1972). Hartree-Fock calculations with Skyrme's interaction. I. Spherical nuclei. *Phys. Rev. C*. 5, 626

[5] D. Vautherin (1973). Hartree-Fock calculations with Skyrme's interaction. II. Axially deformed nuclei. *Phys. Rev. C*. 7, 296

[6] H. Flocard, P. Quentin, A. K. Kerman and D. Vautherin (1973). Nuclear deformation energy curves with the constrained Hartree-Fock method. *Nucl. Phys. A*. 203, 433

[7] H. Flocard, P. Quentin, D. Vautherin, M. Veneroni and A. K. Kerman (1974). Self-consistent calculation of the fission barrier of ^{240}Pu. *Nucl. Phys. A*. 231, 176

[8] N. Nikolov, N. Schunck, W. Nazarewicz, M. Bender, and J. Pei (2011). Surface symmetry energy of nuclear energy density functionals. *Phys. Rev. C*. 83, 034305. American Physical Society.

[9] J. D. McDonnell, W. Nazarewicz, and J. A. Sheikh (2013). Third minima in thorium and uranium isotopes in a self-consistent theory. *Phys. Rev. C*. 87, 054327. American Physical Society.

[10] A. Staszczak, A. Baran, and W. Nazarewicz (2013). Spontaneous fission modes and lifetimes of superheavy elements in the nuclear density functional theory. *Phys. Rev. C*. 87, 024320. American Physical Society.

[11] W. Younes and D. Gogny (2009). Microscopic calculation of ^{240}Pu scission with a finite-range effective force. *Phys. Rev. C*. 80, 054313. American Physical Society.

[12] M. Warda and J. L. Egido (2012), Fission half-lives of superheavy nuclei in a microscopic approach. *Phys. Rev. C* 86, 014322. American Physical Society.

[13] R. Rodriguez-Guzman and L. M. Robledo (2014). Microscopic description of fission in uranium isotopes with the Gogny energy density functional. *Phys. Rev. C*. 89, 054310. American Physical Society.

[14] H. Abusara, A. V. Afanasjev, and P. Ring (2010). Fission barriers in actinides in covariant density functional theory: The role of triaxiality. *Phys. Rev. C*. 82, 044303. American Physical Society.

[15] Bing-Nan Lu, En-Guang Zhao, and Shan-Gui Zhou (2012). Potential energy surfaces of actinide nuclei from a multidimensional constrained covariant density functional theory: Barrier heights and saddle point shapes. *Phys. Rev. C*. 85, 011301. American Physical Society.

[16] H. Abusara, A. V. Afanasjev, and P. Ring (2012). Fission barriers in covariant density functional theory: Extrapolation to superheavy nuclei. *Phys. Rev. C*. 85, 024314. American Physical Society.

[17] A. V. Afanasjev and O. Abdurazakov (2013). Pairing and rotational properties of actinides and superheavy nuclei in covariant density functional theory. *Phys. Rev. C*. 88, 014320. American Physical Society.

[18] J. Libert, M. Meyer and P. Quentin (1980). Spectroscopic Properties of ^{237,239}Pu Fission Isomers from Self-Consistent Calculations. *Phys. Lett. B*. 95, 175. Elsevier.

[19] S. Goriely, S. Hilaire, A. J. Koning, M. Sin and R. Capote (2009). Towards a prediction of fission cross sections on the basis of microscopic nuclear inputs. *Phys. Rev. C*. 79, 024612. American Physical Society.

[20] R. Capote, M. Herman, P. Obložinský, P. G. Young, S. Goriely, T. Belgya, A. V. Ignatyuk, A. J. Koning, S. Hilaire and V. A. Plujko, M. Avrigeanu, O. Bersillon, M.B. Chadwick, T. Fukahori, Zhigang Ge, Yinlu Han, S. Kailas, J. Kopecky, V.M. Maslov, G. Reffo, M. Sin, E.Sh. Soukhovitskii and P. Talou (2009). RIPL – Reference Input Parameter Library for Calculation of Nuclear Reactions and Nuclear Data Evaluations. *Nucl. Data Sheets*. 110, 3107. Elsevier.

[21] S. Perez-Martin and L.M. Robledo (2009). Fission properties of odd-A nuclei within a mean field framework. *Int. J. Mod. Phys. E*. 18, 788. World Scientific Publishing.

[22] F. de la Iglesia, V. Martin, S. Perez-Martin and L.M. Robledo (2009). Different aspects of the fission process studied with the Gogny force. *Fourth International Workshop on Nuclear Fission and Fission-Product Spectroscopy*, Cadarache (France), May 13-16, 2009, *AIP Conf. Proc.* **1175** Melville, NY. 199-206

[23] S. Perez-Martin and L. M. Robledo (2008). Microscopic justification of the equal filling approximation. *Phys. Rev. C*. 78, 014304. American Physical Society.

[24] N. Schunck, J. Dobaczewski, J. McDonnell, J. More, W. Nazarewicz, J. Sarich, and M. V. Stoitsov (2010). One-quasiparticle states in the nuclear energy density functional theory. *Phys. Rev. C*. 81, 024316. American Physical Society.

[25] P. Quentin, L. Bonneau, N. Minkov and D. Samsœn (2010). Odd Nuclei, time-reversal symmetry breaking, and magnetic polarization of the even-even core. *Int. J. Mod. Phys. E*. 19, 611. World Scientific Publishing.

[26] L. Bonneau, J. Le Bloas, P. Quentin and N. Minkov (2011). Effects of core polarization and pairing correlations on some ground-state properties of deformed odd-mass nuclei within the Higher Tamm-Dancoff Approach. *Int. J. Mod. Phys. E*. 20, 252. World Scientific Publishing.

[27] L. Bonneau, N. Minkov, Dao Duy Duc, P. Quentin and J. Bartel (2015). Effect of core polarization on magnetic dipole moments in deformed odd-mass nuclei. *Phys. Rev. C*. 91, 054307. American Physical Society.

[28] J. Libert, M. Meyer and P. Quentin (1982). Self-Consistent Description of Heavy Nuclei. II. Spectroscopic Properties of Some Odd Nuclei. *Phys. Rev. C*. 25, 586. American Physical Society.

[29] R. Vandenbosch and R. Huizenga (1973). *Nuclear Fission*. New York and London: Academic Press.

[30] Jutta E. Escher, Jason T. Burke, Frank S. Dietrich, Nicholas D. Scielzo, Ian J. Thompson, and Walid Younes (2012). Compound-nuclear reaction cross sections from surrogate measurements. *Rev. Mod. Phys.* 84, 353. American Physical Society.

[31] https://www-nds.iaea.org/exfor/endf.htm

[32] O. Bouland, J. E. Lynn and P. Talou (2013). R-matrix analysis and prediction of low-energy neutron-induced fission cross sections for a range of Pu isotopes. *Phys. Rev. C*. 88, 054612. American Physical Society.

[33] M. Sin, R. Capote, A. Ventura, M. Herman and P. Obložinský (2006). Fission of light actinides: ^{232}Th(n,f) and ^{231}Pa(n,f) reactions. *Phys. Rev. C*. 74, 014608. American Physical Society.

[34] P. Fröbrich and R. Lipperheide (1996). *Theory of Nuclear Reactions*, Oxford University Press Inc., New York; Chapter 5 and Chapter 4.3

[35] W. Hauser and H. Feshbach (1952). The Inelastic Scattering of Neutrons. *Phys. Rev.* 87, 366. American Physical Society.

[36] J.F. Berger, M. Girod and D. Gogny (1984). Microscopic Analysis of Collective Dynamics in Low Energy Fission. *Nucl. Phys. A*. 428, 23c. Elsevier.

[37] H. Goutte, J.F. Berger, P. Casoli and D. Gogny (2005). Microscopic approach of fission dynamics applied to fragment kinetic energy and mass distributions in ^{238}U. *Phys. Rev. C*. 71, 024316. American Physical Society.

[38] A. Baran, Z. Lojewski, K. Sieja and M. Kowal (2005). Global properties of even-even superheavy nuclei in macroscopic-microscopic models. *Phys. Rev. C*. 72, 044310. American Physical Society.

[39] P. Möller, D.G. Madland, A.J. Sierk and A. Iwamoto (2001). Nuclear Fission Modes and Fragment Mass Asymmetries in a Five-Dimensional Deformation Space. *Nature*. 409, 785.

[40] M. Warda, J. L. Egido, L. M. Robledo, and K. Pomorski (2002). Self-Consistent Calculations of Fission Barriers in the Fm Region. *Phys. Rev. C*. 66, 014310. American Physical Society.

[41] M. Warda (2009). Microscopic analysis of the fission barriers in ^{256}Fm and ^{258}Fm. *Eur. Phys. J. A*. 42, 605. Springer.

[42] M. Sin and R. Capote (2008). Transmission through multi-humped fission barriers with absorption: A recursive approach. *Phys. Rev. C*. 77, 054601. American Physical Society.

[43] S. Hilaire, Ch. Lagrange and A.J. Koning (2003). Comparisons between various width fluctuation correction factors for compound nucleus reactions. *Ann. Phys.* 306, 209. Elsevier.

[44] P. Möller, A.J. Sierk, T. Ichikawa, A. Iwamoto, R. Bengtsson, H. Uhrenholt and S. Åberg (2009). Heavy-element fission barriers. *Phys. Rev. C*. 79, 064304. American Physical Society.

[45] A.J. Koning, S. Hilaire and S. Goriely (2008). Global and local level density models. *Nucl. Phys. A*. 810, 13. Elsevier.

[46] T. Belgya, O. Bersillon, R. Capote, T. Fukahori, G. Zhigang, S. Goriely, M. Herman, A.V. Ignatyuk, S. Kailas, A. Koning, P. Oblozinský, V. Plujko and P. Young (2006). Handbook for calculations of nuclear reaction data, RIPL-2. *IAEA-TECDOC-1506* (IAEA, Vienna, 2006). Available online at http://www-nds.iaea.org/RIPL-2/

[47] S. Hilaire and S. Goriely (2006). Global microscopic nuclear level densities within the HFB plus combinatorial method for practical applications. *Nucl. Phys. A*. 779, 63. Elsevier.

[48] S. Goriely, S. Hilaire and A.J. Koning (2008). Improved microscopic nuclear level densities within the Hartree–Fock–Bogoliubov plus combinatorial method. *Phys. Rev. C*. 78, 064307. American Physical Society.

[49] S. G. Nilsson, J. R. Nix, A. Sobiczewski, Z. Szymanski, S. Wycech, C. Gustafson, and P. Moller (1968). On the spontaneous fission of nuclei with Z near 114 and N near 184. *Nucl. Phys. A*. 115, 545. Elsevier.

[50] T.H.R. Skyrme (1956). The nuclear surface. *Phil. Mag.* 1, 1043

[51] J. Engel, D. Brink, K. Goeke, S. J. Krieger and D. Vautherin (1975). Time-Dependent Hartree-Fock Theory with Skyrme's Interaction. *Nucl. Phys. A*. 249, 215

[52] P. Bonche, H. Flocard and P. H. Heenen (1987). Self-Consistent Calculation of Nuclear Rotations: The complete yrast line of ^{24}Mg. *Nucl. Phys. A*. 467, 115

[53] D. Samsœn, P. Quentin and J. Bartel (1999). Generalized Routhian Calculations within the Skyrme-Hartree-Fock Approximation. *Nucl. Phys. A*. 652, 34.

[54] L. Bonneau (2003). *Fission des noyaux lourds: Etude microscopique des barrieres de fission et du moment angulaire des fragments*. (Ph.D. Thesis). Universite Bordeaux 1, France

[55] J. C. Slater (1951). A Simplification of the Hartree-Fock Method. *Phys. Rev.* 81, 385.

[56] C. Titin-Schnaider and P. Quentin (1974). Coulomb Exchange Contribution in Nuclear Hartree-Fock Calculations. *Phys. Lett. B*. 49, 397.

[57] J. Skalski (2001). Self-Consistent Calculations of the Exact Coulomb Exchange Effects in Spherical Nuclei. *Phys. Rev. C*. 63, 024312. American Physical Society.

[58] J.Le Bloas, Meng-Hock Koh, P. Quentin, L. Bonneau, J.I.A. Ithnin (2011). Exact Coulomb exchange calculations in the Skyrme-Hartree-Fock-BCS framework and tests of the Slater approximation. *Phys. Rev. C*. 84, 014310. American Physical Society.

[59] P. Ring and P. Schuck (1980). *The nuclear many-body problem*. Springer-Verlag. Berlin.

[60] L. Bonneau, P. Quentin and D. Samsœn (2004). Fission barrier of heavy nuclei within a microscopic approach. *Eur. Phys. J. A*. 21, 391. Springer.

[61] J. Bardeen, L. N. Cooper and J. R. Schrieffer (1957). Theory of superconductivity. *Phys. Rev. C*. 108, 1175.

[62] M. Bender, P.-H. Heenen and P.-G. Reinhard (2003). Self-consistent mean-field models for nuclear structure. *Rev. Mod. Phys.* 75: 136-138

[63] N. Pillet, P. Quentin and J. Libert (2002). Pairing correlations in an explicitly particle-number conserving approach. *Nucl. Phys. A*. 697, 141.

[64] M. A. Preston and R. K. Bhaduri (1975). *Structure of the nucleus*. Addison-Wesley. New York.

[65] H.J. Lipkin (1960). Collective motion in many-particle systems: Part 1. The violation of conservation laws. *Ann. Phys.* 9, 272.

[66] M. Bender, P.-H. Heenen and P.-G. Reinhard (2003). Self-consistent mean-field models for nuclear structure. *Rev. Mod. Phys.* 75: 143-144

[67] M. Bender, K. Rutz, P.-G. Reinhard and J.A. Maruhn (2000). Consequences of the Center-of-Mass Correction in Nuclear Mean-Field Models. *Eur. Phys. J. A*. 7, 467.

[68] S.T. Beliaev (1961). Concerning the calculation of the nuclear moment of inertia. *Nucl. Phys. A*. 24, 322.

[69] E.Kh. Yuldashbaeva, J. Libert, P. Quentin and M. Girod (1999). Mass parameters for large amplitude collective motion: A perturbative microscopic approach. *Phys. Lett. B*. 461, 1.

[70] D. J. Thouless and J. G. Valatin (1962). Time-dependent Hartree-Fock equations and rotational states of nuclei. *Nucl. Phys.* 31, 211

[71] J. Libert, M. Girod and J.P. Delaroche (1999). Microscopic descriptions of superdeformed bands with the Gogny force: Configuration mixing calculations in the A $\sim$ 190 mass region. *Phys. Rev. C*. 60, 054301. American Physical Society.

[72] M. Bender, P.-H. Heenen and P. Bonche (2004). Microscopic study of ^{240}Pu: Mean field and beyond. *Phys. Rev. C*. 70, 054304. American Physical Society.

[73] E. Chabanat, P. Bonche, P. Haensel, J. Meyer and R. Schaeffer (1998). A Skyrme parametrization from subnuclear to neutron star densities Part II. Nuclei far from stabilities. *Nucl. Phys. A*. 635, 231.

[74] E. Chabanat, P. Bonche, P. Haensel, J. Meyer and R. Schaeffer (1998). Erratum to "A Skyrme parametrization from subnuclear to neutron star densities. (II) Nuclei far from stabilities". *Nucl. Phys. A*. 643, 441.

[75] Ben. R. Mottelson and J. G. Valatin (1960). Effect of Nuclear Rotation on the Pairing Correlation. *Phys. Rev. Lett.* 5, 511

[76] P. Quentin, H. Lafchiev, D. Samsœn and I.N. Mikhailov (2004). Simple model for the quenching of the moments of inertia due to pairing correlations in rigidly deformed rotational bands. *Phys. Rev. C*. 69, 054315. American Physical Society.

[77] P. Quentin and J. Bartel, *to be summited*

[78] A. Bohr and B.R. Mottelson (1975). *Nuclear Structure, Vol. II*. Benjamin. Reading.

[79] J. Bartel, P. Quentin, M. Brack, C. Guet, H.-B.Håkansson (1982). Towards a Better Parametrisation of Skyrme-Like Effective Forces: A critical study of the SkM Force. *Nucl. Phys. A*. 386, 79.

[80] T. V. Nhan. Hao, P. Quentin, L. Bonneau (2012). Parity restoration in the highly truncated diagonalization approach: Application to the outer fission barrier of ^{240}Pu. *Phys. Rev. C*. 86, 064307. American Physical Society.

[81] A. Staszczak, A. Baran and W. Nazarewicz (2013). Spontaneous fission modes and lifetimes of superheavy elements in the nuclear density functional theory. *Phys. Rev. C*. 87, 024320. American Physical Society.

[82] N. Schunck, D. Duke, H. Carr and A. Knoll (2014). Description of induced nuclear fission with Skyrme energy functionals: Static potential energy surfaces and fission fragment properties. *Phys. Rev. C*. 90, 054305. American Physical Society.

[83] M. Beiner, H. Flocard, Nguyen Van Giai and P. Quentin (1975). Nuclear Ground-State Properties and Self-Consistent Calculations with the Skyrme Interaction (I). Spherical Description. *Nucl. Phys. A*. 238, 29.

[84] N. Tajima, P. Bonche, H. Flocard, P.-H. Heenen, and M.S. Weiss (1993). Self-Consistent Calculation of Charge Radii of Pb Isotopes. *Nucl. Phys. A*. 551, 434

[85] V. Hellemans, P.-H. Heenen and M. Bender (2012). Tensor part of the Skyrme energy density functional. III. Time-odd terms at high spin. *Phys. Rev. C*. 85, 014326. American Physical Society.

[86] K. Washiyama, K. Bennaceur, B. Avez, M. Bender, P.-H. Heenen and V. Hellemans (2012). New parametrization of Skyrme's interaction for regularized multireference energy density functional calculations. *Phys. Rev. C*. 86, 054309. American Physical Society.

[87] A. Pastore, D. Davesne, K. Bennaceur, J. Meyer and V. Hellemans (2013). Fitting Skyrme functionals using linear response theory. *Phys. Scr. T*. 154, 014014. IOP Publishing.

[88] E. Chabanat, P. Bonche, P. Haensel, J. Meyer and R. Schaeffer (1997). A Skyrme parametrization from subnuclear to neutron star densities. *Nucl. Phys. A*. 627, 710.

[89] M. Bender, P.-H. Heenen and P.-G. Reinhard (2003). Self-consistent mean-field models for nuclear structure. *Rev. Mod. Phys.* 75: 131-132

[90] K. Rutz, M. Bender, P. Reinhard, J.A. Maruhn (1999). Pairing Gap and Polarisation Effects. *Phys. Lett. B*. 468, 1.

[91] M. Samyn, S. Goriely, J.M. Pearson (2005). Further explorations of Skyrme-Hartree-Fock-Bogoliubov mass formulas. V. Extension to fission barriers. *Phys. Rev. C*. 72, 044316. American Physical Society.

[92] S. Karatzikos, A.V. Afanasjev, G.A. Lalazissis, P. Ring (2010). The fission barriers in Actinides and superheavy nuclei in covariant density functional theory. *Phys. Lett. B*, 689, 1.

[93] W. Satula, J. Dobaczewski and W. Nazarewicz (1998). Odd-Even Staggering of Nuclear Masses: Pairing or shape effect ?. *Phys. Rev. Lett.* 81, 3599.

[94] T. Duguet, P. Bonche, P.-H. Heenen and J. Meyer (2001). Pairing Correlations. II. Microscopic Analysis of Odd-Even Mass Staggering in Nuclei. *Phys. Rev. C*. 65, 014311. American Physical Society.

[95] M. Bender, K. Rutz, P.-G. Reinhard, and J.A. Maruhn (2000). Pairing Gaps from Nuclear Mean-Field Models. *Eur. Phys. J. A*. 8, 59. Springer.

[96] Jie Zhao, Bing-Nan Lu, Dario Vretenar, En-Guang Zhao and Shan-Gui Zhou (2015). Multidimensionally constrained relativistic mean-field study of triple-humped barriers in actinides. *Phys. Rev. C*. 91, 014321. American Physical Society.

[97] Meng-Hock Koh, Dao Duy Duc, T. V. Nhan Hao, Ha Thuy Long, P. Quentin, and L. Bonneau (*submitted to Eur. Phys. J. A*)

[98] M. Abramowitz and I. A. Stegun (1968). *Handbook of Mathematical Functions*. Dover, New York.

[99] Andrzej Baran, Aurel Bulgac, Michael McNeil Forbes, Gaute Hagen, Witold Nazarewicz, Nicolas Schunck, and Mario V. Stoitsov (2008). Broyden' s method in nuclear structure calculations. *Phys. Rev. C*. 78, 014318. American Physical Society.

[100] D. D. Johnson (1988). Modified Broyden' s method for accelerating convergence in self-consistent calculations. *Phys. Rev. B* 38, 12807

[101] S. Raman, C. W. Nestor and P. Tikkaneny (2001). Transition Probability from the Ground to the First-Excited 2+ State of Even-Even Nuclides. *At. Data Nucl. Data Tables*. 78, 1.

[102] N. J. Stone (2005). Table of nuclear magnetic dipole and electric quadrupole moments. *At. Data Nucl. Data Tables*, 90, 75.

[103] A. K. Jain, R. K. Sheline, P. C. Sood, and Kiran Jain (1990). Intrinsic states of deformed odd-A nuclei in the mass regions ($151 \leq A \leq 193$) and ($A \geq 221$) *Rev. Mod. Phys.* 62(2), 393.

[104] E. Browne and J.K. Tuli (2014). Nuclear Data Sheets for A = 239. *Nucl. Data Sheets*. 122, 293.

[105] E. Browne (2003). Nuclear Data Sheets for A = 235, 239. *Nucl. Data Sheets*. 98, 665.

[106] D. Habs, V. Metag, H.J. Speeht and G. Ulfert (1977). Quadrupole Moment of the 8-μs Fission Isomer in ^{239}Pu. *Phys. Rev. Lett.* 38, 387.

[107] H.Backe, L.Richter, D.Habs, V.Metag, J.Pedersen, P.Singer, H.J.Specht (1979). Spectroscopy in the Second Minimum of the Potential Energy Surface of 239Pu. *Phys. Rev. Lett.* 42, 490.

[108] S. Bjørnholm and J. Lynn (1980). The double-humped fission barrier. *Rev. Mod. Phys.* 52, 725.

[109] D.W.L. Sprung, S.G. Lie, M. Vallieres, P. Quentin (1979). Collective gyromagnetic ration and moment of inertia from density-dependent Hartree-Fock Calculations. *Nucl. Phys. A*. 326, 37.

[110] Jhilam Sadhukhan, K. Mazurek, A. Baran, J. Dobaczewski, W. Nazarewicz and J. A. Sheikh (2013). Spontaneous fission lifetimes from the minimization of self-consistent collective action. *Phys. Rev. C*. 88, 064314. American Physical Society.

[111] G. N. Smirenkin (1993). Preparation of evaluated data for a fission barrier parameter library for isotopes with Z = 82 - 98, with consideration of the level density models used. *IAEA Report No. INDC(CCP)*-359

[112] B. Bally, B. Avez, M. Bender and P.-H. Heenen (2014). Beyond Mean-Field Calculations for Odd-Mass Nuclei. *Phys. Rev. Lett.* 113, 162501. American Physical Society.

[113] H.Naidja, P.Quentin, T.L.Ha and D.Samsoen (2010). Pairing and vibrational correlations in the higher Tamm-Dancoff approximation (HTDA) approach. *Phys.Rev. C*. 81, 044320. American Physical Society.

[114] Koh Meng Hock, L. Bonneau, P. Quentin, and H. Wagiran (2013). Fission barriers of odd-mass nuclei within the HF-BCS and HTDA approaches. *EPJ Web of Conferences*. 62, 04004

[115] B.R. Mottelson and P.G. Valatin (1960). Effect of Nuclear Rotation on the Pairing Correlation, *Phys. Rev. Lett.* 5, 511.

[116] K. Bencheikh, P. Quentin, J. Bartel (1994). Rotations in Nuclei - A Semiclassical Description. *Nucl. Phys. A*. 571, 518.

[117] S.G. Nilsson, C.F. Tsang, A. Sobiczewski, Z. Szymanski, S. Wyceh, S. Gustafson, I.-L. Lamm, P. M*ö*ller and B. Nilsson (1969). On the Nuclear Structure and Stability of Heavy and Superheavy Elements. *Nucl. Phys. A*. 131, 1.

[118] I.N. Mikhailov, P. Quentin and D. Samsœn (1997). Nuclear Intrinsic Vorticity and Its Coupling to Global Rotations. *Nucl. Phys. A*. 627, 259.

[119] R.W. Hasse and W.D. Myers (1988). *Geometrical relationships of macroscopic nuclear physics*. Springer

[120] W.D. Myers and W.J. Swiatecki (1966). Nuclear Masses and Deformations. *Nucl. Phys.* 81, 1

Appendix A

SKYRME PARAMETERS AND THE VARIOUS COUPLING CONSTANTS

The coupling constants entering the expression of the Hamiltonian densities are written in terms of the Skyrme parameters which are listed in Table A.1 for the three Skyrme interactions considered herein. The expression of the coupling constants are written as follows with the values of each coupling constant given in the Table A.2 according to the type of Skyrme parametrization.

$$B_1 = \frac{t_0}{2}\left(1+\frac{x_0}{2}\right) \qquad B_2 = -\frac{t_0}{2}\left(\frac{1}{2}+x_0\right)$$

$$B_3 = \frac{1}{4}\left[t_1\left(1+\frac{x_1}{2}\right)+t_2\left(1+\frac{x_2}{2}\right)\right] \qquad B_4 = -\frac{1}{4}\left[t_1\left(\frac{1}{2}+x_1\right)-t_2\left(\frac{1}{2}+x_2\right)\right]$$

$$B_5 = -\frac{1}{16}\left[3t_1\left(1+\frac{x_1}{2}\right)-t_2\left(1+\frac{x_2}{2}\right)\right] \qquad B_6 = \frac{1}{16}\left[3t_1\left(\frac{1}{2}+x_1\right)+t_2\left(\frac{1}{2}+x_2\right)\right]$$

$$B_7 = \frac{t_3}{12}\left(1+\frac{x_3}{2}\right) \qquad B_8 = -\frac{t_3}{12}\left(\frac{1}{2}+x_3\right)$$

$$B_9 = -\frac{W_0}{2} \qquad B_{10} = \frac{1}{4}t_0x_0$$

$$B_{11} = -\frac{1}{4}t_0 \qquad B_{12} = \frac{1}{24}t_3x_3$$

$$B_{13} = -\frac{t_3}{24} \qquad B_{14} = -\frac{1}{8}\left(t_1x_1+t_2x_2\right)$$

$$B_{15} = \frac{1}{8}\left(t_1-t_2\right) \qquad B_{18} = -\frac{1}{32}\left(3t_1x_1-t_2x_2\right)$$

$$B_{19} = \frac{1}{32}\left(3t_1+t_2\right)$$

Table A.1: Values of the Skyrme parameters as a function of the Skyrme interaction.

Parameter	SIII	SkM*	SLy5*	SLy5
t_0	1128.75	-2645.00	-2495.31	-2484.88
t_1	395.00	410.00	484.02	483.13
t_2	-95.00	-135.00	-469.48	-549.40
t_3	14000.0	15595.00	13867.43	13763.0
x_0	0.45	0.09	0.620	0.778
x_1	0	0	-0.086	-0.328
x_2	0	0	-0.947	-1.000
x_3	1.0	0	0.934	1.267
α	1.0	1/6	1/6	1/6
W_0	120	130	120.250	126.0

Table A.2: The values of the coupling constants for each Skyrme interaction.

Coupling constant	SIII	SkM*	SLy5*
B_1	-691.359375	-1382.0125	-1634.42805
B_2	536.15625	780.275	1397.3736
B_3	-583.333333	-649.791667	-577.809583
B_4	-61.25	-68.125	2.36832
B_5	-80.0	-85.3125	-102.300165
B_6	34.0625	34.21875	50.68815
B_7	1750.0	1299.583333	1695.293318
B_8	-1750.0	-649.791667	-1657.157885
B_9	-60.0	-65.0	-60.125
B_{10}	-126.984375	-59.5125	-386.77305
B_{11}	282.1875	661.25	623.827500
B_{12}	583.333333	0.0	539.674151
B_{13}	-583.333333	-649.791667	-577.809583
B_{14}	0.0	0.0	-50.37148
B_{15}	0.0	0.0	119.1875
B_{18}	0.0	0.0	17.796085
B_{19}	0.0	0.0	30.705625

Appendix B

HF CALCULATIONS WITH ADJUSTMENT OF LINEAR CONSTRAINTS

B.1 Principle of the method

Let us consider the usual constrained Hartree-Fock calculation with the Hamiltonian given as

$$\hat{H}' \;=\; \hat{H} - \sum_i \lambda_i \, \hat{Q}_i \tag{B.1}$$

where the Lagrange multipliers λ_i are used to constrain the Hartree-Fock Slater determinant to a specific deformation point Q_i. If $|\Psi_0\rangle$ is a solution to the variational problem

$$\delta\big(\langle\Psi_0|H'|\Psi_0\rangle\big) \;=\; 0 \tag{B.2}$$

then the solution of the following variational equation

$$\delta\langle\Psi|(\hat{H}' - \sum_i d\lambda_i \, \hat{Q}_i)|\Psi\rangle = 0 \tag{B.3}$$

is given by the first order perturbation theory as

$$|\Psi\rangle \;=\; |\Psi_0\rangle - \sum_i \lambda_i \sum_{n\neq 0} \frac{\langle\Psi_n|\hat{Q}_i|\Psi_0\rangle}{E_0 - E_n}|\Psi_n\rangle \tag{B.4}$$

The expectation value of the one-body operator $\mathrm{Q_i}$ can be written in matrix form with unknowns $d\lambda_i$ as:

$$\langle\Psi|\hat{Q}_i|\Psi\rangle \;=\; \langle\Psi_0|\hat{Q}_i|\Psi_0\rangle + \sum_j \chi_{ij}\, d\lambda_j \tag{B.5}$$

with

$$\chi_{ij} = 2\sum_{n\neq 0} \frac{\Re e(\langle\Psi_n|\hat{Q}_i|\Psi_0\rangle\langle\Psi_0|\hat{Q}_j|\Psi_n\rangle^*)}{E_n - E_0} \tag{B.6}$$

The solutions to the unknown $d\lambda_i$ is obtained by rearranging the equation and taking the inverse of the χ_{ij} matrix, so that:

$$d\lambda_i = \sum_j \left(\chi^{-1}\right)_{ij} \cdot \left(\langle\Psi|\hat{Q}_i|\Psi\rangle - \langle\Psi_0|\hat{Q}_i|\Psi_0\rangle\right) \tag{B.7}$$

The value of $d\lambda_i$ corresponds to the amount of correction to the constraint λ_i in order to obtain the desired values Q_i of $\langle\Psi|\hat{Q}_i|\Psi\rangle$.

B.2 Application to the constrained Hartree-Fock calculation

In order to obtain an estimate of the correction of $d\lambda_i$, the pairing correlation can be ignored so that the matrix elements of χ_{ij} is calculated from the Slater determinant of the Hartree-Fock ground state $|\Phi_0\rangle$, with the following expression:

$$\chi_{ij} = 2 \sum_{a\in\mathscr{H}(\Phi_0)} \sum_{\alpha\in\mathscr{P}(\Phi_0)} \frac{\Re e(\langle\Phi_0|a_a^\dagger a_\alpha \hat{Q}_i|\Phi_0\rangle\langle\Phi_0|a_a^\dagger a_\alpha \hat{Q}_j|\Phi_0\rangle)}{e_\alpha - e_a} \tag{B.8}$$

where $|a\rangle$ and $|\alpha\rangle$ denotes the hole and particle states respectively with e_a and e_α are their respective single-particle energies.

If $\hat{Q}_i$ is a one-body operator of the form:

$$\hat{Q}_i = \sum_{m,n} \langle m|\hat{q}_i|n\rangle \; a_m^\dagger a_n \tag{B.9}$$

one can then make use of the Wick's theorem to show that:

$$\langle\Phi_0|a_a^\dagger a_\alpha \hat{Q}_i|\Phi_0\rangle = \sum_{j,k}\langle j|\hat{q}_i|k\rangle\langle\Phi_0|a_a^\dagger a_\alpha a_j^\dagger a_k \hat{Q}_i|\Phi_0\rangle = \langle\alpha|\hat{q}_i|a\rangle \tag{B.10}$$

Making use of the expression above, the matrix elements of χ_{ij} can be written as:

$$\chi_{ij} = \sum_{a\in\mathscr{H}(\Phi_0)} \sum_{\alpha\in\mathscr{P}(\Phi_0)} \frac{\Re e(\langle\alpha|\hat{q}_i|a\rangle\langle a|\hat{q}_j|\alpha\rangle^*)}{e_\alpha - e_a} \tag{B.11}$$

It should be noted that the expectation value of the $\hat{Q}_i$ operator in the Hartree-Fock ground state would be written as

$$\langle\Phi_0|\hat{Q}_i|\Phi_0\rangle = \sum_{j\in\mathscr{H}(\Phi_0)} \langle j|\hat{q}_i|j\rangle \tag{B.12}$$

When dealing with a linear constraint, the Hartree-Fock to be diagonalized is such that

$$\hat{h}'_{HF} = \hat{h}_{HF} - \sum_i \lambda_i \hat{q}_i \tag{B.13}$$

If the operator $\hat{q}_i$ is a function of the $\hat{\mathbf{R}}$ position operator, one would then have

$$\langle \mathbf{r}|\hat{h}'_{HF}|\varphi\rangle = \langle \mathbf{r}|\hat{h}_{HF}|\varphi\rangle - \sum_i \lambda_i q_i(\mathbf{r})\varphi(\mathbf{r}) \tag{B.14}$$

At the n^{th} iteration of the Hartree-Fock process, the λ_i value is adjusted by a small amount of $d\lambda_i^{(n)}$ so that the constrained Hamiltonian to be diagonalized in the next iteration would be

$$\hat{h}_{HF}^{(n+1)} = \hat{h}_{HF}^{(n)} - \sum_i \left(\lambda_i^{(n)} + d\lambda_i^{(n)}\right)\hat{q}_i \tag{B.15}$$

with

$$d\lambda_i^{(n)} = \sum_j \left(\chi^{-1}\right)_{ij} \cdot \left(Q_j - \langle \Phi_0^{(n)}|\hat{Q}_j|\Phi_0^{(n)}\rangle\right) \tag{B.16}$$

Appendix C

THE MOMENT OF INERTIA AND $\langle \hat{J}^2 \rangle$ TERM USING BELYAEV FORMULA

The expression for the moment of inertia in the case whereby the time-reversal symmetry is conserved, is given by [109]:

$$\mathcal{I}_{Bel} = \sum_{kl}^{(A)} \frac{|\langle k|j_+|l\rangle|^2}{E_k + E_l}\big(u_k v_l - u_l v_k\big)^2 + \frac{1}{2}\sum_{kl}^{(B)} \frac{|\langle k|j_+|l\rangle|^2}{E_k + E_l}\big(u_k v_l - u_l v_k\big)^2 \tag{C.1}$$

The first summation term of index A sums up all the single-particle states ($|k\rangle$ and $|l\rangle$) with its third component of the total angular momentum operator, $\Omega > 0$. The second summation (index B) only takes into account the states with $\Omega = \frac{1}{2}$. The quasiparticle energy is calculated as:

$$E_k = \sqrt{(e_k - \lambda)^2 + \Delta^2} \tag{C.2}$$

with λ and Δ being the energy of the Fermi level and pairing gap respectively, calculated within the BCS approach. The expectation value of $\hat{J}^2$ for an even-even nucleus has an almost similar form as the equation of the moment of inertia except for the absence of the denominator term:

$$\langle \hat{J}^2 \rangle = \sum_{kl}^{(A)} |\langle k|j_+|l\rangle|^2\big(u_k v_l - u_l v_k\big)^2 + \frac{1}{2}\sum_{kl}^{(B)} |\langle k|j_+|l\rangle|^2\big(u_k v_l - u_l v_k\big)^2 \tag{C.3}$$

In the case of odd-mass nuclei, we shall recall that the experimental I^π quantum numbers is taken equal to the K^π quantum numbers which corresponds to the expectation value of the $\hat{J}_z$ and $\hat{\pi}$ operators of the blocked single-particle state. This is consistent with the unified model ansatz in the absence of Coriolis terms. The moment of inertia for the odd-A nucleus has been calculated from the polarized even-even $(A-1)$ core nucleus, taking into account the time-reversal symmetry breaking. This has been done by first performing the HF-BCS calculations for the desired K^π blocked configuration of the odd-A nucleus. After self-consistency has been achieved, we used this polarized field and perform the calculation of the moment of inertia by excluding the blocked single-particle state denoted by $|m\rangle$ and its pair conjugate state $|\tilde{m}\rangle$ such

that

$$\mathfrak{I}_{Bel} = \frac{1}{2} \sum_{kl \neq m} \frac{|\langle k|j_+|l\rangle|^2}{E_k + E_l} \left(u_k v_l - u_l v_k\right)^2 \tag{C.4}$$

where the summation is taken for all the single-particle states with $\Omega \lessgtr 0$. This is reflected by the factor 1/2 appearing in the expression of the moment of inertia above as opposed to the expression given in equation (C.1).

Appendix D

ROTATIONAL ENERGY AS A FUNCTION OF ANGULAR VELOCITY

In this model, we will discussed about the calculational details of the model proposed by Ref. [77]. This model was originally proposed so as to provide the energies of the rotational band by using simply the energies of the first 2^+ state in the ground-state deformation. The nucleus is viewed as rotating on an axis perpedicular to its symmetry axis with an angular velocity denoted as Ω. In the intrinsic system of the nucleus, the global rotation of the nucleus generates an intrinsic motion denoted as ω which counter-rotates the global nuclear rotation such that the product of both angular velocities $\omega \cdot \Omega < 1$.

The counter-rotating motion ω increases proportionally with the global rotation Ω. On the other hand, it decreases as the pairing correlation do, as a function of Ω with an expression given as:

$$\omega \;=\; -k\,\Omega\Big[1 \;-\; \Big(\frac{\Omega}{\Omega_c}\Big)^2\Big] \tag{D.1}$$

where the parameter k is a positive constant to be determined from the model. The critical angular velocity Ω_c corresponds to the angular velocity where the pairing correlations vanishes, due to the Coriolis anti-pairing which was first discussed in Ref. [115]. The critical angular velocity is estimated from

$$\Omega_c^2 \;=\; \frac{4\,E_0}{\mathcal{I}_R} \tag{D.2}$$

where $\mathcal{I}_R$ is the rigid-body moment of inertia . The moment of inertia of a spherical nuclear shape $\mathcal{I}_R^0$ could be estimated to a good approximation from the expression

$$\frac{\mathcal{I}_R^0}{\hbar^2} \;=\; \frac{A^{5/3}}{68.4}\,\mathrm{MeV}^{-1} \tag{D.3}$$

as reported in the work of Ref. [116]. E_0 is the pair-condensation energy at zero spin which was found to be twice the correlation energy [76]. From Ref. [117], the correlation energy was estimated to be about 2.3 MeV across the whole nuclear chart. Therefore, the condensation energy is taken to be 4.6 MeV.

The total excitation energy $E(\omega,\Omega)$ is assumed to have a quadratic form in the angular velocities ω and Ω, such that

$$E(\omega,\Omega) \;=\; \frac{1}{2}\Big[A\;\omega^2 \;+\; 2\,B\,\Omega\,\omega \;+\; C\,\Omega^2\Big] \tag{D.4}$$

whereby we would get the following expression upon using equation (D.1)

$$E(\omega,\Omega) \;=\; \frac{\Omega^2}{2}\Big[C-2\,B\,k(1-\varepsilon^2)+A\,k^2(1-\varepsilon^2)^2\Big] \;\equiv\; \frac{1}{2}\,\mathfrak{I}(\Omega)\,\Omega^2 \tag{D.5}$$

with $\varepsilon = \frac{\Omega}{\Omega_c}$ and $\mathfrak{I}(\Omega)$ being the moment of inertia as a function of the global nuclear rotation. The expression for the parameters A,B and C are estimated with a semi-classical approximation:

$$A = \eta\Theta F\Big[1-\frac{D}{\eta}\Theta\Big] \qquad B = \eta F\Big[1-\frac{D}{\eta}\Theta\Big] \qquad C = \eta F\Theta\Big[1-\frac{D}{\eta\Theta}\Big] \tag{D.6}$$

with

$$\eta = \mathfrak{I}_R^0\,q^{1/3}, \qquad \Theta = \frac{1}{2}\Big(q+\frac{1}{q}\Big) \tag{D.7}$$

where q is a ellipsoidal deformation parameter being the ratio of the semi-axis along the symmetry z-axis to the perpendicular direction. The renormalization factor F is given by:

$$F \;=\; \frac{1+0.69\,A^{-2/3}}{1-\frac{D}{\eta}} \tag{D.8}$$

The parameter D was obtained from the expression [118]:

$$\frac{D}{\eta} \;=\; 5\Big(\frac{8}{9\,\pi}\Big)^{2/3} f_{NM}\,A^{-2/3} \tag{D.9}$$

where f_{NM} is the (constant) isoscalar nucleon effective mass form factor in nuclear matter and A is the total number of nucleons. For $A = 240$ and the Skyrme SkM* parametrization where $f_{NM} = 1.265$, we have $D \;=\; 0.0706\,\eta$.

In the work of Ref. [77], the deformation parameter q is fixed so as to reproduce the mass quadrupole moment $Q(q)$ of a deformed nuclear shape using the expression [119]:

$$Q(q) \;=\; \frac{2}{5}A^{5/3}\,r_0^2\,q^{-2/3}\,\big(q^2-1\big) \tag{D.10}$$

where $r_0 = 1.2049$ fm according to Ref. [120]. The value of the mass quadrupole moment was obtained using the expression

$$Q \;=\; \frac{A}{Z}\,Q_{ch} \tag{D.11}$$

where Q_{ch} is the charge quadrupole moment taken from Ref. [101].

One of the crucial step in the model is to obtain a good estimate of the parameter k entering the equations (D.1) and (D.5). This has been done by using the the energy of the first 2^+ state. Using the expression for the energy of a rotational band, $E(I) = \frac{\hbar^2}{2\mathcal{I}} I(I+1)$ we have for the first 2^+ state:

$$E(2^+) \;=\; \frac{6\hbar^2}{2\mathcal{I}_2} \;=\; \frac{1}{2}\mathcal{I}_2\,\Omega^2 \tag{D.12}$$

By solving the first two equation on the left, one would obtain an estimate of $\mathcal{I}_2$ which in turns would provide the value of Ω. Using equation (D.12) above and together with equation (D.5), the value of k can be obtained from :

$$k \;=\; \frac{B}{A(1-\varepsilon_{2^+}^2)}\left[1 - \sqrt{1 - \frac{A(C-\mathcal{I}_2)}{B^2}}\right] \tag{D.13}$$

where ε_{2^+} is the value of $\varepsilon = \frac{\Omega}{\Omega_c}$ corresponding to the angular velocity of the 2^+ state.

The total angular momentum I as a function of the global rotation Ω can then be determined from the expression:

$$\bar{I} \;=\; \Big\{\big[C - 2Bk + Ak^2\big] \;+\; \frac{4}{3}\big[Bk - Ak^2\big]\varepsilon^2 \;+\; \frac{3}{5}Ak^2\varepsilon^4\Big\}\Omega \tag{D.14}$$

where $\bar{I} = \sqrt{I(I+1)}$ with $I = 0, 2, 4, 6$ etc. The equation $\bar{I}(\Omega)$ could be inverted so as to obtain the value of Ω as a function of $\bar{I}$. Thereafter, the rotational energy at a specific value of $\Omega(\bar{I})$ could be obtained from equation (D.5).

Figure D.1 shows the rotational bands obtained using the current model extracted from the work of Ref. [77] as compared to the experimental data. The rotational bands of ^{236}U was found to be nicely reproduced up to $I \approx 18$ while it is less satisfactory at higher spins. The agreement for the ^{240}Pu is much more impressive, with good agreement between the calculated values and the experiment even up to $I \approx 30$.

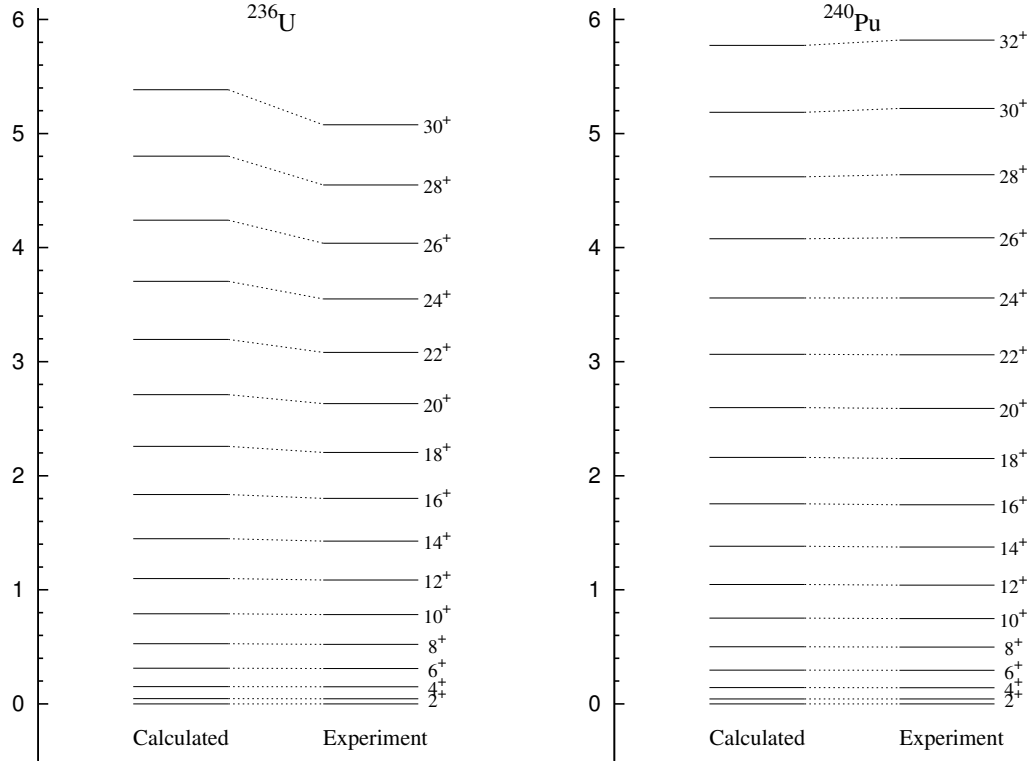

Figure D.1: Excitation energy of the rotational bands in ^{236}U and ^{240}Pu nuclei extracted from the calculations of Ref. [77] and compared to the experiments.